TECHNISCHE UNIVERSITÄT DARMSTADT

The impact of *S*-sulfocysteine in cell culture media

Fachbereich Chemie

der Technischen Universität Darmstadt

zur Erlangung des Grades
Doctor rerum naturalium
(Dr. rer. nat.)

Dissertation
von Martina Zimmermann, M.Sc

Erstgutachter: Prof. Dr. Harald Kolmar
Zweitgutachter: Prof. Dr. Dipl-Ing. Jörg von Hagen

Darmstadt 2020

Zimmermann, Martina: The impact of *S*-sulfocysteine in cell culture media
Darmstadt, Technische Universität Darmstadt
Jahr der Veröffentlichung der Dissertation auf TUprints: 2021
Tag der Einreichung: 08.09.2020

Tag der mündlichen Prüfung: 02.11.2020

Erklärung zur Dissertation

Hiermit versichere ich, Martina Zimmermann, die vorliegende Dissertation ohne Hilfe Dritter und nur mit den angegebenen Quellen und Hilfsmitteln angefertigt zu haben. Alle Stellen, die Quellen entnommen wurden, sind als solche kenntlich gemacht worden. Diese Arbeit hat in gleicher oder ähnlicher Form noch keiner Prüfungsbehörde vorgelegen.
Mir ist bekannt, dass im Falle eines Plagiats (§38 Abs.2 APB) ein Täuschungsversuch vorliegt, der dazu führt, dass die Arbeit mit 5,0 bewertet und damit ein Prüfungsversuch verbraucht wird. Abschlussarbeiten dürfen nur einmal wiederholt werden.
Bei der abgegebenen Thesis stimmen die schriftliche und die zur Archivierung eingereichte elektronische Fassung überein.

Datum: 07.09.2020

Unterschrift: M. Zimmerm

Contribution to publications and patents

Parts of this work are currently under review:

Zimmermann, M., Kolmar, H., Zimmer, A. (in preparation) "*S*-sulfocysteine – Investigation of cellular uptake in CHO cells"

Accepted Poster for the delayed conference Cell culture engineering (CCE XVII):

Zimmermann, M., Arsalan, M., Zimmer, A. "*S*-sulfocysteine – Investigation of cellular uptake in CHO cells"

Publications related to a second project:

Zimmermann, M., Ehret, J., Kolmar, H., Zimmer, A. (2019). "Impact of acetylated and non-acetylated fucose analogues on IgG" Antibodies **8**(1): 9.

Ehret, J., **Zimmermann, M.,** Eichhorn, T., Zimmer, A. (2018). "Impact of cell culture media additives on IgG glycosylation produced in CHO cells" Biotechnology and Bioengineering, **116**(4): 816-830.

Zimmermann, M., Nguyen, M., Schultheiss, C., Kolmar, H., Zimmer, A. (in preparation). „Use of 5-Thio-L-Fucose in cell culture media or feed to modulate binding affinity of therapeutic proteins"

Contribution to Patent: 19218172.5

Zimmermann, M., Ehret, J., Zimmer, A. (one-year grace period) "Methods and compositions for modulating the glycosylation profile of proteins"

Contribution to conferences:

Poster at GlycoBioTec 2019, Berlin:

Zimmermann, M., Ehret, J., Zimmer, A. "Development of a flow cytometry-based high throughput screening method to detect core-fucosylation"

Poster at European Society Animal Cell Technology (ESACT) 2019, Copenhagen which was published in BMC proceedings 2020, **14** (Suppl 1):188:

Zimmermann, M., Ehret, J., Zimmer, A. „Impact of acetylated and non-acetylated fucose analogues on IgG glycosylation" (P-538)

Ehret, J., **Zimmermann, M.,** Zimmer, A. "Impact of cell culture media additives on IgG glycosylation produced in CHO cells" (P-545)

Zusammenfassung

Die Aminosäure L-Cystein wird zur Kultivierung von Säugetierzellen wie chinesische Hamster ovarial (CHO) Zellen benötigt. Aufgrund der geringen Stabilität von Cystein und der geringen Löslichkeit von Cystin bei neutralem pH, wurde *S*-Sulfocystein (SSC) für den Einsatz in hochkonzentrierten Feeds entwickelt. Die Bioverfügbarkeit und der positive Einfluss von SSC wurde bereits mehrfach publiziert, wobei ebenfalls eine Toxizität bei hohen SSC Konzentrationen beobachtet wurde. Sowohl die zelluläre Aufnahme von SSC und die Ursache der Toxizität sind bisher ungeklärt und wurden in dieser Arbeit untersucht. Aufgrund struktureller Ähnlichkeit von SSC zu Cystin und Glutamat wurde vermutet, dass der Cystin/Glutamate-Antiporter (x_c^-) die SSC Aufnahme ermöglicht. Dies wurde einerseits durch die Hemmung des Transporters mittels Sulfasalazin und andererseits über Transporter Überexpression mittels Sulforaphan oder Sulforaphan-*N*-acetylcystein untersucht. Durch die tägliche Zugabe von 50 µM und 100 µM Sulfasalazin während Fed-Batch Experimenten wurde die extrazelluläre SSC-Konzentration um 65% bzw. 177% erhöht, was auf eine verringerte Aufnahme aufgrund der x_c^- Hemmung hinweist. Im Gegensatz dazu wurde eine erhöhte Transporteraktivität durch die Zugabe von 15 µM Sulforaphan und Sulforaphan-*N*-acetylcystein detektiert, indem die extrazelluläre SSC Konzentration um 60% bzw. 52% verringert wurde. Diese entgegengesetzte Wirkung stützt die Hypothese, dass SSC mittels x_c^- transportiert wird. Des weiteren wurde die Toxizität von SSC durch die Sulforaphan-bedingt erhöhte SSC Aufnahme verstärkt. Dies weist darauf hin, dass insbesondere die SSC Konzentration aber auch die x_c^- Antiporteraktivität die toxische Reaktion beeinflussen.

Der zweite Teil dieser Studie zielte darauf ab, Auswirkungen der Feed-Formulierung auf die SSC bedingte Toxizität und die Abhängigkeit verschiedener Zelllinien mittels Hochdurchsatz Fed-Batch Experimenten und multivariater Datenanalyse (MVDA) zu untersuchen. Die unterschiedliche Auswirkung von acht CHO-Zelllinien und 79 verschiedenen Feed-Formulierungen deutet sowohl auf eine klonabhängige SSC Toxizität als auch einen signifikanten Einfluss der Feed-Formulierung hin. Die Identifizierung von Medienkomponenten, welche die SSC Toxizität fördern war nicht möglich, so dass die Feed-Formulierung nur einen indirekten Einfluss auf die SSC Toxizität haben mag. Der letzte Abschnitt diente dazu die Metabolisierung von SSC durch CHO-Zellen zu untersuchen, indem Zelllysate mit SSC versetzt wurden. Die mittels LC-MS/MS identifizierten Metabolite wurden genutzt um neue Hypotheses zu formulieren. Die Erschöpfung von Glutathion und Akkumulation von *S*-sulfo-Glutathion wurden als mögliche Schlüsselmetabolite identifiziert und könnten eine übermäßige Persulfidierung von Cystein-abhängigen Schlüsselproteinen durch die Metabolisierung von SSC fördern.

Abstract

L-Cysteine is a critical amino acid required for the cultivation of mammalian cells such as Chinese hamster ovary cells (CHO). Due to low stability of cysteine and low solubility of the dimer cystine at neutral pH, *S*-sulfocysteine (SSC) was developed to substitute cysteine in highly concentrated feeds. The bioavailability of SSC, the positive impact but also the toxic response at high SSC concentrations was already described in previous studies. The underlying mechanism for cellular uptake and the root cause for the toxicity however remained unclear so far and were studied in the current work.

Due to the structure similarity of SSC to cystine and glutamate, it was proposed that the cystine/glutamate antiporter (x_c^-) allow cellular uptake of SSC and was assessed via transporter inhibition using sulfasalazine and transporter overexpression using either sulforaphane or sulforaphane-*N*-acetylcysteine during fed-batch experiments. Following daily addition of 50 µM and 100 µM sulfasalazine, the extracellular SSC concentration was increased by 65% and 177% respectively, suggesting a reduced uptake due to x_c^- inhibition. In contrast, enhanced transporter activity through 15 µM sulforaphane and sulforaphane-*N*-acetylcysteine treatment, induced a 60% and 52% reduced extracellular SSC concentration, respectively. The inverse cellular response of CHO cells strongly suggests that SSC is transported via x_c^-. Additionally, elevated SSC uptake via sulforaphane treatment was linked to aggravated SSC toxicity indicating that the x_c^- antiporter activity impacts the toxic response by controlling the concentration of intracellular SSC.

The second part of this study was aimed at assessing the impact of the feed formulation and cell line dependency regarding SSC toxicity via a combined approach of high throughput small-scale fed-batch experiments and multivariate data analysis (MVDA). A diverse SSC response was observed for eight different CHO cell lines and 79 different feed formulations indicating a clone dependent SSC response and a significant impact of the feed formulation on the toxicity. However, MVDA was not able to identify cell culture media components which impair the toxic response of SSC, suggesting that the feed formulation has an indirect impact on the SSC toxicity.

The final section sought to clarify the root cause for toxicity after SSC application. For this purpose, SSC metabolization by CHO cells was investigated *in vitro* by spiking SSC to cell lysates. Critical intracellular metabolites were identified using LC-MS/MS, whereby significant responses to SSC treatment were *e.g.* glutathione depletion and the accumulation of *S*-sulfo-glutathione. These might support excessive persulfidation of cysteine-dependent key proteins through SSC metabolization, which was suggested to be the root cause of toxicity.

Content

1. Introduction

1.1. Therapeutic proteins

For clinical use, more than 130 recombinant proteins are approved by the U.S. Food and Drug Administration (FDA) including small hormones like Insulin (about 6 kDa)[1], major growth hormones like erythropoietin (about 38 kDa) [2], complex fusion proteins like etanercept (about 125 kDa) [3] and monoclonal antibodies (mAbs) like rituximab (about 150 kDa) [4]. Insulin, a rather simple therapeutic protein as treatment for diabetes is produced either in yeast or in *Escherichia coli* [5, 6]. According to the International Diabetes Federation, 463 million people are living with diabetes today and increasing numbers with 578 and 700 million are estimated for 2030 and 2045, respectively [7]. This estimation indicates the high demand on therapeutic proteins. Due to high efficiency of mAbs against various diseases, the development of new therapeutic antibodies is rising every year and dominates the pharmaceutical market of biologics [8]. Especially, the approval of muromonab, the first murine mAb in 1986 and adalimumab, the first human mAb, changed the pharmaceutical industry fundamentally [9, 10].

1.1.1. Antibodies

Antibodies, also known as Immunoglobulins (Ig), are the defense system against foreign material by labelling pathogens such as viruses and bacteria or pathogen-infected cells to trigger an immune response [11]. The structure of an antibody comprises two antigen binding fragments (F_{ab}) and a single crystallizing fragment (F_C) consisting of two heavy and two light chains arranged in an overall exterior Y-shape (figure 1). The heavy chain bears three single constant domains C_{H1}, C_{H2} and C_{H3} and one variable domain V_H, whereas the light chain is composed of one constant domain C_{L1} and a variable domain V_L. Two interchain disulfide bonds are present in the hinge region to link both heavy chains and two additional interchain disulfides link each heavy and light chain of the F_{ab} fragment [12, 13]. Additional stability is gained via 12 intrachain disulfide bridges [14]. Antibody functionality depends on high antigen specificity, while allowing a broad variability to recognize various pathogens. Specificity is ensured by three complementary determining regions positioned at each variable domain, whereas random genomic splicing creates variability to recognize an extensive range of antigenic targets with different affinities [15].

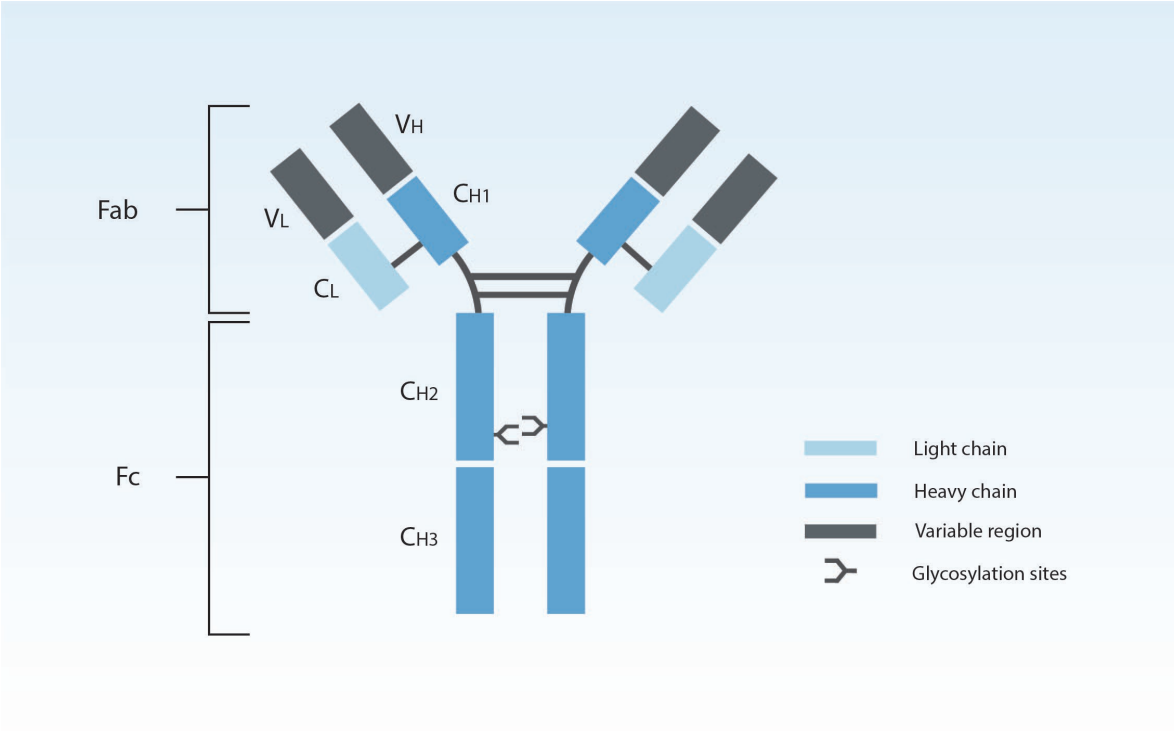

Figure 1. Schematic illustration of a human IgG1. The IgG antibody consists of two light chains (L) and two consecutively numbered heavy chains (H) – forming its typical Y-shape architecture. The F_{ab} region comprises variable (V) and constant (C) domains, responsible for antigen binding. The Fc region is comprised of only constant domains – bearing *N*-linked glycans that are relevant for the biological activity of the antibody.

Furthermore, five different classes (IgG, IgM, IgA, IgE and IgD) differing in structure and functionality are present in humans, whereas IgG1 is the most common subclass for therapeutic antibodies due to their long *in vivo* half-life [16, 17]. Beside a long half-life, desired characteristics during antibody engineering include a high target specificity, lack of immunogenicity and a high efficacy in order to minimize the required therapeutic dose and following side effects. Irrespective of the manufacturing process and the drug format, investigation of the product quality is inevitable to guarantee drug safety.

1.1.2. Quality attributes of therapeutic antibodies

The manufacturing process includes the selection of a production cell line, a cultivation media and a process mode, which are all contributing to the protein quality as major parameter of a therapeutic drug. To ensure a desired product quality, characteristics that might affect safety and efficacy are defined during the development process as critical quality attributes (cQA) including appropriate ranges. The cQA for a monoclonal antibody drug comprise general properties like appearance and pH, excipient levels like surfactants and salts, contaminants like endotoxins, process related impurities like host DNA, generated product variants like aggregates, fragments, and posttranslational modifications and finally the bioactivity like potency and effector functions [18].

Aggregation

Aggregation of therapeutic antibodies needs to be prevented due to loss of drug-efficacy and a possible cause of detrimental immunogenic reactions in patients [19, 20]. Aggregate formation can occur during all steps of the production process [21]. During cell cultivation physicochemical stress like pH shifts, osmolality, temperature, extensive aeration or mechanical stress in form of excessive stirring or shaking can trigger antibody aggregation [22, 23].

Prevention of excessive aggregation during biosynthesis requires proper protein folding in the endoplasmic reticulum (ER) where disulfide bonds are formed. Native disulfide bridge formation is mainly regulated by glutathione (GSH) in combination with several enzymes [24]. Since high productivities were demonstrated to trigger aggregation, lowering the cell culture temperature during the production phase (to 30-33°C) and thereby reducing protein folding stress reduced aggregation significantly [25, 26]. Especially the combination of a temperature shift with redox active compounds like GSH and cystine (CysS) were observed to be highly effective [27]. Another strategy to achieve a low aggregation level during cultivation, is the addition of small organic components like dimethyl sulfoxid (DMSO) and glycerol, which are described to antagonize aggregation by acting as chaperones and stabilizing proteins against thermal denaturation [28-30]. Additionally, the addition of surfactants like Tween 20 were demonstrated to be effective to reduce agitation-induced protein aggregation [31].

Excessive aggregation levels at the point of harvest are removed during the purification processes but will reduce the product yield. To achieve a high purity level, multiple orthogonal purification steps are required. Within the purification, proteins experience physical stress like filtration and pH shifts used for elution. Both might induce aggregation, which is reversible but still unwanted [32, 33]. Consequently, aggregation level and subsequent stability of therapeutic proteins have to be monitored, continuously.

Fragmentation

Fragmentation is considered as cQA, since exposure of patients to different antibody epitopes within fragments might cause immunogenicity *in vivo* [34]. Fragmentation of antibodies can occur during production, harvest and during purification. The misincorporation of amino acids in the protein backbone, is typically eliminated by a control mechanism of the cell, but an increased rate of errors due to improper codon-anticodon pairing in a heterogeneous expression system can lead to undetected errors [35]. Furthermore, proteases released by cells might degrade the protein and radicals might hydrolyze the susceptible hinge region [36, 37]. Fragmentation that occurs during the harvest step was suggested to depend on mechanical cell lysis in large bioreactors which

releases reducing enzymes. However, irreversible inhibition of respective enzymes (*e.g.* Mn^{2+} addition) or chemical inhibition of disulfide reduction (*e.g.* EDTA addition) just before harvest were able to prevent fragmentation [38, 39].

Trisulfides

The insertion of an additional sulfur into the classical disulfide bridge within proteins forms a trisulfide bond ($-CH_2-S-S-S-CH_2-$). In case of IgG, this trisulfide bond occurs at the hinge region, connecting both heavy chains, which was observed in all IgG subclasses but occurs mainly in IgG_2 and IgG_4 due to enhanced accessibility [40]. Although trisulfides do not affect the biological activity of antibodies when investigating antigen binding, they increase undesired antibody heterogeneity. For example, within a fed-batch cultivation a total trisulfide content in a range from <1% and up to 39% was observed, whereby the Cys concentration in the feed was demonstrated to be the root cause. More precisely, the Cys concentration in the supernatant contributes to dissolved hydrogen sulfide which was directly correlated with trisulfide formation [14, 41].

Posttranslational modifications

Various enzymatic modifications following protein synthesis are called posttranslational modifications (PTMs) and are contributing to the broad functional range of mature antibodies [42]. The analysis of more than 530,000 proteins revealed that phosphorylation, acetylation and *N*-linked glycosylation are the most frequent modifications according to both, experimentally observed PTMs and also via databases putative identified modifications [43].

Protein phosphorylation provides a sensitive regulation of various cell processes including growth, apoptosis and many signal transduction pathways [44]. Phosphorylation of serine/threonine kinases are mainly used to convoy messages of extracellular ligands into a cellular response *e.g.* inducing a conformational change upon phosphorylation leading to increased enzyme activity [45]. Acetylation occurs by transferring the acetyl group from acetyl-coenzyme A to the terminal amine on the side chain of lysine residues. This is essential for gene regulation by changing the chromatin interaction to histones leading to chromatin relaxation followed by increased transcription rates [46].

Glycosylation is the most extensive modification and is essential for protein stability and biological activity [47, 48]. Importance of proper glycosylation became clearly notable when diseases of genetic disorders summarized as congenital disorders of glycosylation or carbohydrate-deficient glycoprotein syndromes became apparent [49]. Over 40 disorders of glycosylation have been reported, which are mainly caused by defects during the

synthesis or processing of glycans and are therefore critical for therapeutic protein production [50, 51].

Accordingly, glycosylation of therapeutic antibodies is reported to have the most significant impact on pharmacokinetics and physiochemical properties and is therefore of great interest [52, 53]. The attachment of an oligosaccharide to an asparagine residue is called *N*-linked glycosylation, whereas serine or threonine attachment is known as *O*-linked glycosylation. *O*-glycosylation occurs in the hinge region of IgA1 and IgD but is not present in IgG molecules [54]. In case of human IgG, the glycan is typically attached at position Asn^{297} of each Fc-heavy chain and is determined through a consensus sequence (Asn-X-Ser/Thr), whereas X can be any amino acid except proline. Some antibodies bear another glycosylation in the Fab-domain *e.g.* cetuximab (Erbitux®) at position Asn^{88} [55, 56].

Protein glycosylation follows a complex metabolic pathway leading to an enormous structural diversity of proteins. The presence of several consensus sequences with varying degrees of glycan occupancies is referred to as macroheterogeneity and depends on the location within the sequence, protein conformation, host cell line and physiological state of the expressing cell [57]. Microheterogeneity, on the other hand, is defined by the extent of alternation within each glycan attached at those sites [58].

In summary, product quality including aggregation, fragmentation, trisulfides and various PTM affect the safety and efficacy of therapeutic IgG, hence have to be monitored during the production process.

1.2. The production of therapeutic proteins – State of the Art

The production of therapeutic proteins is based on the overexpression of a foreign protein by cells cultivated in a bioreactor. Key parameters contributing to the final product quality are the cell line, cell culture media, and the cultivation process. The industrial production often embraces platform approaches comprising a stable and robust expression systems with optimized cell lines tailored to a specific media and production process to save time during the development of a new drug [59, 60].

1.2.1. Cell lines as expression systems

With focus on human therapy application, approved mAbs were mainly produced in Chinese hamster ovary (CHO) cells and partly in murine myeloma cells like NS0 and SP2/0 [61-65]. The advantage of mammalian cell lines are the production of non-immunogenic therapeutics due to higher similarity of PTMs to endogenous human proteins [66]. Overall, about 70% of all recombinant proteins are produced in CHO [67]. The preference of CHO cells appeared due to their robust growth in suspension allowing high volumetric productivity while having a high cloning efficiency which is powerful during cell line development [66, 68, 69]. Cell line engineering continuously aims at enhancing the process efficacy, which is determined by the time to reach a high cell density, the duration within the production phase at reasonable cell viability, and the cell specific productivity [64]. Several CHO sub cell lines like CHO-K1, CHO-S and CHO-DG44 have emerged on the market to cover various demands by having different metabolisms preferring either mAb expression, cell survival elongation or biomass production [70].

Different selection systems are available to ensure high expression of the protein of interest. Expression systems in CHO cells are commonly based on dihydrofolate reductase (DHFR) and glutamine synthetase (GS) activity but also on arginase [71]. DHFR is essential for nucleotide metabolism whereas glutamine synthetase is required for intracellular glutamine biosynthesis and arginase ensures polyamine production. All systems are based on the transgene co-amplification of these crucial enzymes to prevent growth of non-transfected populations. The selection occurs in the absence of thymidine and hypoxanthine for DHFR-deficient cells, glutamine for GS-deficient cells and L-ornithine and putrescine for arginase-deficient cells. During cell expansion, stringency of the selection process might be increased by supplementing methotrexate, a known DHFR inhibitor, or L-methionine sulfoximine, a GS inhibitor [72-75]. The choice of a cell line is the foundation for general cell performance and furthermore for final product quality.

1.2.2. Manufacturing process

The selection of a production process aims for a low-cost and high-yield production without compromising the product quality. Common cultivation processes are batch, fed-batch and perfusion. In a batch culture, cells are cultivated in a medium until essential metabolites are depleted. Depending on the cell line and media, final titers of about 0.5 to 0.9 g/L are reached in batch mode [76].

In a perfusion culture, the cultivation is extended via continuous media exchange, leading to constant product recovery since the product is typically secreted by the cells. The required media exchange frequency to maintain nutrient requirements of the cells depends on the viable cell density (VCD) and limits the perfusion system. To extend the cultivation in the production phase, a specific VCD is retained in the bioreactor through daily removal of cells (referred to as bleeding). A high VCD level yields in high productivity but increases the media exchange demand causing cellular stress thus needs to be balanced carefully [77].

In case of a fed-batch process, feeds with aligned feeding regimes fulfill cellular demands during different cultivation phases by maintaining appropriate nutrient levels [78, 79]. Fed-batch is commonly used due to simple applicability and adaptability to fit specific demands [80]. To circumvent loss of volumetric productivity due to dilution, feed solutions are typically highly concentrated. Nowadays protein expression can routinely yield in titers of >5 g/L in a typical 14 day fed-batch process [59].

Beside the cultivation mode, cell performance and product quality is influenced by pH, temperature, pCO_2 and pO_2 which are adjustable in common bioreactors [26, 81].

Generally, harvesting has to be accomplished before the product gets exposed to excessive by-products compromising the product quality and is ensured via continuous monitoring of the physiological state of the culture. However, detrimental effects on product quality might also arise by maximizing the productivity of cells by increasing the pressure on the cellular folding and assembly machinery [60]. Thus, product titer and quality have to be considered equally during process development.

1.2.3. Cell culture media

The history of cell culture media goes back to 1882 were the first media-like solution based on salt called Ringers solution was used for *in vitro* cultivation of animal tissue [82]. Driven by industrial applications to produce recombinant proteins, cell culture technology has changed fundamentally. For a long time, serum-containing media were used for cell cultivation due to reliable cell growth promoting effects [78]. Since animal-derived serum bears the risk of virus contamination it was replaced more and more by animal-free protein hydrolysates *e.g.* from soy, wheat and yeast, to compensate for its cell growth and productivity support [83-85]. Considerable lot-to-lot variations of both, serum and

hydrolysates promoted the implementation of chemically defined media (CDM) to enhance production process robustness [78, 83, 84].

Cell culture media is key to gain an economic production process of therapeutic proteins that deliver consistent product qualities with high productivities [78, 86, 87]. A consistent and reproducible production process is supported by a chemically defined and serum-free media containing essential nutrients for cells. The advanced goal is to develop a media applicable to multiple cell lines. A basal media is composed of carbohydrates, amino acids, vitamins, inorganic salts and trace elements to ensure cell survival and productivity. Additionally, lipids, polyamines, nucleosides, reductants, protective additives, buffers and recombinant proteins like growth factors, hormones and carrier proteins might be included to support cell growth and productivity [67, 88]. The function of each component is known and summarized in table 1, whereas the overall composition and the concentration of each compound is decisive for the cell performance as demonstrated by Reinhart *et al.* comparing eight chemically defined media [76]. More precisely, high initial concentrations might be harmful and affect the culture due to high osmolality, but nutrient depletion as well as accumulation of by-products *e.g.* lactate or ammonia are also detrimental for cells [89]. Overall, amino acids are key nutrients for cell growth and productivity and represent a majority of media and feed formulations.

Table 1. Main cell culture media nutrients.

Nutrient	Function	References
Carbohydrates	Main energy source	[78]
Amino acids	Building blocks for proteins and energy source via the amino acid catabolism	[90]
Vitamins	As precursors of various cofactors, vitamins are necessary for cell division and cell growth	[83, 91]
Inorganic Salts	Assure osmotic balance for cells, regulate membrane potential (Na^+, K^+, and Cl^-)	[78, 83, 92]
Trace elements	Function in the active centers of enzymes and other physiologically active substances by undergoing electron transfer reactions within energy metabolism	[91]
Lipids	Development of cellular membranes	[93]
Polyamines	Regulation of cell growth (proliferation, differentiation and apoptosis) and modulation of ion channel functions	[94, 95]
Nucleosides	Building blocks for DNA and RNA	[96]
Reducing agents	If cultivated cells lack cystine transporters, extracellular cystine is converted to cysteine by reductants that can be readily internalized by these cells	[97, 98]
Buffers	Addition of sodium bicarbonate ($NaHCO_3$) allows pH regulation of the culture medium via gaseous CO_2 (5-10 %)	[99]
Surfactants	Reducing shear stress of cultured cells	[100]
Growth factors and hormones	Mandatory to grow some cell lines in serum-free media to induce proliferation and differentiation	[83]

1.3. Cysteine – An exceptional amino acid

1.3.1. Cysteine – structure and reactivity

At least 500 naturally occurring amino acids are known, whereas only 20 amino acids are translated by the genetic code into proteins [101]. Within proteins, the only sulfur-containing amino acids are cysteine (Cys) in form of a thiol (-SH) and methionine (Met) as thioether (-SCH_3). In comparison to a relatively low reactivity of Met, Cys presents a high reactivity and is critical for many biological functions. Cys nucleophilicity and reactivity is enhanced by the deprotonation of the thiol group to a charged thiolate (-S^-). The protonation or rather the relative amount of thiolate to thiol depends on the pH and is indicated via the pK_a value which allows an estimation of the reactivity. At physiological pH, Cys thiols are predominantly protonated due to a pK_a of 8.5. The pK_a of Cys thiols in peptides and proteins can be as low as 3.5, since the local environment of Cys residues is influencing the pK_a value, and by that influencing the reactivity [102, 103]. An electropositive environment tends to lower the pK_a by stabilizing the negatively charged thiolate group of the peptide whereas an electronegative environment tends to raise its pK_a. Accordingly, low pK_a thiols within Cys-containing peptides or proteins are more reactive [104]. Moreover, accessible Cys residues at the surface of proteins were shown to have a pK_a value close to the physiological pH which enables a shift to enhanced nucleophilicity in response to pH changes [105]. These properties enable Cys or rather the Cys residue to sense and regulate cellular mechanisms.

1.3.2. Intracellular cysteine accessibility

Mammalian cells rely on Cys biosynthesis and import of extracellular Cys to accomplish the high cellular Cys demand during production of therapeutic proteins [106]. Cys synthesis is reported via the reverse-transsulfuration pathway utilizing methionine. The removal of the methyl group bound to the sulfur atom of methionine involves the conversion from methionine to *S*-adenosylhomocysteine, homocysteine and cystathionine and finally hydrolysis to Cys [107]. This conversion is reversible so that the expression of involved enzymes as well as the reactivity are tightly regulated via intermediates and post-translational modifications of involved enzymes [108]. However, Cys is considered as essential amino acid, indicating that the transsulfuration pathway might not be active in various cell lines or cultivated cells cannot cope with cellular Cys demand via this pathway [109]. Thus, intracellular Cys needs to be maintained via extracellular Cys uptake as visualized in figure 2. Cells possess several transporters facilitating either extracellular Cys uptake or uptake of the Cys dimer cystine (CysS) with subsequent intracellular reduction to

Cys. Some transporters for mixed disulfides (system L) are also known to be expressed by mammalian cells.

Direct Cys uptake is mainly enabled via the alanine-serine-cysteine (ASC) transporter and the excitatory amino acid transporter (EAAT) also termed x_{AG}^- system [110]. Both belong to the solute carrier family 1 (SLC1) referred to as “high-affinity glutamate and neutral amino acid transporter family” [111]. They are sharing a high degree of amino acid sequence similarity but possess distinct transport characteristics which ensure cellular Cys supply independently of the extracellular pH. At physiological pH, Cys thiols are predominantly protonated and are only transported via ASC, which is specific for neutral amino acids such as alanine, serine and threonine [112]. The transport is concentration driven to ensure equilibration of different neutral amino acid pools, which is mostly in favor of Cys uptake instead of Cys export [113]. In case of an extracellular pH shift, deprotonated Cys uptake is executed by EAAT3, a transporter specific for acidic amino acids. A unidirectional transport was suggested, due to internal re-protonation thereby facilitating intracellular Cys retention [114].

Although ASC and EAAT3 transporters ensure Cys supply, cells rely on additional CysS uptake due to autoxidation of Cys to CysS in the extracellular environment leading to generally low Cys concentrations. The functional CysS/Glu antiporter complex (x_c^-) is a heteromeric complex with two subunits connected via a disulfide bridge [115, 116]. The glycosylated heavy chain encoded by *SLC3A2* gene also called 4F2hc subunit, is required for proper localization of the antiporter to the cell membrane and heterodimerizes with several amino acid transporters of the SLC7 family. The light chain encoded by *SLC7A11* called xCT subunit is known for the 1:1 counter-transport of Glu and CysS with a high substrate specificity [117-119]. Under physiological conditions, influx of CysS into the cells is enhanced by rapid intracellular CysS reduction to Cys and counter-transport of Glu out of the cells [120, 121]. A high intracellular Glu concentration required for the counter-transport is maintained by amino acid transport systems like x_{AG}^- [122], whereas excessive extracellular Glu concentration results in competitive inhibition of the x_c^- transporter [120]. Cells with low CysS uptake capacity were demonstrated to internalize mixed disulfides via the L system, although it is mainly reported to transport branched chain and aromatic amino acids [98, 123].

Regarding CHO cells, ASC, EAAT, x_c^- and system L were reported to be expressed within independent studies [122, 124-126]. However, in a study comparing three CHO cell lines with different productivities, about 40% of the known transporters were differentially expressed, indicating that CHO subclones may handle amino acid demand and Cys supply differently [127].

1.3.3. The physiological role of cysteine

Intracellular Cys is crucial for the biosynthesis of small biomolecules like coenzyme A (CoA) and several antioxidants encountered in cells [128, 129]. CoA is synthesized in a five-step catalyzed reaction via successive phosphorylation and decarboxylation utilizing pantothenate and Cys (figure 2). More precisely, pantothenate is phosphorylated to 4'-phosphopantothenate utilizing ATP and then Cys is fused under further ATP consumption to 4'-phosphopantothenoylcysteine. Subsequent decarboxylation leads to 4'-phosphopantetheine which is first converted to dephospho-CoA by transferring adenosine-monophosphate onto the phosphate and finally to CoA through additional phosphorylation of the 3'-hydroxyl of ribose [128]. Functionally, CoA is a cofactor for enzymes within the tricarboxylic acid (TCA) cycle and is key for a sustained energy supply to ensure cell survival. It functions as acyl group carrier and as carbonyl activating group, within essential biochemical reactions of the TCA cycle. Various enzymes like pyruvate dehydrogenase and α-ketoglutarate dehydrogenase utilize CoA to store energy in form of $NADH_2$ [130, 131].

Cells possess a variety of Cys-derived antioxidants, such as taurine and glutathione (GSH), which create a balance needed to maintain the redox status of the cells. These antioxidants are needed to cope with reactive oxygen species (ROS), which are largely produced in mitochondria as side-product of several enzymatic reactions to generate ATP [132]. Major taurine biosynthesis is accomplished via irreversible Cys catabolism. In a first step, Cys is oxidized to cysteine sulfinic acid (also called cysteine sulfinate) by cysteine dioxygenase (CDO) and in a next step, cysteine sulfinate decarboxylase (CSDA) catalyzes the decarboxylation to hypotaurine. Finally, hypotaurine dehydrogenase oxidizes hypotaurine by utilizing NAD^+ yielding taurine. Since excessive Cys catabolism would cause Cys depletion, the CDO level needs a tight regulation enabled via rapid ubiquitination and subsequent CDO degradation at low intracellular Cys levels [133]. Minor taurine synthesis is achieved through cysteine lyase (CL) which is able to convert Cys to L-cysteate utilizing sulfite (SO_3^{2-}), which is further decarboxylated to taurine by CSDA. The sulfur in taurine (2-aminoethanesulfonic acid) is completely reduced, thus taurine is not able to scavenge ROS directly. The indirect antioxidant activity of taurine is based on the upregulation of enzymes of the antioxidant defense system and targeting the root cause i.e. ROS generation within mitochondria [129, 134].

GSH, the most prominent Cys-derived antioxidant, is an essential cellular component [135]. GSH, a ɣ-L-glutamyl-L-cysteinyl-glycine tripeptide, is synthesized from constituent amino acids by generation of γ-glutamylcysteine via the glutamate-cysteine ligase (GCL) and subsequent *C*-terminal transfer of glycine by γ-glutamyl cysteine synthetase (γGCS). Within GSH synthesis, Cys was demonstrated to be the limiting substrate since glutamate and

glycine are generally higher concentrated intracellularly [136]. Consequently, intracellular Cys depletion disrupts *de novo* GSH synthesis.

GSH functions as intracellular antioxidant protecting cells by scavenging highly destructive ROS like hydrogen peroxide (H_2O_2) and reactive nitrogen species (RNS) like NO_2 [137]. The monomer GSH is oxidized by ROS/RNS (direct interaction or enzymatically) to its disulfide-linked dimer GSSG and reduced back to GSH via glutathione reductase (GR) to restore the antioxidant pool [138]. However, important to know is that ROS are not generally harmful for cells. Depending on the concentration, ROS can be viewed as mediators of physiological processes, whereas hydroperoxides are produced by the cells as second messenger. Oxidative stress is defined as imbalance of oxidants and antioxidant response and the ratio of GSH/GSSG as main redox couple serves as indicator of the cellular redox state [139, 140]. Within subcellular compartments, distinct redox requirements are reflected by the GSH/GSSG ratio. To maintain the overall cellular redox state in the cytosol, GSH is predominantly found in the reduced form leading to a GSH/GSSG ratio of 10:1 or up to 100:1 [141, 142]. A similar ratio was observed in mitochondria having a high demand of GSH, since ROS are mainly generated as byproduct of aerobic metabolism to generate ATP [132]. Overall, cytosolic GSH accounts for about 85% of the total GSH pool, whereas about 15% is present in the mitochondria, which is high considering the small matrix volume of mitochondria compared to the cytosol [143, 144]. The role of the GSH/GSSG ratio is quite different in the secretory pathway. An oxidative environment with a nearly equal GSH/GSSG ratio in ER and Golgi supports disulfide bridge formation [141, 145-147]. In summary, Cys derived molecules contribute to the cellular defense system against oxidative stress, whereas GSH is the most abundant low molecular weight thiol. Via the GSH/GSSG ratio cells are able to regulate specific requirements for biochemical reactions.

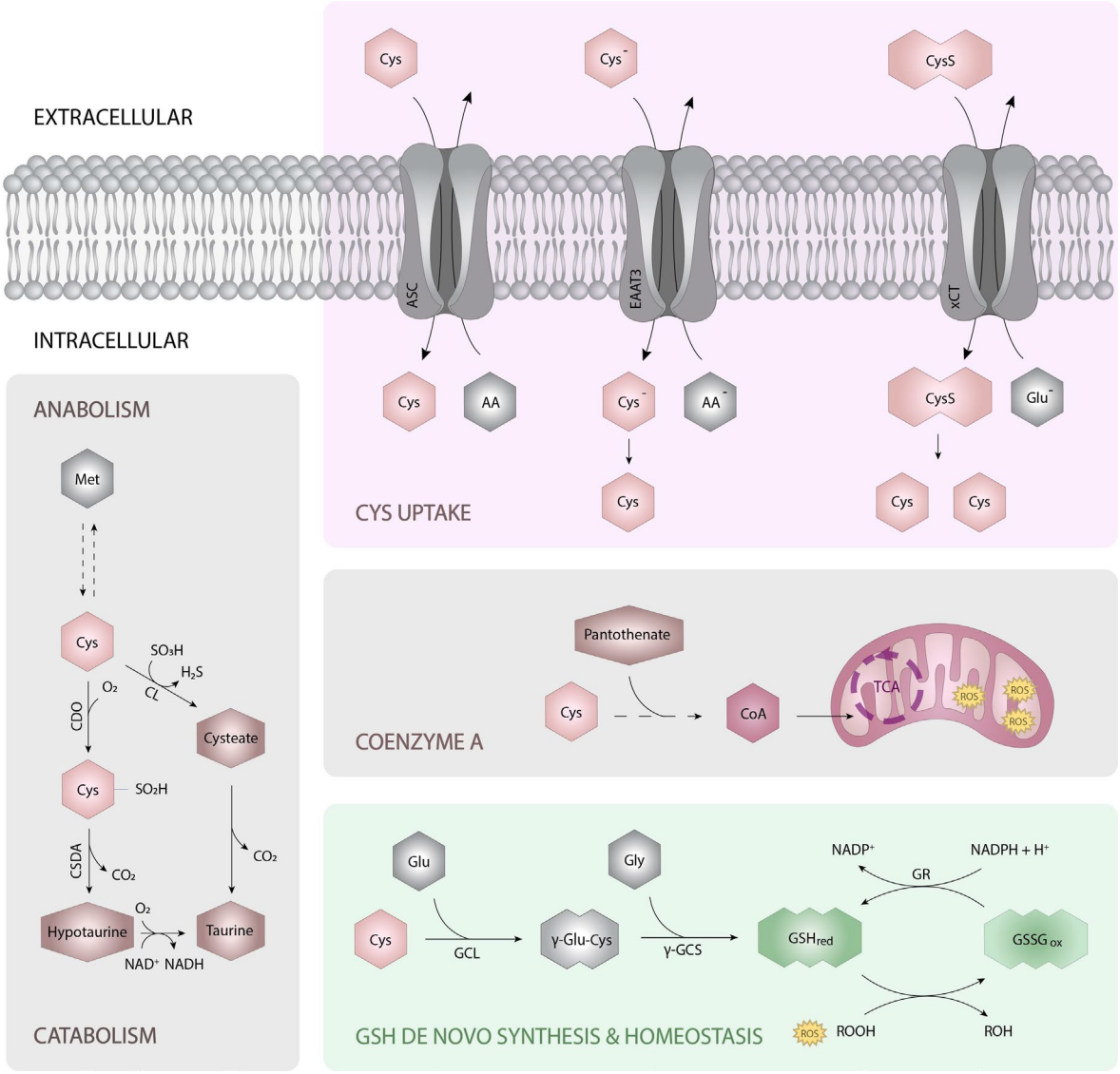

Figure 2. Overview of cysteine (Cys)-related mechanisms. **Cys uptake** is enabled via alanine-serine-cysteine (ASC) and excitatory amino acid transporter (EAAT) or xCT antiporter transporting cystine (CysS), which is intracellularly reduced to Cys. Cys **anabolism** is utilizing Methionine (Met) and Cys **catabolism** yields several antioxidants such as taurine. **Coenzyme A** (CoA) is synthesized by a five-step reaction utilizing Cys and pantothenate and CoA is then transported into mitochondria and used in the tricarboxylic acid (TCA) cycle. The major antioxidant is glutathione (GSH), whereby **GSH *de novo* synthesis** requires Cys, glutamic acid (Glu) and glycine (Gly). Reactive oxygen species (ROS) are scavenged by GSH leading to glutathione disulfides (GSSG) and intracellular **GSH Homeostasis** is enabled via glutathione reductase (GR), which can reduce GSSG back to GSH consuming NADPH. Cysteine dioxygenase (CDO), cysteine sulfinate decarboxylase (CSDA), cysteine lyase (CL), glutamate-cysteine ligase (GCL), γ-glutamyl cysteine synthetase (γGCS).

1.3.4. Redox active cysteine residues in proteins

Cys residues are highly conserved in structural or functional regions of proteins. Structural thiols play a central role in the folding and the subsequent stabilization of proteins via disulfide bridges [148]. Oxidative protein folding in the lumen of the ER starts with initial disulfide formation via spontaneous condensation of a thiol with sulfenic acid (Cys-SOH) or enzymatic catalyzed disulfide formation via endoplasmic reticulum oxidoreductin 1 (Ero1p). Subsequent rearrangement of incorrectly formed disulfide bonds is promoted via protein disulfide isomerase (PDI) until mature protein is present [149, 150]. The latter step is crucial, especially with increasing amount of Cys residues or rather disulfide bonds within a protein, which is positive correlated with the length for proteins >200 amino acids [148].

Functional protein thiols are implicated in several cellular processes such as redox related gene regulation. At increasing oxidative stress, redox related protective genes are upregulated to ensure cell survival. The mechanism (figure 3) is triggered by the transcription factor NF-E2-related factor 2 (Nrf2), which is linked to the Kelch-like ECH-associated protein 1 (Keap1), a Cys-rich protein [151]. In unstressed conditions, i.e. low ROS concentrations, Nrf2 is bound to Keap1 which inhibits translocation of Nrf2 to the nucleus and moreover initiates constant Nrf2 ubiquitination and subsequent Keap1 dissociation and Nrf2 degradation in proteasomes. In comparison, high ROS concentrations lead to oxidation of distinct Keap1 thiols, which results in Nrf2 translocation to the nucleus, where Nrf2 heterodimerizes with small musculoaponeurotic fibrosarcoma (sMaf) proteins and transactivates the antioxidant response element (ARE) and thereby the expression of several antioxidant defense proteins [152]. Major genes are contributing to the GSH biosynthesis like the x_c^- transporter responsible for CysS supply and both subunits of GCL catalyzing the rate-limiting transfer of Cys. In combination with genes regulating *e.g.* NADPH and GST level, GSH homeostasis is ensured [153]. In summary, oxidative stress sensing is enabled via Cys-rich Keap1 and triggers several antioxidant genes.

Functional thiols are also implicated in the regulation of the catalytic activity of enzymes in response to the redox environment. For instance, in reducing environments, Cys is predominantly present as thiolate anion, which is critical for enzyme activity relying on a thiolate in the active site. For example, the proteolytic activity of Cys proteases depends on a thiolate anion that is needed for the nucleophilic attack of carbons in the amide bonds of peptides to hydrolyze the linkage. This is accomplished in lysosomes containing various hydrolytic enzymes in an acidic environment to hinder oxidation of the thiol [154, 155].

Furthermore, in oxidizing environments, functional thiols are susceptible to reversible and irreversible oxidation (figure 3). Initial oxidation of protein thiols leads to highly unstable and thus reactive sulfenic acid intermediates (Cys-SOH), which have a unique ability to function as nucleophiles but also as electrophiles [156]. At high GSH concentrations, sulfenic acid

is reduced back to its active thiol, whereas strong oxidizing metabolites convert Cys-SOH to sulfinic acids (Cys-SO_2H) having an even lower nucleophilicity than sulfenic acid [157-159]. Several reviews reported that oxidation to sulfinic acid is typically an irreversible modification [160, 161], whereby Biteau *et al.* demonstrated that sulfiredoxin, an enzyme conserved in eukaryotes is able to catalyze the reduction to sulfenic acid utilizing ATP [162]. It was suggested that the enzyme accessibility of the modified thiol defines whether sulfinic acid is irreversible. At increasing ROS concentrations, sulfinic acid might be oxidized to sulfonic acids (Cys-SO_3H), which is definitely regarded as irreversible modification [151, 163, 164]. Degradation of irreversibly oxidized proteins is enabled via proteasomes, which exhibit enhanced activity through oxidation to promote self-regulation [165].

Protection of protein thiols from irreversible overoxidation is achieved by either *S*-glutathionylation (P-SSG) or persulfidation (P-SSH). Both are redox-sensitive, reversible PTMs, which occur predominantly at low pK_a thiols (figure 3) [166, 167].

The transfer of GSH onto the protein thiols may proceed spontaneously at high concentrations but is highly promoted by either oxidized protein thiols (Cys-SOH) or oxidized GSH (GS-SOH) [168]. Furthermore, glutathione-*S*-transferase (GST) was reported to catalyze glutathionylation [168]. At low ROS levels, < 0.1% of total proteins are *S*-glutathionylated, which is increased to > 15% by extensive oxidative stress [169]. This modification protects protein thiols from irreversible oxidation but needs to be removed at decreasing ROS concentrations to restore protein activity. Deglutathionylation is mainly attributed to glutaredoxin (Grx) having a redox-active mono- or dithiol motive (Cys-X-X-Ser/Cys) [157-159]. At low ROS levels, thiols in the active site of Grx are present as reactive thiolate. This thiolate initiates the cleavage of GSH mixed disulfides (P-SSG) leading to a glutaredoxin-glutathione intermediate (Grx-GSH) and releasing the reduced protein thiol. Grx activity is restored by formation of a new disulfide bridge to another GSH leading to GSSG release. In case of the Grx with a dithiol motive, the second Cys-residue remains as thiol at high GSH concentrations, whereas high ROS concentrations promote oxidation of one thiol triggering interchain disulfide bridge formation of the dithiol motive due to close proximity. Thereby, enzymatic deglutathionylation activity is lost, and proteins remain glutathionylated and are moreover protected for irreversible oxidation at high ROS levels. The interchain disulfide bridge is reduced back when GSH level is increasing due to lower oxidative stress [160, 170].

Protein persulfidation (also called perthiolation or sulfhydration) was reported to have similar redox signaling and protecting functions as oxidized thiols (the mechanism is visualized in the appendix figure 42). Initial protein persulfidation (P-SSH), might result enzymatically from CysS conversion to cysteine hydropersulfide (Cys–SSH) via two major sulfurtransferases: cystathionine γ-lyase (CSE) and cystathionine β-synthase (CBS),

whereby the persulfide moiety can be transferred onto GSH and subsequently onto various proteins [171, 172]. Additionally, protein persulfidation occurs through an interaction of hydrogen sulfide (H_2S) with oxidized thiols like sulfenic acids or with disulfides. However, H_2S seems to be incapable to react with reduced thiols, thereby preventing persulfidation at low ROS levels [167, 173]. After initial persulfidation, further oxidation occurs through hydrogen peroxide - analogue to the oxidation of thiols - leading to perthiosulfenic acid (P-Cys-S-SOH) or perthiosulfenate (P-Cys-S-SO^-). Further oxidation to perthiosulfinic acid (P-Cys-S-SO_2H) and subsequentially to perthiosulfonic acid (P-Cys-S-SO_3H) occurs in presence of high ROS [174]. Although, persulfidation protects enzymes from overoxidation, persulfide formation inactivates enzyme activity and needs to be reversed at low ROS [175]. Reduction of protein persulfidation is preliminary enabled via the thioredoxin (Trx) system. Trx is an oxidoreductase, which possesses, similar to Grx, a dithiol motif (Cys-X-X-Cys) readily interacting with persulfides. The catalytic activity is based on a nucleophilic attack of a protein persulfide by a Trx thiolate leading to an intermolecular mixed disulfide and release of either the protein thiol or H_2S in case of perthiosulfenic acid. The counterpart is subsequently reduced through the nucleophilic attack of the second nearby Trx thiolate leading to an intramolecular disulfide of the oxidoreductase. In case of higher oxidized persulfides, the respective SO_x are released similarly [176]. To regain Trx activity, the Trx intramolecular disulfide bridge is subsequently reduced by the NADPH-dependent thioredoxin reductase (TrxR) [174, 177]. Inhibition of the Trx system increased the persulfide level significantly, indicating that Trx is crucial for persulfide homeostasis [178].
In summary, protein thiols enable ROS mediated regulation of protein functions, whereby glutathionylation and persulfidation protects these thiols from excessive oxidative stress.

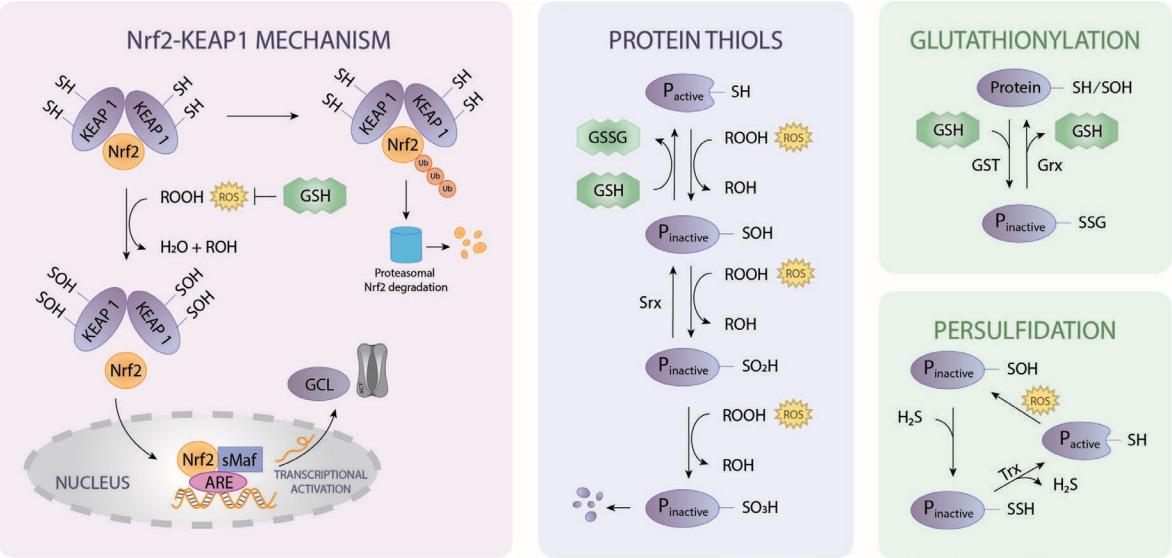

Figure 3. Mechanisms of protein thiols. Redox gene regulation via **Nrf2-KEAP1 mechanism** is based on Cys-rich Keap1 coupled to Nrf2. At low reactive oxygen species (ROS) level, Nrf2 ubiquitination occurs, which triggers Keap1 dissociation and proteasomal degradation of Nrf2. In presence of high ROS, KEAP1 thiols are oxidized and Nrf2 is transported into the nucleus, where Nrf2 heterodimerizes with sMaf proteins and activating antioxidant response element (ARE). Major genes are then transcribed, and their proteins are contributing *e.g.* to the GSH biosynthesis like the x_c^- transporter responsible for CysS supply and glutamate-cysteine ligase (GCL) catalyzing the rate-limiting transfer of Cys within glutathione (GSH) *de novo* synthesis. **Protein thiols** are oxidized via ROS to sulfenic acid, sulfinic acid and irreversibly to sulfonic acid. Overoxidation of protein thiols is prevented by glutathionylation or persulfidation. **Glutathionylation** can occur spontaneously and is promoted in oxidizing environment or can be catalyzed through glutathione-*S*-transferase (GST). Glutaredoxin (Grx) catalyzes deglutathionylation to restore the protein activity at low ROS. **Persulfidation** is *e.g.* initiated through hydrogen sulfide (H_2S) reacting with sulfenic acid and is reversed by the thioredoxin (Trx) system.

1.3.5. Cell culture media comprising cysteine

Addition of Cys during cell cultivation is crucial for cell survival and protein production, making Cys an essential compound in cell culture media and feeds [179, 180]. The reactivity of Cys described in previous chapters restricts the applicable concentration range and stability of cell culture media. Autoxidation of Cys to CysS in presence of air is enhanced by catalysts such as copper and cannot be prevented during media preparation [181]. CysS has a much lower solubility limit (0.46 mM at 25°C in water) compared to Cys (2.3 M at 25°C in water) and might precipitate during storage and thereby reduce the bioavailable Cys concentration [182]. Another challenge is Cys reactivity to other media components during storage, especially for high concentrated media. Cys reactivity is enhanced at increasing temperature and after light exposure due to production of reactive species which oxidizes the thiol (*e.g.* by the photosensitizer riboflavin). Thereby enhanced Cys reactivity induces degradation of essential feed components [183, 184]. This unpredictable degradation of medium and feed components prior to use is detrimental, since it adds an element of uncertainty which can affect the quality of the final product. To reduce degradation in general, prepared media feeds are commonly stored at 4°C and light protected.

Furthermore, several strategies with the attempt to stabilize Cys in neutral pH feed have been investigated to reduce unwanted side reactions, while remaining bioavailable for the cells.

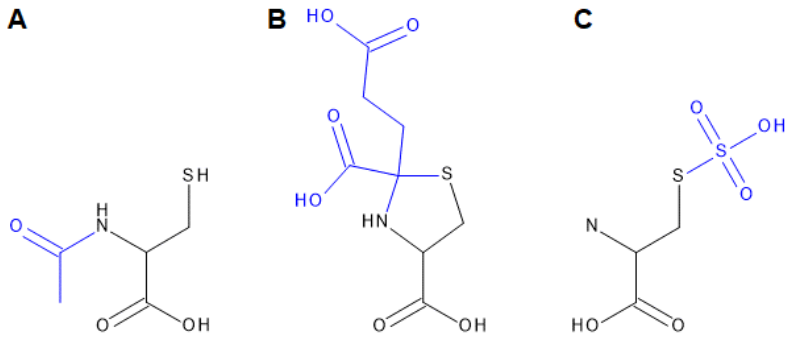

Figure 4. Cysteine derivatives used in cell culture media. (A) *N*-acetylcysteine, (B) 2-(2-carboxyethyl)-1,3-thiazolidine-2,4-dicarboxylic acid, and (C) *S*-Sulfocysteine. Modifications are highlighted in blue.

N-acetylcysteine

The acetylation of the amine group in Cys is stabilizing the thiol group and is known as *N*-acetylcysteine (NAC) as visualized in figure 4 A. The chemical modification increases the pK_a of Cys (8.3) to about 9.5 and thereby reducing the thiol nucleophilicity at physiological pH and thereby increasing feed stability [185]. However, bioavailability of NAC needs to be ensured to allow Cys replacement in feeds. Acetylation as common modification was reported to enhance permeability by increased hydrophobicity of NAC [186]. Intracellularly, acetylation is hydrolyzed by aminoacylases and remaining Cys boosts GSH biosynthesis demonstrating indirect antioxidant activity of NAC [185].

Interestingly, cellular cytotoxicity was observed at increasing concentrations of NAC, whereas reduced toxicity was observed for *N*-acetylcysteine amide, a NAC derivative [187]. Along with *N*-acetylcysteine ethyl ester, NAC derivatives are reported to be hydrolyzed intracellularly to Cys and NAC leading to enhanced antioxidant activities [187-190].

Thiazolidine

Another approach to stabilize Cys utilizes the ketoacids pyruvate and α-ketoglutaric acid (KG). Both were demonstrated to form a stable thiazolidine ring with Cys. In the non-enzymatic cyclo-condensation, the keto group interacts with the thiol and amino group of Cys leading in case of KG to 2-(2-carboxyethyl)-1,3-thiazolidine-2,4-dicarboxylic acid (CKG) as visualized in figure 4 B [191]. As intended, the combination of reduced thiol reactivity and antioxidant activity of excess ketoacids were demonstrated to reduce the oxidative potential of cell culture feeds [192]. Furthermore, bioavailability of CKG for CHO cells increased the GSH pool along with prolonged cultivation and increased productivity during a fed-batch

process [193]. No cellular toxicity was described for CKG, which qualifies it as control condition within this study.

S-Sulfocysteine

Protection of the reactive thiol by a sulfonic acid group via disulfide linkage yields *S*-sulfocysteine (SSC) as visualized in figure 4 C. Replacement of Cys in feeds by SSC was demonstrated to enhance feed stability. More precisely, CysS precipitation in feed solutions containing 15 mM Cys was observed within 24h, whereas SSC was stable over 3 months without detection of increased Cys or CysS [194]. Moreover, SSC was bioavailable for cultivated CHO cells leading to similar growth and enhanced product quality with reduced aggregation and trisulfides (insertion of a sulfur atom in a disulfide bond) [195]. A prolonged viability and increased titer in presence of SSC was suggested to result from direct antioxidant activity in combination with an increased GSH pool. Furthermore, SSC was demonstrated to interact with GSH leading to cysteine glutathione (GS-Cys) and *S*-sulfo-glutathione (GS-SO_3) suggesting that GS-Cys acts as intracellular Cys storage, supporting further GSH synthesis [194].

Nevertheless, the use of SSC is not yet understood completely, since increasing SSC concentrations can induce cellular toxicity in spin tubes observed as a drastic drop in cell viability correlated with a reduced extracellular pH. The toxic threshold varies depending on the cultivated subclone and was prevented in pH controlled bioreactor processes, via addition of glutamic acid, $CuSO_4$ or buffering compounds like HEPES [196].

2. Objective

The modified amino acid SSC was developed as Cys replacement for fed-batch processes to enhance the feed stability. The objective of this study was to investigate consequences of SSC integration in cell culture feed formulations used to manufacture therapeutic proteins with industry relevant cell lines. This goal is based on the fact that SSC leads to a toxic response when increasing the SSC concentration above a certain level, whereby the mechanism is still unknown.

In a first section, the uptake of SSC by CHO cells was investigated with the goal to identify the responsible transporter and to evaluate whether SSC toxicity correlates with SSC uptake. Due to structure similarity with glutamic acid, the CysS/Glu antiporter (x_c^-) was suggested to enable SSC uptake. Whether SSC acts as substrate for x_c^- was assessed via transporter overexpression and transporter inhibition during fed-batch experiments as visualized in figure 5.

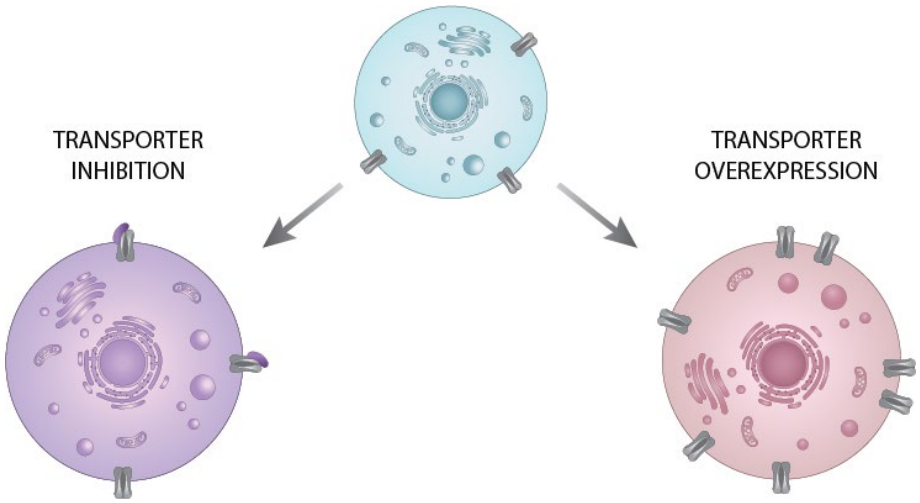

Figure 5. Conceptional strategy to investigate *S*-sulfocysteine uptake. Sulfasalazine is reported to inhibit the x_c^- antiporter, whereas sulforaphane, and sulforaphane-*N*-acetylcysteine are reported to induce x_c^- overexpression.

The second part of this study aimed to understand the possible interactions between SSC and other cell culture media components. In particular, the objective was to identify specific media components, which might amplify or prevent SSC toxicity. This section also focused on the toxic response of different CHO clones to SSC and was used to generate hypotheses on possible mechanisms of toxicity.

The final section sought to enlighten the root cause for toxicity after SSC application. Therefore, SSC metabolization by CHO cells was investigated by spiking SSC to cell lysates. Critical intracellular metabolites, whose concentration was modulated following SSC treatment, were identified using untargeted LC-MS/MS.

3. Materials and Methods

Table 2. Chemicals, reagents, media and kits

Chemicals, reagents, media and kits	Supplier
10 x Dulbecco's phosphate buffered saline	Life Technologies
AccQ-Tag Ultra Derivatization Kit	Waters
AccQ-Tag Ultra Eluent A	Waters
AccQ-Tag Ultra Eluent B	Waters
Acetonitrile	Merck
Amino Acid Standard H	ThermoFisher Scientific
BCA Protein Assay Kit	ThermoFisher Scientific
Bradford solution	Sigma-Aldrich
Buffer Solution (pH 4)	Merck
Buffer Solution (pH 7)	Merck
Buffer Solution (pH 9)	Merck
Calibration solution 300	Gonotec
Calibration solution 850	Gonotec
Calibration solution 2000	Gonotec
CellTiter-Glo® Luminescent Cell Viability Assay	Promega
Cellvento® 4CHO	Merck
Cellvento®Feed220	Merck
Chloroform	Merck
Choline Chloride	Merck
CytoBuster™	Merck
D-(+)-Glucose	Merck
Dimethyl sulfoxide	Merck
Ethanol 96%	Merck
EX-CELL® Advanced™ CHO Feed 1 (without glucose)	Sigma-Aldrich
EX-CELL® Advanced™ CHO Fed-batch Medium	Sigma-Aldrich
Glutathione (reduced)	Sigma-Aldrich
Glutathione (oxidized)	Sigma-Aldrich
Glutathione-cysteine	Cayman Chemical
Halt™ Protease and Phosphatase Inhibitor Cocktail (100X)	ThermoFisher Scientific
HT supplement 100x	Life Technologies
Hydrochloric acid 0.1 M	AppliChem
Insulin	Sigma-Aldrich
L-alanine-L-glutamine	Sigma-Aldrich
L-asparagine	Merck
L-cysteine	Merck

Chemicals, reagents, media and kits	Supplier
L-glutamate	Merck
L-glutamine	Merck
Long R3 IGF-1	Sigma-Aldrich
Methanol	Merck
Norvaline H-NVa-OH	Novabiochem
Phosphotyrosine	Merck
RNAlater	Applied Biosystems
RNase-free PCR Tubes & Caps, 0.2 mL (8-strip format)	ThermoFisher Scientific
RNase-Free 1.5mL Microfuge Tubes	Ambion
RNAse-free water (DEPC-Treated Water)	ThermoFisher Scientific
RNase AWAY®	Sigma
RNeasy mini and midi kits	Qiagen
S-sulfocysteine	Merck (Lot 15/HE/028.01)
S-sulfoglutathione (HCl salt)	synthesized by Pharmaron*
Sodium bicarbonate	Merck
Sodium hydroxide solution 50 %	Merck
Sulfasalazine	Sigma-Aldrich
Sulforaphane	Sigma-Aldrich
Sulforaphane-*N*-acetylcysteine	Cayman Chemical
TaqMan® Fast Universal PCR Master Mix	ThermoFisher Scientific
TaqMan® Reverse Transcription Reagents	ThermoFisher Scientific
Trypan blue	ThermoFisher
Vi-CELL Reagent Pak	Beckman Coulter

* Confirmed via NMR

Table 3. Laboratory consumables

Laboratory consumables	Supplier
96-well white polystyrene microplate	PerkinElmer
96-deep-well plates	Brand
ABI Prism® Optical Adhesive Covers	ThermoFisher Scientific
Amicon® Ultra-0.5 mL centrifugal filter unit, 3 kDa	Merck
Aera Seal™ Film	Sigma-Aldrich
Breath Easy® sealing membrane	Sigma-Aldrich
Chromatography column ACCQ-Tag Ultra C18	Waters
Corning Costar Spin-X® centrifuge tube filters (0.22 µm)	Sigma-Aldrich
Erlenmeyer flask with vented cap	Corning Incorporated
Optical 96-Well Fast Thermal Cycling Plates	ThermoFisher Scientific
ProSep® Ultra Plus column	Merck
Protein A PhyTips®	PhyNexus

Laboratory consumables	Supplier
Spin tube with vented cap Tube spin® Bioreactor 50	TPP
Stericup® Quick Release	Merck
Sterile filter units	Merck
TSKgel FcR-IIIA-NPR column	Tosoh Bioscience
Turbidity meter Turb 550 IR	WTW
Ultrafiltration Discs, 30 kDa	Merck
XSelect® HSS T3 3.5µm C18 reverse phase column	Waters

Table 4. Equipment

Equipment	Supplier
7500 real-time PCR system v2.3	Applied Biosystems
Accuri Flow Cytometer	BD
Biomek 3000	Beckman Coulter
CEDEX Bio HT	Roche Diagnostics
Centrifuge 5418	Eppendorf
Centrifuge 5430 R	Eppendorf
Centrifuge Allegra TM X-22R	Beckman Coulter
Class II safety cabinet: Herasafe TM KS EN12469	ThermoFisher Scientific
Cryoscopic osmometer, Osmomat®	Gonotec
CyBio® FeliX	Analytik Jena
GeneAmp PCR System 9700 Thermocycler	PE Applied Biosystems
Heating block	ROTH
High-resolution mass spectrometer Impact II	Bruker
HPLC Vanquish Horizon	ThermoFisher Scientific
HyperCyt Autosampler	Sartorius
Impact II™	Bruker
Incubator, Climo-Shaker ISF4-XC	Kuhner
IKA® RCT basic	IKA-Werke
Liquid nitrogen tank, 1500 Series-190	German Cryo
Micrtron	Infors
Milli-Q® water purification system	Merck
Multilabel Reader EnVision 2104	PerkinElmer
Multitron Pro	Infors HT
NanoDrop™ One Microvolume UV-Vis Spectrophotometer	ThermoFisher Scientific
pH-Meter Seven Excellence Multiparameter	Mettler Toledo
SpeedVac SPD1030	ThermoFisher Scientific
Ultra performance liquid chromatography	Waters
ViCELL™ XR 2.04	Beckman Coulter
Water bath SW22	Julabo

Table 5. Software

Software	Supplier
7500 Fast Real-Time PCR systems 2.3	Applied Biosystems
Accelrys 4.2	Accelrys
Adobe Illustrator 23.1	Adobe
EndNote™ X8	PDF Tron
Empower 3	Waters
GraphPad Prism 7.05	GraphPad
Progenesis® QI	Waters
SIMCA 16	Sartorius

3.1. SSC uptake

3.1.1. Fed-batch cell cultivation

In general, CHO cell lines were long-time stored in the gas phase of a nitrogen tank (1500 Series-150; German Cryo). For cultivation of CHO-K1 cells producing an IgG1, the respective cryovial containing 1×10^7 cells was thawed at 37°C in a water bath. The cells were then transferred into a 50 mL spin tube with vented cap, previously filled with 30 mL of Cellvento® 4CHO (Merck), a chemically defined CHO cell culture medium that contains all essential components for cell growth. The cells were cultivated at 37°C, 5% CO_2, 80% humidity and a rotation speed of 320 rpm with a shaking diameter of 2.5 cm. The cells were subcultured three times a week as follows: after determining the cell count with the Vi-CELL™ XR 2.04 cell counter (Beckman Coulter), a defined volume of the pre-culture was diluted in 30 mL fresh medium leading to a cell density of either 2×10^5 cells/mL in case of subcultivation over three days or 3×10^5 cells/mL in case of subcultivation over two days.

Cellvento® Feed220, a highly concentrated feed, was used as feeding medium, providing essential components for extended culture duration and productivity (except Cys). Either 15 mM Cys in combination with 50 mM KG or 15 mM SSC (Lot: 15/HE/028.01) with 50 mM KG were added to the feed during reconstitution. The pH of all feeds was adjusted to neutral (pH 7.0 ± 0.2) and osmolality was measured by a cryoscopic osmometer (Gonotec). Afterwards, cell culture media and feeds were sterile filtered (0.22 µm) and stored at 4°C, protected from light until usage.

The fed-batch process conditions were similar to subcultivation, whereby the inoculation density was 2×10^5 viable cells/mL in 30 mL starting volume. 3% feed (v/v) was added on day 3, 5 and 10 and 6% (v/v) was added on day 7. The glucose level was maintained by adding a specific amount of a 400 g/L glucose stock solution on demand to up to 6 g/L during the week and up to 12 g/L over the weekend. Cell counts and viability of at least four

biological replicates were measured with a Vi-CELL™ XR 2.04 cell counter. Spent media (supernatant) analysis including glucose and IgG was performed with the bioprocess analyzer CEDEX Bio HT (Roche) after centrifugation of the sample for 5 min at 4500 rpm (2287 g). Supernatant samples were stored at -20°C for extracellular amino acid analysis and cells for quantification of mRNA levels were stored at -80°C until analysis.

3.1.2. Transporter inhibition

The compound sulfasalazine (SAS; Art. No S0883 Sigma; figure 6) was shown to be a potent inhibitor of the x_c^- antiporter [197-199]. As treatment during fed-batch experiments, daily addition of 50 µM or 100 µM SAS was achieved via a 75 mM SAS stock solution in DMSO. To prevent freeze-thaw cycles SAS aliquots were stored at -20°C for single application.

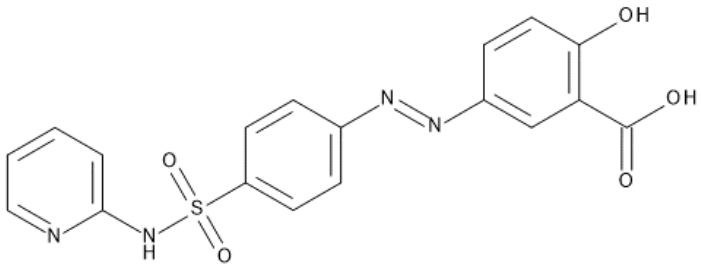

Figure 6. Structure of sulfasalazine.

3.1.3. Transporter overexpression

Sulforaphane (SFN) induces overexpression of the x_c^- antiporter via Nrf2-Keap1 mechanism [200, 201]. SFN is also transferred onto GSH via GST, and further metabolization leads to SFN-*N*-acetylcysteine (SFN-NAC) figure 7 [202]. Whereas SFN lowers the cellular GSH level (and thus might impact negatively growth), no apparent change in the GSH level was observed by SFN-NAC treatment [203]. This suggests that SFN-NAC might induce x_c^- expression as well without impacting the redox level. During fed-batch experiments, 100 mM SFN (Sigma; Art. No 574215) or SFN-NAC (Cayman Chemical; Art. No Cay16098-10) stock solutions solved in DMSO (Sigma) were spiked into the culture to yield 15 µM SFN or SFN-NAC on day 3, 4, 6 and 7 of the cultivation.

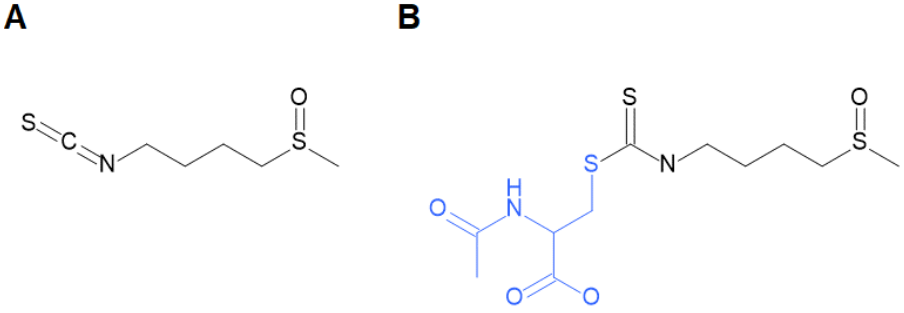

Figure 7. Structure of two isothiocyanates. (A) Sulforaphane and (B) Sulforaphane-*N*-acetylcysteine, whereby the additional *N*-acetylcysteine moiety is highlighted in blue.

3.1.4. Antiporter mRNA analysis

The functional CysS/Glu antiporter complex (x_c^-) is a heteromeric complex with two subunits encoded by the genes *SLC7A11* and *SLC3A2.* The relative messenger ribonucleic acid (mRNA) expression level of *slc7a11* and *slc3a2* were investigated using the TaqMan® technology. At least 12×10^6 viable cells were used to isolate RNA with RNeasy mini/midi kits according to standard procedures (Qiagen). RNA was converted into complementary deoxyribonucleic acid (cDNA) using the RNAse-Free DNase Set in combination with TaqMan® reverse transcriptase, according to standard procedures (ThermoFisher). The relative RNA expression levels were obtained by quantitative polymerase chain reaction (qPCR) using TaqMan® universal PCR master mix and specific primer listed in table 2 on a 7500 real-time PCR system v2.3 (Applied Biosystems).

Table 6. Primer sequence to detect transporter RNA level.

	Forward	**Reverse**	**Dual-labeled probe**
SLC7A11	TGGGAAATTTCTCATTAGC	GAGGCAACATAGAATAACC	CTCTCCTGCTTCGGCTCCAT
SLC3A2	GCTCTGAGTTCTTGGTTG	GGTCACAATTTGCTGCAG	CAATCAAGAGCCTATCCTCACTGAAGT

Data sets were normalized against an endogenous control that is non-regulated by the treatment, namely Glyceraldehyde-3-phosphate dehydrogenase (GAPDH; Cg04424038_gH TaqMan from ThermoFisher). The fold change compared to the control was calculated by applying the $2^{-\Delta\Delta Ct}$ method according to Livak *et al.* [34]. A fold change value between 0 and 1 was transformed using the formula $-1/(2^{-\Delta\Delta Ct})$ to represent a negative fold change.

1. Normalize of the cycle threshold (Ct) values:

   $\Delta Ct_{\text{sample}} = Ct(\text{target gene})_{\text{sample}} - Ct(GAPDH)_{\text{sample}}$

   $\Delta Ct_{\text{control}} = Ct(\text{target gene})_{\text{control}} - Ct(GAPDH)_{\text{control}}$

2. Calculation of the relative expression:

   $\Delta\Delta Ct = \Delta Ct_{\text{sample}} - \Delta Ct_{\text{control}}$

3. Calculation of the fold change in gene expression:

   $\text{Fold change} = 2^{-\Delta\Delta Ct}$

   $\text{Fold change between 0 and 1} = 1/(2^{-\Delta\Delta Ct})$

Genes with at least two-fold increased RNA levels were considered as differentially expressed.

3.1.5. Amino acid analysis

Extracellular amino acid concentrations of cell culture experiments were analyzed by reversed phase ultra-performance liquid chromatography (RP-UPLC). Samples were alkylated with 20 mM iodoacetamide to prevent oxidation of Cys to CysS and afterwards samples were derivatized with AccQ-Tag Ultra® reagent (Waters) for 10 min at 55°C according to standard procedures. Separation was achieved via Ultra C18 column (1.7 µm) heated at 60°C and using a flow rate of 0.7 mL/min. Eluent A (Waters) and a continuous gradient of increasing acetonitrile (Eluent B) was used for elution. After separation via RP-UPLC, amino acids were detected by a photodiode array optical detector detecting the UV active derivatized amino acid. Subsequent data analysis was performed with Empower 3 (Waters). Amino acid quantification was performed with external standard curves analyzed within each run (standard H from Thermo Scientific and SSC from Merck). For data comparison, the AUC of measured amino acid concentrations over the time course of the fed-batch experiment was calculated and normalized to the control condition using a Cys feed. To identify changes in amino acid concentrations caused by different growth, the mean difference of antiporter non-transported amino acids compared to the control was calculated and are visualized as stacked bar in grey.

3.1.6. *In vitro* analysis of SFN interaction

A 15 mM Cys stock solution in water was stabilized with 50 mM KG and the same KG concentration was added in the 15 mM SSC stock solution. 50 µM and 100 µM SFN or SFN-NAC was incubated with either 1.5 mM Cys or 1.5 mM SSC in water. To reflect cell cultivation, a Cys-depleted cell culture medium was added in an additional setup. All mixtures were analyzed directly after mixing and after incubation for 1.5 h at 37°C. To stop further reactions samples were placed on ice until analyzed via RP-UPLC. As control conditions were samples without SFN or SFN-NAC, Cys or SSC and also the Cys-depleted media.

3.2. Relationship between media components and SSC toxicity

3.2.1. Feed hydration

To investigate the impact of SSC, a diverse feed panel containing different levels of common cell culture media components was produced inhouse without Cys, CysS, β-Mercaptoethanol and GSH (internal feed lots summarized in table 3). The milled cell culture powder was hydrated with the standard procedure of the respective unmodified feed and stirred for at least 30 min. To ensure hydration of all components within these modified feeds, the turbidity was measured using the Turbidity meter 550 IR (WTW). Whenever the turbidity of hydrated feeds was above 5 nephelometric turbidity unit (NTU), an additional

titration step to pH 9.5 using 50% NaOH solution was performed. After pH adjustment, the feed was stirred for 10 min and the pH was lowered to either 7.0 or 8.5 using 25% HCl solution and stirred for another 10 min. Thereafter, Milli-Q® water was added until the final volume was reached, followed by measurement of the osmolality ranging from 162 mOsmol/kg (feed2) to 2016 mOsmol/kg (feed10) and final turbidity in a range from 0.48 NTU (Feed9) to 4.5 NTU (Feed10) as summarized in table 3. Supplementation of 50 mM SSC into each feed mixture, increased the final osmolality about 100 mOsmol/kg, whereas the turbidity remained unchanged.

Table 7. Modified feeds

	Feed1	**Feed2**	**Feed3**	**Feed4**	**Feed5**	**Feed6**	**Feed7**	**Feed8**	**Feed9**	**Feed10**
Lot	19_013	19_010	19_003	19_009	19_006	19_011	19_012	19_004	19_014	NA*
conc [g/L]	17.7	19.4	23.2	25.9	30.6	31.1	34.4	72.5	89.5	123
pH	7.00	7.02	7.01	7.01	7.01	7.00	8.50	7.01	7.02	7.0
NTU	2.00	0.76	0.5	1.06	0.86	1.93	0.73	0.76	0.48	4.5
Osmo [mOsmol/kg]	163	162	378	472	272	290	495	832	920	2016
Osmo + SSC [mOsmol/kg]	260	256	472	564	366	386	582	916	1014	2145

*Cellvento Feed220 was used

3.2.2. *In vitro* toxicity assay

Toxicity is the degree to which a chemical substance or a mixture of substances can damage cells. In general, each component can be toxic to cells in high concentrations. The toxicity of components can be estimated within a cell-based assay to test applicability as media or feed additives. Therefore, the respective component is diluted in media or feed solutions. SSC was diluted in media in a range from 0 to 6 mM and in feeds from 0 to 50 mM. About 3×10^5 viable cells/well were seeded in a multiwell-plate with increasing concentrations of the compound of interest. After covering the plate with a Breath Easy® sealing membrane (Sigma), cells were incubated at 37°C, 80% humidity and 5% CO_2, over three days.

The toxicity was assessed via the intracellular ATP level, which correlates with the amount of metabolically active cells. After 30 min equilibration of the plate at room temperature, 100 µL CellTiter-Glo® Luminescent solution (Promega) was added. Thereby, cells were lysed, and ATP-depending luminescence signal was generated during incubation at room temperature for 10 min. More precisely, the intracellular ATP was used as a substrate for the luciferase to convert luciferin to oxyluciferin, which is degraded due to instability and emits luminescence. The stable luminescence signal was measured using the EnVision 2104 Multilabel Reader (PerkinElmer). If a chemical compound shows a toxic effect on cells,

the ATP production stops due to the destruction of the cells. After subtraction of the blank, the metabolic viability of cells with treatment was normalized to the metabolic activity of cells without treatment. Evaluation was performed with GraphPad Prism version 7.05 via a 4-point logistic fit.

3.2.3. Deep-well fed-batch

Eight different CHO cell lines producing seven different mAbs were used in a pre-screening as summarized in table 4. From these, all clones except clone 1 and clone 3 were used in further experiments.

Table 8. CHO cell lines and respective target proteins

Clone 1	Clone 2	Clone 3	Clone 4	Clone 5	Clone 6	Clone 7	Clone 8
IgG1	Rituximab®	IgG1	IgG1	Rituximab®	IgG1	IgG1	Humira®

The previous described fed-batch process (chapter 3.1.1) was adapted to deep-well plates cultivation at 37°C, 5% CO_2, 80% humidity and a rotation speed of 1000 rpm at a diameter of 3 mm. The inoculation density was 2×10^5 viable cells/mL in 1 mL starting volume using 4CHO media. 50 µL feed was added on day 3, 5, 7 and 10 via CyBio Felix. By mixing 12 main feeds (including two feed10 dilutions) containing the same SSC concentration in a 1:1 manner (BioMek 3000), 78 feed mixtures and two control feeds were produced (table 11 appendix), which were tested in one plate (n=2). Cellular response was assessed via the VCD and viability (Hypercyt Autosampler with Accuri Flow Cytometer).

3.2.4. Multivariate data analysis

Multivariate data analysis (MVDA) such as partial least squares (PLS) regression is a known method of analysis for large amounts of variables and was performed via SIMCA 16 (Sartorius AG). The main objective of this method is to create a model, which relates *X*-matrices (predictor matrix: known variables) to *Y*-matrices (response matrix: experimental observations). This enables identification of correlations between X variables and Y variables. Here, the *X*-matrix was built with the concentration of each compound within all feed mixtures. The observed VCD for each feed mixture might be used as *Y*-matrix, but since the SSC response was not clearly assignable, each condition was clustered in either toxic or not toxic (observation class). Separate models for each clone having a distinct SSC concentration were used, since a specific media formulation can lead to different Y responses for different clones.

Based on PLS, statisticians have developed an extended method called orthogonal partial least squares projection discriminant analysis (OPLS-DA). This model filters out variation

that is not directly linked to the observation (orthogonal variation) from correlated (predictive variation) and is therefore easier to interpret and was used in this study [204]. Preliminary scaling of the raw data was necessary for these datasets due to the feed formulations. For example, trace elements have a much lower concentration compared to amino acids but might influence the SSC response significantly. In other words, an unscaled model is dominated by high concentrated compounds resulting in a poor prediction of low concentrated compounds. Thus, each compound is mean centered at zero. Additionally, large relative changes will receive the most weighting in the model. Since relative changes of compounds results from feed formulations and not from experimental measurements, a unit variance scaling was performed leading to a net variance of one. Finally, the predictability of a model is influenced by the distribution of each component. Components which are present in all main feeds lead to a broad distribution by mixing different concentrations, whereas some compounds are rare in the main feeds or compounds are at the same level, leading to a poor distribution. However, this cannot be scaled or normalized and needs to be kept in mind.

The built model is assessed by R^2 values indicating the goodness of fit and Q^2 giving an estimation about the model predictability via cross-validation. For Q^2 calculation, data is divided into seven parts whereby 6/7 of the data is used to build the model and 1/7 of the data is used to validate the model. This is repeated for each data part and the total predicted data is used to calculate the squared errors to the original data and displayed as Q^2. According to the SIMCA users guide, R^2 are admitted at 0.5 or higher for biological attempts and Q^2 above 0.5 is expected for good predictability [205].

The resulting score plot provides information about the relationship between observations separating toxic and non-toxic observations. The positioning of each observation is determined by a predictive principal component, indicating the variation of the samples within the data set and is visualized through the distance from the origin. In case of one or several orthogonal components the most dominant components are positioned in a two-dimensional plot which is visualized as ellipse. Statistical outliers are outside the 95% probability level based on Hotelling's T^2 as multivariate counterpart of a common t-test [206, 207]. Coefficient plots visualize the contribution of each variable to the respective observation classes (toxic and not toxic) including the confidence interval.

3.3. SSC metabolism

The metabolome comprises the overall set of small organic compounds (< 1800 Da), which reflects the cellular state and moreover the response to environmental changes such as the addition of SSC [208].

3.3.1. Extraction of the cellular metabolome

The first step to explore the impact of SSC on intracellular metabolites is the extraction of the metabolome, including amino acids, lipids, nucleotides and sugars. Day three is commonly the first feeding day during fed-batch experiments and thus the time point of first SSC addition. Therefore, intracellular metabolome of two separately cultivated CHO-K1 cells was extracted after three days of cultivation starting with a cell density of 2×10^5 viable cells/mL in a final volume of 30 mL. Quenching the cellular metabolism quickly is prerequisite to extract all metabolites including highly reactive species. 10 mL of a cell suspension with 5×10^6 viable cells/mL were mixed with 40 mL of a 0.9% (w/v) NaCl solution (0.5°C). Afterwards, cells were centrifugated (1000 g, 1 min at 0°C) and the supernatant was discarded. Due to the quenching step, a carry-over of molecules coming from the medium was minimized and allows to skip additional washing of the cells to prevent intracellular metabolite leakage [209].

Subsequent extraction of the metabolome requires a proper solvent selection, since different solvents enable the extraction of distinct compounds from the diverse metabolome. Ice-cold aqueous acetonitrile, -40°C aqueous methanol and -40°C 1:3 methanol-chloroform mixture were used as solvents to extract the metabolome. After quenching of the cell metabolism, 1 mL of the solvent was added to 5×10^6 cells and rigorous mixing caused cell membrane disruption. Intracellular small molecules were solved in the respective solvent during 10 min incubation on ice. Extracted proteins precipitate in the solvent and were removed together with cell debris by centrifugation at 18,000 g, 1 min at 0°C. The supernatant was aliquoted and dried via a vacuum concentrator (SpeedVac SPD1030). Furthermore, extractions without cells were performed to identify solvent impurities. Finally, all dried extracts were stored at -80°C until further analysis.

3.3.2. *In vitro* interaction studies of SSC and cellular extracts

To identify small molecules interacting with SSC, intracellular extracts were incubated with increasing SSC concentrations. Addition of equimolar Cys concentrations were used to identify SSC specific changes during data analysis. Therefore, dried extracts of 5×10^6 cells were dissolved in 200 µL Milli-Q® water and 10 µL of either 0.84 mM or 8.4 mM Cys/SSC stock solutions were spiked into the solution to reach 40 µM and 400 µM, respectively. These mixtures were incubated at 25°C with a rotation speed of 550 rpm over 210 min,

whereby sampling was performed at 0, 100 and 210 min. Afterwards, samples were frozen in liquid nitrogen to stop further reactions and stored at -20°C until analysis.

3.3.3. Preparation of cell lysate

Exploring the impact of SSC on the metabolome in presence of proteins was enabled by cell lysis of CHO-K1 cells. Fed-batch cultivated CHO-K1 cells (feed containing 15 mM Cys) were quenched according to chapter 3.3.1 on day seven. After centrifugation at 1000 g, 1 min at 0°C, cells were washed two times with ice-cold 1x PBS and 2×10^8 cells were lysed in 1 mL CytoBuster™ by mixing at room temperature for 5 min. To remove cell debris, the lysate was centrifuged at max speed and the supernatant containing metabolites and proteins with a protein level of about 1 g/L (determined via Bradford standard procedure; Sigma) was stored at -20°C until further analysis. To exclude impurities from the lysis buffer, pure CytoBuster™ was diluted similarly to the cell lysate with Milli-Q® water.

3.3.4. *In vitro* interaction studies of SSC and cell lysates

40 µM and 400 µM SSC and Cys were applied to cell lysates (pH 7.2) and compared to an untreated control by addition of an equivalent amount of Milli-Q® water. The prepared mixtures were incubated at 37°C at 550 rpm and sampling was performed at 0, 30, 100 and 210 min. To stop enzymatical reactions, a 3 kDa Amicon® Ultra-0.5 mL centrifugal filter unit (four times washed) was used to remove proteins (centrifugation setting: 10,000 x g, 4°C, 30 min). Afterwards filtrate was frozen in liquid nitrogen and stored at -20°C until analysis.

3.3.5. Liquid chromatography coupled with a mass spectrometer

Liquid chromatography coupled to mass spectrometry (LC-MS) is a powerful technique to analyze the metabolome. Within this study, high-performance liquid chromatography (Vanquish Horizon, ThermoFisher Scientific) coupled to a high-resolution mass spectrometer (Impact II; Bruker) was used. Samples (4 µL injection volume) or standard solutions (1 µL injection volume) were loaded on a C18 reverse phase column (XSelect HSS T3 3.5 µm) operated at 40°C with a flowrate of 0.3 mL/min. The separation of analytes was carried out using a 12 min gradient (table 5) consisting of 20 mM ammonium formate / 0.1% formic acid (eluent A) and 100% methanol (eluent B).

Table 9. Continuous gradient of Eluent B to separate small molecules

Gradient step	Retention time [min]	Eluent A [%]	Eluent B [%]
1	0-2	100	0
2	2-4	80	20
3	4-6	70	30
4	6-8	20	80
5	8-8.5	1	99
6	8.5-10	1	99
7	10-12	100	0

MS analyzes were performed using an Impact II mass spectrometer equipped with an electrospray ionization source (ESI) set at -4500V (positive mode) or +3500 V (negative mode). After ionization of analytes during the nebulization process, positively or negatively charged ions (depending on the voltage polarity) are introduced into the MS instrument and then transferred in a quadrupole acting as an ion guide or a mass filter depending on the acquisition mode (MS or MS/MS). In MS/MS mode (tandem mass spectrometry), an ion with a specific m/z is isolated in the quadrupole and then transferred into the collision cell to be fragmented into product ions. Then, ions (MS mode) or product ions (MS/MS mode) are pulsed into a Time of Flight (ToF) analyzer where the ions (or product ions) are separated depending on their mass to charge ratio (m/z). The time required by an ion to reach the detector is directly related to its m/z. MS and MSMS acquisitions were performed within a 20-100 m/z window using Data Dependent Acquisition (DDA) mode. The MS scan rate was set at 12 Hz and the MSMS scan rate was ranging from 12 to 16 Hz depending on ion intensity. Internal calibration was performed using a sodium formate solution.

Relative quantification of compounds detected by mass spectrometry were performed using Progenesis® QI software (Waters). First, MS data were loaded into the software and processed to detect all the unique ions (retention time and m/z pairs) using the default threshold parameter. Then, all the unique ions released from the LC-MS system and those corresponding to poloxamer (a polymer used during cell cultivation with m/z ranging from 288 and 1000 and eluted from 7.6 to 11.5 min) were excluded from the analysis. Afterwards, a deconvolution step was performed using specific adducts (such as M+H, 2M+H, M+Na for positive mode) to group all detected unique ions into features (group of unique ions corresponding to the same compound). All features with maximal abundances < 10000 (positive mode) and < 5000 (negative mode) were not considered in the study.

To identify the remaining features, additional software such as MetFrag in combination with databases (PubChem, Chemspider, HMDB) were used. The mass accuracy for MS and MSMS were set at 5 ppm and 0.01 Da, respectively.

Beside internal standards, a unique identification is rare, since mass-based identification cannot discriminate between isomers having the same elemental composition [210]. In that case, annotation of the fragments might allow a putative identification of a compound. For clarity during data revision, three distinct confidence levels corresponding to the annotation certainty as proposed by Blaženović *et al.* were used in this study. Whenever the precursor mass of a molecular ion matches a database entry it is considered as putative identified compound (level 3), which needs further confirmation. If the database result is matching another criterion i.e. retention time or fragmentation pattern, the feature is considered as likely identified (level 2). The highest level of confidence in the annotation (level 1) is achieved by measuring a pure standard [211].

4. Results

4.1. SSC uptake

High producing clones have a high demand in amino acids to support cell growth and productivity. Cys supply during cell cultivation is ensured via Cys transporter and a CysS/Glu antiporter (x_c^-). In this section, the uptake of SSC by CHO cells when applied to a cell culture feed was studied with the goal of identifying the receptor involved in its transport through the plasma membrane. The x_c^- antiporter was hypothesized to facilitate SSC uptake, due to the structure similarity of SSC to both, Glu and CysS. This hypothesis is visualized in figure 8, whereby only the light chain (xCT, gene *SLC7A11*) of the functional CysS/Glu antiporter x_c^- is included since the heavy chain is not required for the actual transport. Transporter inhibition using sulfasalazine (SAS) and overexpression of the antiporter via sulforaphane (SFN) or sulforaphane-*N*-acetylcysteine (SFN-NAC) treatment was investigated in presence of Cys or SSC during fed-batch experiments with CHO cells (for chemical structures see figure 6 and figure 7).

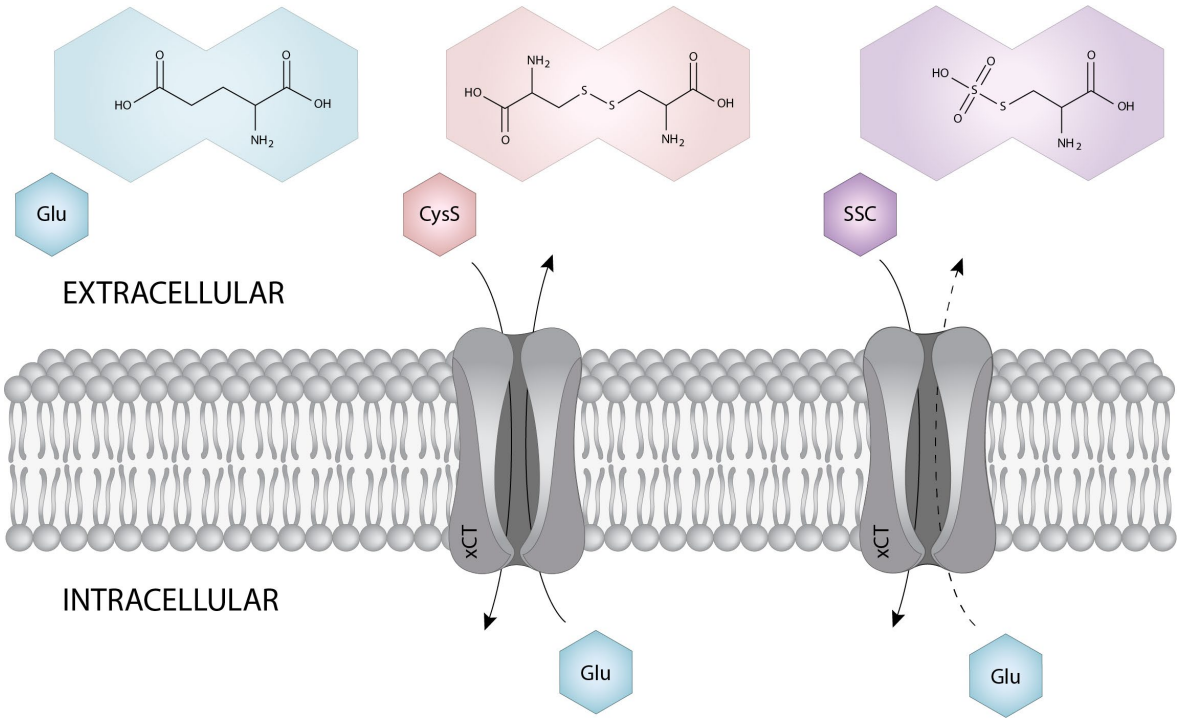

Figure 8. Known xCT antiporter activity and proposed SSC uptake. The left xCT antiporter (gene *SLC7A11*) visualizes the known cystine (CysS) import and glutamate (Glu) export activity with arrows. Due to structure similarity of *S*-sulfocysteine (SSC; purple) to CysS (pastel) and Glu (blue), cellular uptake of SSC was proposed via xCT as visualized on the right. Potential cotransport of Glu is indicated as dashed arrow.

4.1.1. CysS/Glu antiporter inhibition reduces SSC uptake

Transporter inhibition via SAS treatment

In a first test, suitable SAS concentrations to reduce x_c^- transporter activity in CHO cells were evaluated. Gout *et al.* reported single additions of 100 µM up to 300 µM SAS as effective concentration inhibiting growth by limited Cys supply using a Nb2 lymphoma culture [212]. Based on this publication, SAS additions of either 50 µM or 500 µM on day 3, 5 and 7 during a fed-batch using a Cys-feed (stabilized with ketoglutaric acid) were investigated. The goal of this experiment was to find suitable concentrations leading to reduced CysS uptake without being toxic for CHO cells. The impact of different treatments was evaluated by monitoring the VCD and by daily measurement of extracellular amino acids. The area under the curve (AUC) of the VCD or the extracellular amino acid concentration was calculated and compared to an untreated condition.

A lethal response was observed after addition of 500 µM SAS on day 3 (figure 9 A). In contrast, repetitive addition of 50 µM SAS (150 µM SAS condition) showed no apparent effect on the VCD of cultivated cells, but extracellular CysS was only increased 22% compared to the untreated control (figure 9 B) which was considered insufficient to study SSC uptake.

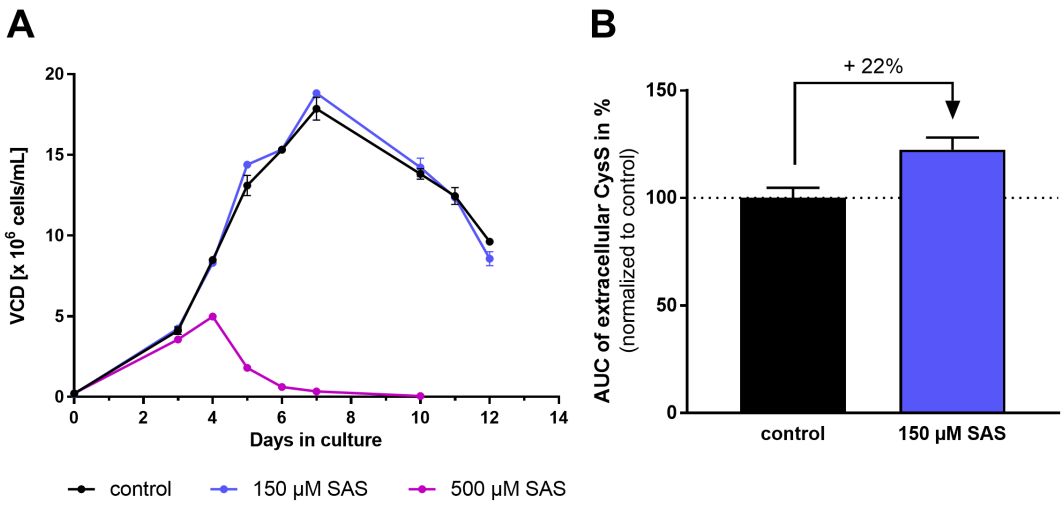

Figure 9. Dose response of sulfasalazine on CHO cells during a fed-batch. Suspension CHO cells were seeded at 2×10^5 cells/mL, incubated at 37°C, 5% CO_2, 80% humidity and agitated at 320 rpm. Feed containing Cys was added on day 3, 5, 10 and 12 (3%; v/v) and day 7 (6%; v/v). 50 µM sulfasalazine (SAS) was added on day 3, 5 and 7 leading to 150 µM SAS in total or 500 µM SAS was added on day 3. (A) Viable cell density (VCD) expressed as mean values ± SEM (n=4). (B) Extracellular cystine (CysS) was measured via RP-UPLC after iodoacetamide treatment and AccQ-Tag derivatization and Area under the curve (AUC) of CysS was normalized to control without SAS treatment. Data are expressed as mean values ± SEM (n=2).

A second experiment was designed to find a SAS concentration balancing reduced VCD and increased CysS concentration in the supernatant by increasing the addition frequency from three additions to daily treatment. Reduced VCD of 8% and 25% was observed at daily

addition of either 50 µM or 100 µM SAS, respectively (calculated as % difference of the AUC of VCD visualized in figure 10 A). Even though a reduced VCD is known to impact the amino acid consumption, amino acids were quantified extracellularly in these conditions, hoping that the impact of the treatment would be more important than the effect of the decreased growth. Results indicate that the extracellularly concentration of CysS was increased with increasing SAS treatment (figure 10 B) but an increase was also observed for all the amino acids, as represented exemplarily for arginine (Arg) in figure 10 C (all the other amino acid data are presented in appendix figure 44), confirming that reduction of VCD is resulting in a lower amino acid consumption from the medium.

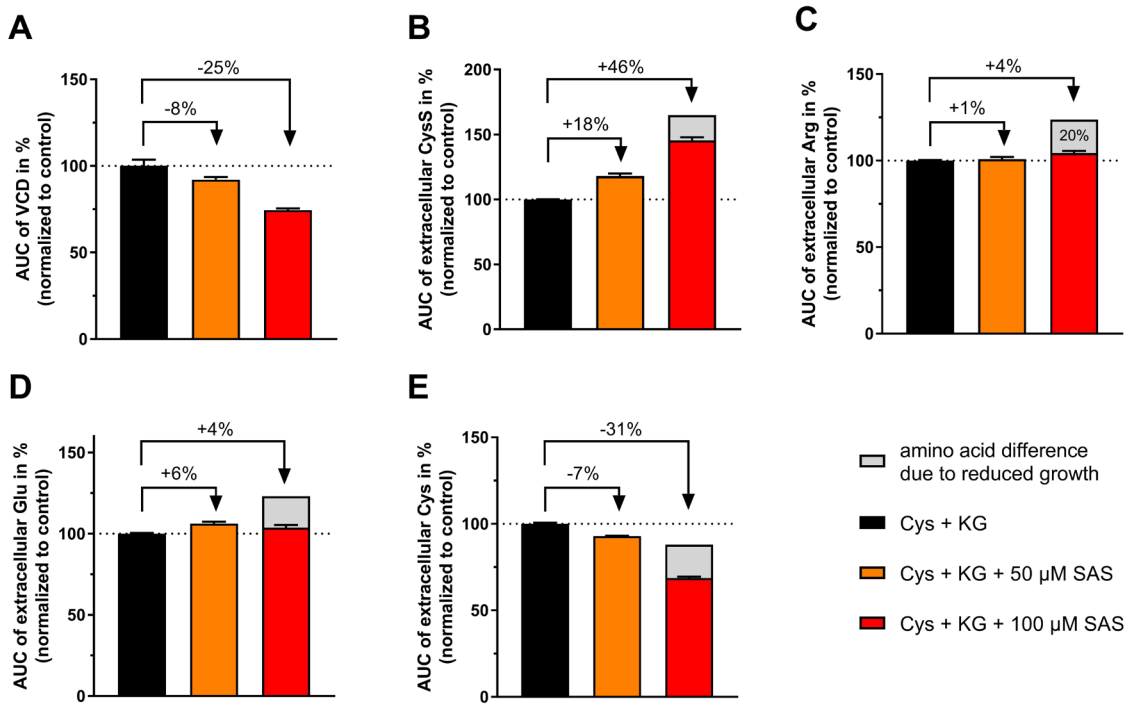

Figure 10. Extracellular amino acids during a fed-batch experiment intended to inhibit the CysS/Glu antiporter. CHO cells were treated daily with 50 µM or 100 µM sulfasalazine (SAS) and feed containing cysteine (Cys) stabilized with ketoglutaric acid (KG). Area under the curve (AUC) of (A) viable cell density (VCD), (B) extracellular cystine (CysS), (C) arginine (Arg), (D) glutamate (Glu) and (D) Cys was measured via RP-UPLC after iodoacetamide treatment and AccQ-Tag derivatization and was normalized to Cys containing feed. Effects due to different growth are calculated as average difference of x_c^- antiporter non-transported amino acids compared to the control and are visualized as stacked bar in grey. Data are expressed as mean values ± SEM (n=2).

To be able to focus on only the increase in amino acid concentration resulting from the transporter inhibition, the amino acid values had to be corrected to take into account the bias introduced by the decreased VCD. Therefore, the mean increase of all extracellular amino acids (not transported by the x_c^- system) was calculated in response to SAS treatment. In response to 50 µM SAS, a minor increase of 1% of the extracellular amino acid concentrations was calculated, whereas 20% higher extracellular amino acid concentrations were detected after 100 µM SAS treatment. This increase did not result from

the x_c^- mediated transport and was thus subtracted from all extracellular amino acid values and is visualized as stacked grey bar on the graphs of figure 10. As an example, Arg known to be transported by system y+ (gene: *SLC7A3*) via facilitated diffusion [127], was increased about 24% via 100 µM SAS treatment. After subtraction of the amino acid concentration that was not consumed due to the lower VCD, the concentration of Arg was only increased about 4% after 100 µM SAS treatment.

In contrast, the increased CysS concentration observed in the supernatant after either 50 µM or 100 µM SAS treatment was increased by 18% and 65% and was still apparent after subtraction of the amino acid concentration that was not consumed due to the lower VCD. Daily addition of 100 µM SAS resulted in 46% higher extracellular CysS concentration (figure 10 B), indicating that independently of the reduction in VCD, less CysS was transported through the x_c^- transporter in presence of SAS.

Extracellular Glu concentration was assessed to link reduced CysS uptake with Glu transport, since x_c^- functions as antiporter. After subtraction of the relative amino acid differences due to growth, 6% and 4% increased extracellular Glu were observed for 50 µM and 100 µM SAS, respectively (figure 10 D). These data indicate no significant change of the Glu concentration at increasing inhibitor concentrations, which might be explained by the availability of several Glu transporters in CHO cells allowing a constant Glu level independently of x_c^- inhibition.

In a next step, extracellular Cys was evaluated and data showed a 7% and 31% reduced concentration through 50 µM and 100 µM SAS, respectively (figure 10 E). These data suggest that in response to reduced CysS uptake, cells may promote Cys import via SAS independent transporters, *e.g.* EAAT3 to counteract intracellular Cys depletion.

Overall, inhibition of the x_c^- antiporter through SAS showed a dose-dependent increase in extracellular CysS concentration suggesting reduced CysS uptake. Due to the low impact of the 50 µM daily addition on the CysS uptake in CHO cells and the high impact of 100 µM SAS on VCD, both treatments were selected for further experiments.

Transporter inhibition in presence of SSC

Next, the impact of the SAS mediated inhibition of x_c^- was evaluated in a fed-batch using SSC containing feed. As in the previous experiment, extracellular amino acids were measured daily and the calculated AUC was normalized to Cys fed cells to allow comparison of both feeds (different Cys-sources) and the respective effect of SAS treatment. If SSC uptake is facilitated by the x_c^- transporter, the transporter inhibition was hypothesized to result in increased extracellular SSC concentrations, as was previously observed for CysS with Cys feeding.

In presence of SSC, daily addition of either 50 µM or 100 µM SAS resulted in 14% and 30% reduced VCD, respectively, when compared to the Cys containing feed (figure 11 A). The increased extracellular amino acid concentration caused by the lower VCD was calculated analogous to Cys fed cells. In presence of SSC, a mean concentration difference of 9% was calculated in response to 50 µM and 31% in response to 100 µM SAS and these values were subtracted from all extracellular amino acid values (visualized as stacked grey bar). Resulting extracellular SSC concentrations were assessed in response to transporter inhibition. A 65% increased extracellular SSC concentration was observed after 50 µM SAS treatment and a 177% higher extracellular SSC concentration was observed after 100 µM SAS treatment demonstrating that subtraction of the amino acid concentration differences due to growth did not disturb the significant cellular response (figure 11 B). Concluding, SSC uptake was reduced in response to x_c^- inhibition through SAS treatment.

To investigate whether reduced SSC uptake triggered Cys uptake as previously observed with Cys feeding, extracellular Cys was evaluated. In untreated SSC fed conditions, extracellular Cys was 37% reduced compared to the control (figure 11 C). This striking difference of the Cys and SSC control condition is due to the fact that the SSC feed does not contain any Cys, so that the overall applied Cys concentration is lower compared to Cys fed conditions. Therefore, SAS treated conditions are compared to the SSC control condition. With 50 µM and 100 µM SAS, the extracellular Cys concentration was 11% and 32% reduced, respectively (figure 11 C) suggesting that cells promote Cys import via SAS independent transporter to compensate reduced SSC uptake.

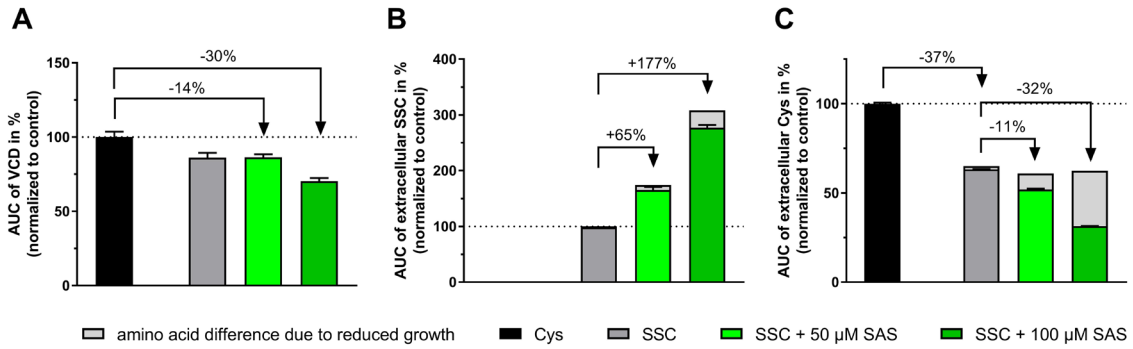

Figure 11. Extracellular amino acids in response to CysS/Glu antiporter inhibition during a fed-batch experiment using an SSC-containing feed. CHO cells were treated daily with 50 µM or 100 µM sulfasalazine (SAS) and feed containing either Cys or SSC. (A) Area under the curve (AUC) of viable cell density (VCD), (B) extracellular SSC, and (C) Cys was measured via RP-UPLC after iodoacetamide treatment and AccQ-Tag derivatization and was normalized to Cys containing feed. Effects due to different growth are calculated as average difference of x_c^- antiporter non-transported amino acids compared to the control and are visualized as stacked bar in grey. Data are expressed as mean values ± SEM (n=2).

Overall, data suggest that cellular uptake of SSC is accomplished via x_c^- antiporter, since significantly less SSC is consumed in presence of SAS (independent of the reduced amino acid consumption due to a lower VCD). The increased Cys consumption indicates that cells

are trying to cope with the lower supply in Cys equivalent via the uptake of more Cys, most likely through a x_c^- independent transporter. To bring additional evidence supporting the x_c^- mediated SSC transport in CHO cells, the impact of x_c^- overexpression on the SSC uptake will be studied next.

4.1.2. Elevated CysS/Glu antiporter expression facilitates SSC uptake

Addition of sulforaphane increases the x_c^- antiporter gene expression level

In contrast to SAS that can be used as x_c^- inhibitor, SFN is known to increase the expression of the transporter and thus was hypothesized to promote SSC uptake. Initially, an SFN dose-response experiment was performed with CHO cells to define a concentration which can upregulate the x_c^- antiporter expression, while maintaining cell performance. The cellular response was assessed via gene expression (mRNA level) and VCD. During a fed-batch process using a Cys containing feed, concentrations of 5 or 25 µM SFN were spiked to the cultures on day 3, 5 and 7 and 50 µM SFN was spiked on day 3 and 5. To compare the impact of different treatments on cell growth, the AUC of the VCD was calculated. Whereas 5 µM SFN had no significant impact on growth, reduced VCD of 30% and 67% were observed for 25 µM and 50 µM SFN, respectively (figure 12 A).

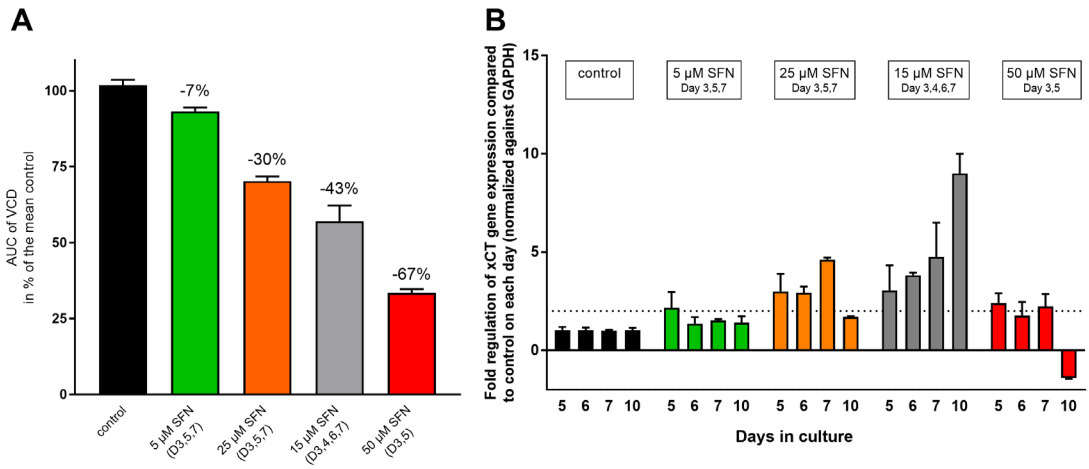

Figure 12. Dose response of sulforaphane on CHO cells. Suspension CHO cells were seeded at 2×10^5 cells/mL, incubated at 37°C, 5% CO_2, 80% humidity and agitated at 320 rpm. Feed was added on day 3, 5 and 10 (3%; v/v) and day 7 (6%; v/v) whereas 5, 25 or 50 µM sulforaphane (SFN) was added on day 3, 5, 7 and 15 µM SFN was added on Day 3, 4, 6 and 7. (A) Area under the curve (AUC) of the Viable cell density (VCD) was calculated. Bars represent normalized values to the untreated Cys control condition (n=4) and the absolute difference compared to the control is shown above. (B) CysS/Glu antiporter (xCT; gene *SLC7A11*) mRNA expression as fold change relative to the untreated control on each day and normalized to Glyceraldehyde 3-phosphate dehydrogenase (GAPDH) with n=2. Two-fold increased mRNA levels were considered as differentially expressed.

Exploration of the antiporter mRNA levels (gene *SLC7A11)* was used to assess x_c^- antiporter upregulation as CHO specific antibodies were not commercially available to detect antiporter expression via Western Blot. 5 µM SFN treatment induced a 2.2-fold

increased *SLC7A11* mRNA level on day 5, while 25 µM SFN resulted in a max upregulation of 4.6-fold on day 7 (figure 12 B) indicating that 25 µM was more suitable than 5 µM SFN to induce antiporter expression. In both cases, the heterodimeric subunit *SLC3A2* was not upregulated (appendix figure 43).

Since the *SLC7A11* gene expression was only transitory with 5 µM SFN and the VCD was impacted by the 25 µM SFN treatment, an intermediate concentration of 15 µM SFN and a more frequent addition during the growth phase (day 3, 4, 6 and 7) was tested to minimize the impact on VCD while maintaining a significant overexpression of the transporter.

Using 15 µM SFN, a reduced VCD of about 40% was observed (figure 12 A), but treatment yielded a 9.0-fold upregulated *SLC7A11* mRNA level on day 10 compared to the control (figure 12 B). Although the RNA level was efficiently upregulated, the highly impacted cellular growth was suggested to influence the amino acid consumption significantly, so that a reduced CysS uptake rate might not be distinguishable from lowered consumption. Thus, treatment was not yet satisfactory and required further adaption.

Addition of sulforaphane-N-acetylcysteine circumvents reduced VCD

Reduced VCD caused by SFN treatment might be linked to a detrimental reduction of the intracellular GSH concentration, since SFN is known to interact with GSH. To circumvent a reduced GSH level potentially leading to the reduced VCD, sulforaphane-*N*-acetylcysteine (SFN-NAC), the interaction product of SFN and GSH, was tested in an additional experiment. To compare both treatments, the impact of equimolar concentrations of SFN and SFN-NAC (15 µM) on CHO cell growth, as well as *SLC7A11* mRNA expression level, was explored.

Results obtained using the Cys feed indicate that the SFN treatment resulted in about 43% reduced VCD compared to the control, while SFN-NAC reduced VCD only by 10% (figure 13 A), thus confirming the hypothesized lower toxicity of the interaction product SFN-NAC on CHO cells. However, SFN treatment increased the mRNA levels of the antiporter by up to 6.1-fold at day 4 and 4.8-fold at day 7, whereas SFN-NAC treatment increased the mRNA level only 4.0-fold on day 4 and 2.8 fold on day 7 (figure 13 B), indicating that SFN-NAC is a slightly less effective inducer of the *SLC7A11* expression than SFN. Thus, both treatments were used in the next experiment to be able to study the potential impact of the reduced VCD following SFN treatment and the potential limited overexpression of the receptor mRNA following SFN-NAC treatment, on the CysS and SSC uptake.

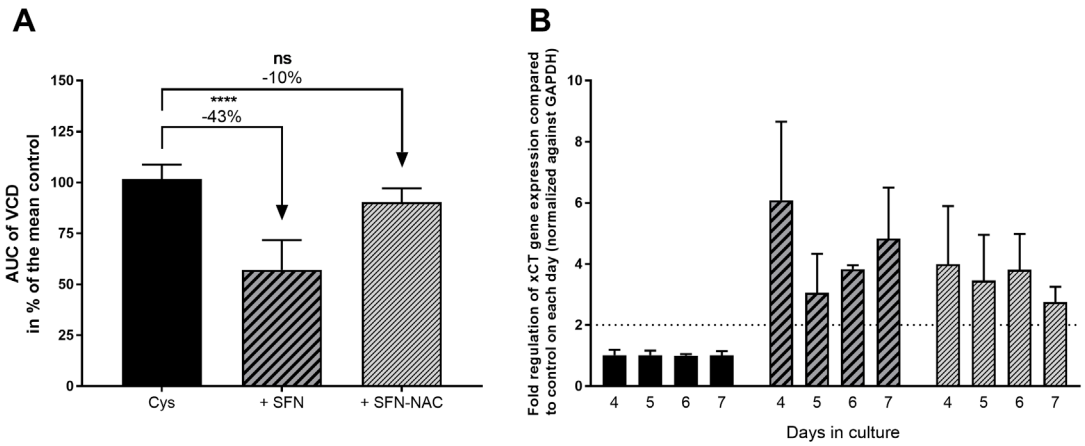

Figure 13. Impact of SFN and SFN-NAC on CHO cells during a fed-batch using a cysteine feed. Suspension CHO cells were seeded at 2×10^5 cells/mL, incubated at 37°C, 5% CO_2, 80% humidity and agitated at 320 rpm. Feed containing 15 mM Cys stabilized with 50 mM KG was added on day 3, 5, 10 and 12 (3%; v/v) and day 7 (6%; v/v) whereas 15 µM SFN or SFN-NAC were added on day 3, 4, 6 and 7. (A) Area under the curve (AUC) of the viable cell density (VCD) was calculated. Bars represent normalized values to the untreated Cys control condition of two independent experiments (n=8). (B) Fold regulation of the CysS/Glu-antiporter (xCT) gene expression relative to the control on each day and normalized to GAPDH (n=2). Data are expressed as mean values ± standard error of the mean (SEM). Statistical analysis of the VCD was performed with one-way ANOVA and subsequent Dunn's multiple comparison, whereas p-values indicate the following: **** p<0.0001, ns = not significant.

SFN and SFN-NAC treatment facilitate CysS uptake

Since the increase of the *SLC7A11* mRNA does not necessarily correlate with an enhanced transporter activity, extracellular amino acid analysis was performed on supernatants from fed-batch experiments to confirm increased transporter activity after SFN or SFN-NAC treatment.

The upregulation of the transporter is expected to yield a lower extracellular CysS concentration compared to the control, since this transporter is reported to be solely responsible for CysS uptake. Quantification of each amino acid in the supernatant of the CHO cell culture as a function of time was used to calculate the AUC and was normalized to the control. The previously described reduced VCD of SFN and slightly reduced VCD of SFN-NAC treated cells compared to the control yielded in general higher extracellular amino acid concentrations due to the lower consumption but independently of the antiporter overexpression. Thus, similarly to transporter inhibition experiments, the respective amino acid concentration differences due to the lower VCD were subtracted and visualized as stacked grey bar for each condition (appendix figure 45). As an example, the concentration of Arg, was increased about 24% due to SFN treatment and 18% due to SFN-NAC (figure 14 A). After subtraction of the amino acid concentration differences due to growth, the concentration of Arg varied less than 2% following both SFN treatments, confirming that the

correction is needed to focus only on the amino acid changes that are related to the x_c^- transporter.

When considering corrected amino acid values, extracellular CysS concentrations were significantly reduced by SFN and SFN-NAC treatment by 31% and 30%, respectively (figure 14 B), whereby no significant change of extracellular Glu was observed (-2% and -5% for SFN and SFN-NAC, respectively) (figure 14 C), most probably suggesting the involvement of another Glu transporter. Altogether, data support elevated antiporter activity, which qualified 15 µM SFN and SFN-NAC treatment on days 3, 4, 6 and 7 to study SSC uptake.

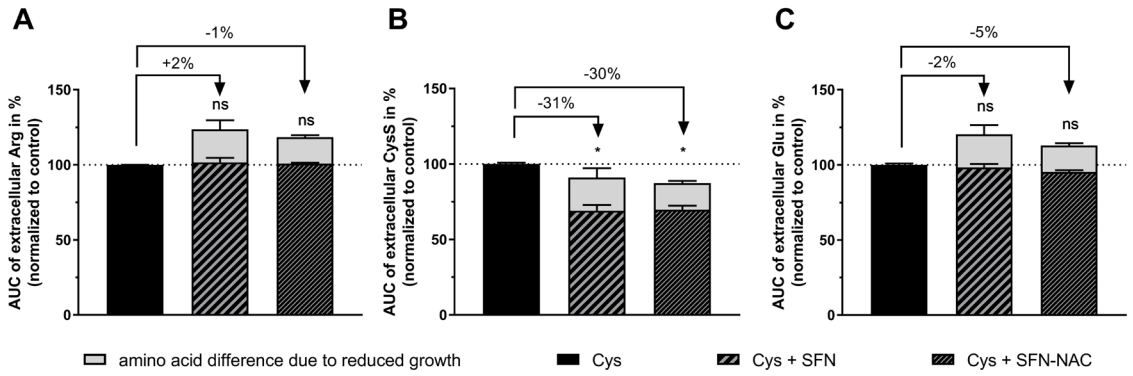

Figure 14. Extracellular amino acids in response to SFN and SFN-NAC during two independent fed-batch experiments with feed containing Cys. With the intention to increase the expression of the CysS/Glu antiporter (xCT), cells were treated with either SFN or SFN-NAC. Area under the curve (AUC) of extracellular (A) arginine (Arg), (B) CysS and (C) Glu was measured via RP-UPLC after iodoacetamide treatment and AccQ-Tag derivatization and was normalized to Cys containing feed. Effects due to different growth are calculated as average difference of antiporter unrelated amino acids to the control and are visualized as stacked bar in grey. Data are expressed as mean values ± SEM (n=6). Statistical analysis was performed with one-way ANOVA and subsequent Dunn's multiple comparison, whereas *p*-values are indicated as followed: * $p<0.05$, ns = not significant.

Elevated CysS/Glu antiporter expression facilitates SSC uptake

SFN and SFN-NAC addition were applied in a fed-batch experiment using SSC-containing feed as sole Cys source. As in previous experiments, different treatments were compared on basis of VCD, mRNA levels and extracellular amino acid analysis. Data sets were normalized to untreated Cys feeding to observe differences regarding the Cys source as well as SFN and SFN-NAC treatment.

Feeding with SSC in place of Cys resulted in a non-significant reduction of the VCD of about 3%, whereas the combination of SSC feeding with SFN and SFN-NAC treatment resulted in a reduced VCD of 27% and 16%, respectively (compared to the SSC control figure 15 A). The feeding with SSC had no effect on the *SLC7A11* mRNA expression, whereas the combination with SFN and SFN-NAC treatment led to 6.5 and 4.3-fold increased mRNA level after 7 days, respectively (figure 15 B). Since SSC feeding alone did not affect the mRNA levels of the antiporter, both SFN and SFN-NAC treatments may be used to study the cellular uptake of SSC in cells overexpressing the x_c^- antiporter.

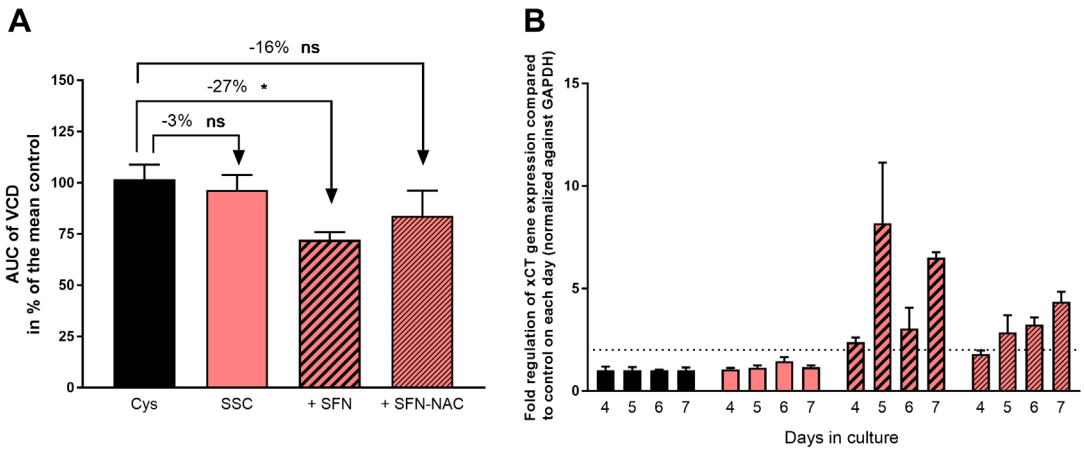

Figure 15. Impact of SFN and SFN-NAC on CHO cells during a fed-batch using an SSC feed. Suspension CHO cells were seeded at 2×10^5 cells/mL, incubated at 37°C, 5% CO_2, 80% humidity and agitated at 320 rpm. Feed containing 15 mM SSC was added on day 3, 5, 10 and 12 (3%; v/v) and day 7 (6%; v/v) whereas 15 µM SFN or SFN-NAC were added on day 3, 4, 6 and 7. (A) Area under the curve (AUC) of the Viable cell density (VCD) was calculated. Bars represent normalized values to the untreated Cys control condition of two independent experiments (n=8). (B) Fold regulation of the CysS/Glu-antiporter (xCT) gene expression relative to the control on each day and normalized to GAPDH (n=2). Data are expressed as mean values ± SEM. Statistical analysis of the VCD was performed with one-way ANOVA and subsequent Dunn's multiple comparison, whereas p-values indicate the following: * p<0.05, ns = not significant.

In presence of SSC, an averaged increase of about 10% extracellular amino acid concentration was detected for both treatments as a result from the reduced VCD as exemplarily shown for Arg (figure 16 A). Transporter overexpression caused a reduction of extracellular CysS of about 29% (p=0.005) after SFN addition and about 28% (p=0.014) after SFN-NAC addition (figure 16 B), indicating a similar enhanced transporter activity in presence of both treatments.

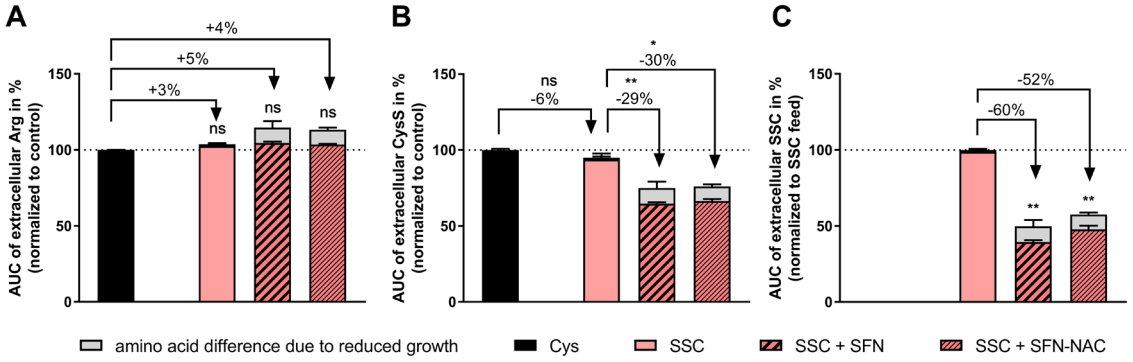

Figure 16. Extracellular amino acids during two independent fed-batch experiments with feed containing 15 mM SSC. With the intention to increase the expression of the CysS/Glu antiporter (xCT), cells were treated with either SFN or SFN-NAC. Area under the curve (AUC) of extracellular (A) Arg, (B) CysS, and (C) *S*-Sulfocysteine (SSC) was measured via RP-UPLC after iodoacetamide treatment and AccQ-Tag derivatization and was normalized to Cys containing feed. Effects due to different growth are calculated as average difference of antiporter unrelated amino acids to the control and are visualized as stacked bar in grey. Data are expressed as mean values ± SEM (n=6). Statistical analysis of the amino acids was performed either with one-way ANOVA and subsequent Dunn's multiple comparison or in case of SSC by the Mann-Whitney test, whereas p-values are indicated as followed: * p<0.05, ** p<0.01, ns = not significant.

Additionally, significantly reduced extracellular SSC concentrations of approximatively 60% (p=0.0022) and 52% (p=0.0022) were observed when cells were treated with either SFN or SFN-NAC, respectively (figure 16 C). Considering that the SSC feed alone did not influence the mRNA expression levels of the antiporter, the amino acid quantification after SFN and SFN-NAC treatment suggests that, enhanced SSC uptake is mediated by elevated antiporter expression and thus support the hypothesis of SSC uptake via x_c^- antiporter.

SSC does not interact with SFN or SFN-NAC

Experiments with SFN and SFN-NAC treatment indicate that increased x_c^- transporter expression can promote the uptake of extracellular CysS and SSC. Since SFN is known to react with Cys residues in proteins such as Keap1, it might as well react with Cys or SSC in the supernatant. *In vitro* experiments were performed to ensure that reduced extracellular CysS and SSC concentrations following SFN or SFN-NAC treatment were not caused by a chemical interaction.

During previous fed-batch experiments, four additions of either 15 µM SFN or SFN-NAC were applied (total 60 µM). To work in a similar range of concentration in the *in vitro* experiments, 50 µM and 100 µM SFN or SFN-NAC were incubated with either 1.5 mM Cys or 1.5 mM SSC in water to explore the possibility of a chemical reaction. Data were normalized to the respective amino acid in water alone after 0 min.

When mixed in water with increasing concentrations of SFN or SFN-NAC (figure 17), neither Cys nor SSC concentrations were decreased after incubation for 1.5 h at 37°C indicating that both SFN and SFN-NAC did not react with Cys or SSC.

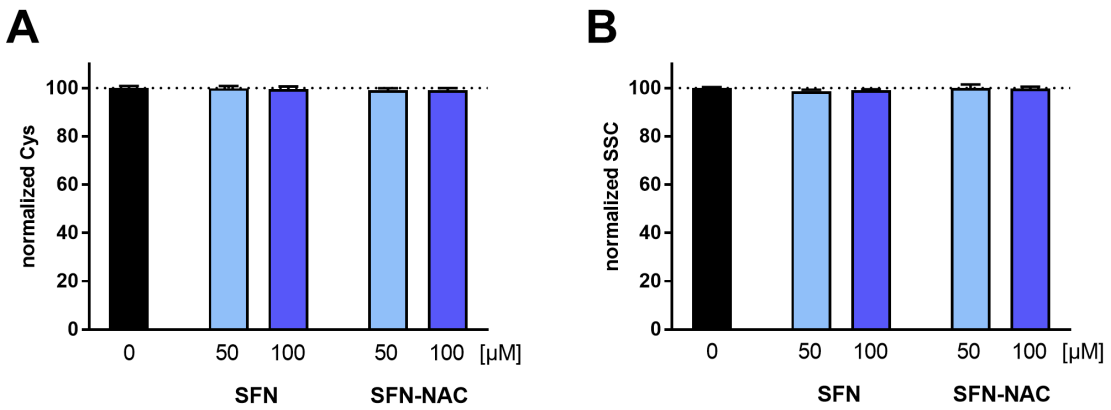

Figure 17. Interaction of SSC or Cys with SFN or SFN-NAC in water. 50 µM and 100 µM sulforaphane (SFN) or sulforaphane-*N*-acetylcysteine (SFN-NAC) were incubated with either (A) 1.5 mM cysteine (Cys) or (B) 1.5 mM *S*-sulfocysteine (SSC). All mixtures were analyzed after incubation for 1.5 h at 37°C. SSC and Cys were measured via RP-UPLC after iodoacetamide treatment and AccQ-Tag derivatization and Cys as well as SSC concentrations were normalized to the water control condition without SFN or SFN-NAC measured after 0 min (n=2).

To reflect the actual cultivation matrix (including trace elements as possible catalyzers), a similar experiment was performed by mixing 1.5 mM Cys and SSC with increasing SFN and

SFN NAC concentrations in Cys-depleted medium. In this experimental setup, a reduced Cys concentration was expected through enhanced autoxidation to CysS in presence of *e.g.* copper (independent of SFN) and overall interaction of Cys with other media components.

Indeed, CysS was detected when Cys was incubated with medium. In the control condition, about 112 µM CysS was detected after 1.5 h incubation at 37°C (figure 18 A). As CysS is the dimer of Cys, the equivalent Cys concentration is 224 µM, which represents 15% of the initially applied 1500 µM. Since 17% of applied Cys was retained and 15% was detected in form of CysS (figure 18 B, whereby CysS is visualized as stacked grey bar) the remaining 68% are likely interacting with other cell culture media components.

Additional treatment did not change the Cys level. For example, about 19% and 17% Cys was observed for 100 µM SFN and SFN-NAC, respectively, indicating that SFN and SFN-NAC do not interact with Cys in the cell culture media matrix.

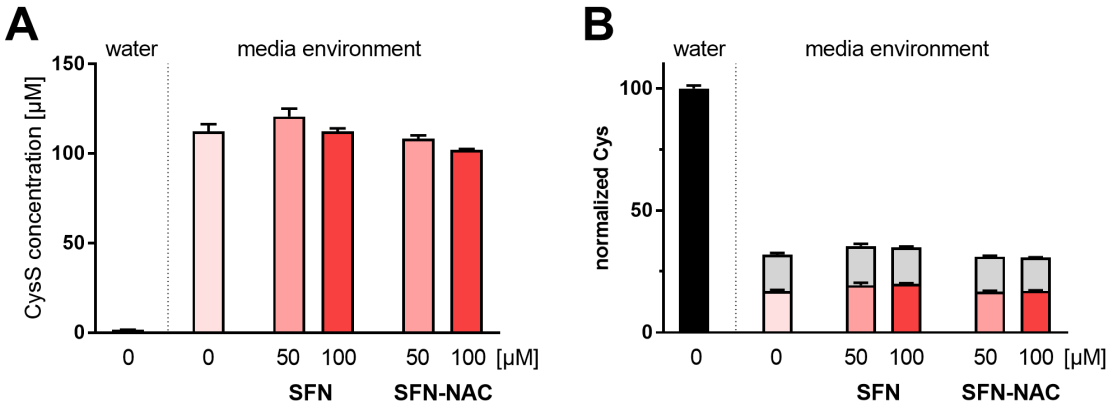

Figure 18. Interaction of Cys with SFN or SFN-NAC in media. 1.5 mM cysteine (Cys) were incubated with either 50 µM and 100 µM sulforaphane (SFN) or sulforaphane-*N*-acetylcysteine (SFN-NAC) in presence of Cys-depleted cell culture medium to reflect cell cultivation. All mixtures were analyzed after incubation for 1.5 h at 37°C. (A) Cystine (CysS) and (B) Cys were measured via RP-UPLC after iodoacetamide treatment and AccQ-Tag derivatization, whereby Cys concentrations were normalized to 1.5 mM Cys in water without SFN or SFN-NAC measured after 0 min. Based on the detected CysS concentration, the equivalent Cys was calculated as percent of the initial applied Cys concentration and visualized as stacked grey bar (n=2).

A reduction of the SSC concentration in presence of medium alone was not expected, since previous studies demonstrated that SSC was more stable compared to Cys. Indeed, about 95% of the applied SSC concentration was recovered without treatment and 96% and 93% was detected in presence of 50 µM SFN and SFN-NAC, respectively (figure 19). Furthermore, no dose dependent effect was observed, as 97% SSC was detected in presence of 100 µM SFN and 96% was detected in presence of SFN-NAC. These data confirm that the decrease in the extracellular SSC concentration observed in the transporter overexpressing cell experiment (> 60%) cannot be caused by an extracellular chemical interaction of SFN and SSC.

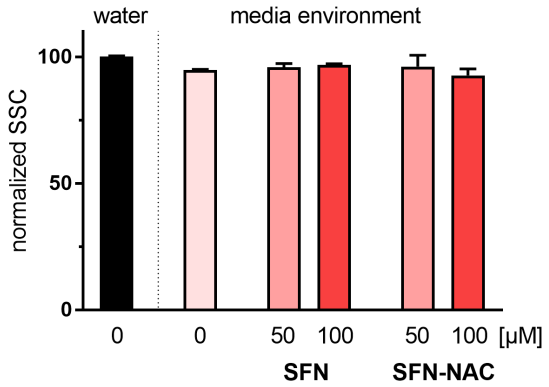

Figure 19. Interaction of SSC with SFN or SFN-NAC in media. 50 µM and 100 µM sulforaphane (SFN) or sulforaphane-*N*-acetylcysteine (SFN-NAC) were incubated with 1.5 mM *S*-sulfocysteine (SSC) in presence of Cys-depleted cell culture medium to reflect cell cultivation. All mixtures were analyzed after incubation for 1.5 h at 37°C. SSC were measured via RP-UPLC after iodoacetamide treatment and AccQ-Tag derivatization and concentrations were normalized to SSC in water without SFN or SFN-NAC measured after 0 min (n=2).

4.1.3. Increased CysS/Glu antiporter activity leads to accelerated SSC toxicity

Exchange of Cys within a feed with equimolar concentrations of SSC was demonstrated in previous studies to yield good cellular performance [194]. However, usage of increased SSC concentrations led to a toxic response. First, an SSC dose response experiment was performed to determine the SSC concentration, which triggers a toxic response with the cell line used herein. To further identify whether the toxic response is triggered by SSC or through elevated Cys availability, two non-toxic SSC concentrations were additionally supplemented with Cys, to increase the overall Cys concentration. Finally, to study whether an increase in SSC uptake prompts toxicity, cells were treated with varying amounts of SSC and with SFN to increase the x_c^- activity.

Increasing SSC concentration causes toxic response

The toxic response of a CHO-K1 cell line was explored via feeding of 15 mM, 20 mM and 30 mM SSC in a Cys-depleted feed. Data were assessed through the VCD, whereby 15 mM SSC was expected to yield a good cell performance, increasing SSC concentration to 20 mM was thought to have an adverse effect, whereas 30 mM SSC was described to be lethal.

As expected, after the second addition of a 30 mM SSC containing feed on day 5 (3% v/v) the VCD was decreased from 8.6×10^6 viable cells/mL on day 5 to 7.6×10^6 viable cells/mL on day 6 and after another day of cultivation no viable cells were detected (figure 20). Lowering the concentration to 20 mM SSC prevented the toxic response. However, the VCD was still lowered compared to 15 mM SSC. More precisely, a max VCD of 14.4×10^6 viable cells/mL was observed on day 7 when 20 mM SSC was applied and a max VCD of 17.4×10^6 viable cells/mL on day 7 when 15 mM SSC was applied. Concluding, both non-toxic SSC

concentrations were thought to be suitable to investigate the impact of additional Cys in the feed.

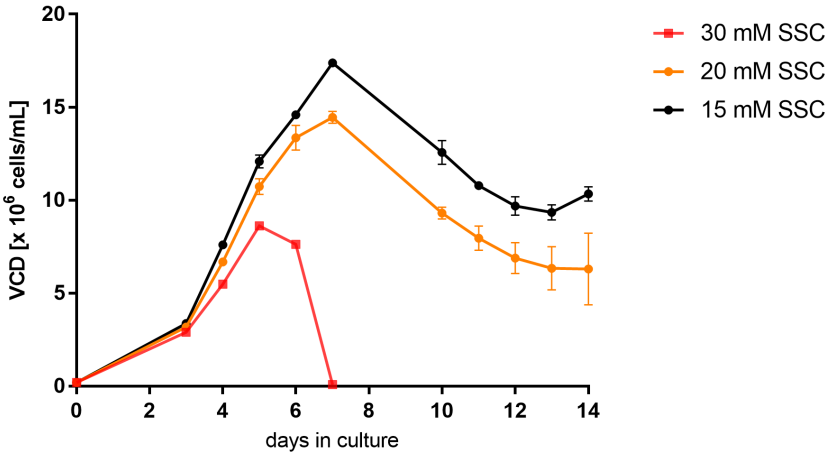

Figure 20. Dose dependent SSC toxicity. Suspension CHO cells were seeded at 2×10^5 cells/mL, incubated at 37°C, 5% CO_2, 80% humidity and agitated at 320 rpm. Feed containing increasing concentrations of 15 mM, 20 mM or 30 mM SSC were added on day 3, 5, 10 and 12 (3%; v/v) and day 7 (6%; v/v). Viable cell density (VCD) represent mean values ± SEM (n=4).

Additional Cys does not impact the toxic response

To investigate if the total Cys concentration or the amount of SSC causes the toxic response, 15 mM and 20 mM SSC conditions were supplemented with the respective amount of Cys to yield 30 mM total Cys equivalent, as this was the SSC concentration leading to a toxic response. Due to Cys autoxidation, each condition was further supplemented with KG to stabilize Cys in all feeds. For clarity, 15 mM SSC was supplemented with 15 mM Cys and 50 mM KG, whereas 20 mM SSC was supplemented with 10 mM Cys and 33 mM KG to maintain the same Cys:KG ratio. Feeds without additional Cys (SSC treatment controls) were still supplemented with the respective KG concentration (50 mM and 33 mM KG), since the antioxidant activity of KG might as well impact the cell performance. Data were compared by calculating the AUC of VCD from four biological replicates normalized to 15 mM SSC, as this concentration is equimolar to the commonly applied Cys concentration and was expected to yield a similar cell performance. Comparing both feeds containing 15 mM SSC with and without additional Cys a non-significant reduction of about 5% was observed when Cys was available (figure 21). A similar non-significant reduction of about 1% was observed for 20 mM SSC compared to 20 mM SSC with additional 10 mM Cys. Data indicate that the SSC concentration determines the cellular fate, whereby additional Cys did not alter the VCD significantly.

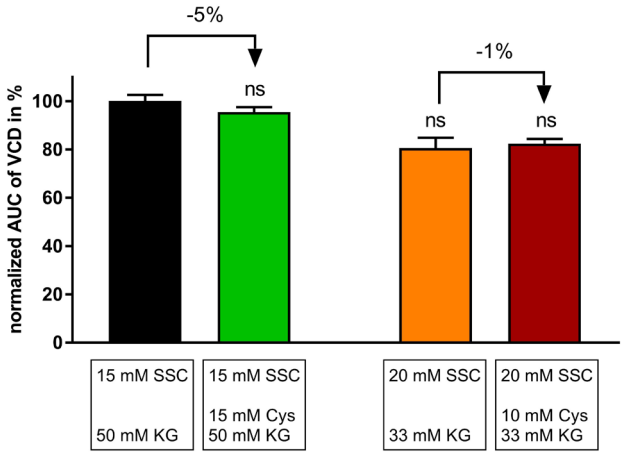

Figure 21. Cellular response to different SSC:Cys ratios. Suspension CHO cells were seeded at 2×10^5 cells/mL, incubated at 37°C, 5% CO_2, 80% humidity and agitated at 320 rpm. Feed containing either a 1:1 ratio; 15 mM *S*-sulfocysteine (SSC) and 15 mM cysteine (Cys) or a 2:1 ratio; 20 mM SSC and 10 mM Cys were supplemented with either 50 mM or 33 mM ketoglutaric acid (KG) to stabilize Cys and added on day 3, 5, 10 and 12 (3%; v/v) and day 7 (6%; v/v). Area under the curve (AUC) of the Viable cell density (VCD) was calculated. Bars represent normalized values to the 15 mM SSC control condition. Data are expressed as mean values ± SEM. Statistical analysis was performed with one-way ANOVA and subsequent Dunn's multiple comparison, ns = not significant.

x_c^- *upregulation aggravates SSC toxicity*

Based on these results, it was hypothesized that x_c^- overexpression and thereby increased SSC uptake might induce a toxic response at lower SSC concentrations. To induce transporter upregulation, the previously established addition of 15 µM SFN on day 3, 4, 6 and 7 was applied within this experiment and cellular response was assessed by the VCD. In presence of 15 mM SSC, SFN treatment triggered a 6.2-fold higher *SLC7A11* RNA level on day 7 suggesting successful upregulation of the transporter (appendix figure 46).

Through SFN treatment, AUC of VCD was 20% reduced, indicating that 15 mM SSC in combination with an upregulated transporter expression was not lethal for cells and reduced VCD is most likely due to SFN treatment (figure 22 A). However, when 20 mM SSC was applied in combination with SFN treatment 10.7×10^6 viable cells/mL on day 5 was reduced to 5.8×10^6 viable cells/mL on day 6, whereas no viable cells were detected on day 7 as already observed for 30 mM SSC (figure 22 B). Thereby, the AUC of VCD was significantly reduced about 58% (p=0.0147), indicating that 20 mM SSC was toxic for cells when x_c^- mRNA was upregulated via SFN treatment.

To support these results, SSC feeds with additional Cys (similar to the previous experiment) were also treated with SFN. In presence of 15 mM SSC and 15 mM Cys, SFN treatment triggered a 5.0-fold higher *SLC7A11* RNA level on day 7 suggesting successful upregulation of the transporter (appendix figure 46), whereby a reduced VCD of about 15% was observed.

In comparison, a reduction of about 58% was observed for 20 mM SSC in presence of 10 mM Cys (p=0.0342) indicating that the toxic response was not influenced through Cys.

In summary, the toxic SSC response is mainly driven by the cellular SSC uptake, which is influenced by the extracellular SSC concentration and x_c^- transporter activity, whereas Cys has no significant influence.

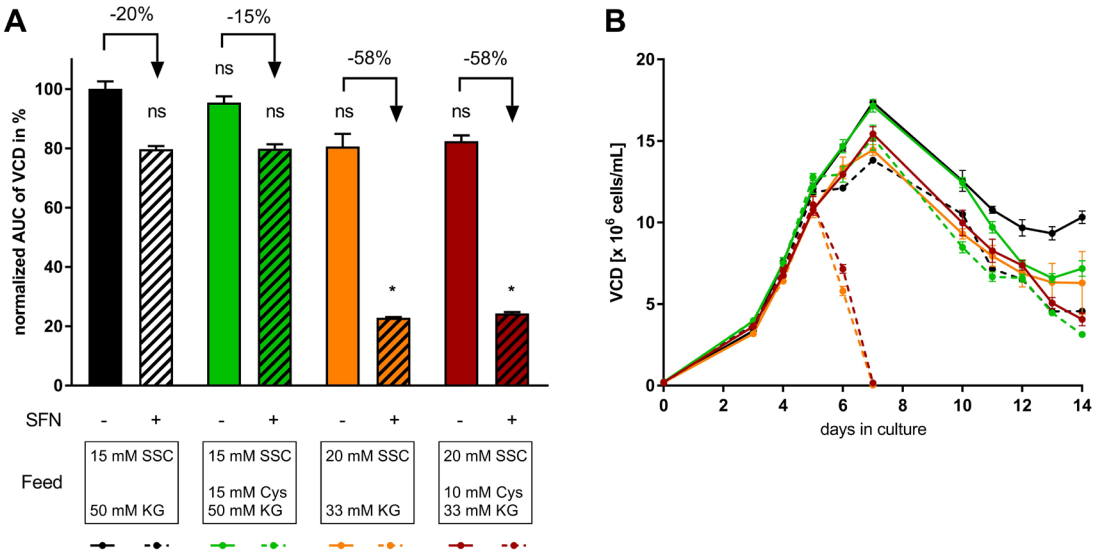

Figure 22. Aggravated SSC toxicity through x_c^- overexpression. Suspension CHO cells were seeded at 2×10^5 cells/mL, incubated at 37°C, 5% CO_2, 80% humidity and agitated at 320 rpm. Feed containing increasing concentrations of 15 mM or 20 mM *S*-sulfocysteine (SSC) with or without additional cysteine (Cys) and ketoglutaric acid (KG) were added on day 3, 5, 10 and 12 (3%; v/v) and day 7 (6%; v/v), whereas 15 µM sulforaphane (SFN) were supplemented on day 3, 4, 6 and 7. (A) Area under the curve (AUC) of the Viable cell density (VCD) was calculated. Bars represent normalized values to the 15 mM SSC control condition. (B) VCD. Data are expressed as mean values ± SEM. Statistical analysis was performed with one-way ANOVA and subsequent Dunn's multiple comparison, whereas *p*-values are indicated as followed: * $p<0.05$, ns = not significant.

Key learnings: SSC uptake and toxicity

Inhibition of the x_c^- antiporter through SAS showed a dose-dependent increase in extracellular CysS and SSC concentration suggesting a reduced uptake.

In contrast, lower extracellular CysS and SSC concentrations were observed in response to increased x_c^- antiporter activity through SFN or SFN-NAC treatment suggesting an enhanced uptake.

Elevated SSC uptake was linked to aggravated SSC toxicity indicating that in particular the SSC concentration and x_c^- antiporter activity impacts the toxic response.

4.2. Relationship between media components and SSC toxicity

Cell performance, in general, is highly influenced by the media formulation and previous experiments have shown that the toxicity of SSC is impacted by other cell culture media components. As an example, Hecklau *et al.* demonstrated that supplementation of Glu or $CuSO_4$ prevented SSC toxicity hence highlighting SSC interacting partners within cell culture media and emphasizing the necessity to identify further components which influence SSC toxicity. The goal of these experiments is to deepen the understanding of the toxic mechanism of SSC but also to identify components that can be adjusted to further improve the performance of cell culture media.

To identify specific components which have an impact on SSC toxicity, a fed-batch screening of a diverse feed panel containing different levels of each component was designed. The idea of such a feed panel was to create a design space, where each component varies within a defined concentration range and can be linked to specific performance parameters such as VCD and titer using multivariate data analysis (MVDA).

Since the existing feed panel was designed using Cys, a pre-screening was performed to investigate the optimal SSC concentration that should be used to replace Cys. To be able to focus during data analysis on the feed components that may interact with SSC, a constant SSC concentration was targeted in all feed mixtures. Furthermore, since SSC is known to be instable or impacted by redox reactions in presence of many sulfur containing compounds, the intended feeds were slightly modified by excluding components suggested to impact SSC stability such as Cys, GSH (interacting with SSC) and reducing agents like β-mercaptoethanol. Following the pre-screening, high throughput fed-batch experiments were performed with the designed SSC containing feeds and MVDA analysis was applied to identify the cell culture media components impacting the SSC mediated toxicity.

4.2.1. Pre-screening linking metabolic viability and SSC toxicity

An assay detecting the metabolic viability can be used to sense SSC toxicity

To analyze the SSC dose response of various cell lines, a cell-based toxicity assay was used to narrow down a suitable SSC concentration for the fed-batch screening. A suitable SSC concentration should induce cell death in some feeds but should not be toxic for other feeds. Indeed, the broad distribution of components within all the cell culture media formulations is supposed to generate a design space with a variability for each component which can either promote or mitigate SSC toxicity. An initial feasibility study was performed with a CHO cell line, which was cultivated at different cell densities over three days in presence of increasing Cys or SSC concentrations. The toxicity was evaluated by monitoring the metabolic viability which correlates with the total intracellular ATP level. A

defined SSC concentration was expected to lower the ATP level significantly, whereas the same Cys concentration was not expected to lead to cell death, thus validating the assay. Both treatments were evaluated by normalization of the ATP level to untreated cells.

Increasing Cys concentrations from 0.38 mM to 6 mM did not alter the metabolic viability of cultivated CHO cells significantly, whereas the ATP level was lowered by SSC in a dose dependent manner. For example, the metabolic viability of a CHO cell line inoculated with 2.6×10^5 cells decreased below 3% in presence of 1.5 mM SSC, whereas the metabolic viability of 1.5 mM Cys treated cells was at 99.7% (figure 23 A). Interestingly, a metabolic viability of 82.1% was observed at 1.5 mM SSC when 1.3×10^5 cells were inoculated, indicating that the detection of a toxic SSC response requires high cell densities. Since the metabolic viability of Cys treated cells were unaffected at both cell densities (100.4% for 1.3×10^5 cells at 1.5 mM Cys), SSC toxicity is detectable within this assay. For further tests, an inoculation density of about 3×10^5 cells was targeted.

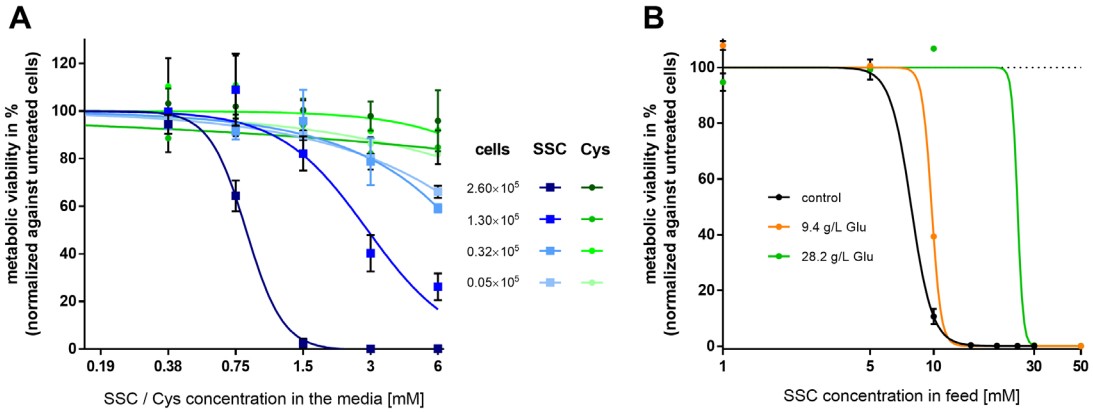

Figure 23. Feasibility study of a cell-based assay to detect SSC toxicity. (A) Serial diluted CHO cells were treated with increasing SSC or Cys concentrations in the media. (B) 3.2×10^5 CHO cells were treated with 10% (v/v) feed with increasing SSC concentrations. Additionally, the regular Glutamate (Glu) concentration (control) was compared to additional 9.4 g/L and 28.2 g/L Glu. After cell cultivation over three days at 37°C, the ATP level was measured (CellTiter-Glo Assay, Promega) and the resulting metabolic viability was normalized to cells cultivated in media without supplementation or feed without any SSC nor Glu and mean values are presented ± SEM (n=2). A non-linear regression of the data is visualized as solid line.

MV_{50} value at a high cell density mimics toxic SSC concentration in fed-batch experiments

In a next step, to better mimic the fed-batch cultivation mode, the assay setup was modified by supplementation of SSC containing feed instead of SSC containing media. Addition of 10% feed was selected representing two feeding steps (5% v/v each) within the intended fed-batch screening. The tested feed contained SSC in a range from 1 to 50 mM and the metabolic viability was decreased to 10.7 % in presence of 10 mM SSC when 3.2×10^5 CHO cells were inoculated (figure 23 B). To assess the cellular response, the SSC concentration leading to 50% metabolic viability (MV_{50}) was determined via non-linear regression. In this setup, a MV_{50} was calculated for a 7.8 mM SSC concentration in the feed.

To proof that the toxicity assay can be used as model to mimic the SSC toxic response in fed-batch experiments, the impact of Glu was analyzed, since Glu supplementation during fed-batch experiments is known to prevent SSC toxicity. Thus, feeds with increasing SSC concentrations were supplemented with either 9.4 g/L and 28.2 g/L Glu leading to a preserved metabolic viability of 39% and 106%, respectively at 10 mM SSC (figure 23 B). Overall, the toxic response was shifted to higher SSC concentrations leading to a calculated MV_{50} of about 9.8 mM SSC when 9.4 g/L Glu was applied and a MV_{50} of about 25 mM SSC by addition of 28.2 g/L Glu (3.2-fold higher MV_{50} than without Glu supplementation). Data indicate that additional Glu supplementation up to 28.2 g/L is not able to completely prevent SSC toxicity but decreases the cell sensitivity to higher SSC concentrations.

To examine whether the previous determined inoculation density of 3×10^5 cells allows a good prediction of the SSC toxicity in a fed-batch experiment (via MV_{50} value) a comparability study was performed with three different inoculation densities. When using a CHO-K1 cell line in combination with feed220, a toxic response was observed at SSC concentrations above 20 mM. Following addition of 10% feed within two independent cell-based assays, a MV_{50} of 17.7 mM, 19.8 mM and 47 mM SSC was calculated when about 6×10^5, 3×10^5 and 1.5×10^5 CHO cells were inoculated, respectively (appendix figure 47). Data confirm that the calculated MV_{50} with an inoculation density of $>3\times10^5$ cells correlates to the toxic concentration observed in a fed-batch. Overall, data confirm that the cell-based assay is suitable to narrow down an appropriate SSC concentration for different feeds intended for the high throughput screening.

High feed concentrations are not suitable for the cell-based assay

A screening of the feed panel without any Cys-source was performed to explore effects triggered by the feed diversity alone. Eight CHO cell lines were selected to screen the influence of a consistent feed addition (10%), whereby no toxicity was expected for feeds without SSC. To compare the feeds, ATP level of cells was normalized to cells cultivated in media without feed addition. For simplicity, feeds were numbered relative to increasing feed concentrations (g/L).

Minor changes were observed for feed 1 to 9 with a maximal ATP reduction of 16% when clone 6 was supplemented with 10% feed 6 (figure 24). This was considered to be within the biological variability of the method. In comparison, the addition of the most concentrated feed 10 with 123.3 g/L reduced the ATP level of all clones except for clone 6. For example, about 79% ATP reduction was observed for clone 5. Data indicate an overfeeding through feed 10 in most of the cell lines, which is either toxic for the cells or triggered a reduced growth. By diluting feed 10 to 80 g/L, the overfeeding was reduced, which was confirmed by higher ATP level. For example, the ATP level of clone 5 was only 40% lower compared

to media for feed 10 at 80 g/L. Further dilution to 25 g/L resulted in similar growth of all clones compared to cultivation without feed addition. Thus, both diluted feed 10 versions (80 and 25 g/L) were integrated into the pre-screening, whereby the original concentration was not excluded as utilization of the undiluted feed was intended for the determining screening at the end.

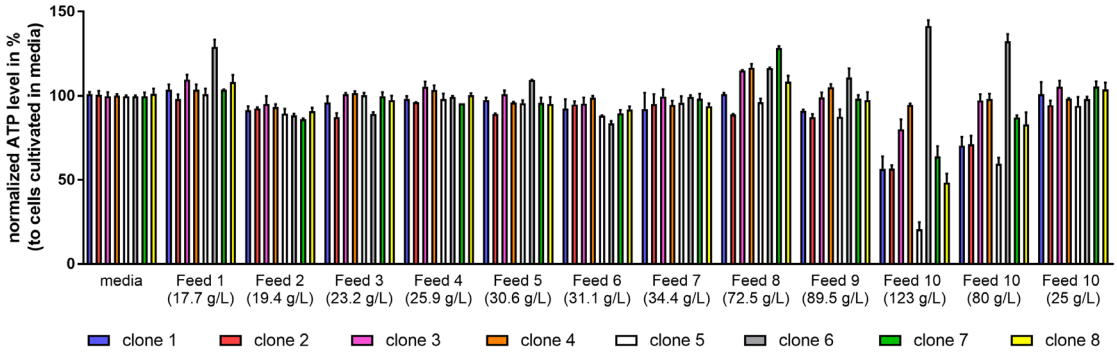

Figure 24. Impact of selected feeds within cell-based assay. About 3×10^5 cells of eight different clones were treated with 10% (v/v) of ten different Cys depleted feed, whereby feed 10 was additionally diluted from 123 g/L to 80 g/L and 25 g/L. After cell cultivation over three days at 37°C, the ATP level was measured (CellTiter-Glo Assay, Promega) and the resulting ATP level was normalized to cells cultivated in media without supplementation and mean values are presented ± SEM (n=2).

4.2.2. SSC toxicity is influenced by the feed formulation and the cell line

To link SSC toxicity to feed components, the selection of a proper SSC concentration for the fed-batch experiments is most critical. To be able to use MVDA linking feed components with the toxicity of SSC, a diverse SSC response with some toxicity is required. Therefore, the cell-based assay was applied to determine appropriate SSC concentrations for the following fed-batch experiments. Key learnings from a first fed-batch experiment using two clones and two SSC concentrations were used to adapt the experimental setup within the second screening using four clones and only one SSC concentration.

SSC toxicity within a toxicity assay is impacted by the feed formulation

A screening of the feed panel with increasing SSC concentrations from 1 mM to 50 mM SSC was performed to define a suitable SSC concentration for the fed-batch experiment. To detect SSC toxicity, data from three independent experiments were normalized to the respective feed without SSC, to adjust changes of the metabolic viability caused by the feed formulation only.

Cultivation of clone 1 with addition of 10 mM SSC reduced the metabolic viability *e.g.* to 92% using feed 9, to 54% by feed 8 and the highest reduction was observed with feed 2 to about 20% indicating a diverse SSC response due to different feed formulations (figure 25). In presence of 30 mM and 50 mM SSC in feed 1 to 9 as well as in feed 10 at 25 g/L, no metabolic viability was observed indicating that all cells were dead due to SSC treatment.

Via non-linear regression, MV_{50} values in a range from 7.8 mM (feed 4) to 14.6 mM SSC (feed 9) were calculated (table 6). In comparison, a metabolic viability of 78% and 22% was observed for cells treated with the high concentrated feed 10 (123 g/L) and the diluted feed 10 (80 g/L) at 30 mM SSC, respectively. Addition of the highest SSC concentration (50 mM) in feed 10 at 123 g/L and 80 g/L reduced the metabolic viability of clone 1 to approximately 60% and below 1% respectively. Therefore, an ambiguous MV_{50} value was calculable for feed 10 diluted to 80 g/L (27.1 mM SSC), whereas no calculation was possible for the high concentration (123 g/L). Data obtained with feed 10 and different dilutions demonstrate that the feed concentration is critical for the toxicity of SSC in the cell-based assay. The addition of increasing feed concentrations (feed 1 to 9) resulted in MV_{50} values of 12.2 mM, 7.9 mM, 9.3 mM, 7.8 mM, 11.7 mM, 12.8 mM, 12.2 mM, 10.2 mM and 14.6 mM SSC. Whether the feed concentration correlates with the calculated MV_{50} for SSC toxicity was assessed by correlating the MV_{50} values obtained from all feeds to the feed concentration. A low R^2 value of 0.25 was obtained which indicates that there is no overall correlation of the feed concentration to the SSC toxicity for clone 1 for all ten feeds independently of the feed formulation.

Finally, the calculation of an average MV_{50} was based on data from feed 1 to 9 and feed 10 at 25 g/L. A mean MV_{50} of 11.2 mM SSC was calculated, which is the SSC concentration intended to result in 50% toxicity for clone 1 in a fed-batch screening using these feeds.

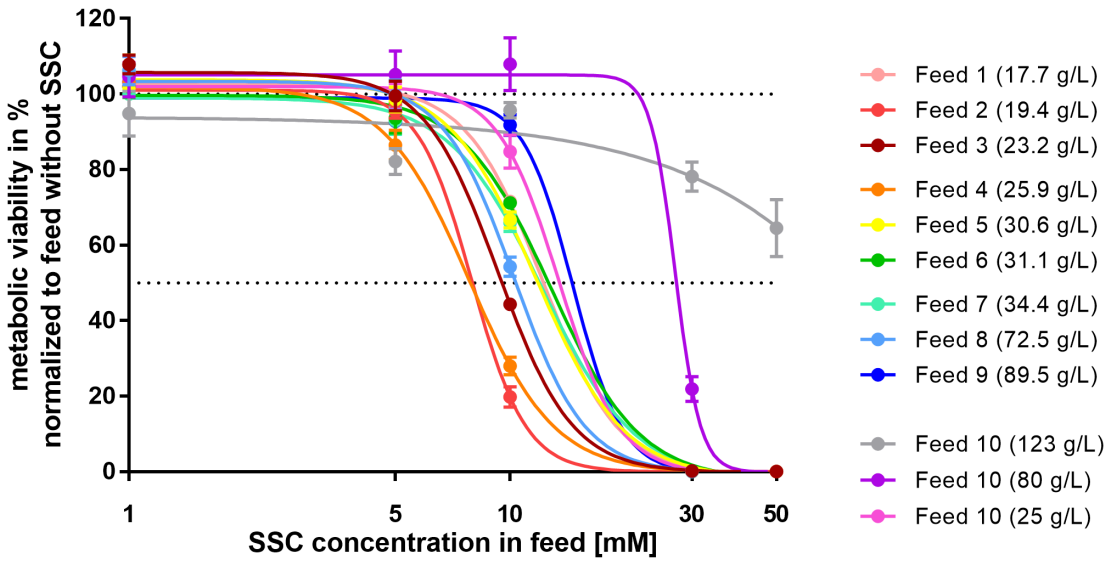

Figure 25. Feed dependent SSC dose response of CHO clone 1. About 3×10^5 cells were treated with 10% (v/v) of 10 Cys depleted feeds (feed 10 with two additional dilutions) supplemented with increasing SSC concentrations in a range from 1 to 50 mM. After cell cultivation over three days at 37°C, the ATP level was measured (CellTiter-Glo Assay, Promega) and the resulting ATP level was normalized to cells cultivated in the respective feed without SSC. Data is expressed as mean values ± SEM (n=4). A non-linear regression of the data is visualized as solid line and was used to calculate the SSC concentration leading to 50% metabolic viability.

Toxic SSC response is cell line dependent

In a next step, the response of seven additional cell lines upon SSC treatment was investigated. At least two independent experiments were performed per clone and the normalized data was merged similar to clone 1. The SSC dose response data from all cell lines are visualized in appendix figure 48 and the calculated MV_{50} values of each clone in combination with each feed are summarized in table 6.

Table 10. Calculated SSC concentration in mM leading to 50% metabolic viability (MV_{50}) using ten feeds and eight CHO clones. The average MV_{50} was calculated per clone for feed 1-9 and feed 10 diluted to 25 g/L.

Feed	[g/L]	Clone 1 (n=3)	Clone 2 (n=3)	Clone 3 (n=3)	Clone 4 (n=2)	Clone 5 (n=2)	Clone 6 (n=4)	Clone 7 (n=3)	Clone 8 (n=2)
1	17.7	12.2	12.3	13.3	11.9	12.7	13.0	13.9	23.1
2	19.4	7.9	7.8	7.9	8.8	9.8	10.8	12.4	15.6
3	23.2	9.3	9.6	11.2	10.2	11.8	11.7	13.7	17.3
4	25.9	7.8	7.9	7.8	8.5	12.1	11.9	13.2	16.7
5	30.6	11.7	12.9	12.4	12.8	11.1	9.2	15.5	20.9
6	31.1	12.8	11.5	11.8	12.7	11.3	12.0	14.0	21.4
7	34.4	12.2	11.6	10.2	12.9	13.1	12.4	13.2	16.4
8	72.5	10.2	11.3	10.5	10.6	12.2	10.4	13.5	19.0
9	89.5	14.6	17.8	16.0	14.1	12.2	21.4	14.8	26.6
10	123.3*	NA	NA	NA	NA	NA	NA	NA	NA
10	80.0**	27.1	37.2	33.0	29.6	33.9	31.1	49.1	68.6
10	25.0	13.4	10.7	13.1	13.4	14.7	24.4	14.7	21.2
Avg.		**11.2**	**11.3**	**11.4**	**11.6**	**12.1**	**13.7**	**13.9**	**19.8**

* MV_{50} of feed 10 was not calculated due to overfeeding using the original feed concentration. ** Feed 10 was diluted to 80 g/L and calculated MV_{50} values from the fitted curves were ambiguous. Not applicable (NA)

The cellular response of all cell lines to one feed was used to assess a cell line dependency. Regarding the response to feed 4, calculated MV_{50} values were in a range from 7.8 mM (clone 1 and clone 3) to 16.7 mM SSC for clone 8. The more than 2-fold calculated difference, demonstrates that the toxic SSC concentration is clone dependent and thus has to be defined independently for each clone.

Similar to clone 1, an average MV_{50} was calculated for each clone with values from feed 1 to 9 and the diluted feed 10 (25 g/L). Afterwards, clones were numbered by increasing mean MV_{50} values (table 6). The average MV_{50} values ranged from SSC sensitive to less sensitive clones with SSC concentrations of 11.2 mM (clone 1), 11.3 mM (clone 2), 11.4 mM (clone 3), 11.6 mM (clone 4), 12.1 mM (clone 5), 13.7 mM (clone 6), 13.9 mM (clone 7) and 19.8 mM (clone 8), demonstrating different SSC sensitivities of the tested cell lines.

Setting the SSC concentration to the average MV_{50} values was expected to result in a balanced SSC response triggering a toxic response with some feeds due to a prolonged cultivation during fed-batch experiments in combination with a broad distribution of components accelerating but also mitigating SSC toxicity. However, within a first fed-batch screening, two SSC concentrations adjacent to the calculated MV_{50} value per clone were

tested to reduce the probability that the selected SSC concentration yields in a toxic response for either all or no feed conditions. Based on the calculated MV_{50} value of 13.7 mM for clone 6, supplementation of 16 mM SSC in all feeds was tested to a toxicity in more than 50% of the conditions, whereas 9 mM was selected to ensure the survival of cells. For simplicity, 16 mM SSC was also tested for clone 7 with an average MV_{50} of 13.9 mM, whereas 13 mM SSC was selected as second SSC concentration being closer to the calculated MV_{50}. Further clones were tested in an additional experiment to allow experimental adjustments.

Increasing SSC concentration leads to elevated toxicity using two CHO clones

The cell-based assay allowed an estimation of the SSC toxicity, but in contrast to the assay with a cultivation time of three days, a common fed-batch experiment lasts 14 days. To assess the SSC response within this cultivation process, two cell lines producing an IgG1 were used in a small-scale fed-batch screening to test the impact of the feed panel.

Although feed 10 diluted to 25 g/L was used for calculation of the mean MV_{50}, the undiluted feed 10 was used in the fed-batch screening. This decision was based on the fact, that the high concentrated feed 10 formulation was balanced for cellular demand during fed-batch experiments. Thus, the use of a diluted feed might induce depletion of specific components by extending the cultivation time from three days in the assay to 14 days in the fed-batch experiment. To increase the diversity of the tested feeds, the ten main feeds containing the same SSC concentration were mixed in a 1:1 manner, reaching a total of 55 feed mixtures that were used in the fed-batch. Additionally, a control feed without SSC (with 13.9 mM Cys) was applied to estimate the growth of the respective clone with this feeding strategy.

The cellular response was assessed via the VCD, whereby SSC toxicity was evaluated manually, since neither the VCD as function of the time nor the viability were able to illustrate the SSC specific response. More precisely, SSC concentration was not selected for optimal growth but to induce toxicity, so that cellular growth might be lowered by addition of SSC-containing feeds. As consequence, a reduced growth might yield a similar AUC of VCD as a toxic response after initial high growth. Therefore, only a drastic reduction of the VCD within a short time was regarded as SSC specific toxicity. Whenever a toxic response was observed for at least one biological replicate, this feed mixture was classified as toxic for subsequent MVDA. For simplicity, figure 26 visualizes the SSC response of the ten main feeds in different colors, whereas the resulting feed mixtures are visualized in light grey. The final classifications of the SSC response are summarized for all cell lines in the appendix table 12.

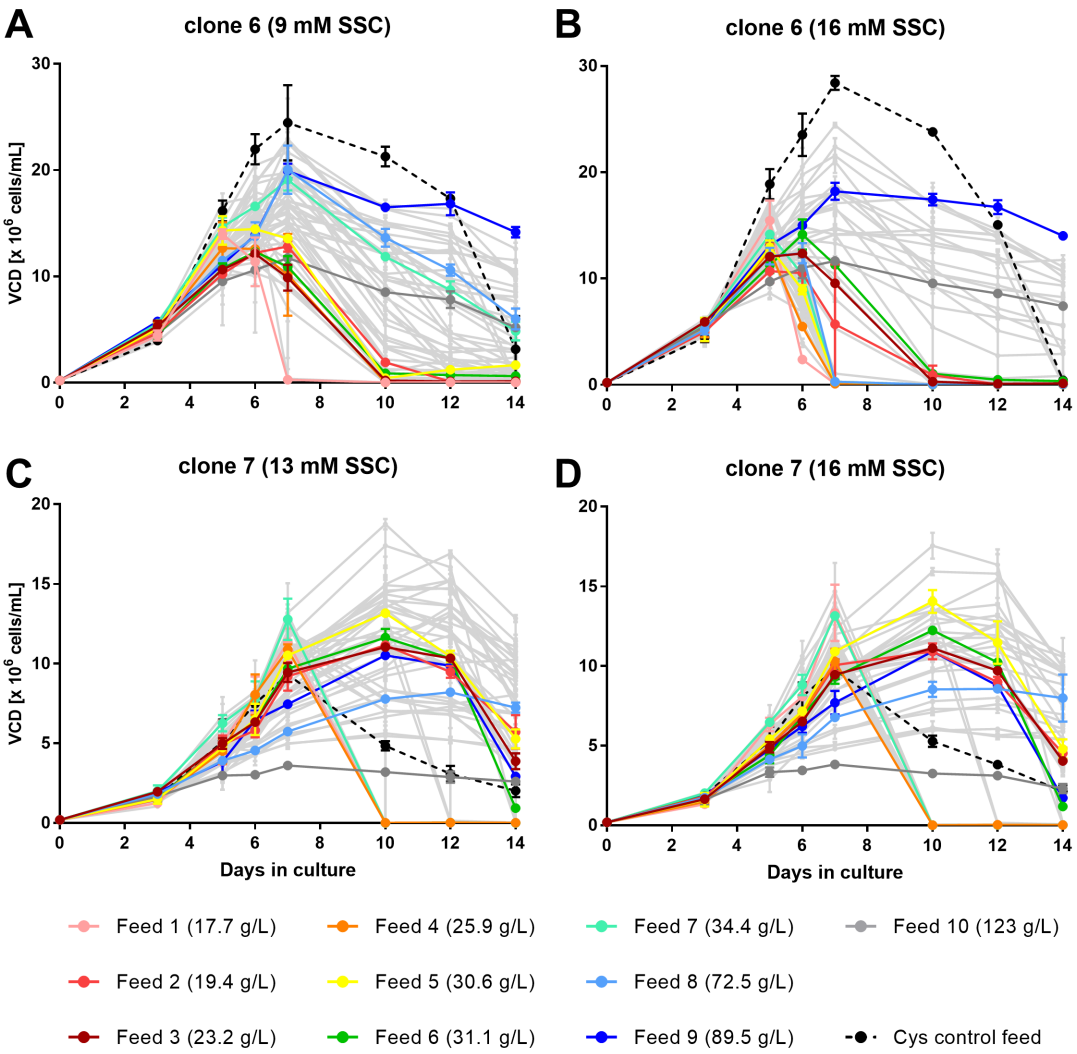

Figure 26. SSC response of clone 6 and clone 7 during fed-batch experiments. Suspension CHO cells were seeded at 3×10^5 cells/mL in deep-well plates, incubated at 37°C, 5% CO_2, 80% humidity and agitated at 320 rpm. Ten main feeds with a distinct SSC concentration were mixed in a 1:1 manner leading to 55 feed mixtures (visualized in light grey). 50 µL of each feed mixture was added on day 3, 5, 7 and 10. Viable cell density (VCD) is visualized of clone 6 with feeds containing either (A) 9 mM SSC or (B) 16 mM SSC, whereas VCD of clone 7 was fed with feeds containing either (C) 13 mM SSC or (D) 16 mM SSC. Data presents mean values of two biological replicates ± SEM.

First, the cellular response of clone 6 in presence of 9 mM SSC was assessed. A drastic toxic response was observed for feed 1 on day 7 (figure 26 A). During further cultivation, feed addition on day 7 triggered a toxic response by feed 2 to 6, whereby feed 7 and 8 reduced the VCD compared to feed 9, but no toxicity was detected. Regarding all feed mixtures tested within this fed-batch experiment, 24 conditions showed a toxic response, which presents 42.1% of all tested conditions (appendix table 12).

By increasing the SSC concentration from 9 mM to 16 mM SSC, the toxic response of *e.g.* feed 5 was shifted from a detection on day 10 to day 7 (figure 26 B). This shift to an earlier time point was also observed for feed 1, 4, 7, 8 and one replicate of feed 2. The VCD of the second replicate (feed 2) indicated a delayed toxic response on day 10 (of note: on day 8

and 9, no measurement was performed). Additionally, application of feed 3 and 6 caused a toxic response observed on day 10, whereas the VCD of feed 9 and feed 10 were higher compared to the Cys control on day 14. Regarding all feed mixtures, supplementation of 16 mM SSC yielded in a toxic response within 36 conditions which represents 63.2% of all conditions (appendix table 12). The data sets indicate that the toxic response was enhanced by increasing the concentration from 9 to 16 mM SSC, since more cells died, and the response was also shifted to earlier time points, thus demonstrating the importance of an appropriate SSC concentration. Overall, the observed toxicity in response to both selected SSC concentrations for clone 6 (52.7% toxicity at 9 mM and 76.4% toxicity at 16 mM SSC) are suitable for a statistical analysis.

Regarding clone 7, the addition of feed 1, 4 and 7 with 13 mM SSC induced a toxic response, which was detected on day 10 (figure 26 C). All remaining main feeds showed a high VCD until day 12, whereby the reduction on day 14 was not assigned to SSC toxicity, since SSC unrelated toxic by-products might have accumulated until the end of cultivation. Considering all feed mixtures, a toxic response was observed in 14 conditions (24.6%) when 13 mM SSC was applied (table 12).

By increasing the SSC concentration from 13 mM to 16 mM, the same feeds (feed 1,4 and 7) triggered a toxic response, observed on day 10 (figure 26 D). However, a slightly increased number of feed mixtures (20 conditions; 35.1%) triggered a toxic response when using 16 mM SSC (table 12). Although addition of 16 mM SSC was higher than the calculated MV_{50} value of 13.9 mM, a toxic response was observed in less than 50% of the conditions.

Whether a reduced growth of this cell line is responsible for a reduced toxicity was investigated next. Irrespective of the applied SSC concentration, a reduced growth was observed for feed 10 (123 g/L) reaching a max VCD on day 7 with about 3.8×10^6 cells/mL and a slightly reduced growth was observed for feed 8 (72.5 g/L) reaching 8.6×10^6 cells/mL on day 12. However, feed 9 (89.5 g/L) with a higher concentration compared to feed 8 reached a max VCD with about 10.9×10^6 cells/mL, indicating that the feed concentration alone is not determining the toxic response. Still overfeeding might counteract SSC metabolism.

Overall, the observed toxic response of clone 7 was lower compared to clone 6, but data set is still applicable for MVDA. Concluding, selection of the SSC concentration for each clone based on the calculated MV_{50} proved to be useful to narrow down the concentration but a slightly higher SSC concentration than the calculated MV_{50} was thought to be advantageous for the next screening.

Four additional CHO clones demonstrated a diverse SSC response

With the aim to increase the biological variability of the SSC response, four additional CHO clones with different growth rates and productivities were investigated next. Based on the previous study, the experimental setup was slightly modified. Both feed 10 dilutions (80 g/L and 25 g/L) were included in this second fed-batch screening to increase the feed diversity and to overcome possible overfeeding of the cells.

By mixing these twelve feeds with the same SSC concentration in a 1:1 manner, a total of 78 feed mixtures plus a Cys control was tested next. Due to the testing of four clones, only one SSC concentration was applied, which was slightly higher than the calculated MV_{50}. 14 mM SSC was applied for clone 2, 4 and 5 having a similar average MV_{50} of 11.3 mM, 11.6 mM and 12.1 mM, respectively. The toxicity assay indicated that clone 8 was the least sensitive to SSC toxicity (MV_{50} of 19.8 mM) and was treated with feed mixtures containing 22 mM SSC. Toxic response was assessed by daily VCD measurement (except the weekend).

First, the impact of the high concentrated feed 10 and respective dilutions (in presence of 14 mM SSC) was assessed to evaluate if the feed dilutions cause a nutrient limitation during the fed-batch experiment. The high concentrated feed 10 (123 g/L) yielded a max VCD of 4.9×10^6 cells/mL on day 5, whereas the dilution to 80 g/L yielded a max VCD of 6.4×10^6 cells/mL on day 7 (figure 27 A). By further dilution of feed 10 to 25 g/L a max VCD of 11.6×10^6 cells/mL was observed on day 7. The higher VCD correlating with the dilution indicated no depletion of crucial cell nutrients during the 14-days fed-batch experiment, whereas overfeeding inhibited the cell growth, significantly. However, with this data set it was not possible to judge if this overfeeding interferes with SSC metabolism.

Regarding the additional main feeds, addition of 14 mM SSC was not toxic for clone 2 except for feed 5 with a toxic response detected on day 7. This low toxicity was highly unexpected, since the calculated MV_{50} was rather low with 11.3 mM. Considering all feed mixtures, only six conditions induced a toxic response through the addition of 14 mM SSC, which reflects only 7.5% of all conditions (appendix table 12). This overall low toxic response observed for clone 2 makes the data set unsuitable for statistical analysis.

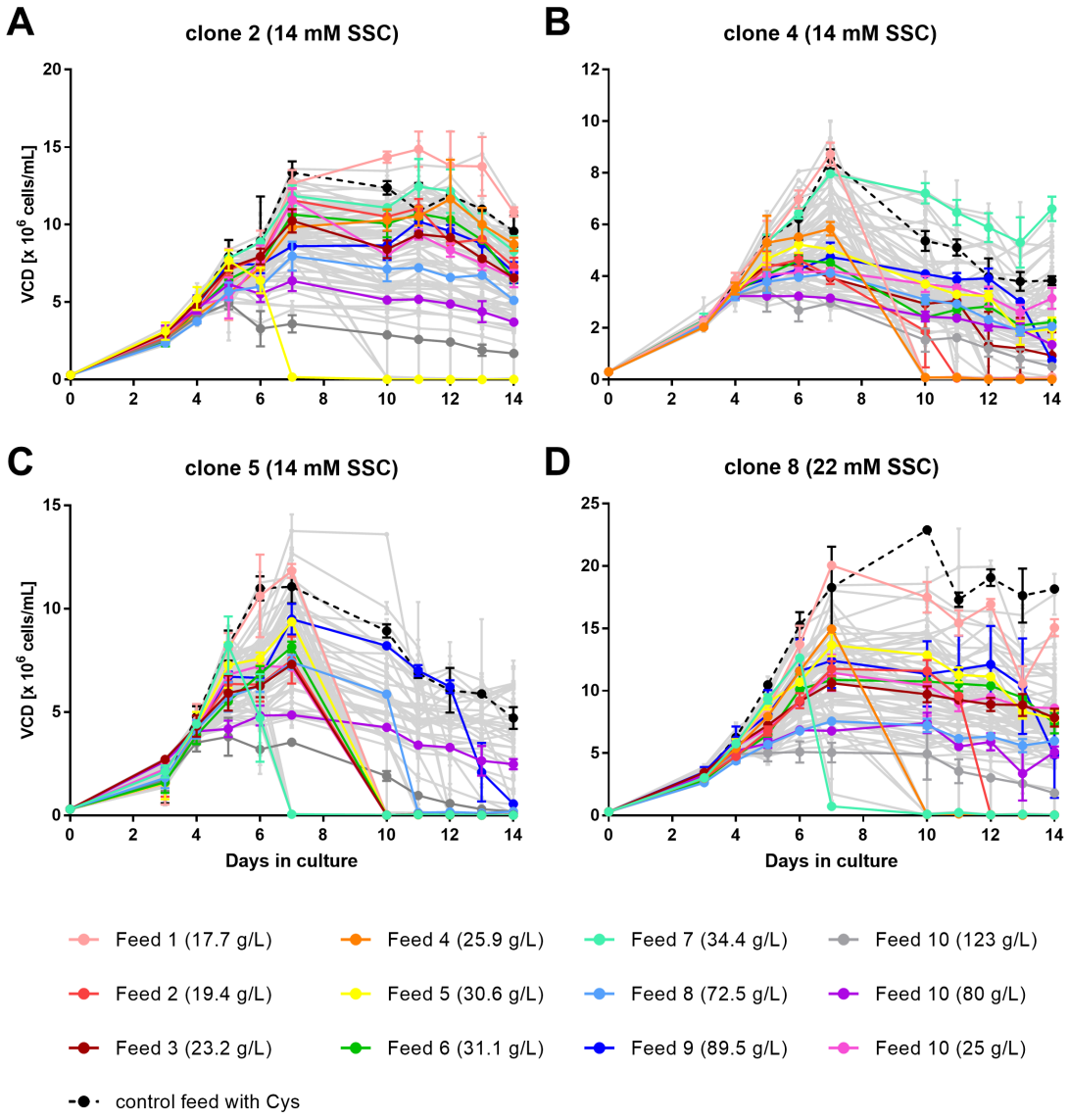

Figure 27. SSC response of four CHO clones during fed-batch experiments. Suspension CHO cells were seeded at 3×10^5 cells/mL in deep-well plates, incubated at 37°C, 5% CO_2, 80% humidity and agitated at 320 rpm. Ten main feeds and two additional feed 10 dilutions with a distinct SSC concentration were mixed in a 1:1 manner leading to 78 feed mixtures (visualized in light grey). 50 µL of each feed was added on day 3, 5, 7 and 10. Viable cell density (VCD) is visualized of (A) clone 2 fed with 14 mM SSC (B) clone 4 fed with 14 mM SSC, (C) clone 5 fed with 14 mM SSC and (D) clone 8 fed with 22 mM SSC. Data present mean values of two biological replicates ± SEM.

Regarding clone 4, feed mixtures were similarly supplemented with 14 mM SSC, whereby after addition of feed 1 and feed 4, a toxic response was observed on day 10 (figure 27 B). Here it is important to mention that a slow decrease in VCD of *e.g.* feed 2 was thought to be an unspecific response and was not counted as SSC toxicity. Overall, a toxic response was observed in 22 conditions using clone 4, which reflects 27.5% of all conditions (appendix table 12).

Cultivation of clone 5 in presence of 14 mM SSC caused a fast viability drop on day 7 when feed 7 was applied (figure 27 C). A similar drop was observed on day 10 for feeds with increasing concentrations (feed 1 – 6) and feed 10 (25 g/L), whereas feed 8 triggered toxicity was observed on day 11. Addition of feed 9 and both high concentrated feed 10 (80 and 123 g/L) showed no SSC toxic response. Including all feed mixtures, a toxic response was induced in 47 conditions, which reflects 59.5% of 79 conditions (one condition lacking due to inoculation error) making this data set highly suitable for statistical analysis (appendix table 12).

The pre-screening indicated that clone 8 is the least SSC sensitive clone tested so far and thus a higher SSC concentration of 22 mM was applied. Addition of SSC-containing feed resulted in toxic response on day 7 for feed 7, day 10 for feed 4, and day 12 for feed 2 (figure 27 D). Including all feed mixtures, a toxic response was observed in 13 conditions which represents 16.3%, which indicates that the SSC concentration was still too low for clone 8 (appendix table 12).

In summary, statistical analysis requires a balanced SSC response to correlate SSC toxicity with the feed composition. Clone 2 and clone 8 showed minor toxic response with 7.5% and 16.3% of all conditions leading to an SSC mediated cell death, respectively. In comparison, data of clone 4 (27.5% of all conditions leading to an SSC mediated cell death), clone 5 (59.5%), clone 6 (63.2%) and clone 7 (35.1%) were thought to be suitable for statistical analysis.

4.2.3. Use of multivariate data analysis to link feed formulation and SSC toxicity

The biological complexity of the toxic SSC response makes a regression and furthermore the prediction of feed components which might trigger SSC toxicity difficult. A powerful statistical data analysis is required to build biologically relevant conclusions from the fed-batch screenings using four different CHO clones and up to 80 different feed mixtures containing 93 components with a broad concentration range.

The SSC response was assessed via a model describing the relation between the feed components and the observed cellular response. More precisely, the *X*-matrix was built by the concentration of all components in each feed mixture (plus the overall feed concentration), whereby the *Y*-matrix was defined through the fed batch observation by classifying each feed mixture as either toxic or not-toxic (appendix table 12). To focus on data variation which only correlates with the observed toxicity, the orthogonal projection to partial least squares discriminant analysis (OPLS-DA) was applied. Thereby, the non-correlated systematic variation in the *X*-matrix is removed, which reduces model complexity. Separate models were used for each clone since the response (*Y* variables) might be different for two clones using the same feed formulation (*X* variable).

Assessment of the models indicates modest predictability of components correlating with SSC toxicity

In a first step, the scatter plots showing the relationship of all observations for a specific cell clone was used to evaluate whether each model is able to discriminate between toxic and not toxic observations. The assessment of each model was then based on the resulting goodness of fit and predictability of the model and the coefficient plots were used to pinpoint components with either a negative or a positive correlation to SSC toxicity. In a final step, identified components correlating with the toxicity were tested through the cell-based assay. The OPLS-DA model explaining the SSC toxicity observed for clone 6 treated with feeds containing 16 mM SSC was built by two principle components. The predictive component (separating toxic and non-toxic observations) explained 22.0% of the data variance, and an orthogonal component explained 14.1% of the variance as visualized in the two-dimensional score plot (figure 28 A). The score plot revealed a good discrimination of both classes, whereby four mixtures are apparently misclassified (feed mixture 17, 18, 22 and 23). Further investigation revealed that *e.g.* mixture 18 displayed an ambiguous result with one biological replicate having a reduced VCD whereas the other was viable until the end of cultivation. Since classes were defined as toxic whenever one replicate showed a toxic response, the observed toxicity might not be SSC related. However, this cannot be proven hence class assignment was not modified. Additionally, four high concentrated feeds, namely feed 8 (72.1 g/L), feed 10 (123 g/L), feed 9 (89.7 g/L) and mixture 62 (mix of feed 9 and 10 see appendix table 11; 106.4 g/L) are plotted outside of the confidence ellipse with a significance level of 0.05, indicating that these feeds have a different cellular impact which is not modeled using OPLS-DA. However, the model of clone 6 yielded a R^2X of 0.361, R^2Y of 0.683 and Q^2 of 0.529 (figure 28 B). The low R^2X values indicate that the concentration distribution of all feed mixtures is rarely explained within this model, which is uncritical for the study purpose, whereas R^2Y above 0.5 indicates a proper model to discriminate between toxic and not toxic. Similarly, Q^2 above 0.5 suggests a good predictability of the model and allows further investigation.

Additional validation of the built model was achieved by the coefficient plots visualizing the relationship of each component to the class. Regarding the toxic class, positive regression coefficients were expected for components aggravating SSC toxicity, whereas negative coefficients for those counteracting the toxicity. Addition of two feed compounds, namely Glu and Copper, were demonstrated to circumvent SSC toxicity in fed batch experiments and were expected to be negatively correlated with the toxic class in the model. Indeed, a negative correlation for Glu (-0.0329 $\pm$ 0.0105) and Copper (-0.0195 $\pm$ 0.0157) was observed within the coefficient plot of clone 6 (figure 28 C). On the other hand, four components had a positive correlation with the toxic response, namely the amino acid L-

tyrosine (0.0481 ± 0.0434), the growth factor insulin (0.0221 ± 0.0183), a synthetic analogue of an insulin-like-growth factor 1 (IGF-1) having an Arg at the third position instead of Glu (R3) and additional 13 amino acids at the N-terminus (Long) thus known as Long R3 IGF-1 (0.0217 ± 0.0169) and the dipeptide L-Ala-L-Gln (0.0107 ± 0.0083). The data set suggests that increasing concentrations of these components might increase SSC toxicity. However, the rather high error bars indicate a low confidence within this prediction, so that evaluation of the other clones is necessary.

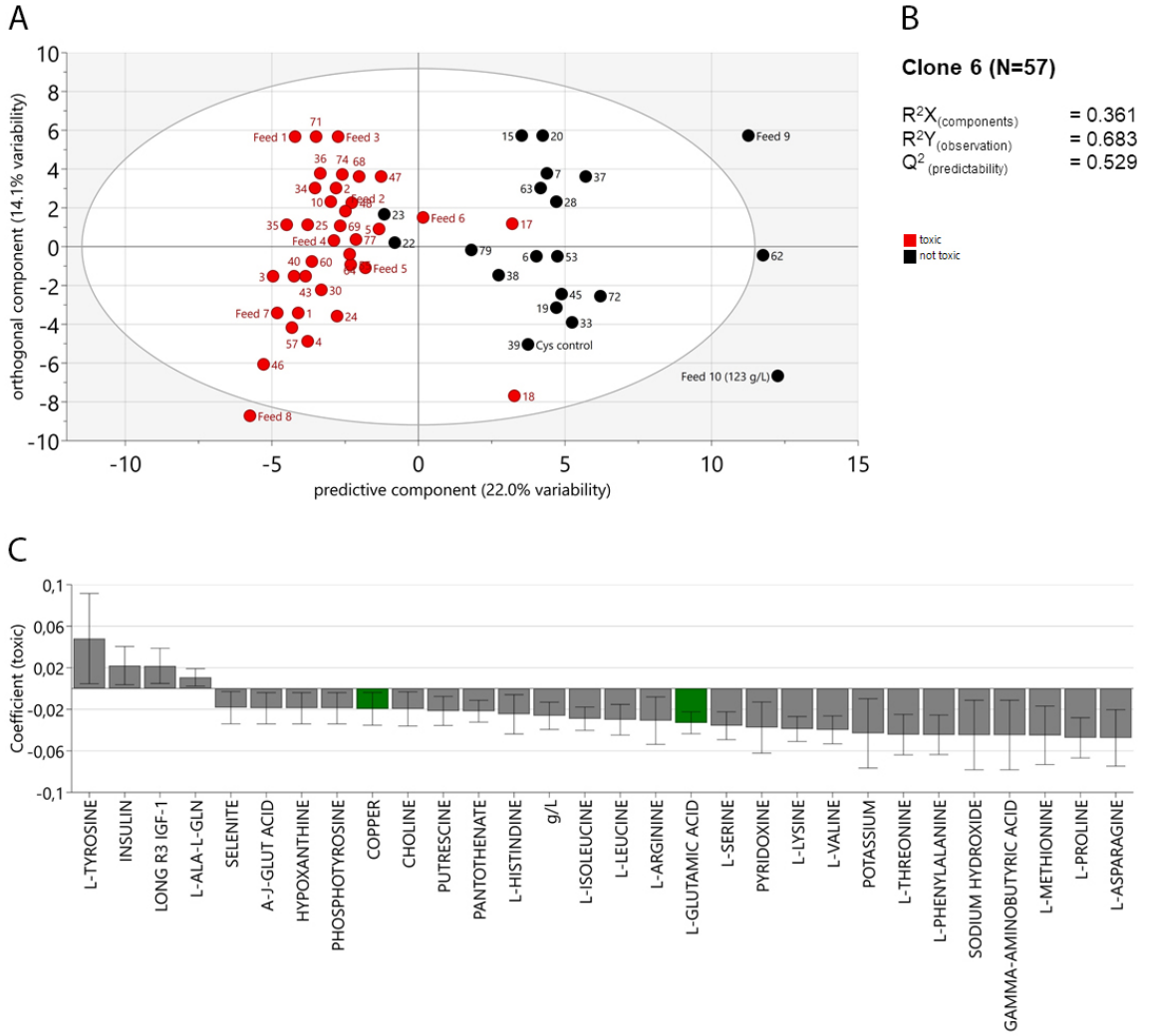

Figure 28. OPLS-DA model describing the SSC response of clone 6. The *X*-matrix was built by the composition of 57 feed mixtures and the *Y*-matrix was defined through the observed SSC response within a fed-batch screening using the respective feeds (toxic in case of a sharp reduction of the viable cell density). (A) 2D-score plot of the feed mixtures classified as either toxic (red) or not toxic (black). The predictive component explains 22.0% of the data variance and an orthogonal component explains 14.1% of the variance. The ellipse defines the confidence level with a significance level of 0.05 based on Hotelling's T². (B) The model of clone 6 yielded a R^2X of 0.361, R^2Y of 0.683 and Q^2 model predictability of 0.529. (C) The coefficient plot visualizes components correlating positively or negatively with the toxic response. Known components to reduce SSC toxicity are highlighted in green with a negative correlation to the toxic response.

Modeling the response of clone 7 upon treatment with 16 mM SSC was based on a predictive component explaining 16.3% of the variability, whereby three orthogonal components explain 20.0%, 13.4% and 11.9% of the variability in the data set (figure 29 A). The fact that the orthogonal component explains a higher variability of the data than the predictive component indicates that other factors impact the data more importantly than the factors explaining the difference between toxic and not toxic. Only feed 10 was positioned beyond the ellipse and a proper discrimination was observed between the toxic and not toxic observation classes. Using these components to explain the data for clone 7, a R^2X of 0.618 was reached within this model (figure 29 B). Furthermore, the model yielded a R^2Y of 0.650 and Q^2 of 0.510 indicating a modest model.

However, the negative correlation of Glu to the toxic SSC response (-0.0131 $\pm$ 0.0118) had high error bars, whereby the negative correlation of copper was not significant (figure 29 C). On the other hand, eleven components were observed with a positive correlation with phosphate having the highest coefficient of 0.0984 ± 0.0587. Decreasing coefficients were observed for L-Ala-L-Gln (0.0765 ± 0.0145), Long R3 IGF-1 (0.0720 ± 0.0169) and insulin (0.0684 ± 0.0184), which were already observed in clone 6. Further components with positive coefficients are a fatty acid mix (0.0519 ± 0.0161), citrate (0.0517 ± 0.0153), pyruvate (0.0498 ± 0.0456), iron (0.0420 ± 0.0186), ethanolamine (0.0416 ± 0.0183), α-tocopherol (0.0322 ± 0.0242) and hydrocortisone (0.0288 ± 0.0196).

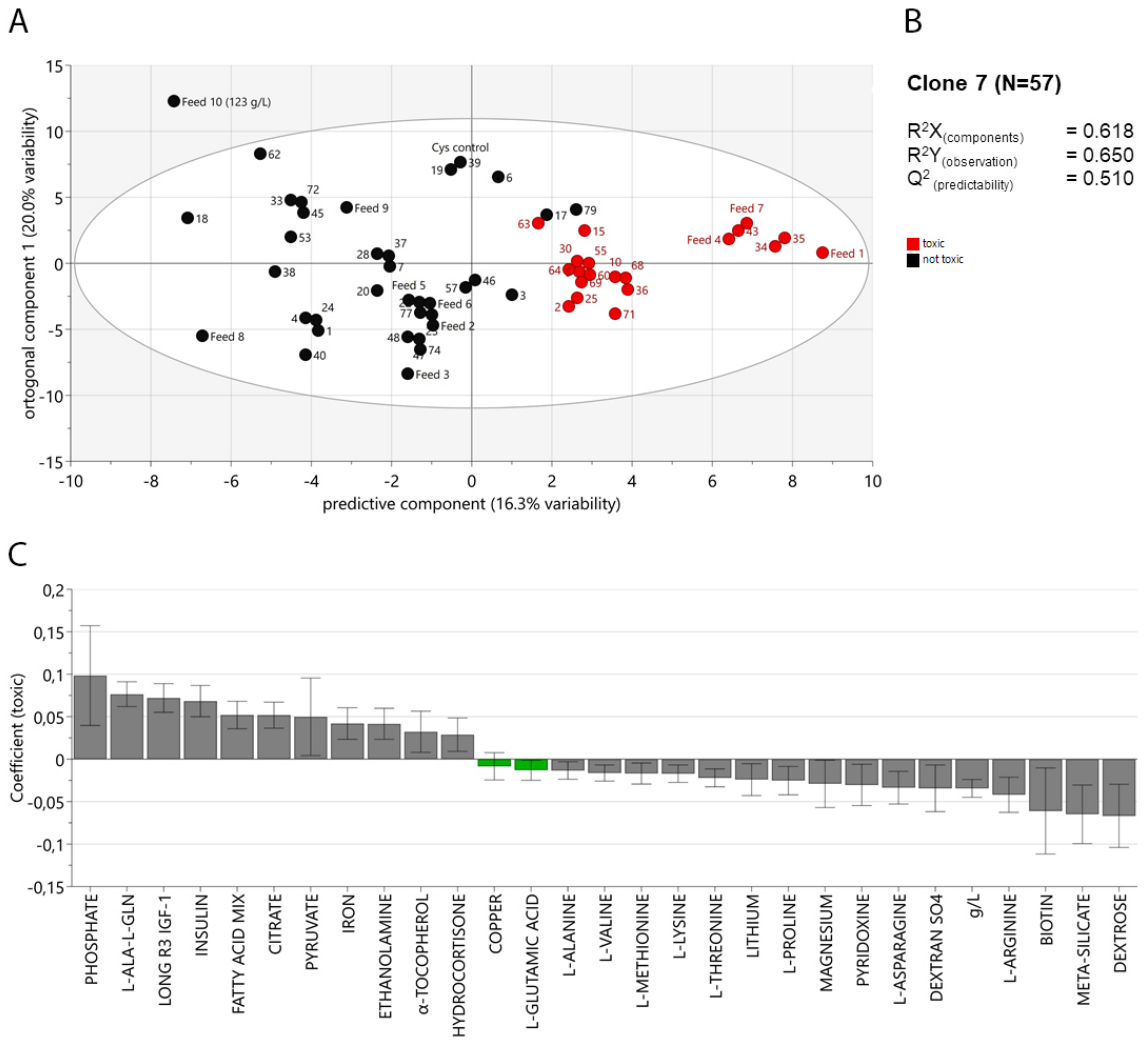

Figure 29. OPLS-DA model describing the SSC response of clone 7. The X-matrix was built by the composition of 57 feed mixtures and the Y-matrix was defined through the observed SSC response within a fed-batch screening using the respective feeds (toxic in case of a sharp reduction of the viable cell density). (A) 2D-score plot of the feed mixtures classified as either toxic (red) or not toxic (black). The predictive component explains 16.3% of the data variance and three orthogonal components explain 20.0%, 13.4% and 11.9% of the variance. The ellipse defines the confidence level with a significance level of 0.05 based on Hotelling's T². (B) The model of clone 7 yielded a R2X of 0.618, R2Y of 0.650 and Q2 model predictability of 0.510. (C) The coefficient plot visualizes components correlating positively or negatively with the toxic response. Glutamic acid and copper as known components to reduce SSC toxicity is highlighted in green with a negative correlation.

The OPLS-DA model explaining the SSC toxicity observed for clone 4 with 80 feed mixtures (79 mixtures containing 14 mM SSC) was built by just one predictive component explaining 26.6% of the data variance and yielded a good discrimination of the SSC response with the toxic response below zero and not toxic above zero (figure 30 A). Only feed 10 was positioned above the 3-fold significance level, whereby mixture 8 and mixture 62 were positioned above the 2-fold significance level. Thereby, the model yielded R^2X of 0.266, a R^2Y of 0.402 and Q^2 of 0.361 indicating a rather weak model to predict feed components triggering a toxic response (figure 30 B). However, a negative correlation of Glu (-0.0212 ± 0.0039) and copper (-0.0160 ± 0.0043) were observed and thereby supporting the model

predictability. Feed components with positive coefficients were calcium (0.0221 ± 0.0161), a fatty acid mix (0.0174 ± 0.0138), the dipeptide L-Ala-L-Gln (0.0169 ± 0.0119), the base uridine (0.0144 ± 0.0115), α-tocopherol (0.0144 ± 0.0140), adenosine (0.0143 ± 0.0110), cytidine (0.0143 ± 0.0110), guanosine (0.0143 ± 0.0110), hydroxyproline (0.0138 ± 0.0091), taurine (0.0129 ± 0.0122), and Long R3 IGF-1 (0.0064 ± 0.0053).

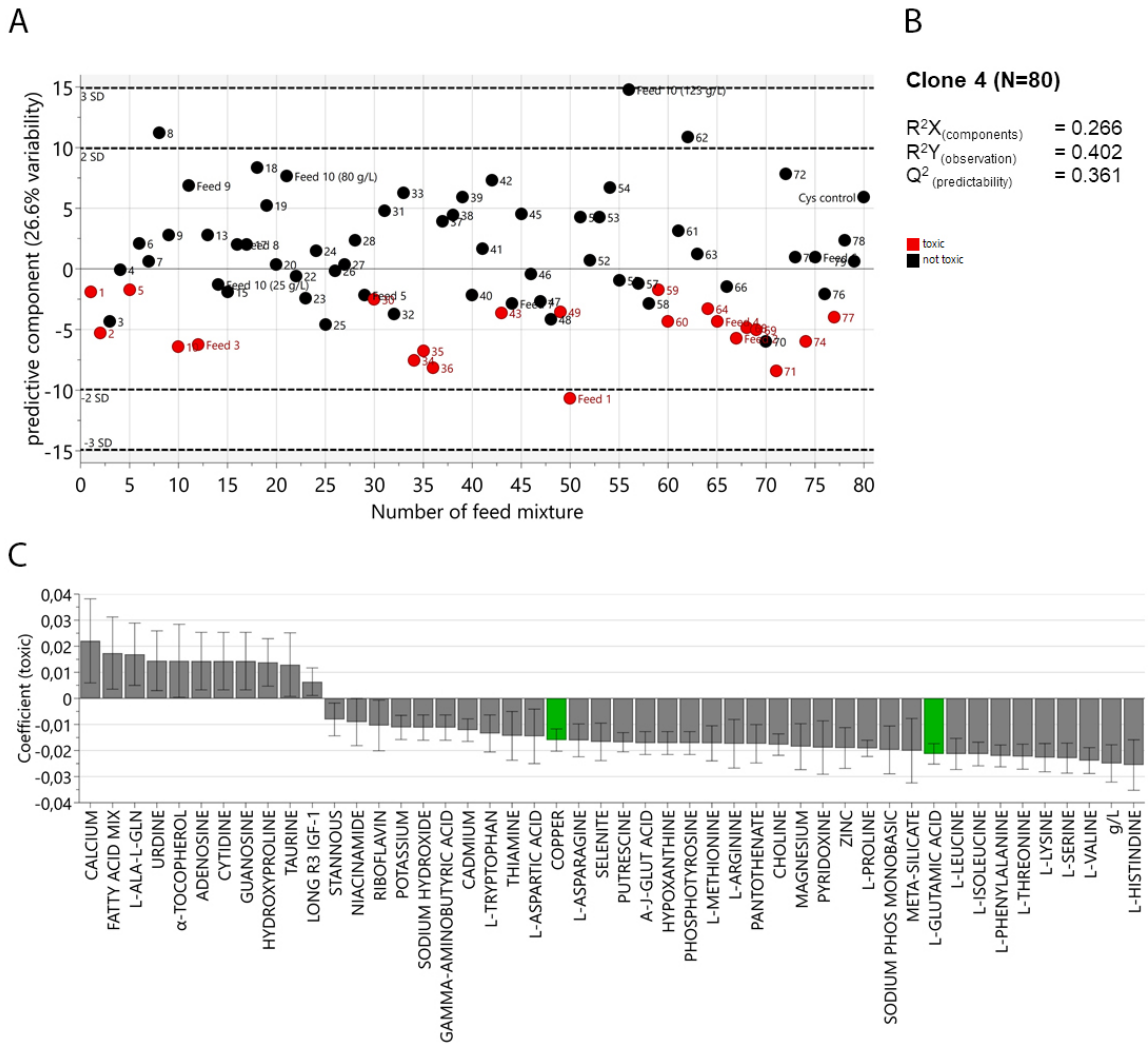

Figure 30. OPLS-DA model describing the SSC response of clone 4. The *X*-matrix was built by the composition of 80 feed mixtures and the *Y*-matrix was defined through the observed SSC response within a fed-batch screening using the respective feeds (toxic in case of a sharp reduction of the viable cell density). (A) 2D-score plot of the feed mixtures classified as either toxic (red) or not toxic (black). The predictive component explains 26.6% of the data variance. (B) The model of clone 4 yielded a R^2X of 0.266, R^2Y of 0.402 and Q^2 model predictability of 0.361. (C) The coefficient plot visualizes components correlating positively or negatively with the toxic response. Known components to reduce SSC toxicity are highlighted in green with a negative correlation to the toxic response.

Finally, the model of clone 5 using 79 feed mixtures (78 mixtures containing 14 mM SSC) was built by just one predictive component explaining 26.6% of the data variance and yielded a good discrimination of the SSC response. Similar to the previous described model feed 10, feed mixtures 8 and 62 and additionally feed 1 were positioned outside of the 2-

fold significance level. The OPLS-DA model yielded a R^2X of 0.275, a R^2Y of 0.678 and Q^2 of 0.634 having the best predictability among all tested clones.

A negative correlation of Glu (-0.0332 ± 0.0122) and copper (-0.0293 ± 0.0105) were observed. Feed components with positive coefficients were L-tyrosine (0.0168 ± 0.0112), pyruvate (0.0168 ± 0.0122), linoleic acid (0.0144 ± 0.0099), L-Ala-L-Gln (0.0135 ± 0.0055), hydroxyproline (0.0129 ± 0.0094), ethanolamine (0.0119 ± 0.0080), taurine (0.0119 ± 0.0067), ethylenediaminetetraacetic acid (EDTA; 0.0115 ± 0.0085), fatty acid mix (0.0114 ± 0.0061), 3-(N-morpholino)-propanesulfonic acid (MOPS; 0.0106 ± 0.0055), uridine (0.0106 ± 0.0103), Long R3 IGF-1 (0.0095 ± 0.0080), α-tocopherol (0.0090 ± 0.0074), citrate (0.0088 ± 0.0070), insulin (0.0085 ± 0.0083) and phosphate (0.0061 ± 0.0052).

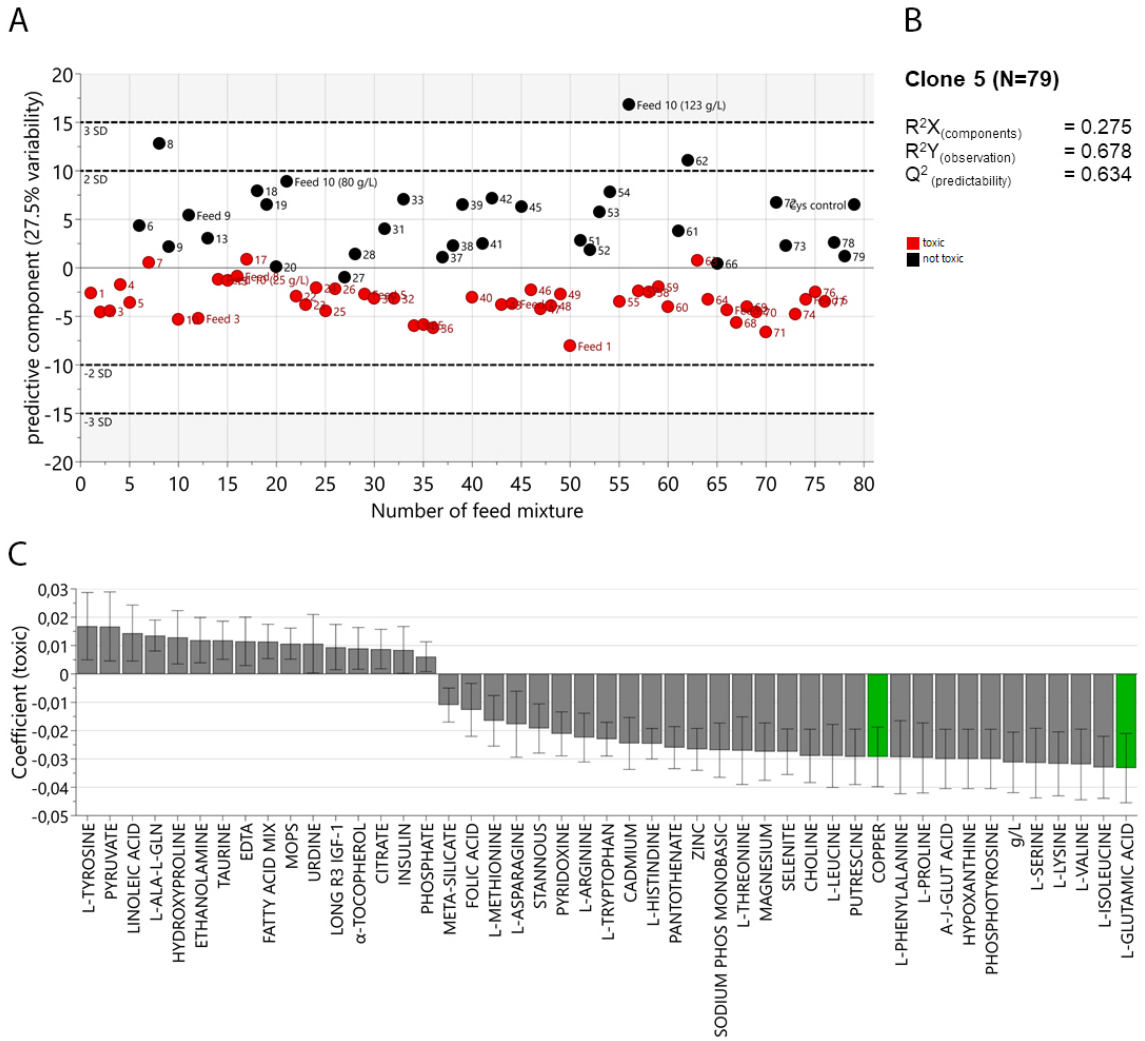

Figure 31. OPLS-DA model describing the SSC response of clone 5. The *X*-matrix was built by the composition of 79 feed mixtures and the *Y*-matrix was defined through the observed SSC response within a fed-batch screening using the respective feeds (toxic in case of a sharp reduction of the viable cell density). (A) 2D-score plot of the feed mixtures classified as either toxic (red) or not toxic (black). The predictive component explains 26.6% of the data variance. (B) The model of clone 5 yielded a R^2X of 0.275, R^2Y of 0.678 and Q^2 model predictability of 0.634. (C) The coefficient plot visualizes components correlating positively or negatively with the toxic response. Known components to reduce SSC toxicity are highlighted in green with a negative correlation to the toxic response.

Overall, the most promising compound which demonstrated a positive correlation to SSC toxicity within all four cell lines was the dipeptide L-Ala-L-Gln suggesting that L-Ala-L-Gln may induce SSC related toxicity (table 7). A positive correlation in three cell lines was observed for four components, namely Long R3 IGF-1, Insulin, α-tocopherol and a fatty acid mix. Since clone 4 had the lowest model predictability, the dipeptide, Long R3 IGF-1 and insulin were further investigated.

Table 11. MVDA hitlist. Feed components correlating positively with SSC toxicity, i.e. components that aggravate SSC toxicity according to the model.

	Clone 5	**Clone 6**	**Clone 7**	**Clone 4**
Model predictability Q^2	0.634	0.529	0.510	0.361
L-Ala-L-Gln	x	x	x	x
Long R3 IGF-1*	x	x	x	
Insulin	x	x	x	
α-tocopherol	x		x	x
Fatty acid mix	x		x	x

* A synthetic analogue of an insulin-like-growth factor 1 (IGF-1) having an arginine at the third position instead of glutamic acid (R3) and additional 13 amino acids at the N-terminus (long).

L-Ala-L-Gln, Long R3 IGF-1 and insulin did not influence SSC toxicity significantly

The most promising components were tested within the cell-based toxicity assay to assess the influence on SSC toxicity using clone 7. This clone was chosen since it showed the highest coefficient values and rather small error bars. The treatments were expected to aggravate SSC toxicity and were tested in the concentration range of the fed-batch screening in combination with increasing SSC concentration. The initial test was performed without any feed as a preferably high effect of the components was intended and the feed formulation was demonstrated to impact the metabolic viability. To support the data a similar experiment with additional 10% feed was performed.

The dipeptide L-Ala-L-Gln was supplemented to cultivated clone 7 in a range from 6.37 mg/mL to 637 mg/mL since the tested feeds were in a range from 63.7 mg/mL to max 500 mg/mL. Compared to untreated cells, the metabolic viability was decreased in presence of 1 mM SSC to 69%, and with increasing dipeptide concentrations to 80% (6.37 mg/mL), 79% (63.7 mg/mL) and 66% (637 mg/mL) as visualized in figure 32 A. At higher SSC concentrations the metabolic viability was always below 2%. The calculated MV_{50} was not significantly impacted with MV_{50} values in a range from 1.02 mM SSC without the dipeptide to 1.07 mM SSC in presence of 637 mg/mL of the dipeptide, whereas a MV_{50} value of 1.17 mM SSC was calculated in presence of 6.37 mg/mL L-Ala-L-Gln.

In all feed mixtures, insulin was used in a range from 1.7 mg/mL to max 14 mg/mL so that the impact of 0.1 mg/mL, 1 mg/mL and 10 mg/mL was tested similar to the dipeptide. Compared to untreated cells, the metabolic viability was reduced in presence of 1 mM SSC to 65%, and with increasing insulin concentrations to 61% (0.1 mg/mL), 48% (1 mg/mL) and 35% (10 mg/mL) as visualized in figure 32 B. The calculated MV_{50} was slightly reduced from 1.02 mM SSC (without insulin) in a dose dependent manner to 0.99 mM SSC through 1 mg/mL insulin and 0.92 mM SSC by 10 mg/mL insulin.

Regarding Long R3 IGF-1 with 16 µg/mL to max of 100 µg/mL in the feeds, only a small impact was observed with a MV_{50} reduction from 1.0 mM to 0.97 mM, 0.84 mM and 0.72 mM SSC for 6 µg/L, 60 µg/L and 600 µg/L Long R3 IGF-1, respectively (figure 32 B). This minor effect indicates that Long R3 IGF-1 might have an effect but cannot account for the huge differences between the feeds especially since several feeds are lacking Long R3 IGF-1 but showed a toxic response anyway.

To bring additional evidence that these components do not influence SSC toxicity, insulin was tested in the same concentration range, but with additional 10% of feed 7, as this feed was toxic for clone 7 (figure 29 A) and a positive correlation was observed for insulin (figure 29 C). After normalization of the metabolic viability to feed without SSC, the impact of Insulin was assessed. Compared to untreated cells, the metabolic viability was reduced in presence of 10% feed containing 10 mM SSC to 11.5%, and with increasing insulin concentrations to 18.8% (0.1 mg/mL), 28.2% (1 mg/mL) and 3.5% (10 mg/mL) as visualized in figure 32 D.

In summary, data indicate that the feed formulation impacts SSC toxicity, but a single component does not aggravate SSC toxicity significantly. In combination with previous experiments, data suggest that feed formulation effects rather the cell metabolism as well as cell growth and thereby SSC metabolization, which requires further investigation.

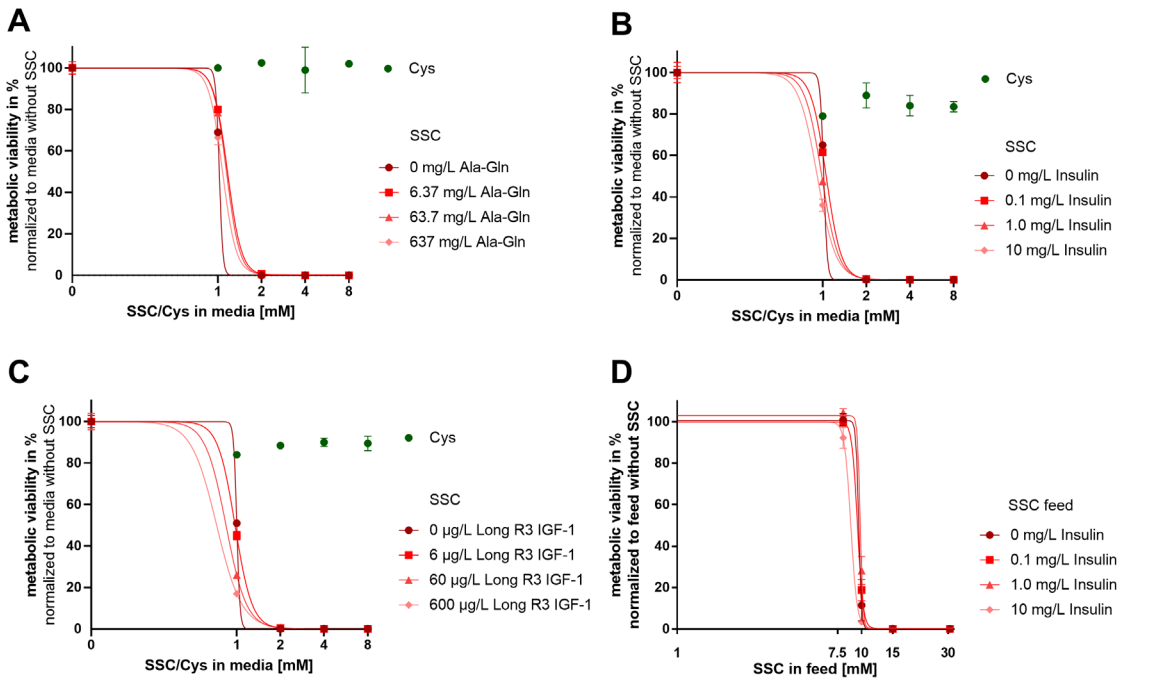

Figure 32. Impact of L-Ala-L-Gln, Long R3 IGF-1 and insulin on SSC toxicity. SSC dose response in presence of increasing concentrations (A) L-Ala-L-Gln in a range from 6.37 to 637 mg/mL (B+D) Insulin in a range from 0.1 to 10 mg/mL and (C) Long R3 IGF-1 in a range from 6 to 600 µg/L. 3.2×10^5 CHO cells (clone 7) were treated with increasing SSC (red) or Cys (green) concentrations in the media or (D) with increasing concentrations of SSC in feed. After cell cultivation over three days at 37°C, the ATP level was measured (CellTiter-Glo Assay, Promega) and the resulting ATP level was normalized to cells cultivated in media without supplementation and mean values are presented ± SEM (n=2). A non-linear regression of the data is visualized as solid line.

Key learnings: Feed formulation and SSC toxicity

High cell densities enhance SSC toxicity within a cell-based assay which suggests that metabolization of SSC by cells might be required to trigger the toxic effect.

A diverse SSC response was observed for eight different CHO cell lines cultivated in either a cell-based assay or a small-scale fed-batch experiment using a broad feed panel. Results indicate a clone dependent SSC response and a significant impact of the feed formulation on the toxicity.

However, MVDA was not able to predict specific cell culture media components triggering SSC toxicity. The identified hits did not aggravate SSC toxicity within a cell-based assay, whereas addition of Glu (known previously) was able to decrease cell sensitivity to higher SSC concentrations about 3.2-fold.

From a methodology standpoint, these results underline that even though MVDA is a powerful method to generate hypothesis, validation of the data is mandatory to confirm the suggested correlations.

4.3. SSC metabolism

The intracellular metabolome reflects the cellular state and the response of a cell to environmental changes such as the addition of a non-native amino acid. Cellular metabolization of SSC was demonstrated to increase the GSH level within cells but increased uptake through high extracellular SSC concentrations or upregulated transporter expression triggered a toxic response. Identification of SSC interaction products with intracellular metabolites was intended to deepen the understanding of SSC metabolism and furthermore identify metabolites which might cause cellular toxicity upon SSC feeding. The strategy was to analyze chemical reactions of extracted metabolites with SSC and extend this knowledge with enzymatic catalyzed reactions in presence of SSC using untargeted LC-MS/MS to generate new hypotheses regarding the toxicity.

4.3.1. Acetonitrile as suitable solvent to extract intracellular metabolites

Exploring SSC interactions with the intracellular metabolome requires an efficient extraction of the metabolites. Due to the wide range of physical and chemical properties of metabolites, different extraction efficiencies were reported for various solvents [213]. For example, highly polar compounds like nucleotides are less soluble in relatively nonpolar solvents, whereas polar solutions are likely to extract nucleotides. Regarding CHO cells, 12 different solvents were compared, whereby 50% aqueous acetonitrile (ACN_{aq}) was suggested as most suitable to extract intracellular metabolites [214]. Additional metabolites might be extracted by solvents accounting for other extraction specificities such as 50% aqueous methanol ($MeOH_{aq}$) and a 1:3 MeOH - chloroform (MC) mixture, which are predominantly used in several studies [213]. Thus, an initial experiment was intended to compare solvent efficiencies to define the most suitable solvent for further experiments.

The metabolome of a CHO-K1 clone was extracted after three days of cultivation (n=2) with ACN_{aq}, $MeOH_{aq}$ and a MC mixture. After extraction, cell debris and proteins were removed, and the respective solvent was evaporated via vacuum concentration. The dried extracts were dissolved in water and analyzed via LC-MS in positive and negative ionization mode to cover diverse properties of intracellular metabolites. Data were analyzed using Progenesis® QI by excluding LC-MS system released compounds and features with a low abundance as described in chapter 3.3.5.

To compare solvent efficiencies, detected features were clustered in a Venn diagram visualized in figure 33 (annotated compounds are summarized in appendix table 13 for positive mode, and table 14 for negative mode). Overall, 305 features were detected in positive mode, whereas 179 were detected within all solvents and only 26 features were observed using either $MeOH_{aq}$ (12) or MC (14), but not ACN_{aq}. 67 features were solely

detected in ACN_{aq} extracts, leading to a total of 288 observed features using ACN_{aq}, whereas a total of 230 and 188 features were observed in $MeOH_{aq}$ and MC extracts, respectively. A similar trend was observed in negative mode, whereby 201 features were detected in total and most of these were detected in ACN_{aq} extracts (178 features). In summary, ACN_{aq} was the most suitable extraction solvent within this setup, since it allowed the extraction of a maximum of small molecules and the detection in both ionization modes of 288 (ESI^+) and 178 (ESI^-) features, whereby application of both electrospray ionization modes was thought to be advantageous for the screening of global SSC interaction products.

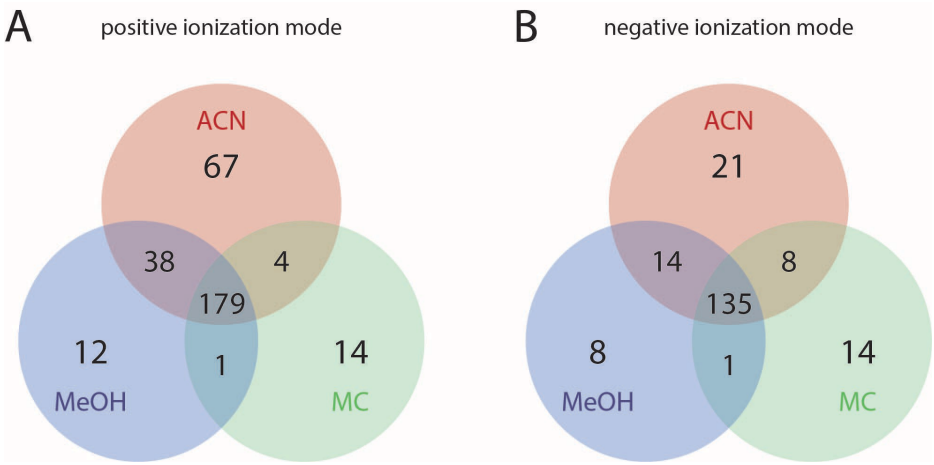

Figure 33. Intracellular metabolite extraction efficiency of different solvents. Venn diagram visualizes the detected features after filter application described in chapter 3.3.5, extracted from $5x10^6$ cells (at least level 3) in (A) positive (305) and (B) negative (201) ionization mode using three different extraction solvents: 50% aqueous acetonitrile (ACN) in red, 50% aqueous methanol (MeOH) in blue and a 1:1 MeOH - chloroform mixture (MC) in green.

4.3.2. GSH is the main intracellular metabolite interacting with SSC

In this section, the chemical interaction of SSC with intracellular metabolites was explored. Prior to the SSC interaction experiment, an appropriate SSC concentration range was determined by analyzing the intracellular GSH level of extracts via the common amino acid analysis described in chapter 3.1.5. This was based on previous results [194] indicating that SSC reacts 1:1 with GSH in the intracellular compartment. An average GSH + GSSG level of approximately 44 µM was detected within three ACN_{aq} extracts (data not shown). Accordingly, extracts were supplemented with either 40 µM or 400 µM SSC in subsequent experiments to work with the known 1:1 ratio as well as an excess of SSC. To identify effects specifically induced by SSC treatment, extracts were similarly treated with Cys and both treatments were compared to untreated extracts via LC-MS (n=2). Changes over time were monitored in all conditions after incubation at 25°C for 100 min and 210 min. The filter described in chapter 3.3.5 was applied leading to 475 remaining features in total (both detection modes within all samples) which were further explored to evaluate the influence of SSC.

Internal standards allow confident identification

The intracellular antioxidant GSH was described as main interaction product of SSC leading to glutathione-cysteine (GS-Cys) and sulfoglutathione (GS-SO_3). To allow confident identification of all Cys-sources (Cys, CysS and SSC) as well as GSH, GSSG and respective mixed disulfides (GS-Cys and GS-SO_3), pure standards were analyzed via LC-MS. Table 8 summarizes the key metrics of all standards and the extracted ion chromatograms are visualized in the appendix figure 49. All standards were detected in positive mode expect for the GS-SO_3 compound which was only detected in negative mode since in-source fragmentation was observed in positive mode. More precisely, the protonated GS-SO_3 molecule was shown to lose SO_3 (-79.9568 Da) during the ionization process leading the formation of an in-source fragment with the same m/z than GSH (m/z 308.0912, M+H). However, GSH and in-source fragment of GS-SO_3 can be easily discriminated based on their distinct retention time equal to 2.07 and 1.39 min, respectively (appendix figure 50).

Table 12. Key metrics of highly relevant standards.

	Retention time [min]	**m/z M±H**	**ionization mode**	**Neutral mass [Da]**
SSC	1.17	201.9839	pos	200.9760
Cys	1.25	122.0272	pos	121.0197
CysS	1.15	241.0311	pos	240.0238
GSH	2.07	308.0912	pos	307.0838
GSSG	3.59	307.0839	pos	612.1525
GS-Cys	1.42	427.0955	pos	426.0879
GS-SO_3	1.39	308.0913*	pos	387.0406
GS-SO_3	1.39	386.0333	neg	387.0406

* m/z of main in-source fragment of GS-SO_3 (neutral loss of SO_3) observed in positive mode

SSC interacts with GSH leading to GS-Cys and GS-SO_3

Detection of the mixed disulfides GS-Cys and GS-SO_3 in presence of SSC was expected, whereas it was unclear if Cys reacts similarly with GSH leading to GS-Cys and whether GS-SO_3 might occur without SSC as well. Hence, the targeted approach was intended to explore differences between Cys and SSC interacting with GSH from the intracellular metabolome.

First, the Cys specific response was assessed to allow subsequent identification of SSC specific response. A constant GSH abundance in a range from about 1.22×10^6 (t_{210}) to 1.26×10^6 (t_{100}) was observed when 40 µM Cys was added, which was similar to untreated extracts having an average abundance of about 1.16×10^6 (t_0) to 1.22×10^6 (t_{210}) over time (figure 34 A). Addition of 400 µM Cys reduced the average abundance of GSH in untreated extracts about 25% to 0.87×10^6 at t_0, indicating a fast, chemical reaction of GSH and Cys. Further incubation increased GSH abundance to 0.92×10^6 (t_{100}) and 0.96×10^6 (t_{210}) when 400 µM Cys was applied.

The interaction product GS-Cys was not detected in untreated extracts and in the 40 µM Cys condition. At 400 µM Cys, GS-Cys was unambiguously detected with an abundance of about 9.5×10^4 at t_0, which was then reduced over time to 9.0×10^4 (t_{100}) and 8.4×10^4 (t_{210}) as visualized in figure 34 B. Data indicate, that extracts exposed to Cys yields GS-Cys via quick chemical reactions with GSH, which is then slowly degraded at 25°C over time. Within the acquired data, minor changes were observed over time, whereas supplemented extracts showed significant changes at t_0 indicating quick chemical reactions already during sample preparation. For statistical analysis, data from all time points were applied to increase statistical robustness.

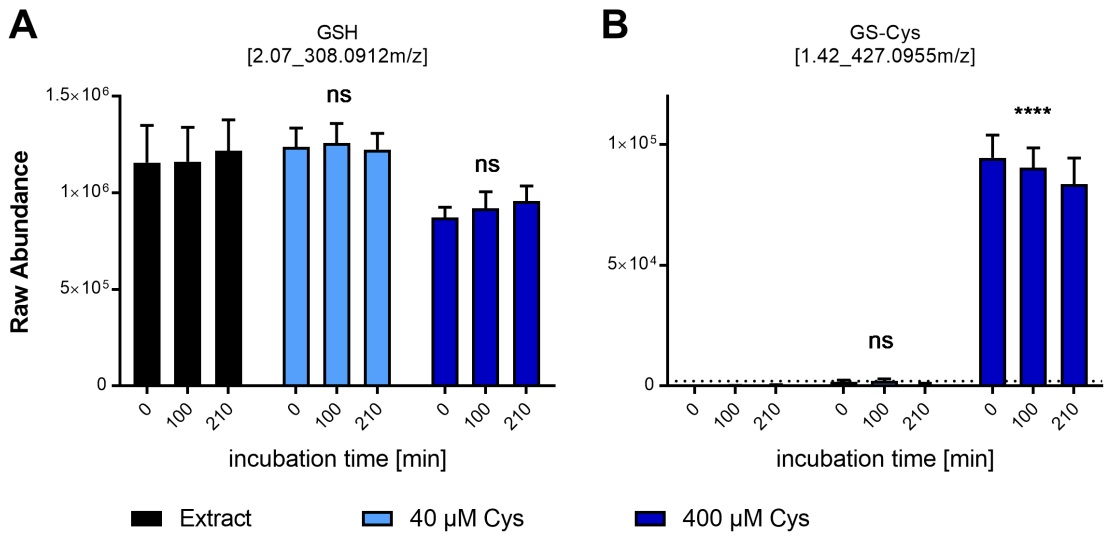

Figure 34. Chemical interaction of Glutathione (GSH) with L-Cysteine (Cys) leading to GS-Cys. Intracellular metabolites were extracted with a 50% aqueous acetonitrile solution. Extracts from $5x10^6$ cells were incubated with 40 and 400 µM Cys for 210 min at 25°C. Samples were analyzed after 0, 100 and 210 min by LC-MS/MS and raw abundance (positive ionization mode) of (A) GSH and (B) GS-Cys are visualized as mean values ± SEM (n=4). An abundance below 2000 is not distinguishable from background noise and is indicated as dotted line. Since minor changes were observed over time, statistical comparison was performed with data from all time points (n=12) using one-way ANOVA and subsequent Dunn's multiple comparison, whereas p-values indicate the following: ****p<0.0001, ns = not significant.

Next, the SSC specific response was assessed. After addition of 40 µM SSC, no signal corresponding to this molecule (m/z 201.9839) was detected indicating either SSC depletion due to quick reactions with metabolites or that the concentration was below the limit of detection (LOD) of the method (figure 35 A). In comparison, 400 µM SSC increased the abundance significantly to about 2.3×10^6 (t_0), which stayed constant at a high level over time ($p<0.0001$).

GSH was clearly interacting with SSC leading to a significantly reduced GSH abundance of about 43% through 40 µM SSC and 86% through 400 µM SSC (figure 35 B). More precisely, GSH abundance was reduced from 1.16×10^6 (t_0) in the untreated control to 0.65×10^6 (t_0) through addition of 40 µM SSC ($p=0.0047$) and to 0.16×10^6 (t_0) by 400 µM SSC ($p<0.0001$). This dose dependent reduction correlated with increasing GS-Cys and GS-SO_3 (figure 35 C+D). In extracts supplemented with 40 µM SSC, an average GS-Cys abundance of 2.4×10^4 ($p=0.0096$) and a GS-SO_3 abundance of 3.0×10^4 ($p<0.0001$) was observed. 400 µM SSC yielded in further increased average abundances of 5.8×10^4 ($p<0.0001$) for GS-Cys and 11.3×10^4 ($p<0.0001$) for GS-SO_3. Data indicate that GS-Cys and GS-SO_3, the mixed disulfides of GSH and SSC arise from dose dependent chemical reactions. Furthermore, GS-Cys level and GS-SO_3 level are stable at 25°C as the initial reached abundance is constant over time.

In comparison to 40 µM Cys showing no effect on the GSH abundance, 40 µM SSC was able to decrease the amount of GSH. Additionally, 400 µM SSC depleted most of the GSH pool, whereas 400 µM Cys reduced the GSH pool only slightly supporting a higher reactivity of SSC with GSH compared to Cys (figure 35 B).

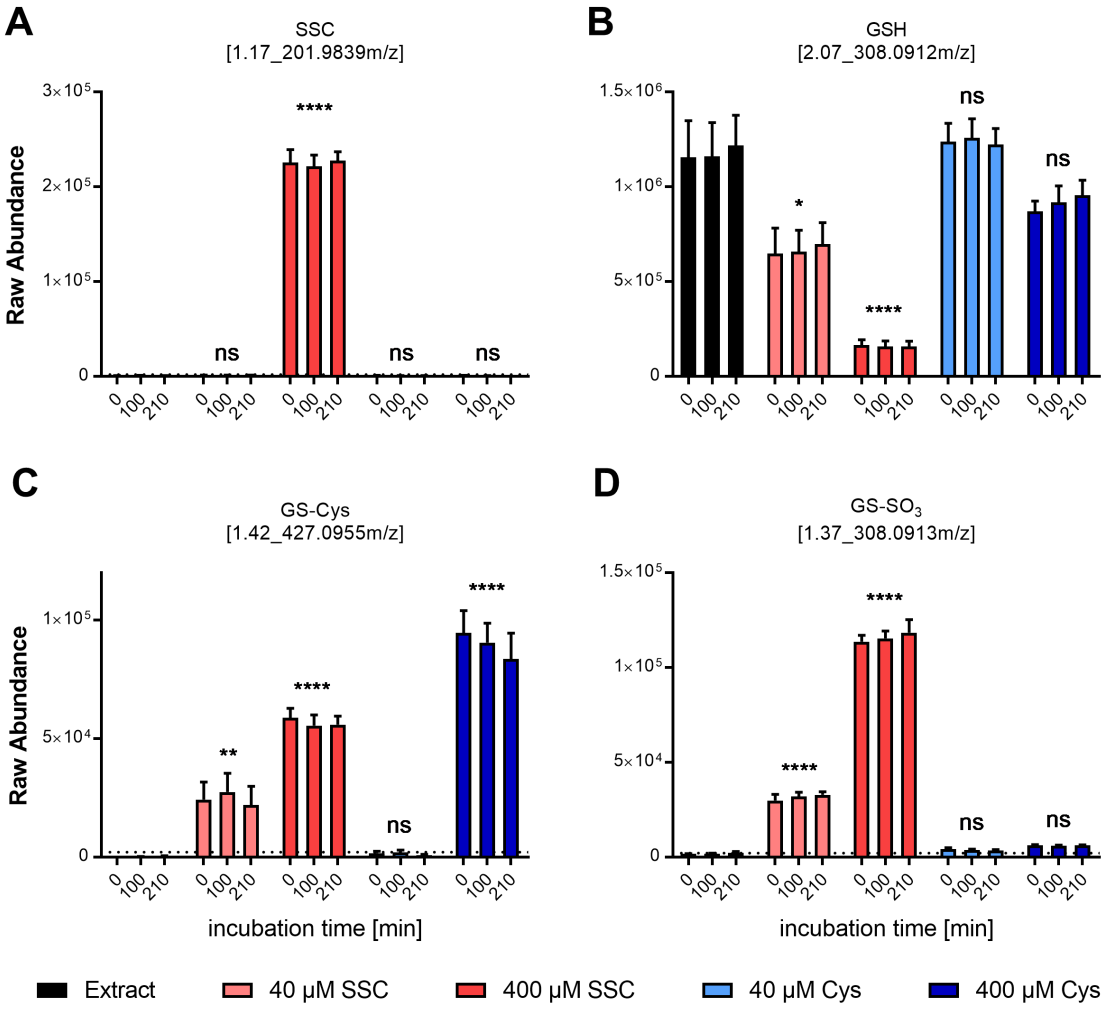

Figure 35. Chemical interaction of Glutathione (GSH) with L-Cysteine (Cys) and *S*-sulfocysteine (SSC) leading to mixed disulfides. Intracellular metabolites were extracted with a 50% aqueous acetonitrile solution. Extracts from 5x10^6 cells were incubated with 40 and 400 µM SSC or Cys for 210 min at 25°C. Samples were analyzed after 0, 100 and 210 min by LC-MS/MS and raw abundance (positive ionization mode) of (A) SSC, (B) GSH, (C) GS-Cys and (D) GS-SO_3 are visualized as mean values ± SEM (n=4). An abundance below 2000 is not distinguishable from background noise and is indicated as dotted line. Since minor changes were observed over time, statistical comparison was performed with data from all time points (n=12) using one-way ANOVA and subsequent Dunn's multiple comparison, whereas p-values indicate the following: ****p<0.0001, *** p<0.0002, ** p<0.002, * p<0.033, ns = not significant.

Two hits identified via untargeted approach

The untargeted approach aimed to identify metabolites which are either influenced by SSC treatment or to reveal metabolites which are naturally not produced by the cells in the presence of SSC. Therefore, data was screened for specific abundance patterns. First, features were identified where the abundance of the untreated extract differs from SSC treated extracts. The effect was thought to be SSC specific, whenever the abundance of the Cys treated samples showed a different profile. Two features meeting these criteria were identified with a mass to charge ratio (m/z) of 255.1011 and 470.1443.

The abundance of the first feature of interest (m/z 255.1011) was at about 3500 ($t_{0\text{-}210}$) in untreated extracts and 40 µM SSC increased the abundance significantly about 2.0-fold (figure 36 A) to an abundance of about 6700 at t_0 (p=0.0217). 400 µM SSC increased the abundance of 255.1011 m/z further about 2.9-fold to 10,600 at t_0 (p<0.0001). In contrast, the abundance was similar to the untreated control when 40 µM and 400 µM Cys were added with an abundance of 3400 (t_0) and 3300 (t_0), respectively. The data set suggests that the increased abundance of this feature is SSC specific and therefore of high interest. Based on the fragmentation pattern, this compound was putatively identified as HEPES peroxide (figure 36 C). HEPES, a zwitterionic sulfonic acid buffering agent used in cell culture media, is able to scavenge ROS leading to HEPES peroxide, whereby the localization of the additional hydroxy group cannot be annotated within the fragmentation pattern. To validate the compound in general, HEPES might be treated with hydrogen peroxide, singlet oxygen or a superoxide radical to achieve a heterogenous HEPES peroxide mixture. In case the feature m/z 255.1011 is detected, the identification needs to be further verified by analyzing pure standards of various oxidized HEPES structures. However, this was not performed, since this compound is not commercially available. Additionally, the presence of HEPES peroxide might be linked to an overall higher ROS level resulting from the decreased level of GSH observed intracellularly after SSC spiking. Indeed, GSH is the main intracellular scavenging molecule and its depletion might lead to an increased oxidation of other intracellular molecules.

The abundance of the second feature of interest (m/z 470.1443) was slightly increased over time from about 2.4×10^4 at t_0 to 2.8×10^4 (t_{210}) in untreated extracts (figure 36 B). The incubation of the lysate with 40 µM Cys had no impact on the abundance of this feature (2.4×10^4) whereas the addition of 400 µM Cys led to a decreased abundance of about 1.4×10^4 (t_0) and 1.6×10^4 after 210 min (t_{210}), which is 1.6-fold lower compared to the untreated control (p=0.18). This decrease was more prominent in presence of SSC. A significant 2.4-fold reduction to about 1.0×10^4 (t_0) was observed in presence of 40 µM SSC (p=0.0034), whereby 400 µM SSC reduced the abundance 20.8-fold below the LOD (p<0.0001). Based on the fragmentation pattern, this compound (m/z 470.1443) was

putatively identified as glucoglutathione, which might be a thermal maillard reaction product of GSH with glucose (figure 36 D). However, a pure standard has to be analyzed to validate the component identification. Unfortunately, this compound was not commercially available, but another possibility in order to confirm the identification might be to incubate GSH with glucose including an iron source to catalyze the maillard reaction. Less interaction of glucose and GSH in presence of Cys or SSC might as well be explained by the observed lower GSH abundance, which correlates with the glucoglutathione abundance level. Thus, GSH is more likely to react with thiol containing compounds than with glucose or glucoglutathione reacts readily with SSC.

In summary, HEPES peroxide and glucoglutathione were putatively identified as metabolites which are influenced by the addition of SSC. Whether these arise through SSC directly or if rather the GSH reduction via SSC interaction triggers the changed abundance profile needs to be verified. Since cellular GSH homeostasis is regulated by several enzymes, SSC interaction studies in whole cell lysates was targeted next.

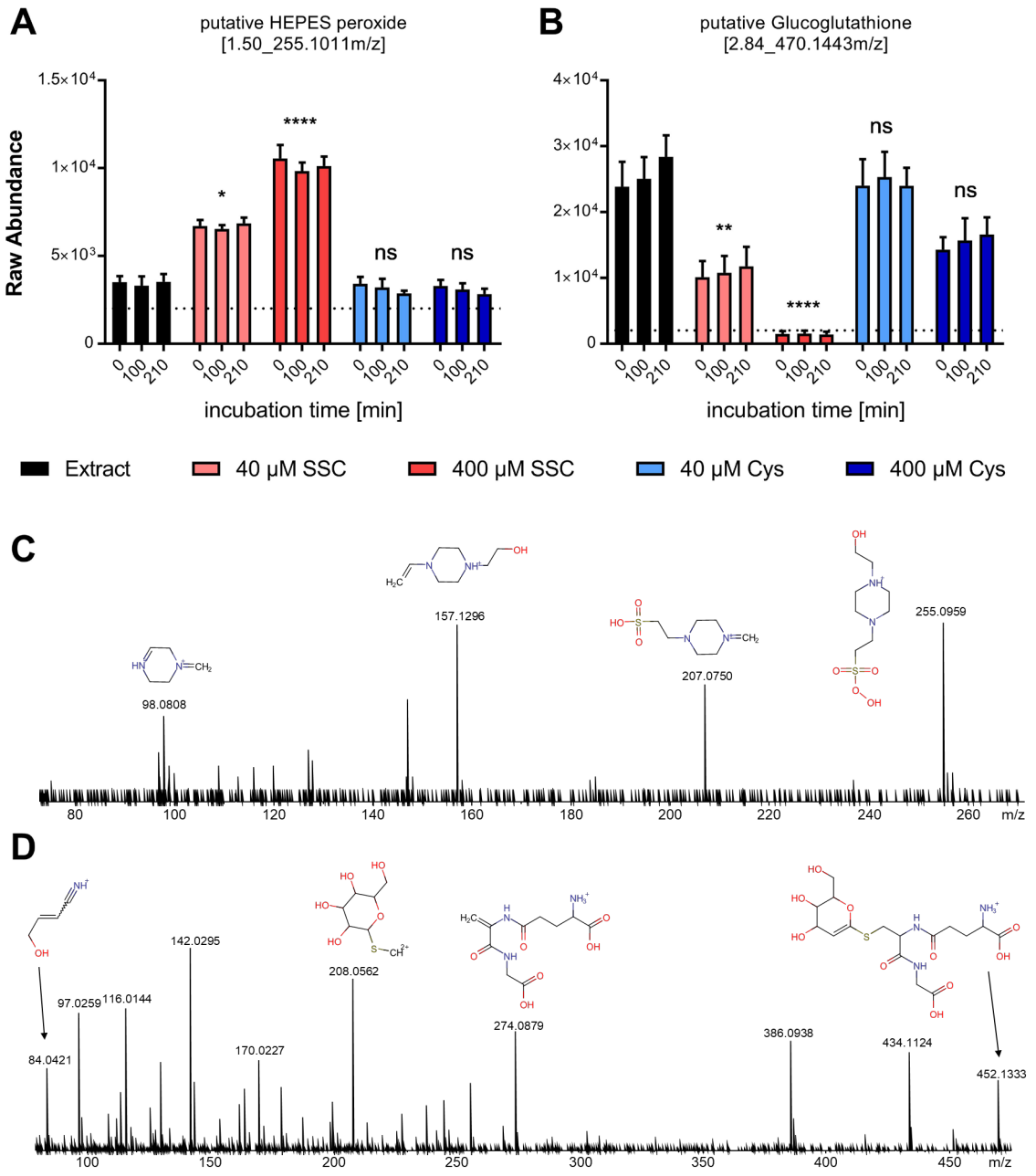

Figure 36. Putative identified compounds influenced by SSC interactions with intracellular metabolites. Intracellular metabolites were extracted with a 50% aqueous acetonitrile solution. Extracts from 5x10^6 cells were incubated with 40 and 400 µM SSC or Cys for 210 min at 25°C. Samples were analyzed after 0, 100 and 210 min by LC-MS/MS and abundance of (A) 255.1011 m/z (ESI+) and (B) 470.1443 m/z (ESI+) are visualized as mean values ± SEM (n=4). An abundance below 2000 is not distinguishable from background noise and is indicated as dotted line. Since minor changes were observed over time, statistical comparison was performed with data from all time points (n=12) using one-way ANOVA and subsequent Dunn's multiple comparison, whereas p-values indicate the following: **** p<0.0001, *** p<0.0002, ** p<0.002, * p<0.033, ns = not significant. (C) Fragmentation pattern of 255.1011 m/z was putatively annotated as HEPES peroxide. The additional hydroxy group compared to HEPES was exemplarily positioned at the sulfonic acid group but can be located at several positions. (D) Fragmentation pattern of 470.1443 m/z was putatively annotated as glucoglutathione, whereby the structure of the parental ion is exemplarily shown as *S*-linked structure.

4.3.3. Enzymatical SSC metabolization

SSC interaction studies in presence of proteins is essential to estimate the influence of SSC on cellular functions. Especially thiol-dependent enzyme activity is crucial for cells and might be impacted by SSC. For this purpose, lysates of seven days cultivated CHO-K1 cells were incubated with increasing SSC concentrations. Based on the previous experiment with cell extracts, 40 µM and 400 µM SSC or Cys were applied although the detected GSH concentration of the lysate was 2-fold lower (22 µM) compared to ACN_{aq} extracts (data not shown). All mixtures and an untreated lysate as control were incubated at 37°C to support enzymatic reactions and subsequent sampling was performed after 0, 30, 100 and 210 min. Enzymatic reactions were directly stopped by removing the proteins from metabolites at 4°C using a 3 kDa Amicon® Ultra centrifugal filter unit and filtrate was analyzed via LC-MS/MS.

GS-Cys is metabolized and GS-SO_3 accumulates in presence of SSC and a cell lysate

To explore whether the SSC interaction with GSH is solely chemically driven or whether enzymes impact the abundance of mixed disulfides, a targeted LC-MS approach was used. Based on the previous experiment, chemical reactions were expected to be fast and thus predominantly observed at t_0, whereas enzymatically reactions might be observed over time. Enzymes relevant for GSH metabolization and homeostasis can either support GS-Cys and GS-SO_3 synthesis or participate in their reduction thus restoring the respective building blocks.

SSC abundances in presence of enzymes were lowered over time *e.g.* from 3.8×10^4 (t_0) to 3.3×10^4 (t_{210}) for 400 µM SSC treated lysates, indicating that either slow reactions occur at 37°C or SSC is enzymatically metabolized (figure 37 A). Similar to previous experiments with extracts, a quick chemical reaction of GSH and SSC was observed. More precisely, the abundance of GSH in untreated lysates was at 2.3×10^5 (t_0), which was 2-fold decreased to 1.2×10^5 (t_0) when 40 µM SSC was added and was further decreased over time to 1.0×10^5 (t_{210}) (figure 37 B). In presence of 400 µM SSC, GSH abundance was directly 41.1-fold lowered to an abundance of 0.5×10^4 (t_0) and further decreased to 0.3×10^4 (t_{210}), indicating fast GSH depletion.

GS-Cys product was not observed in untreated lysates and largely detected in presence of 40 µM SSC with a raw abundance of 2.7×10^4 at t_0 (figure 37 C). As previous results without any proteins indicated a constant GS-Cys abundance over time (figure 35 C), a decrease over time was interpreted as enzymatic catalyzed. Thus, enzymatic degradation was detected over time by a 1.8-fold GS-Cys decrease to an abundance of 1.5×10^4 after 210 min when treated with 40 µM SSC. This effect was dose dependent as 400 µM SSC resulted in a higher initial GS-Cys abundance of 3.4×10^4 (t_0) which was 4.1-fold decreased to 0.8×10^4

(t_{210}). In comparison, the abundance of GS-SO_3, another mixed disulfide, was mainly increased over time (figure 37 D). In presence of 40 µM SSC, GS-SO_3 abundance was 2.7-fold increased from 0.5×10^4 (t_0) to 1.4×10^4 (t_{210}). In presence of 400 µM SSC, GS-SO_3 abundance was initially 1.9-fold increased from 2.6×10^4 (t_0) to 4.9×10^4 after 100 min. Afterwards, a slight decrease of the GS-SO_3 abundance to 4.4×10^4 (t_{210}) was observed. Data set suggests that GS-SO_3 might be less susceptible to enzymatic metabolization compared to GS-Cys and might accumulate intracellularly.

In summary, different effects in presence of SSC were observed for both mixed disulfides over time. Both were present at t_0 due to chemical interaction and GS-Cys was subsequently metabolized during incubation, whereas GS-SO_3 was enriched over time. Data suggest that intracellular enzymes known to restore the GSH pool such as glutathione reductase are able to reduce GS-Cys but might not be able to reduce GS-SO_3 properly. To demonstrate whether this is true, the substrate specificity of reducing enzymes needs to be assessed.

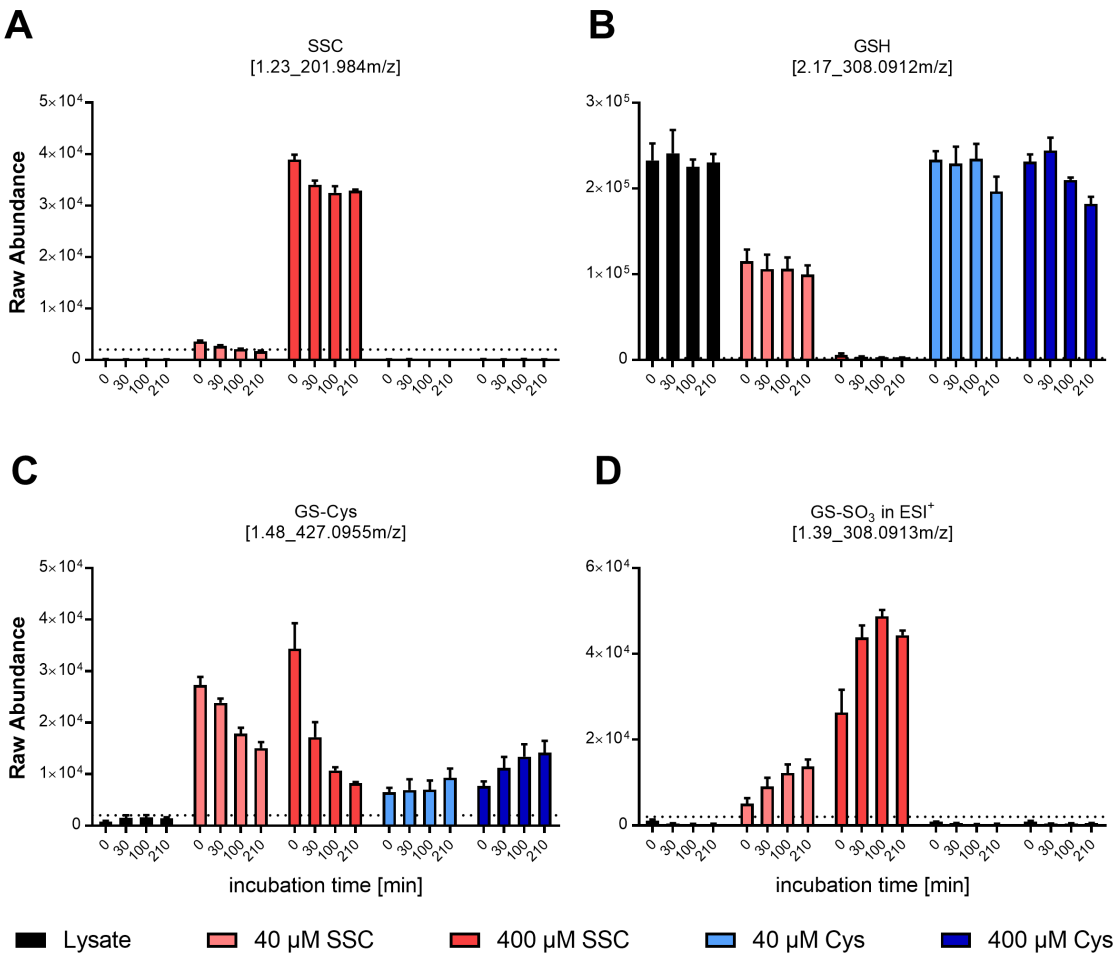

Figure 37. Interaction of GSH with Cys and SSC in presence of proteins. Lysates from $2x10^8$ cells were incubated with 40 µM and 400 µM SSC or Cys for 210 min at 37°C. Samples were analyzed after 0, 30, 100 and 210 min by LC-MS/MS and raw abundance (positive ionization mode) of (A) SSC, (B) GSH, (C) GS-Cys and (D) GS-SO_3 are visualized as mean values ± SEM (n=4). An abundance below 2000 is not distinguishable from background noise and is indicated as dotted line.

Twelve hits within the untargeted approach

The untargeted approach was aimed to formulate new hypotheses regarding the observed SSC toxicity. After incubation of cell lysates with 40 µM and 400 µM SSC or Cys over 210 min, the filtrate was analyzed via LC-MS. Data were analyzed using Progenesis® QI by excluding solvent impurities, and features with low abundance i.e. < 10000 for positive and < 5000 for negative mode. Similar to the experiment using lysates, data was screened for specific abundance patterns. More precisely, features where the abundance of the untreated extract differed from SSC treated extracts were thought to be of interest, whereas an SSC specific response was identified by assessing the response after Cys addition (features with a similar response to Cys and SSC were not of interest). Twelve features summarized in table 9 were identified as interesting and were further investigated.

Table 13. SSC influenced intracellular metabolites classified via untargeted approach.

Feature RT [min]_m/z	**Ion**	**Neutral mass**	**Mass Error [ppm]**	**Identification (confidence level)**
1.06_203.2230m/z	M+H	202.2151	0.3	Spermine (1)
1.07_146.1652m/z	M+H	145.1573	0.4	Spermidine (1)
1.44_256.9909m/z	M-H	257.9987	0.1	$C_5H_9N_2O_6S_2$ (3)
1.75_324.0593m/z	M+H	323.0514	0.0	Cytidine monophosphate (1)
3.03_244.0933m/z	M+H	243.0854	1.3	Cytidine (1)
4.57_267.0588m/z	M+Na	244.0690	1.5	Uridine (1)
4.65_282.1199m/z	M+H	281.1120	-3.2	1-Methyladenosine (1)
4.66_664.1163m/z	M+H	663.1099	1.2	NAD^+ (1)
5.89_298.1146m/z	M+H	297.1067	0.1 0.1 0.1 0.1	2-Methylguanosine (3) Nelarabine (3) 7-Methylguanosine (3) 1-Methylguanosine (3)
5.95_283.1037m/z	M+H	282.0958	0.0 0.0	7-Methylinosine (3) 1-Methylionosine (3)
6.14_359.1037m/z	M+H	358.0958	0.3	Pantetheine 4'-phosphate (1)
8.94_204.1233m/z	M+H	203.1158	2.0	4-[2-Hydroxyethyl(propan-2-yl)amino] -4-oxobutanoic acid (3)

A prominent effect due to SSC supplementation was observed for the feature "3.03_244.0933m/z". In the untreated lysate, the abundance was 26-fold increased over time from 0.4×10^4 (t_0) to 10.5×10^4 (t_{210}) and similarly 24-fold increased when treated with 400 µM Cys from 0.4×10^4 (t_0) to 9.8×10^4 at t_{210} (figure 38 A). In contrast, the abundance increased only from 0.4×10^4 (t_0) to 1.4×10^4 (t_{210}) in lysates treated with 400 µM SSC (3.5-fold). Consequently, the abundance at t_{210} was 7.2-fold higher in lysates without SSC although the abundance at t_0 was similar. This feature was identified with an internal standard as cytidine, an RNA building block.

The same trend, but less prominent response was observed for five additional features. A 1.5-fold difference was calculated for m/z 324.0593 after 210 min, which was identified as cytidine monophosphate, a 2.2-fold difference for m/z 267.0588 (uridine), a 2.9-fold difference for m/z 282.1199 (1-methyladenosine), a 1.3-fold difference for m/z 298.1146 putatively annotated as methylguanosine and a 1.6-fold difference for m/z 283.1037 putatively annotated methylinosine (figure 38 B-F). For the two putative annotated components the methyl group positioning is uncertain, whereas the other features were identified with internal standards. These effects suggest that SSC or an SSC interaction product influences the formation of nucleosides *e.g.* via enzyme inhibition. However, if this blocked formation triggers toxicity in a production process such as a fed-batch is not clear and requires further experiments.

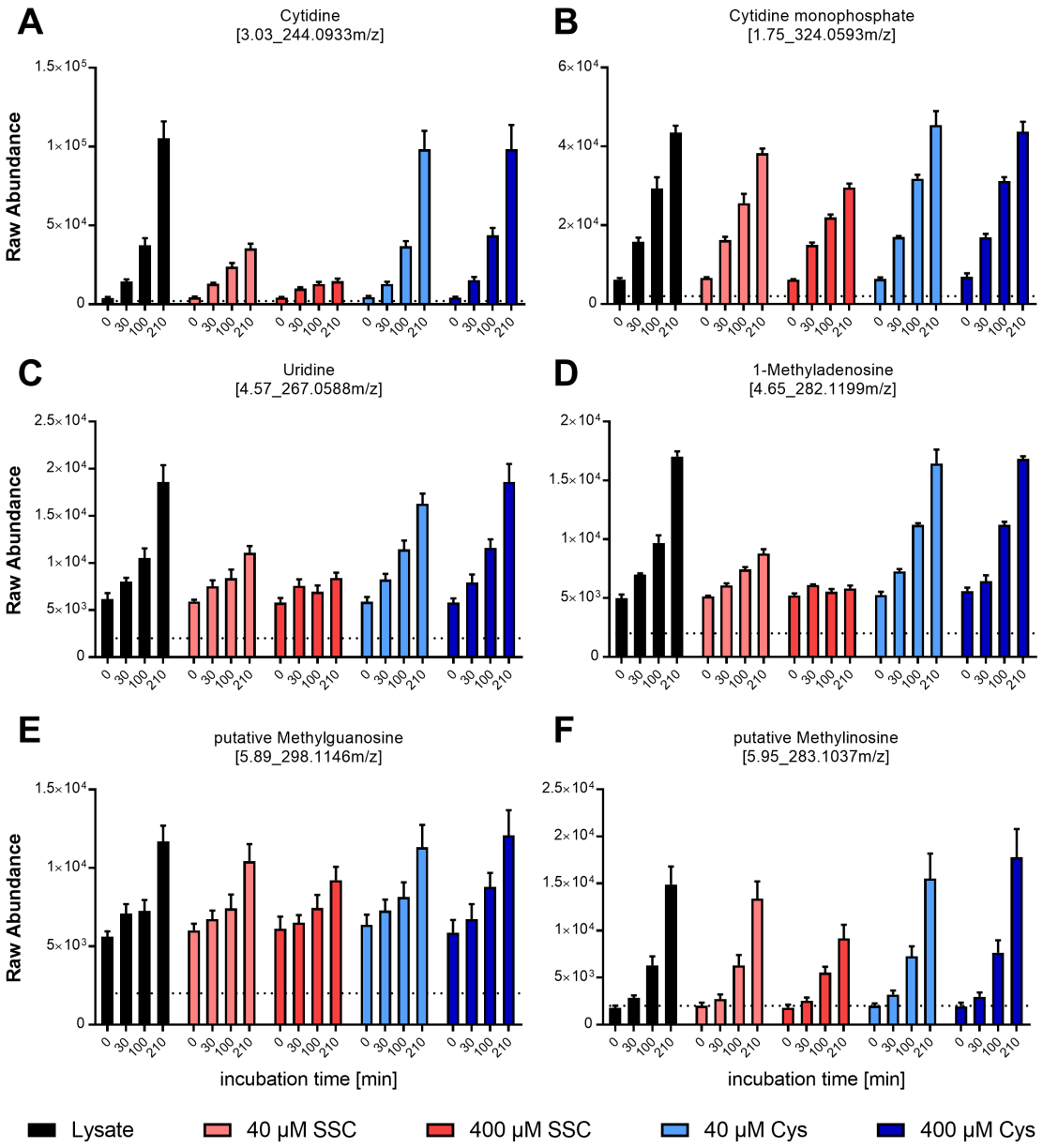

Figure 38. Influence of SSC on metabolism of RNA building blocks. Lysates from 5x10^8 cells were incubated with 40 µM and 400 µM SSC or Cys for 210 min at 37°C. Samples were analyzed after 0, 30, 100 and 210 min by LC-MS/MS and raw abundance (positive ionization mode) of (A) cytidine, (B) cytidine monophosphate, (C) uridine, (D) 1-methyladenosine, (E) putative identified methylguanosine and (F) putative identified methylinosine are visualized as mean values ± SEM (n=4). An abundance below 2000 is not distinguishable from background noise and is indicated as dotted line.

Two compounds (m/z 203.223 and m/z 146.52) showed an increasing abundance over time in both controls (untreated and Cys treated lysate), whereby the abundance of 400 µM SSC treated lysates remained constant (figure 39). After 210 min incubation, a 1.9-fold and 2.0-fold higher abundance was observed within the controls for m/z 203.223 and m/z 146.1652, respectively (figure 39 A and B). These features were identified by internal standards as spermine (m/z 203.223) and spermidine (m/z 146.1652), which are directly linked i.e. spermidine as intermediate within spermine synthesis. The data set suggests that either the

catalyzing enzyme yielding spermidine (spermidine synthase having ten Cys residues) is inhibited by SSC or one of the substrates, putrescine or *S*-adenosylmethionineamine are depleted via SSC treatment.

From the four remaining features, a prominent SSC effect was observed for m/z 359.1037, which was 1.7-fold lowered within 40 µM SSC treated lysates, whereas 400 µM SSC lowered the abundance significantly about 21-fold (figure 39 C). This feature was identified as pantetheine 4-phosphate via internal standard. It contains a thiol group and is a key substrate of CoA biosynthesis, which is moreover essential for biochemical reactions within the tricarboxylic acid cycle (TCA). Thus, depletion of pantetheine 4-phosphate as consequence of SSC treatment is likely to affect CoA biosynthesis and might disturb the energy cycle in cells.

Furthermore, the abundance of m/z 664.1163 was reduced in the untreated lysate from 1.3×10^4 (t_0) to 0.2×10^4 (t_{210}), whereas the reduction was less prominent when treated with SSC (figure 39 D). More precisely, the abundance of this compound was decreased from 1.3×10^4 (t_0) to 0.9×10^4 (t_{210}) in lysates treated with 400 µM SSC resulting in a 4.6-fold higher abundance compared to the control and a 2.8-fold higher level when lysates were treated with 40 µM SSC. This feature was identified as Nicotinamide adenine dinucleotide (NAD^+), a redox active metabolite, which is reduced to NADH within several reactions of the TCA. Thus, reduced NAD^+ consumption might be a consequence of pantetheine 4-phosphate depletion in SSC treated lysates.

A similar effect was observed via SSC treatment for the feature m/z 204.1233. The abundance was decreased from 1.9×10^4 (t_0) to 0.6×10^4 (t_{210}) in the untreated lysate, whereas the reduction in presence of 400 µM SSC was less prominent leading to a reduced abundance from 1.8×10^4 (t_0) to 1.5×10^4 (t_{210}), which is 2.4-fold higher after 210 min compared to the control (figure 39 E). In comparison, 400 µM Cys treatment caused a 1.4-fold higher abundance compared to the control indicating that this effect might be caused by excessive Cys as well. This feature was putative annotated as 4-[2-Hydroxyethyl(propan-2-yl)amino]-4-oxobutanoic acid (confidence level 3). As this feature was only detected in positive ionization mode, the possibility that this feature is an insource fragment has to be taken into account, especially since the SO_3 group can be lost during positive ionization as observed for GS-SO_3. This reinforces the demand for standard validation of putative identified features.

The feature at m/z 256.9909 showed a significantly increased raw abundance from below the LOD at t_0 (404) to 1.3×10^4 (t_{210}) in the lysate treated with 400 µM SSC (32-fold), whereas the raw abundance in the untreated and Cys treated lysate was not detectable (figure 39 F). The feature was only detected in negative ionization mode and has not been identified yet. Due to a poor MS/MS spectra quality, no putative annotation was possible either. However,

based on mass accuracy (0.1 ppm) and isotopic pattern, the neutral sum formula $C_5H_9N_2O_6S_2$ was determined for this compound (assuming a deprotonated molecular ion $[M-H]^-$).

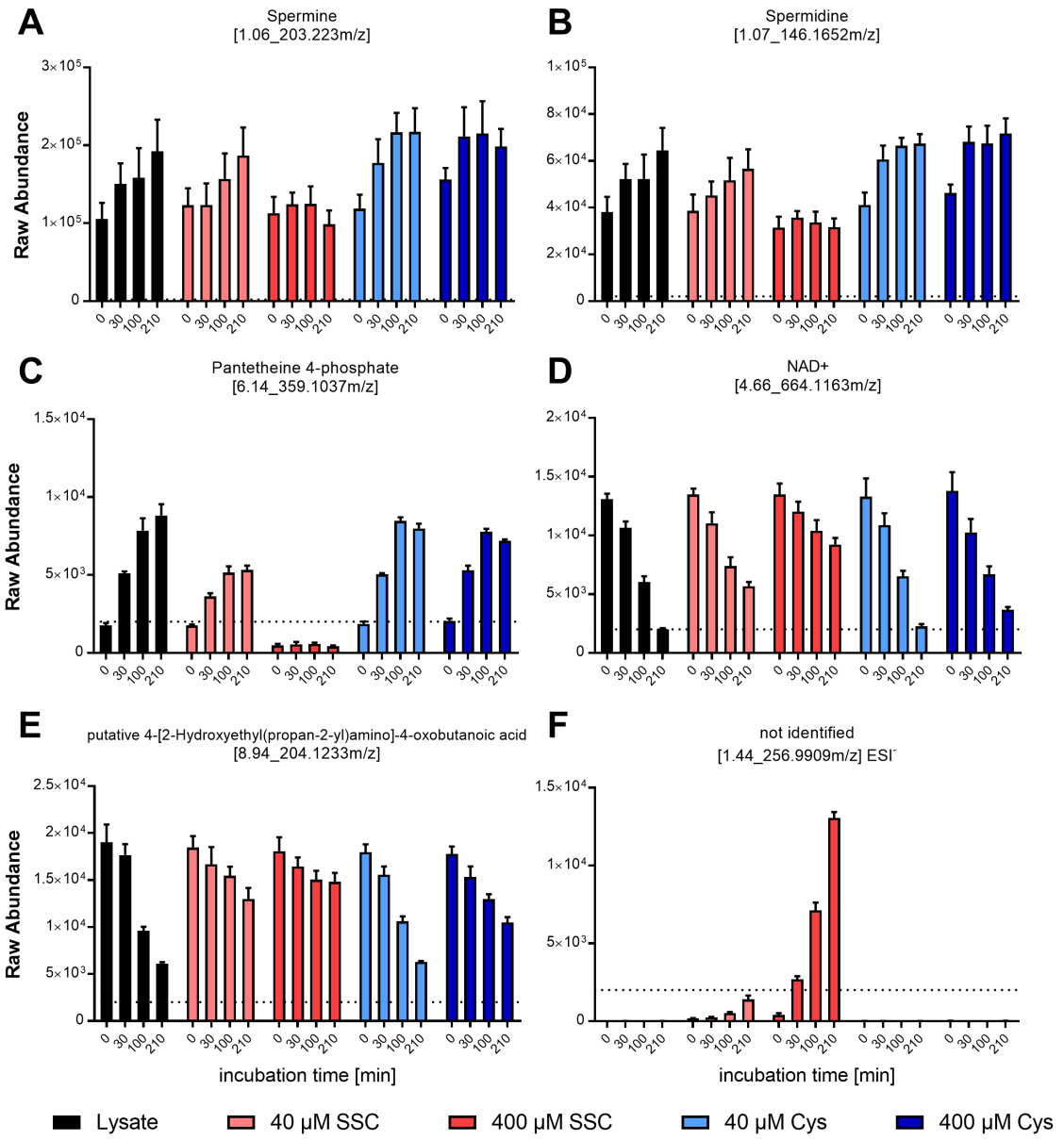

Figure 39. Influence of SSC on intracellular metabolites. Lysates from $5x10^8$ cells were incubated with 40 and 400 µM SSC or Cys for 210 min at 37°C. Samples were analyzed after 0, 30, 100 and 210 min by LC-MS/MS and raw abundance (positive ionization mode) of (A) Spermine, (B) spermidine, (C) pantetheine 4-phosphate, (D) Nicotinamide adenine-dinucleotide (NAD^+), (E) putative identified 4-[2-Hydroxyethyl(propan-2-yl)amino]-4-oxobutanoic acid and (F) unknown feature with 256.9909m/z detected in negative ionization mode are visualized as mean values ± SEM (n=4). An abundance below 2000 is not distinguishable from background noise and is indicated as dotted line.

In summary, 12 features were affected in presence of SSC. The abundance of several RNA building blocks, spermine including the intermediate spermidine and pantetheine 4-phosphate were less increasing over the time within SSC treated lysates. In comparison,

consumption of NAD^+ and putative identified 4-[2-Hydroxyethyl(propan-2-yl)amino]-4-oxobutanoic acid was reduced. Finally, only one feature (m/z 256.9909) detected in negative mode was absent in all control conditions and was increasing over time due to SSC treatment and might cause toxicity.

Key learnings: SSC metabolism

SSC metabolization is likely to occur via GSH interaction yielding mixed disulfides GS-Cys and GS-SO_3. Data suggests that GS-Cys is metabolized in lysates, whereas GS-SO_3, a non-native metabolite, might accumulate over time and thereby influence cellular metabolism.

Within the untargeted LC-MS approach, 12 metabolites were identified to be affected in presence of SSC:

- reduced production or higher consumption:
  six RNA building-blocks, spermine, spermidine and pantetheine 4-phosphate
- higher production or reduced consumption:
  NAD^+ and 4-[2-Hydroxyethyl (propan-2-yl)amino]-4-oxobutanoic acid (putative)
- solely production of an unidentified feature at m/z 256.9909

5. Discussion and outlook

This study focused on the cellular impact of SSC, an unnatural amino acid, which was developed to replace Cys within feed formulations to improve cell culture media stability. Although SSC was demonstrated to be bioavailable and thus can be used as Cys replacement for the production of therapeutic proteins, a drastic response leading to a fast cell death was observed at increasing SSC concentrations. To deepen the understanding of this toxic response, the cellular uptake and the intracellular metabolization of SSC was investigated. Furthermore, the impact of different feed formulations and different CHO cell lines on SSC toxicity was screened to try to identify the main factors in cell culture media impacting SSC performance and to understand the impact of clonal diversity on the toxic effect. Using the data obtained in this study in combination with data from previous studies, a mechanism of action will be proposed in the last section, which might serve as basis for further investigations.

5.1. The CysS/Glu antiporter and the response of CHO cells

Upregulation of the CysS/Glu antiporter

Within this study, expression of the CysS/Glu-antiporter (x_c^-) in CHOK1 cells was upregulated by SFN or SFN-NAC treatment, whereas antiporter inhibition was obtained by SAS treatment. Both treatments, have been reported to influence the antiporter functions for various cell lines [199, 212, 215-222], whereby the response of CHO cells was not reported so far.

As side effect of SFN treatment, a significantly decreased VCD was observed at increasing concentrations, whereby lower SFN concentrations restricted the desired antiporter mRNA upregulation within this study. The diverse cellular response of various cell lines to SFN was highly dose dependent. For example, cell viability of cardiac myoblasts was increased within a study using low SFN concentrations compared to untreated cells. This effect was linked to the upregulation of several detoxifying enzymes, protecting cells against oxidative stress, hence demonstrating that SFN treatment induced several Nrf2 regulated target genes [215]. On the other hand, SFN was reported to cause cell cycle arrest at G_2/M through inhibition of cell cycle regulatory genes *e.g.* in articular chondrocytes [200, 216]. Finally, an apoptotic response to SFN was reported for several cancer cells, which was linked to various mechanisms like DNA hypomethylation or mitochondria-mediated apoptotic pathway leading to increased caspase activity [217-220].

For studies where an adverse effect of SFN treatment was undesired, lower SFN concentrations or shorter incubation time were used to circumvent the detrimental effects. For example, Corssac *et al.* tested the effects of SFN within cardiomyocytes by incubating

the cells for max 24h with two different SFN concentrations. No adverse effect was observed at the lower concentration, whereas a 2-fold higher concentration decreased the cellular viability significantly within that rather short incubation time (compared to fed-batch experiments). In comparison to the observed response in this study, the desired response, which was cellular protection against ROS, was already detectable at the lower SFN concentration [221]. In another study, using primary lung fibroblasts, SFN containing medium was exchanged after 4h to allow further cultivation for 24h, whereby the 4h treatment was sufficient to induce *slc7a11* mRNA upregulation [201]. In the present study, however, a media exchange was undesired, as the accumulated extracellular amino acids were the most interesting functional readouts to prove that the transporter activity was modulated by the treatment. To overcome this, SFN-NAC was tested, which showed a lower impact on the cell viability compared to SFN. A lower toxicity of SFN-NAC was also reported by Liu *et al*. using a colorimetric assay to detect the cell viability of human umbilical vein endothelial cells (HUVECs) in response to SFN and SFN-NAC treatment after 24h. More precisely, both treatments reduced the viability in a dose-dependent manner, whereby SFN showed a stronger cytotoxicity compared to SFN-NAC [202].

Concluding, future experiments to upregulate the transporter may focus on optimizing SFN-NAC treatment as this showed less side effects, while being able to induce transporter upregulation in CHO. Beside SFN-NAC, further intermediates originating from SFN and GSH interaction, like the cysteine-conjugate (SFN-Cys), were demonstrated to exhibit similar protective effects but were less toxic compared to SFN and are therefore interesting for future studies [202]. Beyond that, additional chemicals, which are reported to induce Nrf2 activity might be screened for their ability to trigger antiporter overexpression in CHO, while having less side-effects. For example, Takaya *et al.* described that *tert*-butylhydroquinone, diethylmaleate and dimethylfumarate target the same thiol as SFN within KEAP1 and were successful at inducing Nrf2 activity using embryonic fibroblasts [223]. Dimethylfumarate and diethylmaleate are oxidative stressor and were reported in independent studies to induce antiporter expression [224, 225], suggesting that these chemicals might be good candidates for a screening with CHO. Furthermore, genetically engineered CHO cells, overexpressing the antiporter, might allow cross-validation of the data.

The elevated *SLC7A11* RNA level detected in this study after SFN or SFN-NAC treatment was suggested to correlate with a higher expression of the antiporter and likely explains the observed enhanced transporter activity. Due to the lack of a commercially available antibody with CHO specificity, Western blot analysis was unsuccessful so far. Although several studies demonstrated the correlation of mRNA upregulation and increased antiporter expression, *e.g.* using human cancer cells [226, 227], the detection of this

transporter was inconsistent in the literature. As reviewed by Van Liefferinge *et al.*, different band sizes for the protein were detected within different western blot studies, all claiming to detect the antiporter. Several groups detected the transporter at the predicted molecular weight of about 55 kDa, whereas knock out cell lines demonstrated that the transporter should migrate at about 35 kDa [228]. The 35 kDa band was confirmed by an independent study using a new polyclonal antibody against mouse xCT. A band was detected at 35 kDa in wild type mouse, which was absent when using antiporter knockout mouse (as note: unspecific binding was also observed) [229]. Furthermore, Shih *et al.* demonstrated that the disulfide-linked heterodimer of xCT and 4F2hc migrates at 105 kDa, whereby xCT appeared as 35 kDa band and 4F2hc as 80 kDa band under reducing conditions (via β-ME). Additionally, a 55 kDa band appeared under Nrf2 overexpressing conditions and was suggested to be an alternatively spliced or translationally modified form of the transporter as it did not heterodimerized with 4F2hc [230]. Concluding, a proper control like a *SLC7A11* antiporter knockout cell line would be highly beneficial to assess antibody specificity. To circumvent the lack of antibody specificity, quantitative LC-MS may be performed to monitor antiporter expression level [231].

Inhibition of the CysS/Glu antiporter

In response to SAS, the observed growth reduction of CHO cells was not surprising, as this compound is commonly used as potent tumor growth suppressor, by limiting x_c^- mediated CysS uptake [212]. Further studies demonstrated that reduced CysS uptake causes subsequent GSH depletion, so that cellular protection against ROS is attenuated after SAS treatment [199, 222]. Although a reduced uptake rate through x_c^- was the intended goal of the SAS treatment and not a side effect, supplementation of antioxidants such as taurine (uptake via *SLC6A6* [198]) might be advantageous for the cells to scavenge ROS and thereby diminish the negative response to SAS treatment. In contrast, GSH supplementation is not suitable as it was demonstrated to readily interact with SSC and might be degraded, extracellularly [232]. Still, nonspecific effects of SAS treatment cannot be ruled out and may impact the presented results. Another strategy to cross-validate the obtained data might be the use of noncoding siRNAs to inhibit target *SLC7A11* mRNA translation, leading to reduced transporter expression [233].

SSC uptake via CysS/Glu antiporter

The initial hypothesis of SSC uptake via the CysS/Glu-antiporter is strongly supported by the results of this study, showing increased SSC uptake for cells with enhanced x_c^- transporter activity and reduced SSC uptake via transporter inhibition. Thus, it appears that SSC might be a substrate of the x_c^- transporter. Whereas most amino acid transporters

have a broad substrate specificity, it is generally known that x_c^- has a high specificity for CysS and Glu [117]. However, cystathionine, an intermediate in Cys synthesis, was demonstrated to act as x_c^- substrate using mouse embryonic fibroblasts [234] and L-alanosine was also suggested to be actively transported via x_c^- when analyzing human cancer cell lines [235]. These studies indicate, that the transporter specificity is not as restricted as expected. To verify the transport of SSC via x_c^-, the use of immature eggs (oocytes) co-expressing xCT and 4F2hc seems to be most suitable as the number of endogenous transport systems within oocytes is low and the cells readily express foreign mRNA [236]. Another method like patch clamp is unsuitable, as it is based on ionic currents, whereby the CysS/Glu transport is electroneutral [237]. In addition, *SLC7A11* knockout cells might be useful to analyze if SSC is mainly transported via x_c^- or whether SSC is able to use additional transporter like system L, which is known to transport mixed disulfides [98]. However, due to the significant higher SSC concentrations detected in the supernatant of the culture in response to x_c^- inhibition, SSC transport via further systems is thought to be marginal.

Even though Glu is known to be exported by the x_c^- antiporter, neither transporter inhibition nor transporter upregulation affected the extracellular Glu concentrations in presence of Cys or SSC, significantly. The lack of an impacted Glu transport might be explained by the availability of several Glu transporters in CHO cells *e.g.* EAAT [238], allowing a constant intracellular Glu level independently of x_c^- activity. In contrast to the results presented herein, both SFN and SAS treatments were successfully correlated with Glu transport by Zheng *et al.* through analyzing the cell culture media of treated and untreated fibroblasts over 60 min. More precisely, fibroblasts with a low transporter expression level were treated with SFN (24h before the experiment), leading to an increased Glu release over time, whereas fibroblasts with a high transporter expression were inhibited with SAS, leading to a reduced Glu release [201]. This snapshot however might not represent the dynamic response of cells, when cultivated long-time during a fed-batch experiment. To assess whether co-transport of Glu occurs in response to SSC uptake, the previously described oocytes co-expressing xCT and 4F2hc might be useful to prove or not the exchange of SSC against Glu.

Cellular SSC sensitivity

Within this study, an increased antiporter activity aggravated the toxic response of SSC. In combination with the data derived from eight different CHO cells demonstrating a diverse SSC sensitivity, the antiporter expression level was suggested to determine SSC sensitivity. It is common knowledge, that CHO subclones handle differently both the uptake of nutrients and the intracellular metabolization of metabolites. A broad study investigating three CHO

cell lines with different productivities revealed that about 40% of the known transporters were differently expressed between the clones by studying several time points during cell cultivation. Regarding x_c^-, an upregulation after transition to the stationary phase was observed, whereas no significant difference was observed for the expression level between the three clones. More precisely, a low antiporter expression was observed on day 4, whereas a 13-fold to max 16-fold RNA upregulation was observed on day 6 and 7 [239]. In contrast to the hypothesis made in this study, these observations may indicate that the SSC cell line sensitivity cannot be defined solely by the antiporter level. Therefore, expression of SSC metabolizing or detoxifying enzymes might be critical as well.

The significantly increased extracellular sulfate concentration described in a batch experiment using 1.5 mM SSC compared to 1.5 mM Cys [194], suggests that the cleavage of SSC releases sulfite (SO_3^{2-}) ions which are possibly converted to sulfate (SO_4^{2-}) by sulfite oxidase [240]. The sulfate in turn may be exported by sulfate transporter such as SLC13 and SLC26 [241]. Thus, the differential expression of these enzymes and transporters might impact the response and sensitivity of different clones to SSC. This underlines the necessity to detect intracellular sulfate and sulfite as well as monitor the expression and activity of the mentioned proteins.

5.2. The impact of the feed formulation

Cell culture media and feed are known to be critical for the cellular performance. Within this study, it was shown that not only the SSC concentration but also the feed formulation impacts the toxic response (figure 26 and figure 27).

The fact that *e.g.* insulin and LongR3 IGF-1 were positively correlated with the toxic response through the statistical analysis of the feed screening (table 7), whereas the toxicity assay was not able to detect any influence (figure 32), leaves room for discussion.

MVDA was demonstrated to be a powerful method to assess the cellular response during cell cultivation within several studies [242-244]. For example, cell culture media processing (*e.g.* milling) and raw material impurities were correlated to cell performance using MVDA [242]. However, MVDA generated hypothesis might be wrong due to correlations between several factors or indirect effects, making a careful validation of obtained results essential.

The fact that an identification of compounds which accelerate SSC toxicity was not possible using the toxicity assay, may suggest that these were false positives. On the other hand, the feed formulation might impact the SSC toxicity indirectly by influencing cellular metabolism including SSC metabolization. Thus, the short cultivation during the toxicity assay might be limited to detect such an impact.

Due to the mechanism of action of growth factors like insulin and LongR3 IGF-1 (insulin-like growth factor) [245], SSC toxicity might not be apoptotic nature so that growth factors might influence SSC toxicity indirectly by promoting growth and thereby increase SSC metabolization, which triggers toxicity. The fact that both growth factors were reported to promote cell survival and growth by activating the protein kinase signaling pathway leading to a strong antiapoptotic effect was reported in independent studies and supports this hypothesis [246, 247]. The fact that feed mixtures without insulin triggered SSC toxicity as well, ensures that insulin cannot be the root cause of the toxic response and supports the idea of an indirect impact. The toxicity assay as a fast screening assay, however, was not able to detect a significant difference in the toxic response. Detection of the proposed indirect effect of growth factors might be an assay limitation, as the cultivation is only three days, whereas the statistical analysis is based on the fed-batch screening. Hence, a fed batch with different insulin ratios should be performed to validate this result.

Statistical analysis of the feed screening indicated a negative correlation of Glu to SSC toxicity (table 7), suggesting a mitigating effect, which was confirmed in this study (figure 23 B) and also in a previous study [196]. The fact that Glu and SSC share a high structure similarity might be critical for this effect. The similarity became clear especially in context of the glutamate receptor (NMDA-receptor), as SSC was reported to be a potent agonist of the receptor causing neurotoxicity due to excessive channel activation [248]. Using CHO cells, a toxicity due to excessive NMDA mediated signaling may not be expected, since this receptor is commonly expressed in nerve cells mediating excitatory neurotransmission [249]. Interestingly, several isoforms of this receptor are listed in the CHO databank [250]. To verify the expression of the NMDA-receptor, qPCR analysis may be performed. In case NMDA-receptor is expressed in CHO, the non-competitive NMDA-receptor antagonist (MK801) might be tested, as application of this antagonist was demonstrated to diminish the neurotoxic effect of SSC *in vivo* [251]. A competitive inhibition of a Glu-receptor through SSC might explain the counteracting effect of increasing Glu concentrations as observed in the toxicity assay (figure 23 B).

The negative correlation of copper with the toxic response through the statistical analysis of the feed screening (table 7) was validated in a previous study [196] and might be explained by the oxidizing properties or the sulfur-complexing activity of copper [252]. For example, copper can catalyze oxidizing reactions of GSH to GSSG [253], so that the interaction with SSC might be reduced, although cells might be more susceptible to ROS in case of reduced GSH. Furthermore, SSC might interact directly with accessible protein thiols, whereas the presence of copper might reduce the number of free thiols due to enhanced oxidation. This hypothesis is supported by a study attempted to reduce the number of unpaired thiols in the Fab region of an antibody. Within this study, it was demonstrated that the addition of $CuSO_4$ to the media decreased the free protein thiol content significantly by more than 10-fold in CHO cells [254]. Consequences of a direct interaction of SSC with protein thiols are further discussed in section 5.4.

5.3. SSC metabolization, a hint for SSC toxicity

Interaction studies of SSC with small molecules indicated that SSC reacts predominantly with GSH, a major cellular antioxidant, yielding mixed disulfides GS-Cys and GS-SO_3. After incubation of extracted metabolites with SSC, a high and constant GS-SO_3 abundance was detected (figure 35 D), whereas this abundance was further increased over time using whole cell lysates (figure 37 D). In comparison, GS-Cys abundance was constant over time in presence of extracted metabolites (figure 35 C) but was decreased in presence of enzymes (figure 37 C), hence confirming functional metabolization mechanisms for GS-Cys within this experimental setup. Data suggest that SSC promotes GSH depletion (figure 37 B) and GS-SO_3 formation, which might accumulate intracellularly through the lack of an adequate metabolization mechanism. Both might create an imbalance within functional cellular processes.

Toxicity of SSC due to abrupt GSH depletion

Since high GSH concentrations were reported to protect cells against excessive ROS and other electrophiles [135], the chemical interaction of SSC with GSH might create a disbalanced GSH homeostasis, as more GSH will be bound as GS-SO_3 at high SSC concentrations. Although other redox couples are available within cells (*e.g.* the thioredoxin system), GSH is known to be the major cellular antioxidant and a GSH depletion is very likely to cause a lower redox buffering capacity that can lead to detrimental oxidative damage [135, 255]. The vital role of GSH for cells was demonstrated using several genetically engineered mouse models studying deficiencies in the GSH biosynthesis pathway that led to GSH depletion [256].

Another explanation for the toxic response observed in response to GSH depletion might be a reduced glutathionylation of apoptosis regulating proteins. Caspases are thiol-dependent proteases, which trigger a cascade in response to apoptotic signals. As the proteolytic activity of caspases was inhibited by glutathionylation of the Cys residue in the active site [257], GSH depletion may reduce glutathionylation level of caspases, which in turn sensitize cells to apoptotic stimuli. In line with that, was the apoptotic-resistance of leukemia cells associated with high intracellular GSH levels leading to an elevated glutathionylation level, which was reversed by GSH downregulation using a specific inhibitor preventing GSH *de novo* synthesis [258]. Overall, GSH depletion is generally described as root cause of cell death, which can induce or stimulate apoptosis [259].

In another study, GSH depletion was described to induce lipid peroxidation of human skin fibroblasts when investigating the cytotoxic effect of a disulfide bearing fungicide, whereby the root cause was suggested to be a disulfide exchange of the fungicide with GSH [260].

The increased intracellular GSH concentration observed in a previous study using a non-toxic SSC concentration during a batch experiment [194] is contradictory to GSH depletion observed in the interaction study (figure 37 B). The fact that GSH depletion in the spiking experiment was observed for an SSC:GSH ratio of 10:1 might suggest that such a ratio is not reached intracellularly, especially in an experiment using a non-toxic SSC concentration. But this does not imply, that the intracellular GSH pool cannot be depleted in response to high SSC concentrations applied during fed-batch experiments. An intracellular GSH depletion at a toxic SSC concentration cannot be easily assessed analytically, as cell death is commonly accompanied by GSH depletion, so that a discrimination of whether GSH depletion is the initiator for the toxic response or a consequence of the occurring cell death is not possible.

Additionally, it should be kept in mind, that the SSC interaction experiment using whole cell lysates might not reflect an intact cell, having different cellular compartments. This compartmentation provides the cell an opportunity to perform reactions under specific controlled conditions at a specific pH, whereas the *in vitro* experiment was performed at pH 7.2 to reflect the cytosol as main compartment [261]. For instance, mitochondria possess 10-15% of total GSH and a pH of 8 to ensure a reduced GSH form, whereby the reactivity of GSH to SSC might be impacted at this pH [255, 261]. However, SSC uptake into the cytosol is likely to decrease the cytosolic GSH pool, whereby the mitochondrial GSH pool might be sustained until cytosolic GSH is depleted.

Toxicity of SSC due to GS-SO_3 accumulation

Mixed disulfides are known to be reduced and recycled by enzymes such as the glutathione reductase (GR) [262] and the difference between GS-Cys metabolization and GS-SO_3 accumulation might be a hint for the SSC toxicity root cause.

Winell and Mannervik demonstrated that GS-SO_3 reduction in liver and peas is GSH dependent. More precisely, GS-SO_3 reduction is initiated via GSH interaction releasing sulfite and subsequent GSSG reduction occurs via GR [263]. Data suggest that previous described GSH depletion promotes GS-SO_3 accumulation as GSH is obligatory for this reaction. This dependence might accelerate the toxic response whenever a threshold (low GSH value) is reached.

Within several studies using *e.g.* lung cells, GS-SO_3 was further described as competitive inhibitor of GST which catalyzes *e.g.* the transfer of GSH onto xenobiotics [264, 265]. This inhibition of GST by GS-SO_3 might impact a broad range of cellular functions such as the detoxification of xenobiotics (electrophilic chemicals not produced by the cell), biosynthesis of steroid hormones or proper glutathionylation as described previously for caspases [266]. As a result, reduced GST activity due to GS-SO_3 mediated inhibition might disable cellular response to cellular stressor, which might lead to the observed cell death.

Toxicity of SSC due to metabolic blockage

SSC interaction studies revealed several impacted metabolites, whereby pantetheine 4'-phosphate showing a significant depletion in response to SSC (figure 39 C). In addition, the formation of several RNA building blocks (figure 38) was inhibited in presence of SSC, which might also explain the observed toxicity.

Pantetheine 4'-phosphate was identified as an interesting feature within the LC-MS study presented in this work, since no increase in abundance was observed in lysates following SSC treatment compared to highly increased abundance in Cys treated or untreated lysates. As substrate of CoA biosynthesis (figure 2), pantetheine 4'-phosphate depletion suggests that CoA formation might be affected in cells treated with SSC. CoA is a vital substrate for several oxidative and biosynthetic reactions in mitochondria and cytosol [267]. For instance, CoA is required to produce acetyl-CoA via pyruvate decarboxylation, which in turn is used in the TCA for ATP generation [268]. Several research groups investigated the consequences of CoA depletion in the organism. For instance, Zhang *et al.* blocked CoA synthesis by chemical inhibition of pantothenate kinases, which induced a dramatic metabolic change to maintain the crucial CoA pool using human cell lines. *In vivo* application of this inhibitor revealed a toxic response in mice and confirms that CoA is crucial for cell survival [269]. An independent study supports the importance of CoA by using knockout mice (pantothenate kinase), whereby knockout of one isoform caused a reduced metabolic

flexibility (*e.g.* the pathway fatty acid β-oxidation would be reduced to a minimum), whereas a double knockout of both isoforms was toxic for the cells [270]. It appears that, an organism compensates a decrease in the CoA pool by reducing CoA based metabolic pathways, whereby an organism cannot compensate for a total depletion of the CoA pool. To gain a deeper understanding of the cellular response, the interaction of pantetheine 4'-phosphate (bearing a thiol) with SSC should be studied in depth to determine whether disulfide exchange between the compounds occurs and whether the product prevents CoA formation.

Nucleosides and methylated nucleosides were interesting features in the LC-MS study as well, since no increase in abundance was observed in SSC treated lysates compared to highly increased abundance in Cys or untreated lysates (figure 38), suggesting either an inhibited RNA building block synthesis or a prevention of RNA degradation in presence of SSC.

Inhibition of the ribonuclease A (RNase A) in presence of SSC might explain the reduced abundance of the nucleosides, as this enzyme specifically cleaves on the 3' side of cytidine and uridine [271], which were both depleted in presence of SSC (figure 38 A+C), whereas the other three nucleosides were similar compared to the untreated lysate. The incubation of RNA and RNase A with and without SSC might bring evidence whether the depletion is caused by a RNase A inhibition. If this mechanism can be ruled out, the synthesis of RNA building block might be inhibited in presence of SSC, which is likely detrimental for the cells as this would impair protein translation.

In summary, intracellular SSC metabolization might impact various cellular processes including the cellular redox regulation via GSH depletion, enzyme inhibition via GS-SO_3 accumulation and diverse metabolic dysregulation. All of these hypotheses have to be verified independently to explain the overall complex toxic response induced in SSC treated cells.

5.4. The hypothesis beyond

Within the previous sections, several mechanisms have been described to explain the toxic response of SSC. This last section is aimed to combine results targeting the complex toxic response with results obtained in previous studies describing mostly the positive impact of SSC [194, 195].

Reducing oxidoreductases might accelerate SSC metabolization

Within the interaction study of SSC using whole cell lysates, a reduced SSC abundance was observed over time (figure 37 A), whereby it was constant in extracts (figure 35 A) suggesting that SSC is also enzymatically metabolized. Oxidoreductases, which are known

to accelerate disulfide shuffling during protein folding, might be able to metabolize SSC and thereby contribute to the time dependent reduction of the SSC abundance observed in this study. The catalytic function of oxidoreductases is determined through the p*K*a of the mono- or dithiol motif (Cys-X-X-Cys) and relative stability of the thiolate in the catalytic center [272]. For isomerases like protein disulfide isomerase (PDI), the catalytic center has one solvent exposed thiolate (reactive) and one buried thiolate (stabilized), which enable both reducing and oxidizing activity [149]. In comparison, highly stabilized thiolates found for example in the endoplasmic reticulum oxidoreductin 1 (Ero1p) support mainly oxidation of disulfides, whereas poorly stabilized thiolates found in Trx and Grx, support the reduction of disulfides including persulfides [273]. Based on these different reactivities of oxidoreductases, Gan *et al.* suggested, that SSC may be metabolized by Grx [274]. In a later study, overexpression of different oxidoreductases like Grx and Trx were demonstrated to enhance SSC metabolization with the goal to increase Cys production using *Escherichia coli.* The group demonstrated, that dithiol motifs as in Trx1, Trx2 and Grx2 are able to convert SSC into Cys and sulfite *in vitro*, whereas the other tested oxidoreductases containing monothiol active sites, showed poor activity [275].

Concluding, CHO cells bearing dithiol oxidoreductases might contribute to reduction of SSC to Cys and sulfite as visualized in figure 40. SSC metabolization is likely to be accelerated by Trx1 and Grx2, as these oxidoreductases are present in the cytosol, whereas Trx2 is mainly found in mitochondria [177, 276].

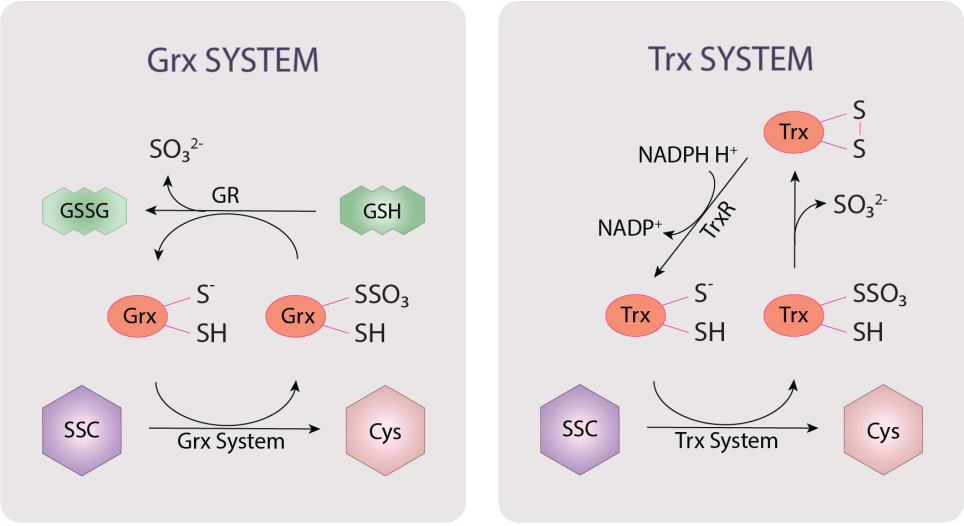

Figure 40. Proposed enzymatic SSC metabolization via oxidoreductases. Glutaredoxin (Grx) and thioredoxin (Trx) bearing a reduced thiol, enables the nucleophilic attack of SSC. Both systems can release sulfite via intrachain disulfide formation (only shown for Trx). Glutathione reductase (GR) catalyzes the reduction of Grx to the active form via reduction of glutathione (GSH) to glutathione-disulfide (GSSG), whereby thioredoxin reductase (TrxR) catalyzes the reduction of Trx to the active form consuming NADPH.

Persulfidation of protein thiols

Increased SSC metabolization raises the question on how cells cope with the increased sulfite released through SSC metabolization. Beside conversion of sulfite to sulfate and subsequent cellular elimination of sulfate, sulfite might be transferred via cysteine lyase onto Cys yielding L-Cysteate (as visualized in figure 2) and hydrogen sulfide, which can in turn trigger persulfidation of oxidized thiols as described in chapter 1.3.3 (figure 42). Additionally, sulfite may interact with intracellular metabolites like GSH leading to GS-SO_3 or might be transferred onto susceptible protein thiols leading to perthiosulfonic acid (P-Cys-S-SO_3H). Perthiosulfonic acid is a highly oxidized persulfide, which is known as an endogenous, oxidative PTM involved in redox-based signaling. However, persulfidation is a dynamic process and SSC metabolization might disbalance this mechanism significantly, which might explain several effects observed in the current and previous SSC studies.

Enhanced cell performance through increased persulfidation via modest SSC concentration

Due to the fact that protein persulfide oxidation occurs naturally and due to reported reversibility of persulfides (including all oxidized persulfide states), SSC induced protein thiol modification to perthiosulfonic acid is not supposed to be directly toxic. Therefore, the eventual impact of protein thiol persulfidation at modest SSC concentration on the production process is discussed. In comparison to Cys-containing feed, the presence of SSC induced an enhanced cell performance and prolonged viability [194]. Since the perthiosulfonic acid modification is reversible, whereas the protein thiol overoxidation to the corresponding sulfonic state is irreversible and leads to protein degradation, slightly increased persulfidation levels through SSC might be advantageous for the cells. Especially during prolonged cultivation with increasing ROS, persulfidation of protein thiols might prevent harmful oxidation of protein thiols and thereby prolong cell viability, when using low SSC concentrations.

If persulfidation occurs in presence of SSC, the probability that the highly overexpressed target protein obtains perthiosulfonic acid modification seems reasonable. Regarding native IgG, proper disulfide formation should ensure that no free sulfhydryl occurs, whereas Zhang *et al.* determined that a small fraction of recombinant produced IgG expressed in CHO contain unpaired thiols [277]. However, peptide mapping of IgG expressed in presence of SSC revealed no SSC integration within a previous study [194]. Consequently, the persulfidation level of IgG is rather uncritical. But it might be reasonable to include the persulfidation level of the therapeutic protein as released criteria in a production processes using SSC.

Persulfidation depends on protein thiol accessibility and reactivity

The protein thiol accessibility which determines the theoretical achievable persulfidation level of host cell proteins needs to be discussed next to evaluate possible persulfidation targets at high SSC concentrations, which might trigger toxicity. In general, Cys has a low abundance in the amino acid sequence of proteins (<2%) and free thiols at the protein surface are generally rare, since most of the Cys residues are conserved in disulfide bridges, which reduces the possibility of PTM persulfidation [278]. The remaining accessible thiols are commonly conserved in the functional center of proteins. These are vulnerable for modification and are in turn crucial for cellular redox-regulation. For example, cultivation of human embryonic kidney cells (HEK293) revealed persulfidation of several proteins *e.g.* epidermal growth factor receptor (EGFR) with about 5-8% persulfidation in unstressed conditions [279]. EGFR regulates several signal transduction cascades and present Cys residues are predominantly buried except for the active-site Cys at the amino acid position 797 (PDB: 3VJO), which is likely the persulfidation target [161, 280]. An even higher persulfidation level of about 15% in unstressed HEK293 cells was observed for Peroxiredoxin (Prx), a multimeric enzyme having two catalytic accessible Cys residues per subunit (*e.g.* Prx4; PDB: 3TKS) [174]. These studies suggest that the persulfidation level in unstressed conditions is determined by the number of accessible protein thiols, since it increases the probability of persulfidation. However, the number of accessible Cys is unlikely the only criteria for persulfidation. The microenvironment is also critical, which defines the pK_a value, thiol nucleophilicity as well as intra-disulfide interactions whenever another thiol is in close proximity. An overview of common protein thiols with a redox-active motif are summarized in table 10 to assess potential target proteins for SSC-induced persulfidation. Proteins can have an accessible monothiol, a dithiol motif (commonly Cys-X-X-Cys) allowing the formation of intrachain disulfides, a 2-Cys motif (two distant, accessible Cys residues) allowing the formation of interchain disulfides or polythiols. As described for Trx, persulfidation of dithiols is unlikely, as an intra-disulfide bridge can release sulfite (figure 40). In comparison, monothiols and proteins with a 2-Cys motif are more susceptible to persulfidation.

Table 14. Proteins with thiol active-sites.

Protein	Abb.	Conserved motif	Compartment	Ref
Thioredoxin	Trx1	dithiol (CXXC)	CYT, NUC	[177, 276]
	Trx2	dithiol (CXXC)	MIT	[177, 281]
Trx reductase	TrxR1	selenolthiol	CYT	
	TrxR2	selenolthiol	MIT	[177, 281]
	TrxR3	selenolthiol	CYT, NUC	
Glutaredoxin	Grx1	dithiol	CYT, NUC	
	Grx2	dithiol	CYT, MIT, NUC	[158, 159,
	Grx3	monothiol	CYT, NUC	282]
	Grx5	monothiol	MIT	
GSH reductase	GR	dithiol (CXXXC)	CYT, MIT	[283]
Peroxiredoxin	Prx1	2-Cys	CYT, PER, NUC	
	Prx2	2-Cys	CYT, NUC	
	Prx3	2-Cys	MIT	[282, 284]
	Prx4	2-Cys	CYT, ER	
	Prx5	2-Cys	CYT, MIT, PER	
	Prx6	2-Cys	CYT, LYS	
GSH peroxidase	GPx	monothiol	CYT	[285]
Sulfiredoxin	Srx	monothiol	CYT, MIT	[162]
Sulfurtransferase	ST	monothiol	MIT	[286]
Protein disulfide isomerase	PDI	dithiol	ER	[150]
ER oxidoreductin 1	Ero1p	CXXCXXC	ER (lumen)	[149, 150]
kelch like ECH associated protein 1	KEAP1	polythiol	CYT	[223]
protein tyrosine phosphatase	PTP	monothiol	ER (CYT)	[287]
Pyruvate kinase M2	PKM2	monothiol	CYT, NUC	[175, 288]
glyceraldehyde-3-phosphate dehydrogenase	GAPDH	Dithiol (CXXXC) + Cys^{247}	CYT	[289]
Superoxide dismutase	SOD1	CXC	CYT	[290]
	SOD2		MIT	
Cys proteases *e.g.* Caspase		monothiol	CYT	[291]

CYT=cytosol (pH 7.2), MIT=mitochondria (pH 8.0), NUC=nucleus (pH 7.2), PER=peroxisome (pH 4.5-5.0), ER=endoplasmic reticulum (pH 7.2), LYS=lysosome (pH 4.5-6.0). *mainly found in yeast and *Escherichia coli*

Excessive persulfidation through high SSC metabolization

High extracellular SSC concentration or x_c^- transporter overexpression can induce increased SSC uptake (figure 22) and subsequent elevated SSC metabolization. Thereby, excessive persulfidation of functional protein thiols via direct transfer of the SO_3 group from SSC or indirectly via GS-SO_3 or reaction with Trx released sulfite might be triggered

(figure 41). As high persulfidation require enhanced activity of the reductase machinery to maintain protein activity, increasing SSC metabolization might disbalance the redox regulating mechanism for proteins and enzymes and moreover trigger a toxic response. For clarity, excessive persulfidation might be comparable with oxidative stress. Cells can cope with a specific amount of ROS, but at a certain threshold, cells collapse. Similar to oxidative stress, persulfidation might be balanced by *e.g.* exporting sulfate and the reducing activity of oxidoreductases. In contrast, high SSC metabolization might trigger excessive persulfidation of various enzymes disabling key cellular functions. The impact of excessive persulfidation was not yet reported in the literature, since sulfur species are rather limited within cells. However, Wedmann *et al.* concluded already that excessive persulfidation might be detrimental [178]. Therefore, persulfidation of a few metabolic key proteins are described hereafter.

For example, persulfidation of protein tyrosine phosphatase (PTP) family was reported to inhibit enzymatical activity, which is commonly initiated through ER stress. Key for this is the monothiol in the active site of PTP with a low pK_a ranging from 4.6 to 5.5 which is susceptible to persulfidation. As consequence, a cascade is triggered which leads to global inhibition of protein translation. More precisely, PTP inhibition leads to increased phosphorylation of protein kinase-like endoplasmic reticulum kinase (pERK), which in turn activates eukaryotic translation initiation factor 2α (eIF2α) leading to attenuation of protein translation [287]. Thus persulfidation of PTP, allows the regulation of several key proteins within signaling pathways as reported by Dóka *et al.* [174]. Similarly, high SSC concentrations might trigger PTP persulfidation leading to loss of protein translation when the reduction machinery cannot cope with the excessive persulfidation level. Additional studies performed by Longen *et al.* demonstrated that increased persulfidation of four Cys residues within Pyruvate kinase M2 (PKM2) monomer (PDB: 3SRH) inhibited the enzyme activity. The enzyme activity is critical for cell survival, since PKM2 catalyzes the last step during glycolysis to produce ATP [175]. Both examples show possible consequences of excessive persulfidation, whereby the broad variety of thiol bearing enzymes having a broad functionality makes it impossible to define the root cause without further studies.

In summary, functional monothiols with a low pK_a are likely deprotonated and thereby susceptible to persulfidation through SSC treatment. SSC metabolization may lead to intracellular GS-SO_3, sulfite and H_2S accumulation, which may contribute to persulfidation of Cys-dependent enzymes. The persulfidation level is balanced by oxidoreductases like Trx, which preserves protein activity. However, oxidoreductases might not be able to cope with excessive persulfidation at increasing SSC metabolization. As functional protein thiols are key for several cellular mechanisms, excessive persulfidation might disable key proteins resulting in a rapid cell death.

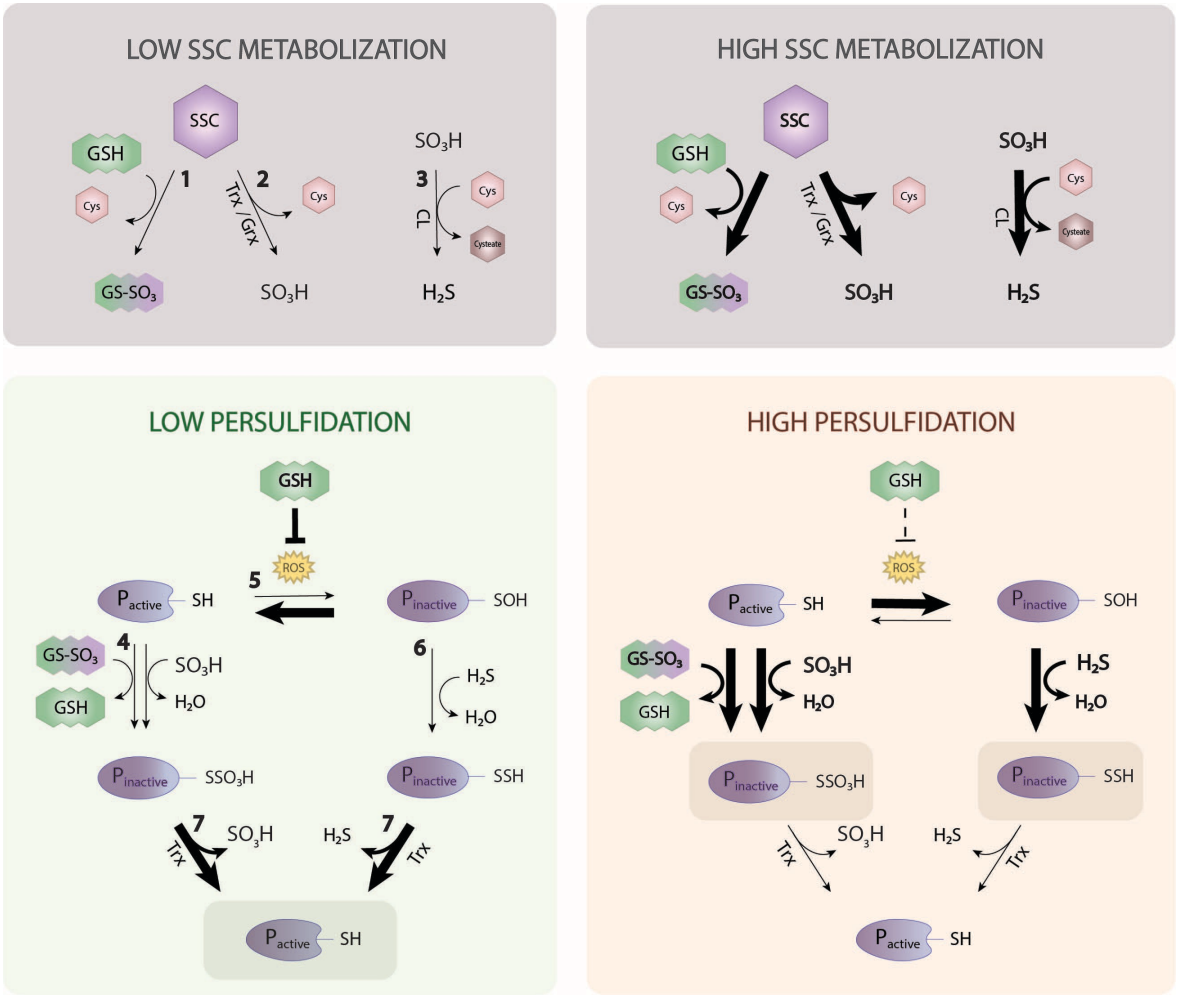

Figure 41. Proposed dose dependent mechanism of SSC. Depending on the extracellular concentration of *S*-Sulfocysteine (SSC) and the x_c^- transporter expression either a low (left side) or a high SSC uptake rate (right side) determines the cellular fate. SSC metabolization is visualized on the top and persulfidation mechanism is visualized at the bottom. (**1**) Chemical interaction of SSC with Glutathione (GSH) leads to *S*-sulfoglutathione (GS-SO_3) and (**2**) enzymatic SSC metabolization via dithiol bearing oxidoreductases like thioredoxin (Trx) releases sulfite, which is in turn catalyzed by (**3**) cysteine lyase (CL) leading to hydrogen sulfide (H_2S). Persulfidation of protein thiols (P-SH) might occur directly via (**4**) GS-SO_3 or sulfite interaction leading to cysteine perthiosulfonic acid (P-SSO_3H). (**5**) In case of low GSH, oxidation of protein thiols to cysteine sulfenic acid (P-SOH) occurs via reactive oxygen species (ROS), whereby (**6**) H_2S can subsequently trigger formation of cysteine hydropersulfide (P-SSH). (**7**) Both persulfide modifications are reversible and are balanced through Trx system, so that protein activity is preserved at a low SSC concentration. In contrast, high SSC concentrations might trigger GSH depletion and accumulation of GS-SO_3, sulfite and H_2S, which causes excessive persulfidation of Cys-dependent key proteins leading inevitably to cell death.

6. References

1. Harfenist, E.J. and Craig, L.C., *The Molecular Weight of Insulin.* J Am Chem Soc, 1952. 74(12): p. 3087-9.

2. Recny, M.A., Scoble, H.A., and Kim, Y., *Structural characterization of natural human urinary and recombinant DNA-derived erythropoietin. Identification of des-arginine 166 erythropoietin.* J Biol Chem, 1987. 262(35): p. 17156-63.

3. Lamanna, W.C., et al., *The structure-function relationship of disulfide bonds in etanercept.* Sci Rep, 2017. 7(3951): p. 1-8.

4. FDA. *U.S. Food and Drug Administration*. [05.05.2020].

5. Kjeldsen, T., *Yeast secretory expression of insulin precursors.* Appl Microbiol Biotechnol, 2000. 54(3): p. 277-86.

6. Zieliński, M., et al., *Expression and purification of recombinant human insulin from E. coli 20 strain.* Protein Expr Purif, 2019. 157: p. 63-9.

7. IDF. *International Diabetes Federation Diabetes atlas*. 2019 [03.02.2020]; 9th:[https://www.diabetesatlas.org/en/].

8. Batra, J. and Rathore, A.S., *Glycosylation of monoclonal antibody products: Current status and future prospects.* Biotechnol Prog, 2016. 32(5): p. 1091-102.

9. Liu, J.K.H., *The history of monoclonal antibody development – Progress, remaining challenges and future innovations.* Ann Med Surg, 2014. 3(4): p. 113-6.

10. Nelson, A.L., Dhimolea, E., and Reichert, J.M., *Development trends for human monoclonal antibody therapeutics.* Nat Rev Drug Discov, 2010. 9(10): p. 767-74.

11. Bonilla, F.A. and Oettgen, H.C., *Adaptive immunity.* J Allergy Clin Immunol, 2010. 125(2): p. 33-40.

12. Dowd, S.E., Halonen, M.J., and Maier, R.M., *Chapter 12 - Immunological Methods*, in *Environmental Microbiology (Second Edition)*, R.M. Maier, Pepper, I.L., and Gerba, C.P., Editors. 2009, Academic Press: San Diego. p. 225-41.

13. Li, X., et al., *Disulfide bond assignment of an IgG1 monoclonal antibody by LC-MS with post-column partial reduction.* Anal Biochem, 2013. 436(2): p. 93-100.

14. Kshirsagar, R., et al., *Controlling trisulfide modification in recombinant monoclonal antibody produced in fed-batch cell culture.* Biotechnol Bioeng, 2012. 109(10): p. 2523-32.

15. Mian, I.S., Bradwell, A.R., and Olson, A.J., *Structure, function and properties of antibody binding sites.* J Mol Biol, 1991. 217(1): p. 133-51.

16. Natsume, A., Niwa, R., and Satoh, M., *Improving effector functions of antibodies for cancer treatment: Enhancing ADCC and CDC.* Drug Des Devel Ther, 2009. 3: p. 7-16.

17. Mankarious, S., et al., *The half-lives of IgG subclasses and specific antibodies in patients with primary immunodeficiency who are receiving intravenously administered immunoglobulin.* J Lab Clin Med, 1988. 112(5): p. 634-40.

18. Schofield, T., Robbins, D., and Miró-Quesada, G., *Critical Quality Attributes, Specifications, and Control Strategy*, in *Quality by Design for Biopharmaceutical Drug Product Development*, F. Jameel, et al., Editors. 2015, Springer New York: New York, NY. p. 511-35.

19. Rosenberg, A.S., *Effects of protein aggregates: an immunologic perspective.* Aaps j, 2006. 8(3): p. 501-7.

20. Ratanji, K.D., et al., *Immunogenicity of therapeutic proteins: influence of aggregation.* J Immunotoxicol, 2014. 11(2): p. 99-109.

21. Cromwell, M.E., Hilario, E., and Jacobson, F., *Protein aggregation and bioprocessing.* Aaps j, 2006. 8(3): p. 572-9.

22. Vázquez-Rey, M. and Lang, D.A., *Aggregates in monoclonal antibody manufacturing processes.* Biotechnol Bioeng, 2011. 108(7): p. 1494-508.

23. Paul, A.J., Schwab, K., and Hesse, F., *Direct analysis of mAb aggregates in mammalian cell culture supernatant.* BMC Biotechnol, 2014. 14(99): p. 1-11.

24. Chakravarthi, S. and Bulleid, N.J., *Glutathione is required to regulate the formation of native disulfide bonds within proteins entering the secretory pathway.* J Biol Chem, 2004. 279(38): p. 39872-9.

25. Gomes, J. and Hiller, G., *Use of low temperature and/or low pH in cell culture*. 2008, Wyeth LLC.

26. Rodriguez, J., et al., *Enhanced production of monomeric interferon-beta by CHO cells through the control of culture conditions.* Biotechnol Prog, 2005. 21(1): p. 22-30.

27. Jing, Y., et al., *Identification of cell culture conditions to control protein aggregation of IgG fusion proteins expressed in Chinese hamster ovary cells.* Process Biochem, 2012. 47(1): p. 69-75.

28. Arakawa, T. and Timasheff, S.N., *The stabilization of proteins by osmolytes.* Biophys J, 1985. 47(3): p. 411-4.

29. Back, J.F., Oakenfull, D., and Smith, M.B., *Increased thermal stability of proteins in the presence of sugars and polyols.* Biochemistry, 1979. 18(23): p. 5191-6.

30. Yoshida, H., et al., *Chemical chaperones reduce aggregate formation and cell death caused by the truncated Machado-Joseph disease gene product with an expanded polyglutamine stretch.* Neurobiol Dis, 2002. 10(2): p. 88-99.

31. Dengl, S., et al., *Aggregation and chemical modification of monoclonal antibodies under upstream processing conditions.* Pharm Res, 2013. 30(5): p. 1380-99.

32. Yigzaw, Y., et al., *Ion exchange chromatography of proteins and clearance of aggregates.* Curr Pharm Biotechnol, 2009. 10(4): p. 421-6.

33. Arosio, P., et al., *Aggregation Stability of a Monoclonal Antibody During Downstream Processing.* Pharm Res, 2011. 28: p. 1884-94.

34. Wang, S., et al., *Characterization of product-related low molecular weight impurities in therapeutic monoclonal antibodies using hydrophilic interaction chromatography coupled with mass spectrometry.* J Pharmaceut Biomed, 2018. 154: p. 468-75.

35. Alam, M.Z., Regioneiri, L., and Santos, M.A.S., *Determination of amino acids misincorporation in recombinant protein by mass spectrometry.* BJAS, 2013. 42(1): p. 1987-95.

36. Vlasak, J. and Ionescu, R., *Fragmentation of monoclonal antibodies.* mAbs, 2011. 3(3): p. 253-63.

37. Robert, F., et al., *Degradation of an Fc-fusion recombinant protein by host cell proteases: Identification of a CHO cathepsin D protease.* Biotechnol Bioeng, 2009. 104(6): p. 1132-41.

38. Kao, Y.H., et al., *Mechanism of antibody reduction in cell culture production processes.* Biotechnol Bioeng, 2010. 107(4): p. 622-32.

39. Trexler-Schmidt, M., et al., *Identification and prevention of antibody disulfide bond reduction during cell culture manufacturing.* Biotechnol Bioeng, 2010. 106(3): p. 452-61.

40. Liu, H. and May, K., *Disulfide bond structures of IgG molecules: structural variations, chemical modifications and possible impacts to stability and biological function.* mAbs, 2012. 4(1): p. 17-23.

41. Pristatsky, P., et al., *Evidence for Trisulfide Bonds in a Recombinant Variant of a Human IgG2 Monoclonal Antibody.* Anal Chem, 2009. 81(15): p. 6148-55.

42. Magdelaine-Beuzelin, C., et al., *Structure-function relationships of the variable domains of monoclonal antibodies approved for cancer treatment.* Crit Rev Oncol Hematol, 2007. 64(3): p. 210-25.

43. Khoury, G.A., Baliban, R.C., and Floudas, C.A., *Proteome-wide post-translational modification statistics: frequency analysis and curation of the swiss-prot database.* Sci Rep, 2011. 1(90): p. 1-5.

44. Kurosawa, N., et al., *Novel method for the high-throughput production of phosphorylation site-specific monoclonal antibodies.* Sci Rep, 2016. 6(25174): p. 1-11.

45. Pawson, T. and Scott, J.D., *Protein phosphorylation in signaling-50 years and counting.* Trends Biochem Sci, 2005. 30(6): p. 286-90.

46. Choudhary, C., et al., *Lysine acetylation targets protein complexes and co-regulates major cellular functions.* Science, 2009. 325(5942): p. 834-40.

47. Varki, A., et al., *Essentials of Glycobiology, 2nd edition*. 2009: Cold Spring Harbor Laboratory Press.

48. Jenkins, N., Parekh, R.B., and James, D.C., *Getting the glycosylation right: Implications for the biotechnology industry.* Nat Biotechnol, 1996. 14(8): p. 975-81.

49. Butler, M., et al., *Detailed glycan analysis of serum glycoproteins of patients with congenital disorders of glycosylation indicates the specific defective glycan processing step and provides an insight into pathogenesis.* Glycobiology, 2003. 13(9): p. 601-22.

50. Grünewald, S., Matthijs, G., and Jaeken, J., *Congenital disorders of glycosylation: a review.* Pediatr Res, 2002. 52(5): p. 618-24.

51. Jaeken, J., *Congenital disorders of glycosylation.* Handb Clin Neurol, 2013. 113: p. 1737-43.

52. Hossler, P., *Protein glycosylation control in mammalian cell culture: past precedents and contemporary prospects.* Adv Biochem Eng Biotechnol, 2012. 127: p. 187-219.

53. Liu, L., *Antibody glycosylation and its impact on the pharmacokinetics and pharmacodynamics of monoclonal antibodies and Fc-fusion proteins.* J Pharm Sci, 2015. 104(6): p. 1866-84.

54. Allen, A.C., Harper, S.J., and Feehally, J., *Galactosylation of N- and O-linked carbohydrate moieties of IgA1 and IgG in IgA nephropathy.* J Clin Exp Immunol., 1995. 100(3): p. 470-4.

55. Abès, R. and Teillaud, J.-L., *Impact of Glycosylation on Effector Functions of Therapeutic IgG.* Pharmaceuticals, 2010. 3(1): p. 146-57.

56. Jefferis, R., *Glycosylation of recombinant antibody therapeutics.* Biotechnol Prog, 2005. 21(1): p. 11-6.

57. Zacchi, L.F. and Schulz, B.L., *N-glycoprotein macroheterogeneity: biological implications and proteomic characterization.* Glycoconj J, 2016. 33(3): p. 359-76.

58. Butler, M., *Optimisation of the cellular metabolism of glycosylation for recombinant proteins produced by Mammalian cell systems.* Cytotechnology, 2006. 50(1-3): p. 57-76.

59. Shukla, A.A., et al., *Evolving trends in mAb production processes.* Bioeng Transl Med, 2017. 2(1): p. 58-69.

60. Gramer, M.J., *Product Quality Considerations for Mammalian Cell Culture Process Development and Manufacturing.* 2013. 139: p. 123-66.

61. Hossler, P., Khattak, S.F., and Li, Z.J., *Optimal and consistent protein glycosylation in mammalian cell culture.* Glycobiology, 2009. 19(9): p. 936-49.

62. Durocher, Y. and Butler, M., *Expression systems for therapeutic glycoprotein production.* Curr Opin Biotechnol, 2009. 20(6): p. 700-7.

63. Satoh, M., Iida, S., and Shitara, K., *Non-fucosylated therapeutic antibodies as next-generation therapeutic antibodies.* Expert Opin Biol Ther, 2006. 6(11): p. 1161-73.

64. Kunert, R. and Reinhart, D., *Advances in recombinant antibody manufacturing.* Appl Microbiol Biotechnol, 2016. 100(8): p. 3451-61.

65. Dumont, J., et al., *Human cell lines for biopharmaceutical manufacturing: history, status, and future perspectives.* Crit Rev Biotechnol, 2016. 36(6): p. 1110-22.

66. Jayapal, K.P., et al., *Recombinant protein therapeutics from CHO Cells - 20 years and counting.*, in *Chem Eng Prog*. 2007. p. 40-7.

67. Li, F., et al., *Cell culture processes for monoclonal antibody production.* mAbs, 2010. 2(5): p. 466-77.

68. Fischer, S., Handrick, R., and Otte, K., *The art of CHO cell engineering: A comprehensive retrospect and future perspectives.* Biotechnol Adv, 2015. 33(8): p. 1878-96.

69. Fan, L., et al., *Improving the efficiency of CHO cell line generation using glutamine synthetase gene knockout cells.* Biotechnol Bioeng, 2012. 109(4): p. 1007-15.

70. Reinhart, D., et al., *Bioprocessing of Recombinant CHO-K1, CHO-DG44, and CHO-S: CHO Expression Hosts Favor Either mAb Production or Biomass Synthesis.* Biotechnol J, 2018. 0(1700686): p. 1-11.

71. Dhara, V.G., et al., *Recombinant Antibody Production in CHO and NS0 Cells: Differences and Similarities.* BioDrugs, 2018. 32(6): p. 571-84.

72. Lin, P.C., et al., *Attenuated glutamine synthetase as a selection marker in CHO cells to efficiently isolate highly productive stable cells for the production of antibodies and other biologics.* MAbs, 2019. 11(5): p. 965-76.

73. Noh, S.M., Shin, S., and Lee, G.M., *Comprehensive characterization of glutamine synthetase-mediated selection for the establishment of recombinant CHO cells producing monoclonal antibodies.* Sci Rep, 2018. 8(5361): p. 1-11.

74. Barnes, L.M., Bentley, C.M., and Dickson, A.J., *Advances in animal cell recombinant protein production: GS-NS0 expression system.* Cytotechnology, 2000. 32(2): p. 109-23.

75. Capella Roca, B., et al., *An arginase-based system for selection of transfected CHO cells without the use of toxic chemicals.* J Biol Chem, 2019. 294(49): p. 18756-68.

76. Reinhart, D., et al., *Benchmarking of commercially available CHO cell culture media for antibody production.* Appl Microbiol Biotechnol, 2015. 99(11): p. 4645-57.

77. Bielser, J.M., et al., *Perfusion mammalian cell culture for recombinant protein manufacturing - A critical review.* Biotechnol Adv, 2018. 36(4): p. 1328-40.

78. Vijayasankaran, N., et al., *Animal Cell Culture Media*, in *Encyclopedia of Industrial Biotechnology*. 2010.

79. Zimmer, A., et al., *Improvement and simplification of fed-batch bioprocesses with a highly soluble phosphotyrosine sodium salt.* J Biotechnol, 2014. 186: p. 110-8.

80. Bibila, T.A. and Robinson, D.K., *In pursuit of the optimal fed-batch process for monoclonal antibody production.* Biotechnol Prog, 1995. 11(1): p. 1-13.

81. Brunner, M., et al., *Investigation of the interactions of critical scale-up parameters (pH, pO(2) and pCO(2)) on CHO batch performance and critical quality attributes.* Bioprocess Biosyst Eng, 2017. 40(2): p. 251-63.

82. Yao, T. and Asayama, Y., *Animal-cell culture media: History, characteristics, and current issues.* Reprod Med Biol, 2017. 16(2): p. 99-117.

83. van der Valk, J., et al., *Optimization of chemically defined cell culture media – Replacing fetal bovine serum in mammalian in vitro methods.* Toxicol in Vitro, 2010. 24(4): p. 1053-63.

84. Richardson, J., et al., *Metabolomics analysis of soy hydrolysates for the identification of productivity markers of mammalian cells for manufacturing therapeutic proteins.* Biotechnol Prog, 2015. 31(2): p. 522-31.

85. Jayme, D.W. and Smith, S.R., *Media formulation options and manufacturing process controls to safeguard against introduction of animal origin contaminants in animal cell culture.* Cytotechnology, 2000. 33(1-3): p. 27-36.

86. Zang, L., et al., *Metabolomics Profiling of Cell Culture Media Leading to the Identification of Riboflavin Photosensitized Degradation of Tryptophan Causing Slow Growth in Cell Culture.* Anal Chem, 2011. 83(13): p. 5422-30.

87. McElearney, K., et al., *Tryptophan Oxidation Catabolite, N-Formylkynurenine, in Photo Degraded Cell Culture Medium Results in Reduced Cell Culture Performance.* Biotechnol Prog, 2016. 32(1): p. 74-82.

88. Landauer, K., *Designing media for animal cell culture: CHO cells, the industrial standard.* Methods in molecular biology (Clifton, N.J.), 2014. 1104: p. 89-103.

89. Hassell, T., Gleave, S., and Butler, M., *Growth inhibition in animal cell culture. The effect of lactate and ammonia.* Appl Biochem Biotechnol, 1991. 30(1): p. 29-41.

90. Franek, F., *Starvation-induced programmed death of hybridoma cells: Prevention by amino acid mixtures.* Biotechnol Bioeng, 1995. 45(1): p. 86-90.

91. Yao, T. and Asayama, Y., *Animal-cell culture media: History, characteristics, and current issues.* Reproductive Medicine and Biology, 2017. 16(2): p. 99-117.

92. Cinátl, J., *Inorganic-organic multimolecular complexes of salt solutions, culture media and biological fluids and their possible significance for the origin of life.* J Theor Biol, 1969. 23(1): p. 1-10.

93. Savonnière, S., et al., *Effects of lipid supplementation of culture media on cell growth, antibody production, membrane structure and dynamics in two hybridomas.* J Biotechnol, 1996. 48(1): p. 161-73.

94. Pegg, A.E., *Functions of Polyamines in Mammals.* J Biol Chem, 2016. 291(29): p. 14904-12.

95. Igarashi, K. and Kashiwagi, K., *Modulation of cellular function by polyamines.* Int J Biochem Cell Biol, 2010. 42(1): p. 39-51.

96. Carvalhal, A.V., et al., *Cell growth arrest by nucleotides, nucleosides and bases as a tool for improved production of recombinant proteins.* Biotechnol Prog, 2003. 19(1): p. 69-83.

97. Bannai, S., *Use of 2-mercaptoethanol in cell culture.* Hum Cell, 1992. 5(3): p. 292-7.

98. Ishii, T., Bannai, S., and Sugita, Y., *Mechanism of growth stimulation of L1210 cells by 2-mercaptoethanol in vitro. Role of the mixed disulfide of 2-mercaptoethanol and cysteine.* J Biol Chem, 1981. 256(23): p. 12387-92.

99. Michl, J., Park, K.C., and Swietach, P., *Evidence-based guidelines for controlling pH in mammalian live-cell culture systems.* Commun Biol, 2019. 2(144): p. 1-12.

100. Clincke, M.F., et al., *Effect of surfactant pluronic F-68 on CHO cell growth, metabolism, production, and glycosylation of human recombinant IFN-γ in mild operating conditions.* Biotechnol Prog, 2011. 27(1): p. 181-90.

101. Wagner, I. and Musso, H., *New Naturally Occurring Amino Acids.* Angew Chem Int Ed, 1983. 22(11): p. 816-28.

102. Roos, G., Foloppe, N., and Messens, J., *Understanding the pK(a) of redox cysteines: the key role of hydrogen bonding.* Antioxid Redox Signal, 2013. 18(1): p. 94-127.

103. Reddie, K.G. and Carroll, K.S., *Expanding the functional diversity of proteins through cysteine oxidation.* Curr Opin Chem Biol, 2008. 12(6): p. 746-54.

104. Poole, L.B., *The basics of thiols and cysteines in redox biology and chemistry.* Free Radic Biol Med, 2015. 80: p. 148-57.

105. Marino, S.M. and Gladyshev, V.N., *Analysis and functional prediction of reactive cysteine residues.* J Biol Chem, 2012. 287(7): p. 4419-25.

106. Shimada, K. and Stockwell, B.R., *tRNA synthase suppression activates de novo cysteine synthesis to compensate for cystine and glutathione deprivation during ferroptosis.* Mol Cell Oncol, 2015. 3(2): p. 1-2.

107. Stipanuk, M.H. and Ueki, I., *Dealing with methionine/homocysteine sulfur: cysteine metabolism to taurine and inorganic sulfur.* J Inherit Metab Dis, 2011. 34(1): p. 17-32.

108. Pajares, M.A. and Pérez-Sala, D., *Mammalian Sulfur Amino Acid Metabolism: A Nexus Between Redox Regulation, Nutrition, Epigenetics, and Detoxification.* Antioxid Redox Signal, 2018. 29(4): p. 408-52.

109. Eagle, H., *Nutrition needs of mammalian cells in tissue culture.* Science, 1955. 122(3168): p. 501-14.

110. Zerangue, N. and Kavanaugh, M.P., *Interaction of L-cysteine with a human excitatory amino acid transporter.* J Physiol, 1996. 493(2): p. 419-23.

111. Hediger, M.A., et al., *The ABCs of solute carriers: physiological, pathological and therapeutic implications of human membrane transport proteins.* Eur J Physiol 2004. 447(5): p. 465-8.

112. Kanai, Y. and Hediger, M., *The glutamate and neutral amino acid transporter family: Physiological and pharmacological implications.* Eur J Pharmacol, 2003. 479: p. 237-47.

113. Zerangue, N. and Kavanaugh, M.P., *ASCT-1 is a neutral amino acid exchanger with chloride channel activity.* J Biol Chem, 1996. 271(45): p. 27991-4.

114. Watts, S.D., et al., *Cysteine Transport through Excitatory Amino Acid Transporter 3 (EAAT3).* PloS one, 2014. 9(10): p. 1-12.

115. Bassi, M.T., et al., *Identification and characterisation of human xCT that co-expresses, with 4F2 heavy chain, the amino acid transport activity system xc.* Eur J Physiol, 2001. 442(2): p. 286-96.

116. Sato, H., et al., *Cloning and expression of a plasma membrane cystine/glutamate exchange transporter composed of two distinct proteins.* J Biol Chem, 1999. 274(17): p. 11455-8.

117. Verrey, F., et al., *Glycoprotein-associated amino acid exchangers: broadening the range of transport specificity.* Eur J Physiol, 2000. 440(4): p. 503-12.

118. Koppula, P., et al., *Amino acid transporter SLC7A11/xCT at the crossroads of regulating redox homeostasis and nutrient dependency of cancer.* Cancer Commun, 2018. 38(12): p. 1-13.

119. Wagner, C.A., Lang, F., and Bröer, S., *Function and structure of heterodimeric amino acid transporters.* Am J Physiol Cell Physiol, 2001. 281(4): p. 1077-93.

120. Lewerenz, J., et al., *The cystine/glutamate antiporter system x(c)(-) in health and disease: from molecular mechanisms to novel therapeutic opportunities.* Antioxid Redox Signal, 2013. 18(5): p. 522-55.

121. Bannai, S., *Exchange of cystine and glutamate across plasma membrane of human fibroblasts.* J Biol Chem, 1986. 261(5): p. 2256-63.

122. Geoghegan, D., *Characterisation of Amino Acid Transport Processes in Chinese Hamster Ovary (CHO) Cells*, in *Department of Chemical and Biological Engineering*. 2015, The University of Sheffield. p. 224.

123. Ishii, T., et al., *Mechanism of growth promotion of mouse lymphoma L1210 cells in vitro by feeder layer or 2-mercaptoethanol.* J Cell Physiol, 1981. 107(2): p. 283-93.

124. Shikano, N., et al., *Radioiodinated 4-iodo-l-meta-tyrosine, a system L selective artificial amino acid: molecular design and transport characterization in Chinese hamster ovary cells (CHO-K1 cells).* Nucl Med Biol, 2010. 37(8): p. 903-10.

125. Bass, R., et al., *The A, ASC, and L systems for the transport of amino acids in Chinese hamster ovary cells (CHO-K1).* J Biol Chem, 1981. 256(20): p. 10259-66.

126. Ji, X., et al., *Existence of an endogenous glutamate and aspartate transporter in Chinese hamster ovary cells.* Acta Biochim Biophys Sin 2007. 39(11): p. 851-6.

127. Kyriakopoulos, S., Polizzi, K.M., and Kontoravdi, C. *Dynamic profiling of amino acid transport and metabolism in Chinese hamster ovary cell culture*. in *BMC Proceedings*. 2013. BioMed Central.

128. Leonardi, R., et al., *Coenzyme A: Back in action.* Prog Lipid Res, 2005. 44(2): p. 125-53.

129. Jong, C.J., Azuma, J., and Schaffer, S., *Mechanism underlying the antioxidant activity of taurine: prevention of mitochondrial oxidant production.* Amino Acids, 2012. 42(6): p. 2223-32.

130. Tretter, L. and Adam-Vizi, V., *Alpha-ketoglutarate dehydrogenase: a target and generator of oxidative stress.* Phil Trans R Soc, 2005. 360(1464): p. 2335-45.

131. Wiegand, G. and Remington, S.J., *Citrate synthase: structure, control, and mechanism.* Annu Rev Biophys Biophys Chem, 1986. 15: p. 97-117.

132. Angelova, P.R. and Abramov, A.Y., *Functional role of mitochondrial reactive oxygen species in physiology.* Free Radic Biol Med, 2016. 100: p. 81-5.

133. Stipanuk, M.H., et al., *Mammalian Cysteine Metabolism: New Insights into Regulation of Cysteine Metabolism.* J Nutr, 2006. 136(6): p. 1652-9.

134. Shimada, K., et al., *Role of ROS Production and Turnover in the Antioxidant Activity of Taurine.* Adv Exp Med Biol, 2015. 803: p. 581-96.

135. Forman, H.J., Zhang, H., and Rinna, A., *Glutathione: overview of its protective roles, measurement, and biosynthesis.* Mol Aspects Med, 2009. 30(1-2): p. 1-12.

136. Griffith, O.W., *Biologic and pharmacologic regulation of mammalian glutathione synthesis.* Free Radic Biol Med, 1999. 27(9-10): p. 922-35.

137. Aquilano, K., Baldelli, S., and Ciriolo, M.R., *Glutathione: new roles in redox signaling for an old antioxidant.* Front Pharmacol, 2014. 5(196): p. 1-12.

138. Lu, S.C., *Glutathione synthesis.* Biochim Biophys Acta, 2013. 1830(5): p. 3143-53.

139. Schafer, F.Q. and Buettner, G.R., *Redox environment of the cell as viewed through the redox state of the glutathione disulfide/glutathione couple.* Free Radic Biol Med, 2001. 30(11): p. 1191-212.

140. Sies, H., Berndt, C., and Jones, D.P., *Oxidative Stress.* Annu Rev Biochem, 2017. 86(1): p. 715-48.

141. Hwang, C., Sinskey, A.J., and Lodish, H.F., *Oxidized redox state of glutathione in the endoplasmic reticulum.* Science, 1992. 257(5076): p. 1496-502.

142. Tobwala, S., et al., *Antioxidant potential of Sutherlandia frutescens and its protective effects against oxidative stress in various cell cultures.* BMC complem altern m, 2014. 14(271): p. 1-11.

143. Meredith, M.J. and Reed, D.J., *Status of the mitochondrial pool of glutathione in the isolated hepatocyte.* J Biol Chem, 1982. 257(7): p. 3747-53.

144. Lambert, A.J. and Brand, M.D., *Reactive oxygen species production by mitochondria.* Methods Mol Biol, 2009. 554: p. 165-81.

145. Chakravarthi, S., Jessop, C.E., and Bulleid, N.J., *The role of glutathione in disulphide bond formation and endoplasmic-reticulum-generated oxidative stress.* EMBO reports, 2006. 7(3): p. 271-5.

146. Sies, H. and Jones, D.P., *Reactive oxygen species (ROS) as pleiotropic physiological signalling agents.* Nat Rev Mol Cell Biol, 2020. 21(7): p. 363-83.

147. Appenzeller-Herzog, C., *Glutathione- and non-glutathione-based oxidant control in the endoplasmic reticulum.* J Cell Sci, 2011. 124(6): p. 847-55.

148. Bošnjak, I., et al., *Occurrence of protein disulfide bonds in different domains of life: a comparison of proteins from the Protein Data Bank.* PEDS, 2014. 27(3): p. 65-72.

149. Bardwell, J.C.A., *The dance of disulfide formation.* Nat Struct Mol Biol, 2004. 11(7): p. 582-3.

150. Gross, E., et al., *Structure of Ero1p, source of disulfide bonds for oxidative protein folding in the cell.* Cell, 2004. 117(5): p. 601-10.

151. Tonelli, C., Chio, I.I.C., and Tuveson, D.A., *Transcriptional Regulation by Nrf2.* Antioxid Redox Signal, 2018. 29(17): p. 1727-45.

152. Ulrich, K. and Jakob, U., *The role of thiols in antioxidant systems.* Free Radic Biol Med, 2019. 140: p. 14-27.

153. Yagishita, Y., Uruno, A., and Yamamoto, M., *Chapter 27 - NRF2-Mediated Gene Regulation and Glucose Homeostasis*, in *Molecular Nutrition and Diabetes*, D. Mauricio, Editor. 2016, Academic Press: San Diego. p. 331-48.

154. Chapman, H.A., Riese, R.J., and Shi, G.P., *Emerging roles for cysteine proteases in human biology.* Annu Rev Physiol, 1997. 59: p. 63-88.

155. Settembre, C., et al., *Signals from the lysosome: a control centre for cellular clearance and energy metabolism.* Nat Rev Mol Cell Biol, 2013. 14(5): p. 283-96.

156. Gupta, V. and Carroll, K.S., *Sulfenic acid chemistry, detection and cellular lifetime.* Biochim Biophys Acta, 2014. 1840(2): p. 847-75.

157. Xiao, Z., et al., *Molecular Mechanisms of Glutaredoxin Enzymes: Versatile Hubs for Thiol-Disulfide Exchange between Protein Thiols and Glutathione.* J Mol Biol, 2019. 431(2): p. 158-77.

158. Iversen, R., et al., *Thiol-disulfide exchange between glutaredoxin and glutathione.* Biochemistry, 2010. 49(4): p. 810-20.

159. Lillig, C.H. and Berndt, C., *Glutaredoxins in thiol/disulfide exchange.* Antioxid Redox Signal, 2013. 18(13): p. 1654-65.

160. Peltoniemi, M.J., et al., *Insights into deglutathionylation reactions. Different intermediates in the glutaredoxin and protein disulfide isomerase catalyzed reactions are defined by the gamma-linkage present in glutathione.* J Biol Chem, 2006. 281(44): p. 33107-14.

161. Truong, T.H. and Carroll, K.S., *Redox regulation of epidermal growth factor receptor signaling through cysteine oxidation.* Biochemistry, 2012. 51(50): p. 9954-65.

162. Biteau, B., Labarre, J., and Toledano, M.B., *ATP-dependent reduction of cysteine-sulphinic acid by S. cerevisiae sulphiredoxin.* Nature, 2003. 425(6961): p. 980-4.

163. Taguchi, K., Motohashi, H., and Yamamoto, M., *Molecular mechanisms of the Keap1-Nrf2 pathway in stress response and cancer evolution.* Genes Cells, 2011. 16(2): p. 123-40.

164. Kansanen, E., et al., *The Keap1-Nrf2 pathway: Mechanisms of activation and dysregulation in cancer.* Redox Biol, 2013. 1(1): p. 45-9.

165. Hugo, M., et al., *Early cysteine-dependent inactivation of 26S proteasomes does not involve particle disassembly.* Redox Biol, 2018. 16: p. 123-8.

166. Zhang, J., et al., *An evolving understanding of the S-glutathionylation cycle in pathways of redox regulation.* Free Radic Biol Med, 2018. 120: p. 204-16.

167. Benchoam, D., et al., *Hydrogen Sulfide and Persulfides Oxidation by Biologically Relevant Oxidizing Species.* Antioxidants, 2019. 8(48): p. 1-23.

168. Gallogly, M.M. and Mieyal, J.J., *Mechanisms of reversible protein glutathionylation in redox signaling and oxidative stress.* Curr Opin Pharmacol, 2007. 7(4): p. 381-91.

169. Hansen, R.E., Roth, D., and Winther, J.R., *Quantifying the global cellular thiol–disulfide status.* PNAS, 2009. 106(2): p. 422-7.

170. Gallogly, M.M., Starke, D.W., and Mieyal, J.J., *Mechanistic and kinetic details of catalysis of thiol-disulfide exchange by glutaredoxins and potential mechanisms of regulation.* Antioxid Redox Signal, 2009. 11(5): p. 1059-81.

171. Ida, T., et al., *Reactive cysteine persulfides and S-polythiolation regulate oxidative stress and redox signaling.* PNAS, 2014. 111(21): p. 7606-11.

172. Ono, K., et al., *Redox chemistry and chemical biology of H2S, hydropersulfides, and derived species: implications of their possible biological activity and utility.* Free Radic Biol Med, 2014. 77: p. 82-94.

173. Zhang, D., et al., *H(2)S-Induced Sulfhydration: Biological Function and Detection Methodology.* Front Pharmacol, 2017. 8(608): p. 1-13.

174. Dóka, É., et al., *Control of protein function through oxidation and reduction of persulfidated states.* Sci Adv, 2020. 6(1): p. 1-20.

175. Longen, S., et al., *Quantitative Persulfide Site Identification (qPerS-SID) Reveals Protein Targets of H2S Releasing Donors in Mammalian Cells.* Sci Rep, 2016. 6(29808): p. 1-12.

176. Millikin, R., et al., *The Chemical Biology of Protein Hydropersulfides: Studies of a Possible Protective Function of Biological Hydropersulfide Generation.* Free Radic Biol Med, 2016. 97(1): p. 136–47.

177. Filipovic, M.R., et al., *Chemical Biology of H(2)S Signaling through Persulfidation.* Chem Rev, 2018. 118(3): p. 1253-337.

178. Wedmann, R., et al., *Improved tag-switch method reveals that thioredoxin acts as depersulfidase and controls the intracellular levels of protein persulfidation.* Chem sci, 2016. 7(5): p. 3414-26.

179. Ghaffari, N., et al., *Effects of cysteine, asparagine, or glutamine limitations in Chinese hamster ovary cell batch and fed-batch cultures.* Biotechnol Prog, 2020. 36(2): p. 1-12.

180. Ali, A.S., et al., *Multi-Omics Study on the Impact of Cysteine Feed Level on Cell Viability and mAb Production in a CHO Bioprocess.* Biotechnol J, 2018(1800352): p. 1-11.

181. Kachur, A.V., Koch, C.J., and Biaglow, J.E., *Mechanism of copper-catalyzed autoxidation of cysteine.* Free Radic Res, 1999. 31(1): p. 23-34.

182. Ralph, T.R., et al., *The electrochemistry of L-cystine and L-cysteine* J Electroanal Chem, 1994. 375((1–2)): p. 1-15.

183. Grzelak, A., Rychlik, B., and Bartosz, G., *Reactive oxygen species are formed in cell culture media.* Acta Biochim Pol, 2000. 47(4): p. 1197-8.

184. Grzelak, A., Rychlik, B., and Bartosz, G., *Light-dependent generation of reactive oxygen species in cell culture media.* Free Radic Biol Med, 2001. 30(12): p. 1418-25.

185. Aldini, G., et al., *N-Acetylcysteine as an antioxidant and disulphide breaking agent: the reasons why.* Free Radic Res, 2018. 52(7): p. 751-62.

186. He, X., et al., *Comparison of N-acetylcysteine and cysteine in their ability to replenish intracellular cysteine by a specific fluorescent probe.* Chem Commun, 2016. 52(60): p. 9410-3.

187. Wu, W., et al., *Effects of N-acetylcysteine amide (NACA), a thiol antioxidant on radiation-induced cytotoxicity in Chinese hamster ovary cells.* Life Sciences, 2008. 82(21): p. 1122-30.

188. Sunitha, K., et al., *N-Acetylcysteine amide: a derivative to fulfill the promises of N-Acetylcysteine.* Free Radic Res, 2013. 47(5): p. 357-67.

189. Ates, B., Abraham, L., and Ercal, N., *Antioxidant and free radical scavenging properties of N-acetylcysteine amide (NACA) and comparison with N-acetylcysteine (NAC).* Free Radic Res, 2008. 42(4): p. 372-7.

190. Giustarini, D., et al., *N-Acetylcysteine ethyl ester (NACET): A novel lipophilic cell-permeable cysteine derivative with an unusual pharmacokinetic feature and remarkable antioxidant potential.* Biochem Pharmacol, 2012. 84(11): p. 1522-33.

191. Schmolka, I.R. and Spoerri, P.E., *Thiazolidine Chemistry. II. The Preparation of 2-Substituted Thiazolidine-4-carboxylic Acids1,2.* J Org Chem, 1957. 22(8): p. 943-6.

192. Andrae, U., Singh, J., and Ziegler-Skylakakis, K., *Pyruvate and related alpha-ketoacids protect mammalian cells in culture against hydrogen peroxide-induced cytotoxicity.* Toxicol Lett, 1985. 28(2-3): p. 93-8.

193. Kuschelewski, J., et al., *Antioxidant effect of thiazolidine molecules in cell culture media improves stability and performance.* Biotechnol Prog, 2017. 33(3): p. 759-70.

194. Hecklau, C., et al., *S-Sulfocysteine simplifies fed-batch processes and increases the CHO specific productivity via anti-oxidant activity.* J Biotechnol, 2016. 218: p. 53-63.

195. Seibel, R., et al., *Impact of S-sulfocysteine on fragments and trisulfide bond linkages in monoclonal antibodies.* MAbs, 2017. 9(6): p. 889-97.

196. Hecklau, C., *Use of S-sulfocysteine (SSC) as a L-cysteine source in Chinese hamster ovary (CHO) suspension batch and fed-batch cultures*. 2016, TU Darmstadt. p. 226.

197. Dixon, S.J., et al., *Pharmacological inhibition of cystine-glutamate exchange induces endoplasmic reticulum stress and ferroptosis.* Elife, 2014. 3: p. 1-25.

198. Geoghegan, D., et al., *Control of amino acid transport into Chinese hamster ovary cells.* Biotechnol Bioeng, 2018. 115(12): p. 2908-29.

199. Chung, W.J., et al., *Inhibition of cystine uptake disrupts the growth of primary brain tumors.* J Neurosci, 2005. 25(31): p. 7101-10.

200. Jeong, H.J., et al., *Sulforaphane inhibits proliferation by causing cell cycle arrest at the G2/M phase in rabbit articular chondrocytes.* Mol Med Rep, 2012. 6(5): p. 1199-203.

201. Zheng, Y., et al., *Age-dependent oxidation of extracellular cysteine/cystine redox state (Eh(Cys/CySS)) in mouse lung fibroblasts is mediated by a decline in Slc7a11 expression.* Free Radic Biol Med, 2018. 118: p. 13-22.

202. Liu, P., et al., *Chemopreventive Activities of Sulforaphane and Its Metabolites in Human Hepatoma HepG2 Cells.* Nutrients, 2018. 10(585): p. 1-16.

203. Kim, B.R., et al., *Effects of glutathione on antioxidant response element-mediated gene expression and apoptosis elicited by sulforaphane.* Cancer Res, 2003. 63(21): p. 7520-5.

204. Trygg, J. and Wold, S., *Orthogonal projections to latent structures (O-PLS).* J Chemom, 2002. 16(3): p. 119-28.

205. Umetrics, M., *User Guide to SIMCA* 2012.

206. Long, F.H., *Chapter 23 - Multivariate analysis for metabolomics and proteomics data*, in *Proteomic and Metabolomic Approaches to Biomarker Discovery (Second Edition)*, H.J. Issaq and Veenstra, T.D., Editors. 2013, Academic Press: Boston. p. 395-407.

207. Hotelling, H., *The Generalization of Student's Ratio.* Ann Math Statist, 1931. 2(3): p. 360-78.

208. Fiehn, O., *Metabolomics--the link between genotypes and phenotypes.* Plant Mol Biol, 2002. 48(1-2): p. 155-71.

209. Sellick, C.A., et al., *Effective quenching processes for physiologically valid metabolite profiling of suspension cultured Mammalian cells.* Anal Chem, 2009. 81(1): p. 174-83.

210. Zhou, B., et al., *LC-MS-based metabolomics.* Mol Biosyst, 2012. 8(2): p. 470-81.

211. Blaženović, I., et al., *Structure Annotation of All Mass Spectra in Untargeted Metabolomics.* Anal Chem, 2019. 91(3): p. 2155-62.

212. Gout, P.W., et al., *Sulfasalazine, a potent suppressor of lymphoma growth by inhibition of the x(c)- cystine transporter: a new action for an old drug.* Leukemia, 2001. 15(10): p. 1633-40.

213. Maharjan, R.P. and Ferenci, T., *Global metabolite analysis: the influence of extraction methodology on metabolome profiles of Escherichia coli.* Anal Biochem, 2003. 313(1): p. 145-54.

214. Dietmair, S., et al., *Towards quantitative metabolomics of mammalian cells: development of a metabolite extraction protocol.* Anal Biochem, 2010. 404(2): p. 155-64.

215. Fernandes, R.O., et al., *Modulation of apoptosis by sulforaphane is associated with PGC-1α stimulation and decreased oxidative stress in cardiac myoblasts.* Mol Cell Biochem, 2015. 401(1): p. 61-70.

216. Singh, S.V., et al., *Sulforaphane-induced G2/M phase cell cycle arrest involves checkpoint kinase 2-mediated phosphorylation of cell division cycle 25C.* J Biol Chem, 2004. 279(24): p. 25813-22.

217. Geng, Y., et al., *Sulforaphane Induced Apoptosis via Promotion of Mitochondrial Fusion and ERK1/2-Mediated 26S Proteasome Degradation of Novel Pro-survival Bim and Upregulation of Bax in Human Non-Small Cell Lung Cancer Cells.* J Cancer, 2017. 8(13): p. 2456-70.

218. Choi, W.Y., et al., *Sulforaphane generates reactive oxygen species leading to mitochondrial perturbation for apoptosis in human leukemia U937 cells.* Biomed Pharmacother, 2008. 62(9): p. 637-44.

219. Pham, N.A., et al., *The dietary isothiocyanate sulforaphane targets pathways of apoptosis, cell cycle arrest, and oxidative stress in human pancreatic cancer cells and inhibits tumor growth in severe combined immunodeficient mice.* Mol Cancer Ther, 2004. 3(10): p. 1239-48.

220. Lewinska, A., et al., *Sulforaphane-Induced Cell Cycle Arrest and Senescence are accompanied by DNA Hypomethylation and Changes in microRNA Profile in Breast Cancer Cells.* Theranostics, 2017. 7(14): p. 3461-77.

221. Corssac, G.B., et al., *Sulforaphane effects on oxidative stress parameters in culture of adult cardiomyocytes.* Biomed Pharmacother, 2018. 104: p. 165-71.

222. Moniruzzaman, R., et al., *Roles of intracellular and extracellular ROS formation in apoptosis induced by cold atmospheric helium plasma and X-irradiation in the presence of sulfasalazine.* Free Radic Biol Med, 2018. 129: p. 537-47.

223. Takaya, K., et al., *Validation of the multiple sensor mechanism of the Keap1-Nrf2 system.* Free Radic Biol Med, 2012. 53(4): p. 817-27.

224. Shin, C.S., et al., *The glutamate/cystine xCT antiporter antagonizes glutamine metabolism and reduces nutrient flexibility.* Nat Commun, 2017. 8(15074): p. 1-11.

225. Lo, M., et al., *The xc− cystine/glutamate antiporter: a mediator of pancreatic cancer growth with a role in drug resistance.* Br J Canc, 2008. 99(3): p. 464-72.

226. Habib, E., et al., *Expression of xCT and activity of system xc− are regulated by NRF2 in human breast cancer cells in response to oxidative stress.* Redox Biol, 2015. 5: p. 33-42.

227. Ji, X., et al., *xCT (SLC7A11)-mediated metabolic reprogramming promotes non-small cell lung cancer progression.* Oncogene, 2018. 37(36): p. 5007-19.

228. Van Liefferinge, J., et al., *Comparative analysis of antibodies to xCT (Slc7a11): Forewarned is forearmed.* J Comp Neurol, 2016. 524(5): p. 1015-32.

229. Massie, A., et al., *Time-dependent changes in striatal xCT protein expression in hemi-Parkinson rats.* Neuroreport, 2008. 19(16): p. 1589-92.

230. Shih, A.Y., et al., *Cystine/glutamate exchange modulates glutathione supply for neuroprotection from oxidative stress and cell proliferation.* J Neurosci Res, 2006. 26(41): p. 10514-23.

231. Tuli, L. and Ressom, H.W., *LC-MS Based Detection of Differential Protein Expression.* J Proteomics Bioinform, 2009. 2: p. 416-38.

232. Nagane, M., et al., *Sulfasalazine, an inhibitor of the cystine-glutamate antiporter, reduces DNA damage repair and enhances radiosensitivity in murine B16F10 melanoma.* PloS one, 2018. 13(4): p. 1-19.

233. Yang, N., et al., *RNAi-mediated SLC7A11 knockdown inhibits melanogenesis-related genes expression in rabbit skin fibroblasts.* J Genet, 2018. 97(2): p. 463-8.

234. Kobayashi, S., et al., *Cystathionine is a novel substrate of cystine/glutamate transporter: implications for immune function.* J Biol Chem, 2015. 290(14): p. 8778-88.

235. Huang, Y., et al., *Cystine-glutamate transporter SLC7A11 in cancer chemosensitivity and chemoresistance.* Cancer Res, 2005. 65(16): p. 7446-54.

236. Pike, S., et al., *Using Xenopus laevis Oocytes to Functionally Characterize Plant Transporters.* Curr Protoc Plant Biol, 2019. 4(1): p. e20087.

237. Bridges, R.J., Natale, N.R., and Patel, S.A., *System xc(-) cystine/glutamate antiporter: an update on molecular pharmacology and roles within the CNS.* Br J Pharmacol, 2012. 165(1): p. 20-34.

238. Kanai, Y., et al., *The SLC1 high-affinity glutamate and neutral amino acid transporter family.* Mol Aspects Med, 2013. 34: p. 108-20.

239. Kyriakopoulos, S., Polizzi, K.M., and Kontoravdi, C., *Comparative analysis of amino acid metabolism and transport in CHO variants with different levels of productivity.* J Biotechnol, 2013. 168(4): p. 543-51.

240. Johnson-Winters, K., Tollin, G., and Enemark, J.H., *Elucidating the catalytic mechanism of sulfite oxidizing enzymes using structural, spectroscopic, and kinetic analyses.* Biochemistry, 2010. 49(34): p. 7242-54.

241. Markovich, D., *Sulfate transport by SLC26 transporters.* Novartis Found Symp, 2006. 273: p. 42-264.

242. Kirdar, A., et al., *Application of Near-Infrared (NIR) Spectroscopy for Screening of Raw Materials Used in the Cell Culture Medium for the Production of a Recombinant Therapeutic Protein.* Biotechnol Prog, 2009. 26: p. 527-31.

243. Kirdar, A.O., Green, K.D., and Rathore, A.S., *Application of multivariate data analysis for identification and successful resolution of a root cause for a bioprocessing application.* Biotechnol Prog, 2008. 24(3): p. 720-6.

244. Powers, D.N., et al., *Multivariate data analysis of growth medium trends affecting antibody glycosylation.* Biotechnol Prog, 2020. 36(1): p. 1-15.

245. Hunt, S.M., et al., *Chinese hamster ovary cells produce sufficient recombinant insulin-like growth factor I to support growth in serum-free medium. Serum-free growth of IGF-I-producing CHO cells.* Cytotechnology, 1997. 24(1): p. 55-64.

246. Zhang, M., et al., *Insulin-like growth factor 1/insulin-like growth factor 1 receptor signaling protects against cell apoptosis through the PI3K/AKT pathway in glioblastoma cells.* Exp ther med, 2018. 16(2): p. 1477-82.

247. Misra, U.K. and Pizzo, S.V., *Up-regulation of GRP78 and antiapoptotic signaling in murine peritoneal macrophages exposed to insulin.* J Leukoc Biol, 2005. 78(1): p. 187-94.

248. Abbas, A.K., et al., *S-sulfo-cysteine is an endogenous amino acid in neonatal rat brain but an unlikely mediator of cysteine neurotoxicity.* Neurochem Res, 2008. 33(2): p. 301-7.

249. Furukawa, H., et al., *Subunit arrangement and function in NMDA receptors.* Nature, 2005. 438(7065): p. 185-92.

250. *Chinese hamster genome database*. http://www.chogenome.org.

251. Plate, J., et al., *S-Sulfocysteine Induces Seizure-Like Behaviors in Zebrafish.* Front Pharmacol, 2019. 10(122): p. 1-6.

252. Rigo, A., et al., *Interaction of copper with cysteine: stability of cuprous complexes and catalytic role of cupric ions in anaerobic thiol oxidation.* J Inorg Biochem, 2004. 98(9): p. 1495-501.

253. Ngamchuea, K., Batchelor-McAuley, C., and Compton, R.G., *The Copper(II)-Catalyzed Oxidation of Glutathione.* Chem Eur J, 2016. 22(44): p. 15937-44.

254. Chaderjian, W.B., et al., *Effect of copper sulfate on performance of a serum-free CHO cell culture process and the level of free thiol in the recombinant antibody expressed.* Biotechnol Prog, 2005. 21(2): p. 550-3.

255. Marí, M., et al., *Mitochondrial glutathione, a key survival antioxidant.* Antioxid Redox Signal, 2009. 11(11): p. 2685-700.

256. Dalton, T.P., et al., *Genetically altered mice to evaluate glutathione homeostasis in health and disease.* Free Radic Biol Med, 2004. 37(10): p. 1511-26.

257. Huang, Z., et al., *Inhibition of caspase-3 activity and activation by protein glutathionylation.* Biochem Pharmacol, 2008. 75(11): p. 2234-44.

258. Friesen, C., Kiess, Y., and Debatin, K.M., *A critical role of glutathione in determining apoptosis sensitivity and resistance in leukemia cells.* Cell Death Differ, 2004. 11 Suppl 1: p. S73-85.

259. Franco, R. and Cidlowski, J.A., *Apoptosis and glutathione: beyond an antioxidant.* Cell Death Differ, 2009. 16(10): p. 1303-14.

260. Cereser, C., et al., *Thiram-induced cytotoxicity is accompanied by a rapid and drastic oxidation of reduced glutathione with consecutive lipid peroxidation and cell death.* Toxicology, 2001. 163(2): p. 153-62.

261. Casey, J.R., Grinstein, S., and Orlowski, J., *Sensors and regulators of intracellular pH.* Nat Rev Mol Cell Biol, 2010. 11(1): p. 50-61.

262. Arscott, L.D., Veine, D.M., and Williams, C.H., Jr., *Mixed disulfide with glutathione as an intermediate in the reaction catalyzed by glutathione reductase from yeast and as a major form of the enzyme in the cell.* Biochemistry, 2000. 39(16): p. 4711-21.

263. Winell, M. and Mannervik, B., *The nature of the enzymatic reduction of S-sulfoglutathione in liver and peas.* Biochim Biophys Acta, 1969. 184(2): p. 374-80.

264. Leung, K.H., Post, G.B., and Menzel, D.B., *Glutathione S-sulfonate, a sulfur dioxide metabolite, as a competitive inhibitor of glutathione S-transferase, and its reduction by glutathione reductase.* Toxicol Appl Pharmacol, 1985. 77(3): p. 388-94.

265. Keller, D.A. and Menzel, D.B., *Effects of sulfite on glutathione S-sulfonate and the glutathione status of lung cells.* Chem-Biol Interact, 1989. 70(1): p. 145-56.

266. Hayes, J.D., Flanagan, J.U., and Jowsey, I.R., *Glutathione transferases.* Annu Rev Pharmacol Toxicol, 2005. 45: p. 51-88.

267. Brass, E.P., *Overview of coenzyme A metabolism and its role in cellular toxicity.* Chem-Biol Interact, 1994. 90(3): p. 203-14.

268. Pietrocola, F., et al., *Acetyl coenzyme A: a central metabolite and second messenger.* Cell Metab, 2015. 21(6): p. 805-21.

269. Zhang, Y.M., et al., *Chemical knockout of pantothenate kinase reveals the metabolic and genetic program responsible for hepatic coenzyme A homeostasis.* Chem Biol, 2007. 14(3): p. 291-302.

270. Garcia, M., et al., *Germline deletion of pantothenate kinases 1 and 2 reveals the key roles for CoA in postnatal metabolism.* PloS one, 2012. 7(7): p. 1-13.

271. Raines, R.T., *Active Site of Ribonuclease A*, in *Artificial Nucleases. Nucleic Acids and Molecular Biology*, Z. M.A., Editor. 2004, Springer, Berlin, Heidelberg. .

272. Nagy, P., *Kinetics and mechanisms of thiol-disulfide exchange covering direct substitution and thiol oxidation-mediated pathways.* Antioxid Redox Signal, 2013. 18(13): p. 1623-41.

273. Cheng, Z., et al., *Reactivity of thioredoxin as a protein thiol-disulfide oxidoreductase.* Chem Rev, 2011. 111(9): p. 5768-83.

274. Gan, Z.R. and Wells, W.W., *Purification and properties of thioltransferase.* J Biol Chem, 1986. 261(3): p. 996-1001.

275. Nakatani, T., et al., *Enhancement of thioredoxin/glutaredoxin-mediated L-cysteine synthesis from S-sulfocysteine increases L-cysteine production in Escherichia coli.* Microb Cell Fact, 2012. 11(62): p. 1-9.

276. Holmgren, A., *Thioredoxin and glutaredoxin systems.* J Biol Chem, 1989. 264(24): p. 13963-6.

277. Zhang, W. and Czupryn, M.J., *Free sulfhydryl in recombinant monoclonal antibodies.* Biotechnol Prog, 2002. 18(3): p. 509-13.

278. Yang, L., et al., *Depletion of cytosolic or mitochondrial thioredoxin increases CYP2E1-induced oxidative stress via an ASK-1-JNK1 pathway in HepG2 cells.* Free Radic Biol Med, 2011. 51(1): p. 185-96.

279. Heppner, D.E., et al., *Cysteine perthiosulfenic acid (Cys-SSOH): A novel intermediate in thiol-based redox signaling?* Redox Biol, 2018. 14: p. 379-85.

280. Truong, T.H., et al., *Molecular Basis for Redox Activation of Epidermal Growth Factor Receptor Kinase.* Cell Chem Biol, 2016. 23(7): p. 837-48.

281. Arnér, E.S. and Holmgren, A., *Physiological functions of thioredoxin and thioredoxin reductase.* Eur J Biochem, 2000. 267(20): p. 6102-9.

282. Hanschmann, E.-M., et al., *Thioredoxins, glutaredoxins, and peroxiredoxins--molecular mechanisms and health significance: from cofactors to antioxidants to redox signaling.* Antioxid Redox Signal, 2013. 19(13): p. 1539-605.

283. Couto, N., Wood, J., and Barber, J., *The role of glutathione reductase and related enzymes on cellular redox homoeostasis network.* Free Radic Biol Med, 2016. 95: p. 27-42.

284. Peskin, A.V., et al., *Glutathionylation of the active site cysteines of peroxiredoxin 2 and recycling by glutaredoxin.* J Biol Chem, 2016. 291(6): p. 3053-62.

285. Ferguson, G.D. and Bridge, W.J., *The glutathione system and the related thiol network in Caenorhabditis elegans.* Redox Biol, 2019. 24(101171): p. 1-12.

286. Nagahara, N., *Catalytic site cysteines of thiol enzyme: sulfurtransferases.* J Amino Acids, 2011. 2011(709404): p. 1-7.

287. Krishnan, N., et al., *H2S-Induced sulfhydration of the phosphatase PTP1B and its role in the endoplasmic reticulum stress response.* Sci Signal, 2011. 4(203): p. 1-13.

288. Masaki, S., et al., *The cysteine residue at 424th of pyruvate kinase M2 is crucial for tetramerization and responsiveness to oxidative stress.* Biochemical and Biophysical Research Communications, 2020. 526(4): p. 973-977.

289. Jeong, J., et al., *Novel oxidative modifications in redox-active cysteine residues.* Mol Cell Proteomics, 2011. 10(3): p. M110.000513.

290. Sheng, Y., et al., *Superoxide dismutases and superoxide reductases.* Chem Rev, 2014. 114(7): p. 3854-918.

291. McIlwain, D.R., Berger, T., and Mak, T.W., *Caspase Functions in Cell Death and Disease.* Cold Spring Harbor Perspectives in Biology, 2013. 5(4): p. 1-29.

7. Appendix

7.1. Supplementary figures and tables

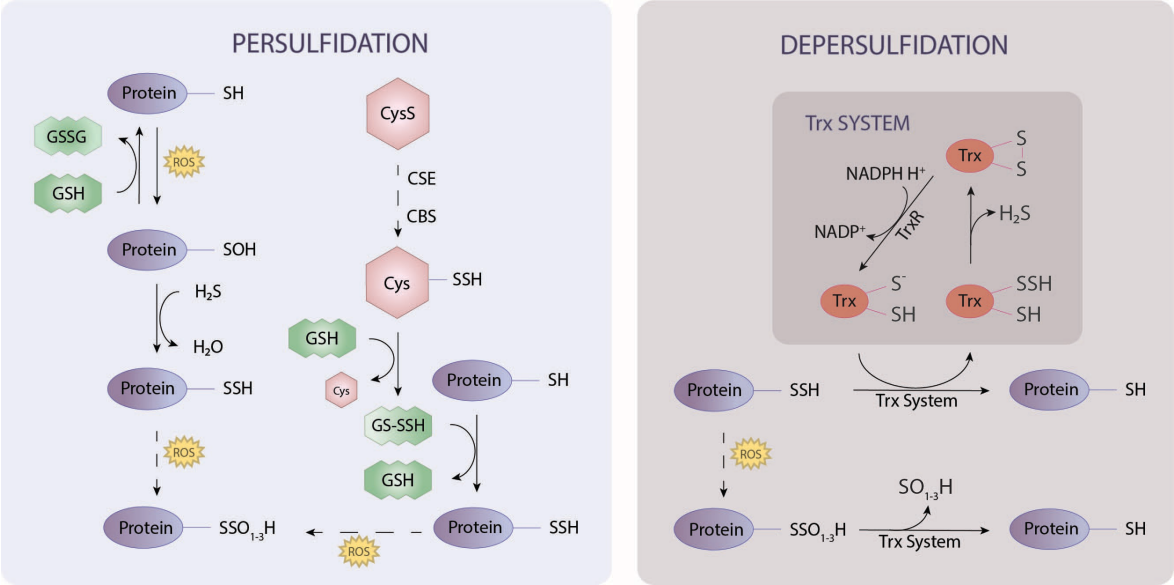

Figure 42. Persulfidation of protein thiols and depersulfidation via Trx system. Native persulfidation occurs either in presence of hydrogen sulfide (H_2S) by reacting with sulfenylated thiols or by stepwise enzymatical conversion of cystine (CysS) to cysteine hydropersulfide (Cys-SSH), which can further transfer the persulfide onto glutathione (GSH) and proteins. Oxidation of protein persulfides occur at high reactive oxygen species (ROS) concentrations, whereby all oxidizing states are reversible. Depersulfidation is enabled via the thioredoxin (Trx) system. Trx has a dithiol motif, which enables the nucleophilic attack of the persulfide, which is subsequently released via intrachain disulfide formation. Thioredoxin reductase (TrxR) catalyzes the reduction of Trx to the active form consuming NADPH. cystathionine γ-lyase (CSE) cystathionine β-synthase (CBS)

Table 15. Feed mixture design for the small-scale fed-batch screening.

Mix	Feed 2	Feed 3	Feed 10 80 g/L	Feed 10 25 g/L	Feed 6	Feed 5	Feed 4	Feed 1	Feed 8	Feed 7	Feed 9	Feed 10 123 g/L
1	0.5	0	0	0	0	0	0	0	0.5	0	0	0
2	0	0.5	0	0	0	0	0.5	0	0	0	0	0
3	0	0	0	0	0	0	0	0.5	0.5	0	0	0
4	0	0	0	0	0	0.5	0	0	0.5	0	0	0
5	0	0	0	0	0.5	0	0.5	0	0	0	0	0
6	0	0	0	0	0	0	0	0.5	0	0	0	0.5
7	0.5	0	0	0	0	0	0	0	0	0	0.5	0
8	0	0	0.5	0	0	0	0	0	0	0	0	0.5
9	0	0	0	0.5	0	0	0	0	0	0	0.5	0
10	0	0	0	0	0	0.5	0	0.5	0	0	0	0
Feed 9	0	0	0	0	0	0	0	0	0	0	1	0
Feed 3	0	1	0	0	0	0	0	0	0	0	0	0
13	0	0	0.5	0	0	0.5	0	0	0	0	0	0
Feed 10 25 g/L	0	0	0	1	0	0	0	0	0	0	0	0
15	0	0	0	0	0	0	0	0.5	0	0	0.5	0
Feed 8	0	0	0	0	0	0	0	0	1	0	0	0
17	0	0	0	0	0	0	0	0	0	0.5	0.5	0
18	0	0	0	0	0	0	0	0	0.5	0	0	0.5
19	0	0	0	0	0	0	0.5	0	0	0	0	0.5
20	0	0.5	0	0	0	0	0	0	0	0	0.5	0
Feed 10 80 g/L	0	0	1	0	0	0	0	0	0	0	0	0
22	0	0	0	0	0.5	0.5	0	0	0	0	0	0
23	0.5	0	0	0	0.5	0	0	0	0	0	0	0

Mix	Feed 2	Feed 3	Feed 10 80 g/L	Feed 10 25 g/L	Feed 6	Feed 5	Feed 4	Feed 1	Feed 8	Feed 7	Feed 9	Feed 10 123 g/L
24	0	0	0	0	0.5	0	0	0	0.5	0	0	0
25	0	0.5	0	0	0	0	0	0	0	0.5	0	0
26	0	0	0	0.5	0.5	0	0	0	0	0	0	0
27	0	0	0	0.5	0	0	0	0	0.5	0	0	0
28	0	0	0	0	0	0.5	0	0	0	0	0.5	0
Feed 5	0	0	0	0	0	1	0	0	0	0	0	0
30	0	0	0	0	0	0.5	0	0	0	0.5	0	0
31	0	0	0.5	0	0	0	0	0	0.5	0	0	0
32	0	0.5	0	0.5	0	0	0	0	0	0	0	0
33	0	0	0	0	0	0.5	0	0	0	0	0	0.5
34	0	0	0	0	0	0	0.5	0.5	0	0	0	0
35	0	0	0	0	0	0	0	0.5	0	0.5	0	0
36	0.5	0	0	0	0	0	0	0.5	0	0	0	0
37	0	0	0	0	0.5	0	0	0	0	0	0.5	0
38	0	0	0	0	0	0	0	0	0.5	0	0.5	0
39	0	0	0	0	0	0	0	0	0	0.5	0	0.5
40	0	0.5	0	0	0	0	0	0	0.5	0	0	0
41	0	0	0.5	0	0	0	0.5	0	0	0	0	0
42	0	0	0.5	0	0	0	0	0	0	0	0.5	0
43	0	0	0	0	0	0	0.5	0	0	0.5	0	0
Feed 7	0	0	0	0	0	0	0	0	0	1	0	0
45	0.5	0	0	0	0	0	0	0	0	0	0	0.5
46	0	0	0	0	0	0	0	0	0.5	0.5	0	0
47	0	0.5	0	0	0.5	0	0	0	0	0	0	0
48	0	0.5	0	0	0	0.5	0	0	0	0	0	0
49	0.5	0	0	0.5	0	0	0	0	0	0	0	0
Feed 1	0	0	0	0	0	0	0	1	0	0	0	0
51	0	0	0.5	0	0.5	0	0	0	0	0	0	0
52	0	0.5	0.5	0	0	0	0	0	0	0	0	0
53	0	0.5	0	0	0	0	0	0	0	0	0	0.5
54	0	0	0	0.5	0	0	0	0	0	0	0	0.5
55	0	0	0	0	0.5	0	0	0	0	0.5	0	0
Feed 10 123 g/L	0	0	0	0	0	0	0	0	0	0	0	1
57	0	0	0	0	0	0	0.5	0	0.5	0	0	0
58	0	0	0	0.5	0	0	0.5	0	0	0	0	0
59	0	0	0	0.5	0	0.5	0	0	0	0	0	0
60	0.5	0	0	0	0	0	0	0	0	0.5	0	0
61	0	0	0.5	0.5	0	0	0	0	0	0	0	0
62	0	0	0	0	0	0	0	0	0	0	0.5	0.5
63	0	0	0	0	0	0	0.5	0	0	0	0.5	0
64	0	0	0	0	0	0.5	0.5	0	0	0	0	0
Feed 4	0	0	0	0	0	0	1	0	0	0	0	0
66	0	0	0.5	0	0	0	0	0.5	0	0	0	0
Feed 2	1	0	0	0	0	0	0	0	0	0	0	0
68	0	0	0	0	0.5	0	0	0.5	0	0	0	0
69	0.5	0	0	0	0	0	0.5	0	0	0	0	0
70	0	0	0	0.5	0	0	0	0.5	0	0	0	0
71	0	0.5	0	0	0	0	0	0.5	0	0	0	0
72	0	0	0	0	0.5	0	0	0	0	0	0	0.5
73	0.5	0	0.5	0	0	0	0	0	0	0	0	0
74	0.5	0.5	0	0	0	0	0	0	0	0	0	0
Feed 6	0	0	0	0	1	0	0	0	0	0	0	0
76	0	0	0	0.5	0	0	0	0	0	0.5	0	0
77	0.5	0	0	0	0	0.5	0	0	0	0	0	0
78	0	0	0.5	0	0	0	0	0	0	0.5	0	0
79	0	0	0	0	0	0	0.68	0	0	0	0.14	0.18
Cys ctrl	0	0	0	0	0	0	0	0	0	0	0	0

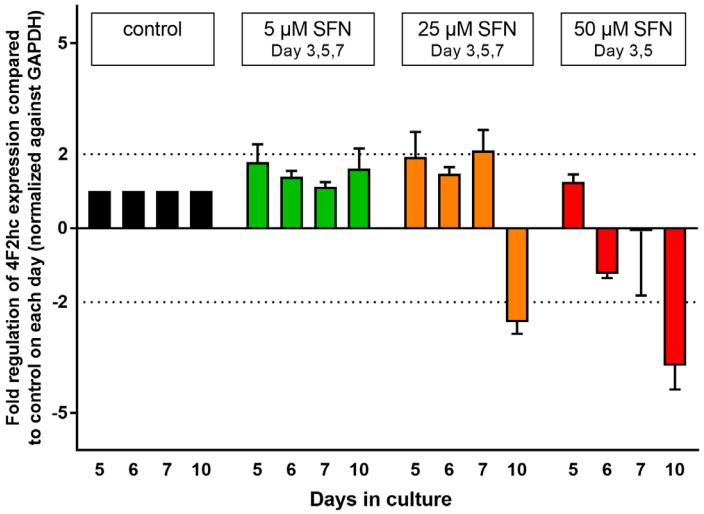

Figure 43. Dose response of Sulforaphane on CysS/Glu antiporter subunit. Suspension CHO cells were seeded at $2x10^5$ cells/mL, incubated at 37°C, 5% CO_2, 80% humidity and agitated at 320 rpm. Feed was added on day 3, 5 and 10 (3%; v/v) and day 7 (6%; v/v) whereas 5, 25 or 50 µM SFN was added on day 3, 5, 7. The mRNA expression of the CysS/Glu antiporter heavy chain (4F2hc) is expressed as fold change relative to the untreated control on each day and normalized to GAPDH (n=2). Two-fold increased mRNA levels were considered as differentially expressed.

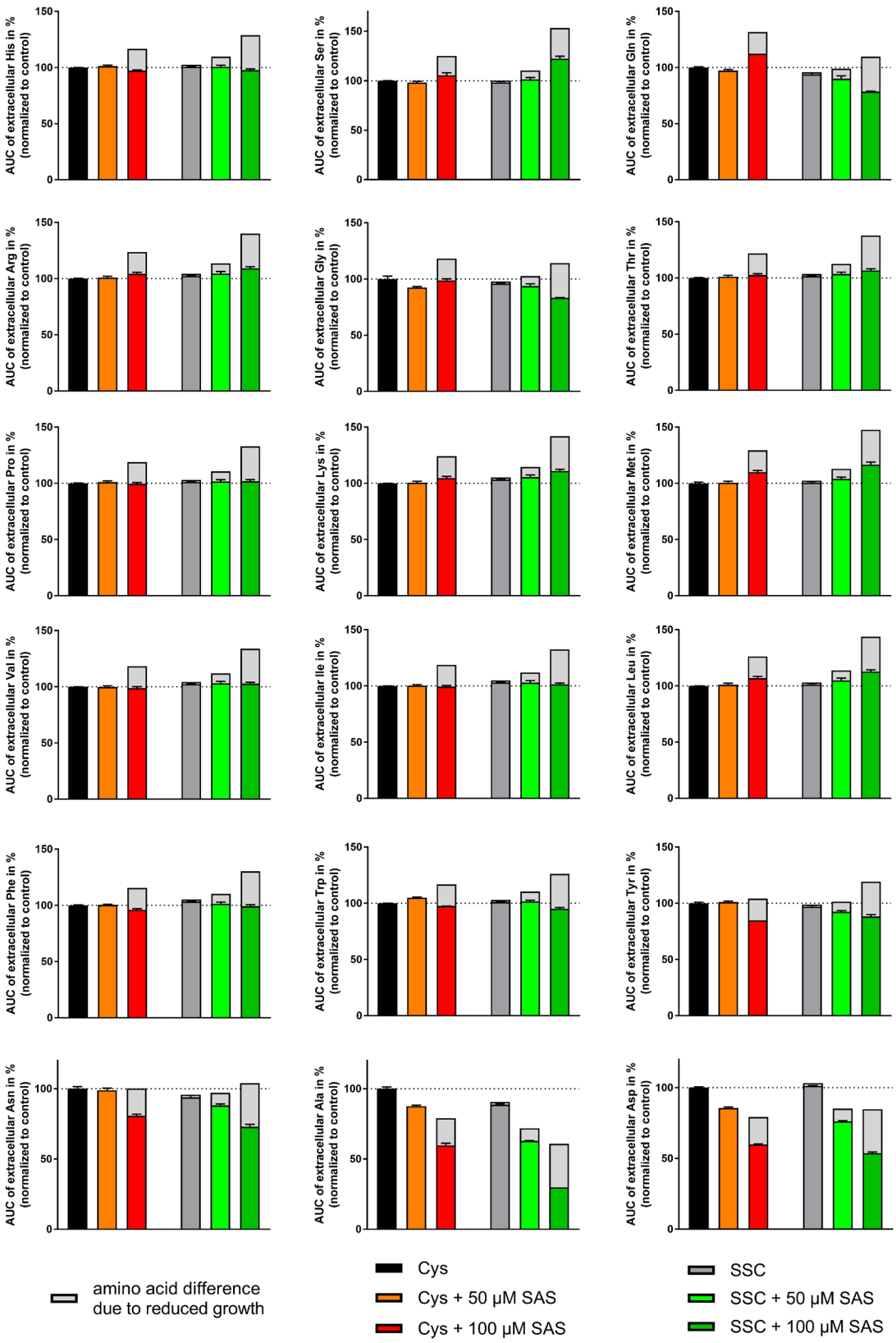

Figure 44. Extracellular amino acids during a fed-batch experiment with feed containing either Cys or SSC. With the intention to inhibit the CysS/Glu antiporter activity, cells were treated daily with either 50 µM or 100 µM Sulfasalazine (SAS). Area under the curve (AUC) of extracellular amino acids was measured via RP-UPLC after iodoacetamide treatment and AccQ-Tag derivatization and was normalized to Cys containing feed. Effects due to different growth are calculated as average difference of antiporter unrelated amino acids to the control and are visualized as stacked bar in grey. Data are expressed as mean values ± SEM (n=2).

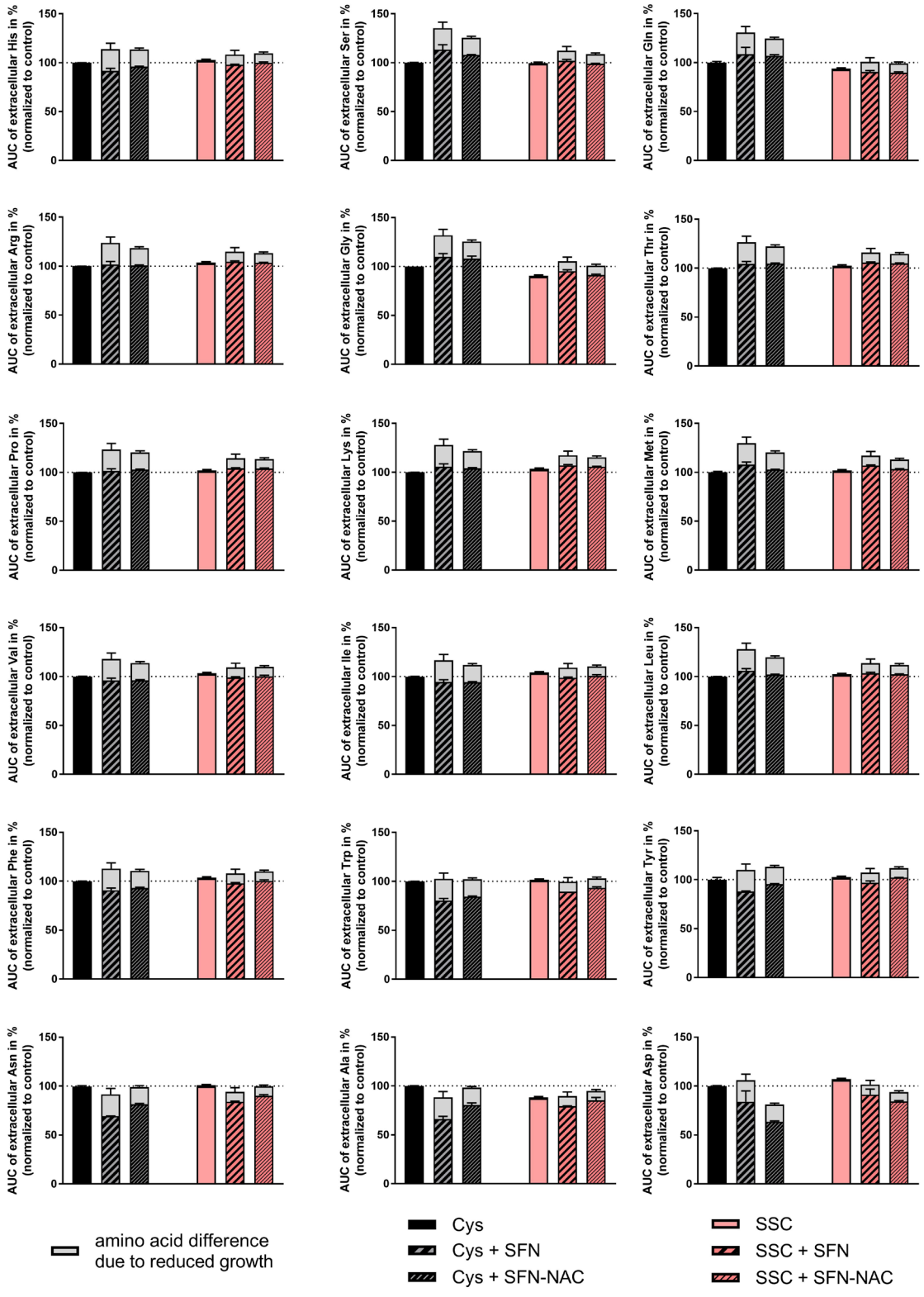

Figure 45. Extracellular amino acids during a fed-batch experiment with feed containing either Cys or SSC. With the intention to increase the expression of the CysS/Glu antiporter, cells were treated with either SFN or SFN-NAC. Area under the curve (AUC) of extracellular amino acids was measured via RP-UPLC after iodoacetamide treatment and AccQ-Tag derivatization and was normalized to Cys containing feed. Effects due to different growth are calculated as average difference of antiporter unrelated amino acids to the control and are visualized as stacked bar in grey. Data are expressed as mean values ± SEM (n=2).

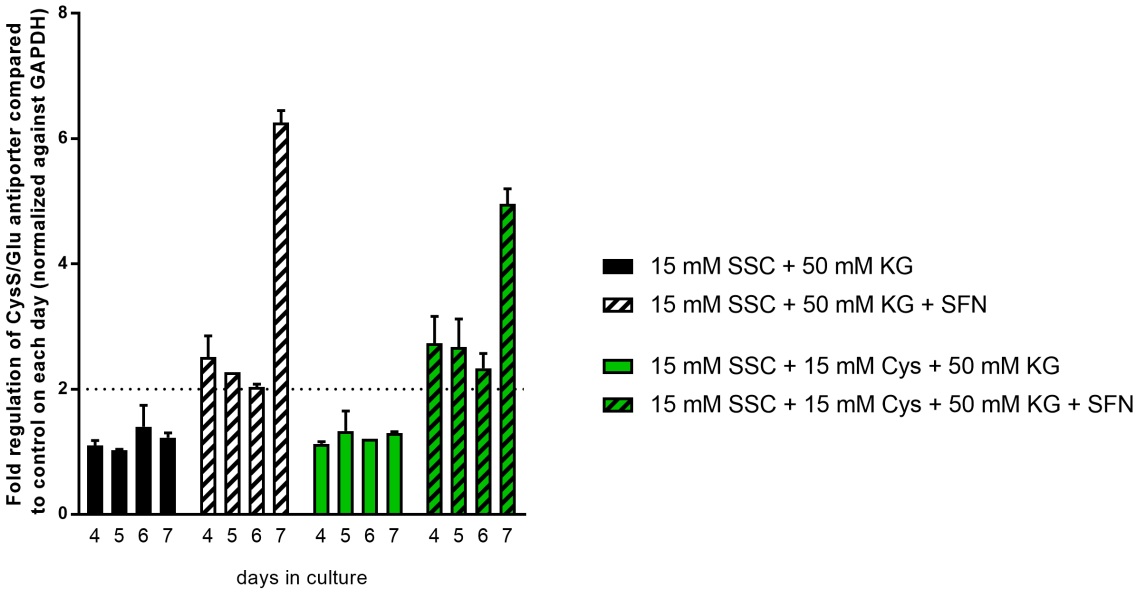

Figure 46. Fold regulation of the CysS/Glu-antiporter (x_c^-) in response to SFN treatment. Suspension CHO cells were seeded at 2×10^5 cells/mL, incubated at 37°C, 5% CO_2, 80% humidity and agitated at 320 rpm. Feed containing increasing concentrations of 15 mM or 20 mM *S*-sulfocysteine (SSC) with or without additional cysteine (Cys) and ketoglutaric acid (KG) were added on day 3, 5, 10 and 12 (3%; v/v) and day 7 (6%; v/v), whereas 15 µM sulforaphane (SFN) were supplemented on day 3, 4, 6 and 7. Fold regulation of the CysS/Glu-antiporter (xCT) gene expression relative to the control on each day and normalized to GAPDH (n=2).

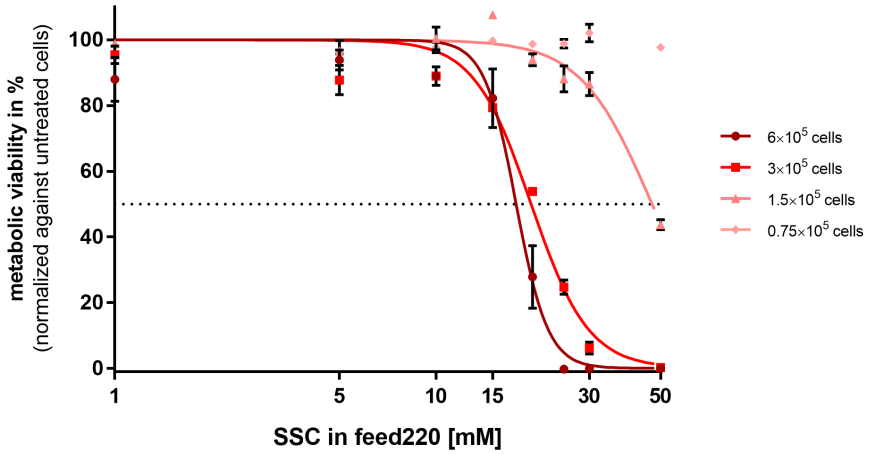

Figure 47. Cell-based response of CHO-K1 cells to SSC. Serial diluted CHO cells were treated with 10% (v/v) of Cys depleted feed220 supplemented with increasing SSC concentrations in a range from 1 to 50 mM. After cell cultivation over three days at 37°C, the ATP level was measured (CellTiter-Glo Assay, Promega) and the resulting ATP level was normalized to cells cultivated in the feed220 without SSC. Data is expressed as mean values ± SEM (n=8). A non-linear regression of the data is visualized as solid line and was used to calculate the SSC concentration leading to 50% metabolic viability (n=2).

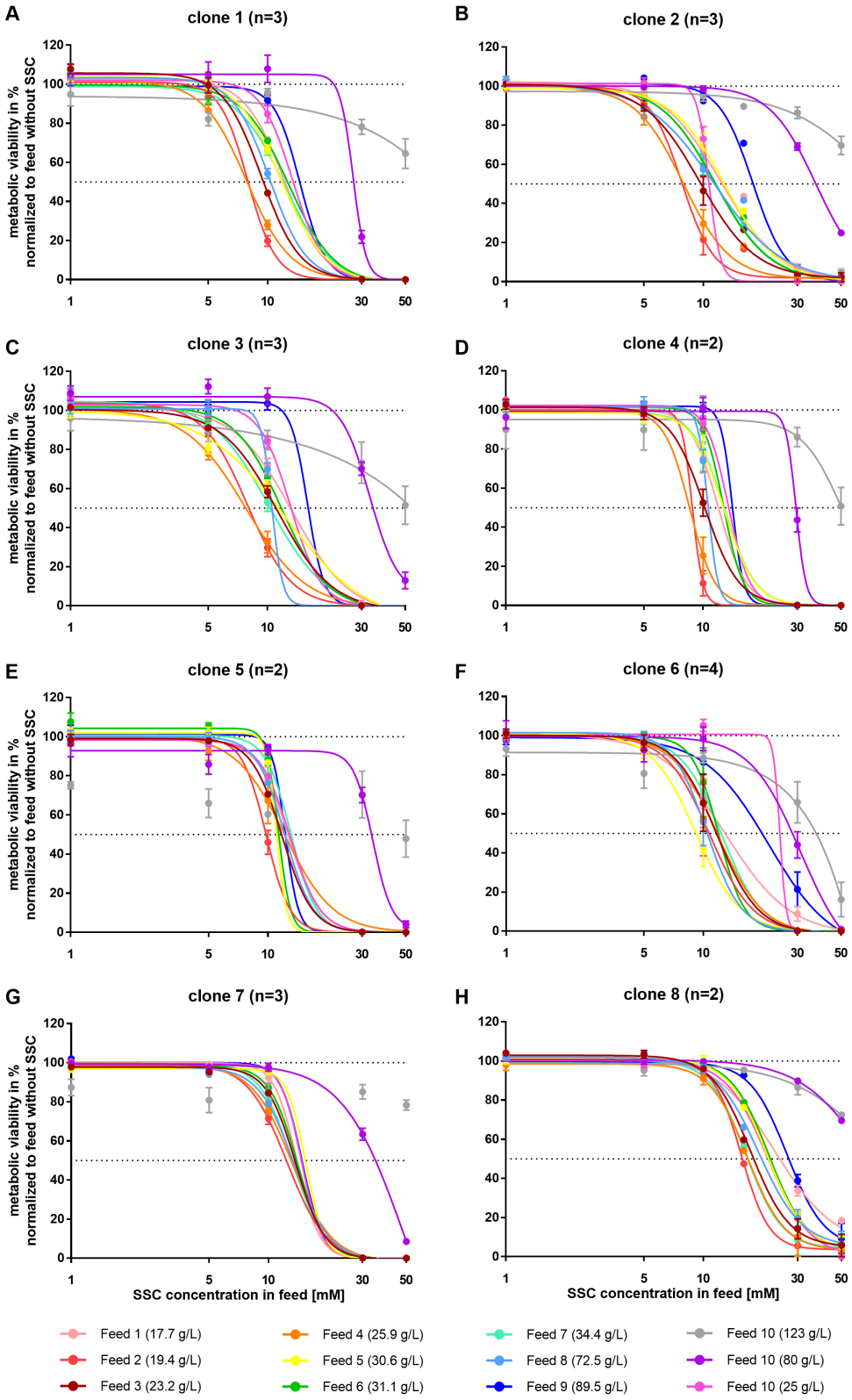

Figure 48. Feed dependent SSC dose response of eight CHO cell lines. About 3×10^5 cells of eight different clones were treated with 10% (v/v) of 12 Cys depleted feed supplemented with increasing SSC concentrations. After cell cultivation over three days at 37°C, the ATP level was measured (CellTiter-Glo Assay, Promega) and the resulting ATP level was normalized to cells cultivated in the respective feed without supplementation and mean values are presented ± SEM. A non-linear regression of the data is visualized as solid line and the calculated SSC concentration leading to 50% metabolic viability are summarized in table 6. A-H) clone 1 – clone 8.

Table 16. Toxic response of six clones through 79 feed mixtures. Each feed contained a specific SSC concentration in a range from 9 to 22 mM.

Feed mixture	Clone6 9 mM	Clone6 16 mM	Clone7 13 mM	Clone7 16 mM	Clone2 14 mM	Clone4 14 mM	Clone5 14 mM	Clone8 22 mM	Summary
1	toxic	toxic	not toxic	not toxic	not toxic	toxic	toxic	not toxic	toxic
2	not toxic	toxic	not toxic	toxic	not toxic	toxic	toxic	not toxic	toxic
3	toxic	toxic	not toxic	not toxic	not toxic	not toxic	toxic	not toxic	toxic
4	toxic	toxic	not toxic	not toxic	not toxic	not toxic	toxic	not toxic	toxic
5	not toxic	toxic	not toxic	toxic	not toxic	toxic	toxic	not toxic	toxic
6	not toxic	not toxic	not toxic	not toxic	not toxic	not toxic	not toxic	not toxic	not toxic
7	not toxic	not toxic	not toxic	not toxic	not toxic	not toxic	toxic	not toxic	toxic
8	NA	NA	NA	NA	not toxic	not toxic	not toxic	not toxic	not toxic
9	NA	NA	NA	NA	not toxic	not toxic	not toxic	not toxic	not toxic
10	toxic	toxic	not toxic	toxic	not toxic	toxic	toxic	not toxic	toxic
Feed 9	not toxic	not toxic	not toxic	not toxic	not toxic	not toxic	not toxic	not toxic	not toxic
Feed 3	toxic	toxic	not toxic	not toxic	not toxic	toxic	toxic	not toxic	toxic
13	NA	NA	NA	NA	not toxic	not toxic	not toxic	not toxic	not toxic
Feed 10 (25 g/L)	NA	NA	NA	NA	not toxic	not toxic	toxic	not toxic	not toxic
15	not toxic	not toxic	toxic	toxic	not toxic	not toxic	toxic	not toxic	toxic
Feed 8	not toxic	toxic	not toxic	not toxic	not toxic	not toxic	toxic	not toxic	toxic
17	not toxic	toxic	not toxic	not toxic	not toxic	not toxic	toxic	not toxic	toxic
18	not toxic	toxic	not toxic	not toxic	not toxic	not toxic	not toxic	not toxic	not toxic
19	not toxic	not toxic	not toxic	not toxic	not toxic	not toxic	not toxic	not toxic	not toxic
20	not toxic	not toxic	not toxic	not toxic	not toxic	not toxic	not toxic	not toxic	not toxic
Feed 10 (80 g/L)	NA	NA	NA	NA	not toxic	not toxic	not toxic	not toxic	not toxic
22	toxic	not toxic	not toxic	not toxic	not toxic	not toxic	toxic	not toxic	toxic
23	toxic	not toxic	not toxic	not toxic	not toxic	not toxic	toxic	not toxic	toxic
24	not toxic	toxic	not toxic	not toxic	not toxic	not toxic	toxic	toxic	toxic
25	toxic	toxic	toxic	toxic	not toxic	not toxic	toxic	toxic	toxic
26	NA	NA	NA	NA	toxic	not toxic	toxic	not toxic	toxic
27	NA	NA	NA	NA	not toxic	not toxic	not toxic	not toxic	not toxic
28	not toxic	not toxic	not toxic	not toxic	not toxic	not toxic	not toxic	not toxic	not toxic
Feed 5	toxic	toxic	not toxic	not toxic	toxic	not toxic	toxic	not toxic	toxic
30	toxic	toxic	toxic	toxic	toxic	toxic	toxic	toxic	toxic
31	NA	NA	NA	NA	not toxic	not toxic	not toxic	not toxic	not toxic
32	NA	NA	NA	NA	not toxic	not toxic	toxic	not toxic	not toxic
33	not toxic	not toxic	not toxic	not toxic	not toxic	not toxic	not toxic	not toxic	not toxic
34	toxic	toxic	toxic	toxic	not toxic	toxic	toxic	toxic	toxic
35	toxic	toxic	toxic	toxic	toxic	toxic	toxic	toxic	toxic
36	not toxic	toxic	not toxic	toxic	not toxic	toxic	toxic	toxic	toxic
37	not toxic	not toxic	not toxic	not toxic	not toxic	not toxic	not toxic	not toxic	not toxic
38	not toxic	not toxic	not toxic	not toxic	not toxic	not toxic	not toxic	not toxic	not toxic
39	not toxic	not toxic	not toxic	not toxic	not toxic	not toxic	not toxic	not toxic	not toxic
40	not toxic	toxic	not toxic	not toxic	not toxic	not toxic	toxic	not toxic	toxic
41	NA	NA	NA	NA	not toxic	not toxic	not toxic	not toxic	not toxic
42	NA	NA	NA	NA	not toxic	not toxic	not toxic	not toxic	not toxic
43	toxic	toxic	toxic	toxic	toxic	toxic	toxic	toxic	toxic
Feed 7	not toxic	toxic	toxic	toxic	not toxic	not toxic	toxic	toxic	toxic
45	not toxic	not toxic	not toxic	not toxic	not toxic	not toxic	not toxic	not toxic	not toxic
46	not toxic	toxic	not toxic	not toxic	not toxic	not toxic	toxic	not toxic	toxic
47	toxic	toxic	not toxic	not toxic	not toxic	not toxic	toxic	not toxic	toxic
48	toxic	toxic	not toxic	not toxic	not toxic	not toxic	toxic	not toxic	toxic
49	NA	NA	NA	NA	not toxic	toxic	toxic	not toxic	toxic
Feed 1	toxic	toxic	toxic	toxic	not toxic	toxic	toxic	not toxic	toxic
51	NA	NA	NA	NA	not toxic	not toxic	not toxic	not toxic	not toxic
52	NA	NA	NA	NA	not toxic	not toxic	not toxic	not toxic	not toxic
53	not toxic	not toxic	not toxic	not toxic	not toxic	not toxic	not toxic	not toxic	not toxic
54	NA	NA	NA	NA	not toxic	not toxic	not toxic	not toxic	not toxic
55	not toxic	toxic	toxic	toxic	not toxic	not toxic	toxic	toxic	toxic
Feed 10 (123 g/L)	not toxic	not toxic	not toxic	not toxic	not toxic	not toxic	not toxic	not toxic	not toxic
57	not toxic	toxic	not toxic	not toxic	not toxic	not toxic	toxic	not toxic	toxic
58	NA	NA	NA	NA	not toxic	not toxic	toxic	not toxic	not toxic
59	NA	NA	NA	NA	not toxic	toxic	toxic	not toxic	toxic
60	not toxic	toxic	toxic	toxic	toxic	toxic	toxic	toxic	toxic
61	NA	NA	NA	NA	not toxic	not toxic	not toxic	not toxic	not toxic
62	not toxic	not toxic	not toxic	not toxic	not toxic	not toxic	not toxic	not toxic	not toxic
63	not toxic	not toxic	toxic	toxic	not toxic	not toxic	toxic	not toxic	toxic
64	toxic	toxic	toxic	toxic	not toxic	toxic	toxic	not toxic	toxic
Feed 4	toxic	toxic	toxic	toxic	not toxic	toxic	NA*	toxic	toxic
66	NA	NA	NA	NA	not toxic	not toxic	not toxic	not toxic	not toxic
Feed 2	toxic	toxic	not toxic	not toxic	not toxic	toxic	toxic	toxic	toxic

Feed mixture	Clone6 9 mM	Clone6 16 mM	Clone7 13 mM	Clone7 16 mM	Clone2 14 mM	Clone4 14 mM	Clone5 14 mM	Clone8 22 mM	Summary
68	toxic	toxic	not toxic	toxic	not toxic	toxic	toxic	not toxic	toxic
69	not toxic	toxic	toxic	toxic	not toxic	toxic	toxic	toxic	toxic
70	NA	NA	NA	NA	not toxic	not toxic	toxic	not toxic	not toxic
71	toxic	toxic	not toxic	toxic	not toxic	toxic	toxic	not toxic	toxic
72	not toxic	not toxic	not toxic	not toxic	not toxic	not toxic	not toxic	not toxic	not toxic
73	NA	NA	NA	NA	not toxic	not toxic	not toxic	not toxic	not toxic
74	toxic	toxic	not toxic	not toxic	not toxic	toxic	toxic	not toxic	toxic
Feed 6	toxic	toxic	not toxic	not toxic	not toxic	not toxic	toxic	not toxic	toxic
76	NA	NA	NA	NA	not toxic	not toxic	toxic	not toxic	not toxic
77	toxic	toxic	not toxic	not toxic	not toxic	toxic	toxic	not toxic	toxic
78	NA	NA	NA	NA	not toxic	not toxic	not toxic	not toxic	not toxic
79	not toxic	not toxic	not toxic	not toxic	not toxic	not toxic	not toxic	not toxic	not toxic
Cys ctrl	not toxic	not toxic	not toxic	not toxic	not toxic	not toxic	not toxic	not toxic	not toxic
# toxic	24	36	14	20	6	22	47	13	43
% toxic	42.1**	63.2**	24.6**	35.1**	7.5	27.5	58.8	16.3	53.8

NA: not applicable * no data due to inoculation error ** toxicity in percent based on 57 tested feed mixtures

Table 17. Detected features in a positive mode using three different solvents. 5×10^6 cells were quenched with 0.5°C NaCl and 50% aqueous acetonitrile (ACN), 50% aqueous methanol (MeOH) and a 1:3 MeOH - chloroform mixture (MC) were used as extraction solvent (n=3). Data of LC-MS analysis in positive ionization mode with an abundance > 10000 were annotated by standards or data base hits including the elemental composition.

Nr	RT [min]	m/z	Solvent			Identification	Formula	Mass error [ppm]
			ACN	MeOH	MC			
1	1.03	203.2230	x	x	x	Spermine tetrahydrochloride	$C_7H_{19}N_3Cl$	1.4
2	1.11	147.1128	x	x	x	D-Lysine	$C_6H_{14}N_2O_2$	0.3
3	1.13	122.9246	x	x	x	more than 1 possible compound		
4	1.15	112.8957	x	x	x	more than 1 possible compound		
5	1.16	131.1179	x	x	x	more than 1 possible compound		
6	1.17	110.0713	x	x	x	more than 1 possible compound		
7	1.17	133.0609	x	x	x	L-Asparagine	$C_4H_8N_2O_3$	1.1
8	1.17	156.0768	x	x	x	L-Histidine	$C_6H_9N_3O_2$	0.6
9	1.18	184.0733	x	x	x	Phosphocholine	$C_5H_{14}NO_4P$	-0.2
10	1.19	124.9999	x	x	x	Brevifolincarboxylic acid 9-sulfate	$C_{13}H_8O_{11}S$	-2.3
11	1.19	216.0632	x	x	x	more than 1 possible compound		
12	1.22	90.0550	x	x	x	L-Alanine	$C_3H_7NO_2$	0.6
13	1.22	120.0656	x	x	x	L-Threonine	$C_4H_9NO_3$	1
14	1.23	148.0606	x	x	x	L-Glutamic acid	$C_5H_9NO_4$	0.8
15	1.23	175.1190	x	x	x	L-Arginine	$C_6H_{14}N_4O_2$	0.4
16	1.24	258.1101	x	x	x	Glycerophosphocholine	$C_8H_{20}NO_6P$	-0.1
17	1.25	145.0497	x	x	x	more than 1 possible compound		
18	1.25	163.0602	x	x	x	more than 1 possible compound		
19	1.25	180.0867	x	x	x	more than 1 possible compound		
20	1.26	496.2089	x	x	x	more than 1 possible compound		
21	1.27	737.2849	x	x	x	more than 1 possible compound		
22	1.29	239.1059	x	x	x	4-(2-Hydroxyethyl)piperazine-1-ethanesulfonic acid	$C_8H_{18}N_2O_4S$	-0.5
23	1.33	104.1070	x	x	x	Choline	$C_5H_{13}NO$	0.3

Nr	RT [min]	m/z	Solvent			Identification	Formula	Mass error [ppm]
			ACN	MeOH	MC			
24	1.40	384.1503	x	x	x	*N*-Acetyl-D-lactosamine	$C_{14}H_{25}NO_{11}$	0.6
25	1.40	405.0100	x	x	x	more than 1 possible compound		
26	1.42	499.2137	x	x	x	more than 1 possible compound		
27	1.44	116.0707	x	x	x	L-Proline	$C_5H_9NO_2$	0.7
28	1.44	447.0679	x	x	x	more than 1 possible compound		
29	1.46	137.0710	x	x	x	more than 1 possible compound		
30	1.49	483.9922	x	x	x	more than 1 possible compound		
31	1.50	192.0326	x	x	x	more than 1 possible compound		
32	1.50	245.0611	x	x	x	more than 1 possible compound		
33	1.50	608.0890	x	x	x	more than 1 possible compound		
34	1.52	157.0608	x	x	x	more than 1 possible compound		
35	1.52	204.0867	x	x	x	more than 1 possible compound		
36	1.55	384.1502	x	x	x	more than 1 possible compound		
37	1.55	501.2294	x	x	x	more than 1 possible compound		
38	1.56	515.2451	x	x	x	more than 1 possible compound		
39	1.58	182.0812	x	x	x	more than 1 possible compound		
40	1.72	431.0731	x	x	x	more than 1 possible compound		
41	1.73	205.0820	x	x	x	more than 1 possible compound		
42	1.75	118.0863	x	x	x	L-Valine	$C_5H_{11}NO_2$	0.4
43	1.77	473.1197	x	x	x	more than 1 possible compound		
44	1.78	112.0505	x	x	x	more than 1 possible compound		
45	1.78	344.0660	x	x	x	more than 1 possible compound		
46	1.83	260.1128	x	x	x	more than 1 possible compound		
47	1.83	278.1234	x	x	x	more than 1 possible compound		
48	1.83	179.1286	x	x	x	more than 1 possible compound		
49	1.84	343.2341	x	x	x	more than 1 possible compound		
50	1.84	428.0368	x	x	x	Adenosine 5'-diphosphate	$C_{10}H_{15}N_5O_{10}P_2$	0.2
51	1.86	215.0163	x	x	x	more than 1 possible compound		
52	1.88	233.0768	x	x	x	more than 1 possible compound		
53	1.89	263.0874	x	x	x	more than 1 possible compound		
54	1.9	228.0979	x	x	x	more than 1 possible compound		
55	1.92	399.1446	x	x	x	*S*-Adenosylmethionine	$C_{15}H_{22}N_6O_5S$	0.3
56	2.02	185.1286	x	x	x	more than 1 possible compound		
57	2.05	346.0463	x	x	x	more than 1 possible compound		
58	2.11	179.0486	x	x	x	more than 1 possible compound		
59	2.11	308.0911	x	x	x	Glutathione	$C_{10}H_{17}N_3O_6S$	-0.1
60	2.17	133.0318	x	x	x	more than 1 possible compound		
61	2.17	150.0584	x	x	x	L-Methionine	$C_5H_{11}NO_2S$	0.6
62	2.22	280.1392	x	x	x	more than 1 possible compound		
63	2.49	146.0923	x	x	x	4-Guanidinobutanoic acid	$C_5H_{11}N_3O_2$	-0.8

Nr	RT [min]	m/z	Solvent			Identification	Formula	Mass error [ppm]
			ACN	MeOH	MC			
64	2.59	361.1832	x	x	x	more than 1 possible compound		
65	2.66	242.6421	x	x	x	more than 1 possible compound		
66	2.71	364.2032	x	x	x	more than 1 possible compound		
67	3.22	132.1019	x	x	x	L-Isoleucine	$C_6H_{13}NO_2$	0.3
68	3.26	275.1602	x	x	x	more than 1 possible compound		
69	3.43	91.0543	x	x	x	more than 1 possible compound		
70	3.43	182.0811	x	x	x	L-Tyrosine	$C_9H_{11}NO_3$	-0.3
71	3.49	132.1019	x	x	x	L-Leucine	$C_6H_{13}NO_2$	0.2
72	3.79	466.1128	x	x	x	more than 1 possible compound		
73	3.96	228.0980	x	x	x	Deoxycytidine	$C_9H_{13}N_3O_4$	0.5
74	4.28	466.1129	x	x	x	more than 1 possible compound		
75	4.28	508.0033	x	x	x	Adenosine 5'-triphosphate	$C_{10}H_{16}N_5O_{13}P_3$	0.5
76	4.41	344.1340	x	x	x	more than 1 possible compound		
77	4.61	664.1157	x	x	x	Nicotinamide adenine dinucleotide (NAD)	$C_{21}H_{27}N_7O_{14}P_2$	0.1
78	4.80	294.1548	x	x	x	more than 1 possible compound		
79	4.82	276.1443	x	x	x	more than 1 possible compound		
80	4.93	123.0553	x	x	x	Niacinamide	$C_6H_6N_2O$	0.5
81	5.16	212.0740	x	x	x	more than 1 possible compound		
82	5.38	247.1290	x	x	x	more than 1 possible compound		
83	5.69	131.0493	x	x	x	more than 1 possible compound		
84	5.70	166.0862	x	x	x	DL-Phenylalanine	$C_9H_{11}NO_2$	-0.1
85	6.02	328.1391	x	x	x	more than 1 possible compound		
86	6.27	202.1074	x	x	x	more than 1 possible compound		
87	6.27	335.1814	x	x	x	more than 1 possible compound		
88	6.27	220.1179	x	x	x	Pantothenic Acid	$C_9H_{17}NO_5$	-0.2
89	6.27	264.1556	x	x	x	more than 1 possible compound		
90	6.71	205.0971	x	x	x	L-Tryptophan	$C_{11}H_{12}N_2O_2$	0.1
91	6.8	367.1501	x	x	x	more than 1 possible compound		
92	7.04	239.1489	x	x	x	more than 1 possible compound		
93	7.38	261.1446	x	x	x	more than 1 possible compound		
94	7.38	276.0844	x	x	x	more than 1 possible compound		
95	7.76	283.1752	x	x	x	more than 1 possible compound		
96	9.33	230.0812	x	x	x	more than 1 possible compound		
97	10.33	133.0863	x	x	x	more than 1 possible compound		
98	3.44	348.0705		x	x	Adenosine monophosphate		0.2
99	3.71	307.0834	x		x	Glutathione, oxidized	$C_{20}H_{32}N_6O_{12}S_2$	0.4
100	4.78	380.1124	x		x	S-Lactoylglutathione	$C_{13}H_{21}N_3O_8S$	0.4
101	11.43	257.2477			x	14-methyl-Pentadecanoic acid	$C_{16}H_{32}O_2$	0.7
102	1.17	106.0499	x	x		D-Serine	$C_3H_7NO_3$	0.5
103	1.17	155.0428	x	x		more than 1 possible compound		

Nr	RT [min]	m/z	Solvent			Identification	Formula	Mass error [ppm]
			ACN	MeOH	MC			
104	1.23	203.0528	x	x		more than 1 possible compound		
105	1.24	258.2424	x	x		more than 1 possible compound		
106	1.26	358.1650	x	x		more than 1 possible compound		
107	1.55	428.1869	x	x		more than 1 possible compound		
108	1.57	406.1321	x	x		N-Acetyl-D-lactosamine	$C_{14}H_{25}NO_{11}$	0.4
109	1.74	203.1503	x	x		NG,NG-Dimethylarginine dihydrochloride		0.5
110	1.96	148.0606	x	x		more than 1 possible compound		
111	2.22	262.1286	x	x		more than 1 possible compound		
112	2.95	470.1442	x	x		more than 1 possible compound		
113	3.05	312.1110	x	x		*N*-(1-Deoxy-1-fructosyl) methionine	$C_{11}H_{21}NO_7S$	-0.4
114	3.13	247.1401	x	x		more than 1 possible compound		
115	4.37	326.1235	x	x		more than 1 possible compound		
116	4.55	207.6392	x	x		more than 1 possible compound		
117	5.24	137.0458	x	x		more than 1 possible compound		
118	5.38	291.0973	x	x		L-*N*-(1H-Indol-3-ylacetyl) aspartic acid	$C_{14}H_{14}N_2O_5$	-1
119	6.02	310.1286	x	x		Tranylcypromine glucuronide	$C_{15}H_{19}NO_6$	0.2
120	7.95	212.0893	x	x		more than 1 possible compound	$C_8H_{15}NO_4$	-1.1
121	8.82	228.0631	x	x		Indolelactic acid	$C_{11}H_{11}NO_3$	-0.1
122	9.81	229.0431	x	x		more than 1 possible compound		
123	1.09	365.2760		x		more than 1 possible compound		
124	1.12	446.8875		x		more than 1 possible compound		
125	1.44	324.0594		x		Cytidine 5'-monophosphate	$C_9H_{14}N_3O_8P$	0.8
126	6.69	243.1831		x		more than 1 possible compound		
127	1.31	342.2059	x			Elemental composition	$C_{13}H_{31}N_3O_5S$	0.6
128	1.47	146.0271	x			Elemental composition	$C_5H_7NO_2S$	0.8
129	1.52	293.1707	x			more than 1 possible compound		
130	1.74	469.0708	x			2-(a-Hydroxyethyl)thiamine diphosphate	$C_{14}H_{22}N_4O_8P_2S$	0.3
131	3.53	263.1966	x			L-Leucine	$C_6H_{13}NO_2$	0.2
132	5.19	350.1018	x			S-(Formylmethyl)glutathione	$C_{12}H_{19}N_3O_7S$	0.4
133	5.94	221.0922	x			more than 1 possible compound		
134	6.70	160.0760	x			more than 1 possible compound		
135	6.73	170.0601	x			more than 1 possible compound		
136	7.22	301.1709	x			more than 1 possible compound		
137	8.39	245.0955	x			D-Biotin	$C_{10}H_{16}N_2O_3S$	0.3
138	8.91	260.0892	x			more than 1 possible compound		
139	10.41	146.0942	x			more than 1 possible compound		

Table 18. Detected features in negative ionization mode using three different solvents. 5×10^6 cells were quenched with 0.5°C NaCl and 50% aqueous acetonitrile (ACN), 50% aqueous methanol (MeOH) and a 1:3 MeOH-chloroform mixture (MC) were used as extraction solvent (n=3). Data of LC-MS analysis in positive ionization mode with an abundance > 5000 were annotated by standards or data base hits including the elemental composition.

Nr	RT [min]	m/z	solvent			Identification	Formula	Mass error [ppm]
			ACN	MeOH	M/C			
1	1.16	140.0119	x	x	x	more than 1 possible compound		
2	1.18	104.0353	x	x	x	L-Serine		-0.3
3	1.18	131.0462	x	x	x	L-Asparagine		0.6
4	1.18	154.0623	x	x	x	L-Histidine		1.0
5	1.18	168.0433	x	x	x	more than 1 possible compound		
6	1.18	201.0518	x	x	x	more than 1 possible compound		
7	1.19	195.0511	x	x	x	more than 1 possible compound		
8	1.19	228.0642	x	x	x	more than 1 possible compound		
9	1.2	215.0329	x	x	x	more than 1 possible compound		
10	1.2	217.0302	x	x	x	more than 1 possible compound		
11	1.22	118.0510	x	x	x	L-Threonine	$C_4H_9NO_3$	0.4
12	1.23	173.1046	x	x	x	L-Arginine		0.9
13	1.24	146.046	x	x	x	L-Glutamic acid		0.9
14	1.24	245.0432	x	x	x	more than 1 possible compound		
15	1.25	135.0300	x	x	x	more than 1 possible compound		
16	1.25	179.0562	x	x	x	more than 1 possible compound		
17	1.25	225.0616	x	x	x	more than 1 possible compound		
18	1.29	237.0915	x	x	x	4-(2-Hydroxyethyl)piperazine-1-ethanesulfonic acid	$C_8H_{18}N_2O_4S$	0.1
19	1.29	293.0491	x	x	x	(2-hydroxy-1,2-diphenylethoxy) sulfonic acid	$C_{14}H_{14}O_5S$	0.5
20	1.39	402.9951	x	x	x	more than 1 possible compound		
21	1.39	565.0477	x	x	x	more than 1 possible compound		
22	1.43	87.0088	x	x	x	L-Glyceric acid	$C_3H_6O_4$	0.0
23	1.44	445.0531	x	x	x	CDP-Ethanolamine		0.1
24	1.49	133.0143	x	x	x	L-Malic acid		0.1
25	1.54	606.0743	x	x	x	more than 1 possible compound		
26	1.62	481.9773	x	x	x	Cytidine triphosphate (CTP)	$C_9H_{16}N_3O_{14}P_3$	0.0
27	1.72	429.0582	x	x	x	more than 1 possible compound		
28	1.73	175.0249	x	x	x	D(+)-Glucuronic acid γ-lactone		-0.7
29	1.74	579.0271	x	x	x	more than 1 possible compound		
30	1.77	517.1108	x	x	x	more than 1 possible compound		
31	1.84	426.0221	x	x	x	ADP	$C_{10}H_{15}N_5O_{10}P_2$	0.0
32	1.85	191.0198	x	x	x	Citric acid	$C_6H_8O_7$	0.2
33	1.85	111.0088	x	x	x	more than 1 possible compound		
34	1.91	89.0244	x	x	x	more than 1 possible compound		
35	1.97	146.0460	x	x	x	more than 1 possible compound		
36	2.02	147.0300	x	x	x	more than 1 possible compound		

37	2.1	613.1602	x	x	x	more than 1 possible compound		
38	2.11	306.0766	x	x	x	Glutathione		0.1
39	2.17	148.0440	x	x	x	L-Methionine		1.3
40	2.21	579.0272	x	x	x	more than 1 possible compound		
41	2.73	147.0300	x	x	x	more than 1 possible compound		
42	2.76	173.0092	x	x	x	more than 1 possible compound		
43	3.21	482.9612	x	x	x	more than 1 possible compound		
44	3.22	130.0874	x	x	x	L-Isoleucine	$C_6H_{13}NO_2$	0.5
45	3.43	180.0666	x	x	x	L-Tyrosine		0.1
46	3.43	346.0558	x	x	x	more than 1 possible compound		
47	3.43	361.1404	x	x	x	more than 1 possible compound		
48	3.48	505.9883	x	x	x	more than 1 possible compound		
49	3.8	464.0980	x	x	x	more than 1 possible compound		
50	4.29	505.9884	x	x	x	more than 1 possible compound		
51	4.31	464.0981	x	x	x	more than 1 possible compound		
52	4.62	662.1018	x	x	x	β-Nicotinamide adenine dinucleotide	$C_{21}H_{27}N_7O_{14}P_2$	-0.1
53	5.71	351.1327	x	x	x	more than 1 possible compound		
54	5.83	131.0351	x	x	x	more than 1 possible compound		
55	5.99	176.0388	x	x	x	N-Formylmethionine		1.0
56	6.27	332.0963	x	x	x	more than 1 possible compound		
57	6.27	445.2002	x	x	x	more than 1 possible compound		
58	6.27	218.1035	x	x	x	Pantothenic acid		0.3
59	6.39	129.0558	x	x	x	D-(-)-Pantolactone		1.3
60	6.68	129.0558	x	x	x	more than 1 possible compound		
61	6.74	203.0826	x	x	x	L-Tryptophan		0.2
62	6.74	407.1724	x	x	x	more than 1 possible compound		
63	6.77	181.0508	x	x	x	Hydroxyphenyllactic acid		0.8
64	7.37	259.1300	x	x	x	more than 1 possible compound		
65	8.88	202.1086	x	x	x	more than 1 possible compound		
66	9.13	145.0872	x	x	x	more than 1 possible compound		
67	9.34	228.0666	x	x	x	more than 1 possible compound		
68	1.21	242.0518		x	x	more than 1 possible compound		
69	1.18	184.9858	x		x	2-Phosphoglyceric acid		0.7
70	10.16	431.1825	x		x	more than 1 possible compound		
71	10.63	681.2957	x		x	more than 1 possible compound		
72	10.68	452.2781	x		x	more than 1 possible compound		
73	10.73	540.3305	x		x	more than 1 possible compound		
74	10.75	478.2937	x		x	more than 1 possible compound		
75	11.01	480.3096	x		x	more than 1 possible compound		
76	11.24	597.3044	x		x	more than 1 possible compound		
77	3.7	611.1447			x	Oxidized glutathione	$C_{20}H_{32}N_6O_{12}S_2$	0.0
78	4.79	378.0976			x	more than 1 possible compound		
79	10.26	748.5135			x	more than 1 possible compound		

80	10.39	686.4766			x	more than 1 possible compound			
81	10.52	774.5288			x	more than 1 possible compound			
82	10.71	307.1586			x	more than 1 possible compound			
83	11.5	776.5441			x	more than 1 possible compound			
84	1.24	302.1010	x	x		more than 1 possible compound			
85	1.27	419.1665	x	x		more than 1 possible compound			
86	1.34	176.0564	x	x		more than 1 possible compound			
87	1.44	114.0561	x	x		L-Proline			0.2
88	1.61	145.0142	x	x		Oxoglutaric acid	$C_5H_6O_5$		-0.1
89	1.96	579.0272	x	x		more than 1 possible compound			
90	3.2	303.0835	x	x		more than 1 possible compound			
91	7.36	252.0877	x	x		more than 1 possible compound			
92	7.96	188.0929	x	x		more than 1 possible compound			
93	8.82	174.0562	x	x		3-(hydroxyacetyl)indole			1.8
94	8.9	236.0928	x	x		more than 1 possible compound			
95	9.82	227.0284	x	x		more than 1 possible compound			
96	1.22	165.0405		x		more than 1 possible compound			
97	1.36	112.0404		x		Trans-4-Hydroxy-L-proline			-0.1
98	1.79	323.0286		x		Uridine 5'-monophosphate	$C_9H_{13}N_2O_9P$		0.0
99	2.24	426.0219		x		more than 1 possible compound			
100	3.81	306.0764		x		more than 1 possible compound			
101	4.34	306.0764		x		more than 1 possible compound			
102	5.04	348.0872		x		more than 1 possible compound			
103	6	326.1246		x		more than 1 possible compound			
104	6.78	365.1354		x		more than 1 possible compound			
105	6.8	401.1122		x		more than 1 possible compound			
106	1.25	166.9751	x			more than 1 possible compound			
107	1.36	381.0432	x			more than 1 possible compound			
108	1.46	112.0404	x			more than 1 possible compound			
109	1.68	351.0568	x			more than 1 possible compound			
110	5.48	179.0349	x			more than 1 possible compound			
111	7.78	440.1322	x			Folic acid			-0.4
112	8.78	165.0558	x			more than 1 possible compound			
113	9.05	144.0456	x			1H-Indole-3-carboxaldehyde			1.1
114	10.53	529.2806	x			more than 1 possible compound			
115	10.82	436.2833	x			more than 1 possible compound			
116	10.88	462.2987	x			more than 1 possible compound			
117	11.2	464.3145	x			more than 1 possible compound			
118	11.48	281.2486	x			more than 1 possible compound			

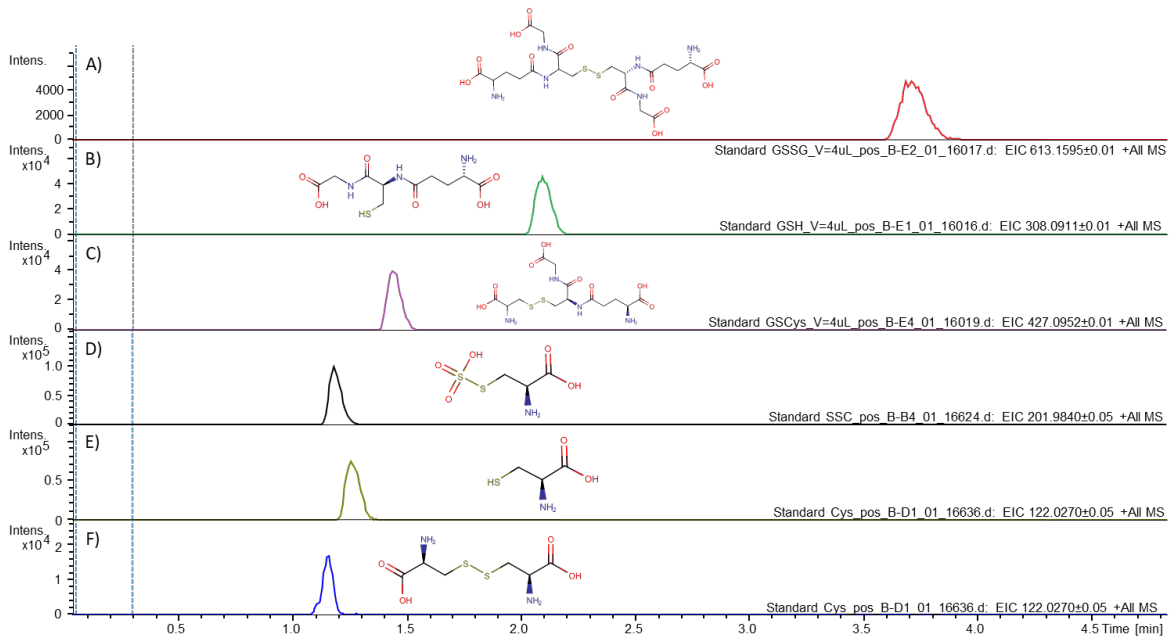

Figure 49. Extracted ion chromatogram of six standards. 500 µM of (A) GSSG, (B) GSH, (C) GS-Cys, (D) SSC, (E) Cys, and (F) CysS were dissolved in water and measured via LC-MS.

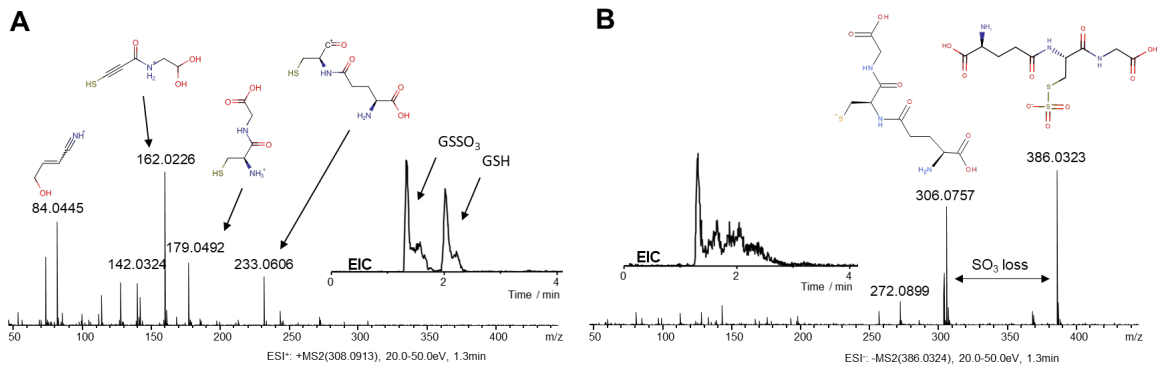

Figure 50. Fragmentation pattern of GS-SO_3 in positive and negative ionization mode. (A) In positive ionization mode 308.0913m/z was observed due to loss of the sulfone group in the ionization source leading to the same m/z as GSH. The respective extracted ion chromatograms are visualized within the graph and highlights the two peaks corresponding to GSH and GS-SO_3. (B) In negative ionization mode 386.0324m/z was detected, whereas the main fragment is due to sulfone loss.

7.2. List of abbreviations

ACN_{aq}	50% aqueous acetonitrile
ARE	antioxidant response element
Arg	arginine
ASC	alanine-serine-cysteine
Asp	asparagine
ATP	adenosine triphosphate
AUC	area under the curve
C	constant domain
CBS	cystathionine β-synthase
cDNA	complementary deoxyribonucleic acid
CDM	chemically defined media
CDO	cysteine dioxygenase
CDR	complementary-determining region
CHO	chinese hamster ovary
cIEF	capillary isoelectric focusing
CKG	2-(2-carboxyethyl)-1,3-thiazolidine-2,4-dicarboxylic acid
CoA	Coenzyme A
cQA	critical quality attributes
CSDA	cysteine sulfinate decarboxylase
CSE	cystathionine γ-lyase
Ct	cycle threshold
Cys	cysteine
CysS	cystine
DDA	data dependent acquisition
DHFR	dihydrofolate reductase
DMSO	dimethyl sulfoxide
DO	dissolved oxygen
EAAT	excitatory amino acid transporter (x_{AG}^{-})
ER	endoplasmic reticulum
Ero1p	endoplasmic reticulum oxidoreductin 1
ESI	electro-spray-ionization
F_{ab}	fragment antigen-binding
F_C	fragment crystallizable
FDA	Food and Drug Administration
γGCS	γ-glutamyl cysteine synthetase
γGT	γ-glutamyl transpeptidase
GAPDH	glyceraldehyde-3-phosphate dehydrogenase
GCL	glutamate-cysteine ligase
GR	glutathione reductase
Grx	glutaredoxins
GS	glutamine synthetase
GS-Cys	cysteine glutathione
$GS\text{-}SO_3$	sulfo-glutathione
GSH	glutathione (reduced)
GSSG	glutathione disulfide (oxidized)
GST	glutathione-*S*-transferase
H_2O_2	hydrogen peroxide
HEPES	4-(2-Hydroxyethyl)-1-piperarzineethanesulfonic acid
Ig	immunoglobulin
IGF-1	insulin-like-growth factor 1
KEAP1	Kelch-like ECH-associated protein 1
KG	α-ketoglutaric acid
mAb	monoclonal antibody
$MeOH_{aq}$	50% aqueous methanol
MC	1:3 MeOH – chloroform mixture
m/z	mass to charge ratio
Met	methionine
mRNA	messenger ribonucleic acid
MS	mass spectrometry
MV_{50}	50% metabolic viability
MVDA	multivariate data analysis
NAC	*N*-acetylcysteine
Nrf2	NF-E2-related factor 2
NTU	nephelometric Turbidity Unit

OPLS-DA	orthogonal partial least squares projection discriminant analysis
PBS	phosphate buffered saline
PDI	protein disulfide isomerase
PTM	post-translational modification
qPCR	quantitative Polymerase chain reaction
RNS	reactive nitrogen species
ROS	reactive oxygen species
rpm	rounds per minute
RT	retention time
RP-UPLC	reverse phase ultra-performance liquid chromatography
SAM	*S*-adenosyl-L-methionine
SAS	sulfasalazine
SEM	standard error of the mean
SFN	sulforaphane
SFN-NAC	sulforaphane-*N*-acetylcysteine
SLC1	solute carrier family 1
SSC	*S*-sulfo-cysteine
ToF	time of flight
Trx	thioredoxin
TrxR	thioredoxin reductase
UPLC	ultra-performance liquid chromatography
UPLC-MS	UPLC coupled to a mass spectrometer
V	variable domain
VCD	viable cell density
x_c^-	CysS/Glu antiporter complex

7.3. List of figures

7.4. List of tables

7.5. Acknowledgements

First of all, I would like to thank Dr. Aline Zimmer for giving me the opportunity to realize my doctoral degree at Merck. Beyond that I want to thank you for the guidance, all the advices and support during the last years. You helped me improving not only my scientific knowledge but also my personal development.

Furthermore, I want to thank Prof. Dr. Harald Kolmar for supervising my doctoral thesis at TU Darmstadt. Especially both trips to Kleinwalsertal were highly appreciated not only for the skiing fun but also for the scientific exchange between the doctoral students.
I want to express my gratitude to Prof. Dr. Jörg von Hagen for serving as Co-referee and Prof. Dr. Katja Schmitz and Prof. Dr. Ulrike Nuber for serving as specialist examiner during my disputation.

Many thanks go to the entire "Advanced Cell Culture Technologies" team. Janike Ehret for making every conference fabulous and for the best US road trip. Corinna Merkel, Alisa Schnellbächer, Susanne Bohl, Maria Wehsling, Maxime Le Mignon, Christine Weiss, Stephanie Bellmaine, Janine Caspari, Ronja Seibel, Corinna Schmidt, Carolina Kunkel, Almut Rapp, Anja Licht, Alice Antonello, Anke Simon, Petra Schott, Tim Hofmann and Dmitry Zabezhinsky for the great discussions during meetings and providing a great work environment.
Special thanks to Melanie Nguyen for showing me Adobe illustrator and Robert Seute for the nice after work time at the boulder house as well as Emily Mayville, Masiha Arsalan and Paul Reindel. You were all great students and contributed to my work.

Additionally, I want to thank the whole St. Louis team for providing me an awesome time during my stay. Especially Laura Hagstrom for the work together but also for being the best tour guide. Avril Lawshe for the nice introduction into SIMCA, Zack Deeds for giving me the opportunity to perform the screening at all, Irfan Hodzic, Chris Kornfeld, Ademola Kassim and Jana Mahadevan for all these nice lunch times. James Ravellette, Jeffrey Galligan and Corey Kretzmer for the best bar hopping tour. David Beattie for giving me the opportunity to present my results but also for explaining me the basic Baseball rules.

I also want to thank all Merck PhD students for the scientific discussions: Marcel Rieker, Sebastian Jäger, Marie Quillmann, Markus Lubda, Sandra Müller, Gregory Som, Anna Kaempffe, Janis Rosskopf and Lukas Roth.

Furthermore, I would like to thank my parents, my sister and my friends for their endless support during my whole life. I certainly could not have done that without you.
Lastly, I would like to express my endless gratitude to Flo. For your encouragement and patience during my studies in the past years and especially during the last months. This would not have been possible without you. Thank you for everything.

8. Affirmations

Martina Zimmermann
Grüner Weg 14
64521 Groß-Gerau

Große-Gerau, 31.08.2020

Erklärung

Ich erkläre hiermit, dass ich meine Dissertation selbstständig und nur mit den angegebenen Hilfsmitteln angefertigt habe.

Martina Zimmermann

Martina Zimmermann
Grüner Weg 14
64521 Groß-Gerau

Große-Gerau, 31.08.2020

Erklärung

Ich erkläre hiermit, noch keinen Promotionsversuch unternommen zu haben.

Martina Zimmermann

Martina Zimmermann
Grüner Weg 14
64521 Groß-Gerau

Große-Gerau, 31.08.2020

Erklärung

Ich erkläre hiermit, dass die elektronische Version der Doktorarbet mit der schriftlichen Version übereinstimmt. Die elektronishe Version liegt dem Prüfungssekretariat vor.

Martina Zimmermann